



Universiteit
Leiden
The Netherlands

Photo-activated drug delivery systems

Kong, L.

Citation

Kong, L. (2018, June 7). *Photo-activated drug delivery systems*. Retrieved from <https://hdl.handle.net/1887/63080>

Version: Not Applicable (or Unknown)

License: [Licence agreement concerning inclusion of doctoral thesis in the Institutional Repository of the University of Leiden](#)

Downloaded from: <https://hdl.handle.net/1887/63080>

Note: To cite this publication please use the final published version (if applicable).

Cover Page



Universiteit Leiden



The following handle holds various files of this Leiden University dissertation:

<http://hdl.handle.net/1887/63080>

Author: Kong, L.

Title: Photo-activated drug delivery systems

Issue Date: 2018-06-07

Photo-activated Drug Delivery Systems

Proefschrift

ter verkrijging van

de graad van Doctor aan de Universiteit Leiden,
op gezag van Rector Magnificus prof.mr.C.J.J.M.Stolker
volgens het besluit van het College voor Promoties
te verdedigen op donderdag 7 juni 2018
klokke 11:15 uur

door

Li Kong

Geboren op 16 oktober 1986 de Qufu, China

Promotiecommissie

Promotor: Prof. dr. A. Kros

Overige leden:

Prof. Dr. H.S. Overkleeft, (voorzitter)

Prof. Dr. J. Brouwer, (secretaris)

Prof. Dr. W. Jiskoot

Prof. Dr. P.Y.W. Dankers

Dr. H.A. Santos

Being, knowing, doing

见自己，见天地，见众生

Table of contents

Preface	6
Chapter 1	7
The Application of Sheddable PEG Coronas in Drug Delivery	
Chapter 2	53
Temporal Control of Membrane Fusion through Photolabile PEGylation of Liposome Membranes	
Chapter 3	83
Spatiotemporal Control of Doxorubicin Delivery from “Stealth-Like” Prodrug Micelles	
Chapter 4	105
Light Induced Modulation of the Very Long Chain Fatty Acid Composition of Cell Membranes	
Chapter 5	127
Charge-Switchable Liposomes for Drug Delivery <i>in Vitro</i> and <i>in Vivo</i>	
Chapter 6	159
Summary and perspective	
Samenvatting	165
Abbreviations	171
Curriculum vitae	173
List of publications	174

Preface:

The work in this thesis focuses on the development of new stimuli-responsive drug delivery systems. All four described systems rely on light as the exclusive trigger of activation and the spatiotemporal precision afforded by this approach is demonstrated, both *in vitro* and *in vivo*, throughout this thesis. Light activation, for three of the four described systems (**chapters 2-4**), leads to dePEGylation of a nanoparticle surface. In this way, the benefits of PEGylation (*e.g.* limited non-specific cellular interactions) are maintained, while the obstacles of PEGylation (*e.g.* limited uptake by targeted cells) can be overcome on demand. In **chapter 5**, light is used to switch the surface charge of a nanoparticle *in situ* and *in vivo*. The effectiveness of this approach is demonstrated within zebrafish embryos. Despite countless reports of stimuli-responsive drug delivery systems in the literature, none have yet made it to the clinic. The work in this thesis is therefore aimed at providing potential solutions to some of the roadblocks slowing the progression of stimulus-responsive drug delivery systems.

1

The Application of Sheddable PEG Coronas in Drug Delivery

Abstract: To prolong *in vivo* circulation times of drug delivery nano-systems, poly(ethylene glycol) (PEG) is often used to sterically shield nanoparticle surfaces. This serves to minimize adsorption of serum proteins to the nanoparticle and recognition and bodily clearance *via* the mononuclear phagocyte system (MPS). However, a PEG corona also inhibits interactions between nano-carriers and target cells, limiting drug delivery and effective therapy. To overcome this dilemma, cleavable PEG coronas have been developed to maintain long circulation lifetimes of nanoparticles while also achieving efficient cellular interactions with targeted cells. In this chapter, various strategies and examples of drug delivery systems with a sheddable PEG corona are reviewed.

1.1 Introduction

In the treatment of cancer, the challenge is how to deliver cytotoxic drugs to cancer cells while minimizing off-target toxicity in healthy cells and tissue. Current chemotherapy is characterized by debilitating side effects^[1] (impaired immune system, nausea, cardiomyopathy, hair loss) and in many cases, the cumulative lifetime dose of an anti-cancer drug must be limited to avoid permanent damage.^[2] Intense efforts have therefore been made to develop drug delivery systems (DDS) capable of delivering drugs specifically to cancer cells (Figure 1).^[3]

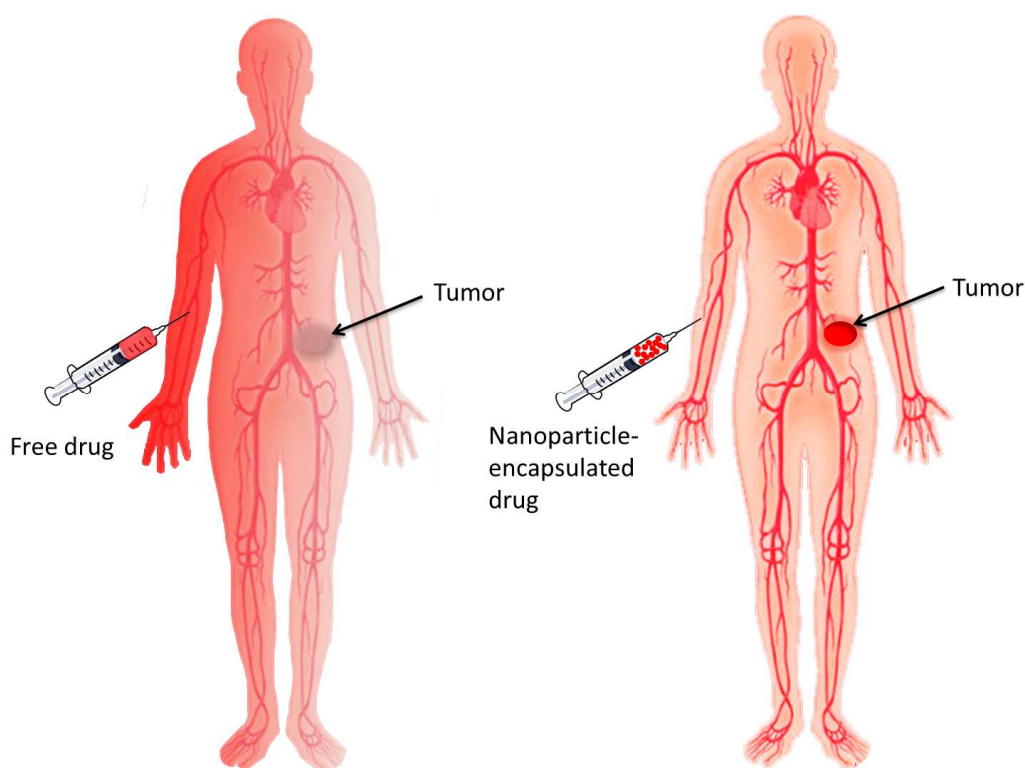


Figure 1. Distribution of free (left) and nanoparticle-encapsulated (right) drugs within the body following systemic (e.g. intravenous) administration. Small molecule drugs freely diffuse through tissue and away from the site of injection (non-targeted). Nanoparticles remain restricted within blood vessels and can passively accumulate within tumors (targeted). Image taken from www.cocoavia.com.

Two principle technologies have emerged: antibody-drug conjugates (ADCs) and nanoparticle-based systems. Currently, 5 ADCs and 12 distinct nanoparticle-based

DDS targeted against a variety of human cancers are on the market.^[4] For ADCs, ‘active’ targeting is achieved through antibody recognition and binding to over-expressed receptors (tumor-associated antigens) on cancer cells.^[5] Once bound, ADCs are endocytosed, the conjugated drug released and ideally the cell is destroyed. Although effective, ADCs are costly to manufacture, can elicit adverse immunogenic responses (limiting repeat dosing) and are largely limited to small molecule drug (and serum stable) cargos.^[6] In the case of nanoparticle-based DDS, drugs are encapsulated within the structure of the self-assembled nanoparticle, hidden and protected from the *in vivo* environment. Pharmacokinetic (PK) profiles are dictated by the nanoparticle and, in theory, it is possible to deliver anything from small molecule drugs to plasmid DNA to target cells and tissue within the body. An enormous variety of nanoparticle-based DDS have been reported, however the most widely investigated are micelles, liposomes and polymersomes (Figure 2).^[7] In the treatment of cancer, the vast majority of nanoparticle-based systems ‘passively’ target tumors *via* the enhanced permeability and retention (EPR) effect.

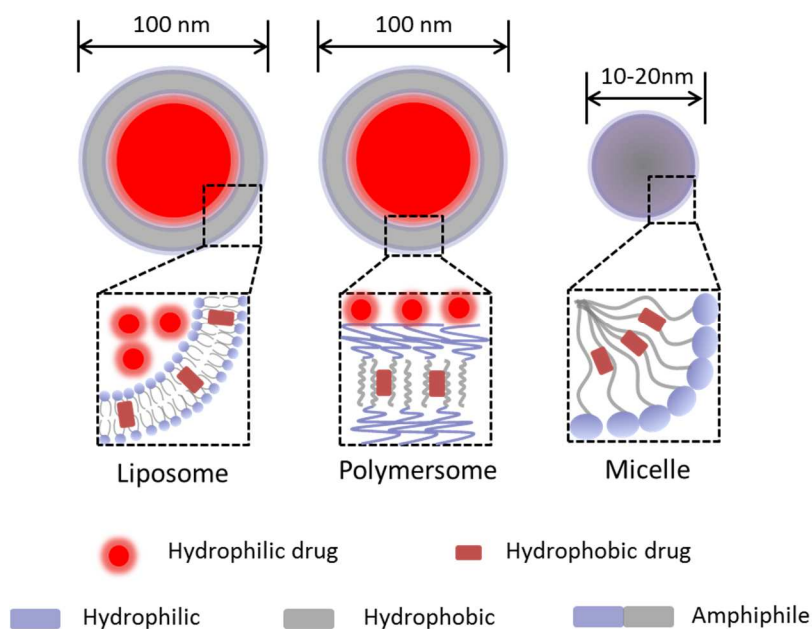


Figure 2. Schematic showing the three most commonly self-assembled nanoparticle- based drug delivery systems. Self-assembly is primarily driven by the burial of hydrophobic functionality of amphiphilic building blocks to limit exposure to water (‘hydrophobic effect’).

1.1.1 The enhanced permeability and retention (EPR) effect

Following administration to the body, small molecule drugs freely diffuse away from the site of injection (Figure 1). In contrast, following intravenous (*i.v.*) injection, nanoparticles are restricted to the circulating blood flow, unable to cross the tightly packed endothelium due to their larger size. For optimal biodistribution, nanoparticles should be larger than 10 nm in diameter – below which they are filtered from the body *via* the kidneys – and smaller than 200 nm in diameter – above which they are recognized and phagocytosed by macrophages (key cells of the mononuclear phagocyte system, MPS) and cleared from the body.^[8]

The EPR effect is a phenomena characterized by the ill-defined ('leaky') vasculature and poor lymphatic drainage of tumors arising from rapid angiogenesis (blood vessel growth) within tumor tissue (Figure 3).^[9] Circulating nanoparticles passing through a tumor can passively diffuse across gaps in the tumor endothelium, accumulate within the tumor and remain there for extended periods of time. Once within the tumor, nanoparticle encapsulated drugs can either passively diffuse from the nanoparticle or an endogenous or exogenous stimulus can trigger release.

A key difference between the various strategies described in this chapter is whether the nanoparticle is internalized prior to drug release or not. If it is first internalized, drug release occurs intracellular and beyond the barrier of the cell membrane. This offers opportunities to deliver membrane impermeable cargos such as DNA, RNA and proteins to cancer cells. If extracellular drug release occurs, the drug must be taken up by cancer cells itself. In either scenario, it is essential cancer cells are exposed to therapeutically relevant doses of cytotoxic drugs if an improved therapeutic index is to be achieved.

There are several nanoparticle-based DDS (*e.g.* Doxil®), currently on the market, designed to passively target chemotherapies to solid tumors *via* the EPR effect.^[10] These have been clinically proven to improve patient quality of life compared to administration of the free drug alone. Nevertheless, the effectiveness of this targeting approach remains contentious.^[11] A recent analysis (>200 separate studies) of nanoparticle uptake in tumors *via* the EPR revealed, for instance, found, on average,

just 0.7% of the injected nanoparticle dose accumulated within the target tumor.^[12] In addition, there is growing evidence that the EPR effect may be more pronounced in experimental animal models than in human patients,^[13] therefore running the risk of false positives entering clinical evaluation. Finally, it is becoming increasingly clear that there is significant physiological heterogeneity within and between tumor types in patients. In other words, the same nanoparticle-based DDS may give very different therapeutic outcomes in two patients suffering from the same cancer.^[14] In light of this, there are growing calls for pre-selection of patients to effectively identify those who would likely benefit from these technologies over those who would likely not.^[15]

1.1.2 Polyethylene glycol (PEG)

To maximize nanoparticle targeting of tumors *via* the EPR effect, nanoparticles with long circulation lifetimes are sought. Put simply, the more times nanoparticles pass through the tumor vasculature, the more will accumulate there. As such, care must be taken to minimize drug leakage from the nanoparticle *en route* to the tumor while at the same time ensuring therapeutically relevant concentrations of drugs are released once there. In the case of liposome-drug formulations – the most widely investigated and major class of nanoparticles approved for clinical use^[16] – this involves careful choice of lipid reagents (*e.g.* cholesterol to rigidify fluid, leaky membranes) to fine tune drug retention/release profiles while at the same time maximizing circulation lifetimes.^[17]

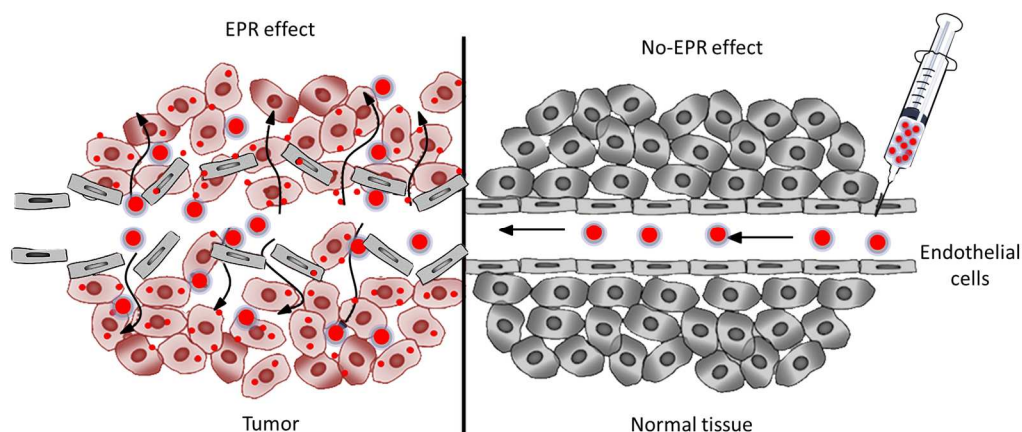
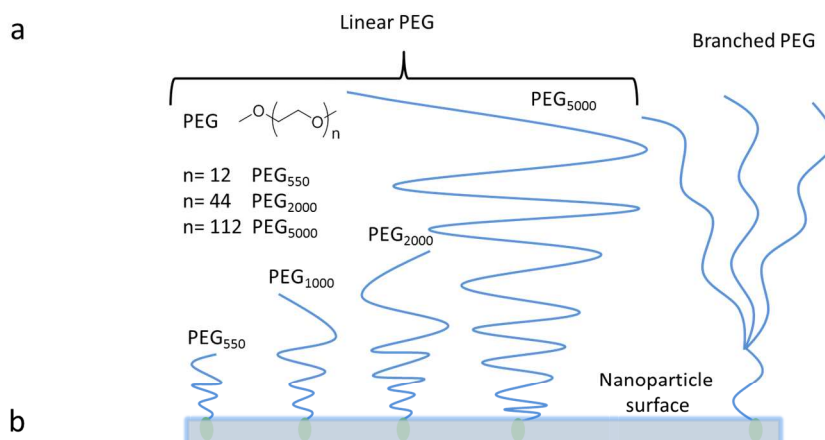


Figure 3. Schematic representation of the EPR effect. Healthy cells are shown in grey and tumor cells in red. The small red dots indicate drug release from the nanoparticle and delivery to cells once nanoparticles have accumulated within the target tumor. Image taken from^[18].

In developing nanoparticles with long circulation lifetimes, the principle biological barrier to overcome is recognition and clearance of nanoparticles by the MPS. The principle organ of the MPS is the liver where hepatic macrophages – Kupffer cells – are highly proficient at recognizing and removing macromolecular, colloidal and pathogenic waste from circulation.^[19] Without any surface modification, up to 99% of nanoparticles are cleared through the liver.^[20] In most cases, it is believed rapid adsorption of blood proteins to the surface of nanoparticles, (a process known as opsonisation), acts as a recognition beacon for the MPS.^[21] For this reason, sterically shielding nanoparticle surfaces with biocompatible polymers such as polyethylene glycol (PEG), has been used to minimize opsonisation and prolong blood circulation times of nanoparticles *in vivo*.^[22]



Therapeutic type	Commercial name	Drug name	PEG (g/mol)	Indications
Enzyme	Adagen	PEGademase bovine	5000 (linear)	severe combined immunodeficiency disease
	Oncaspar	PEGaspargase	5000 (linear)	lymphoblastic leukemia
Interferons	PegIntron	peginterferon-2β	12000 (linear)	hepatitis B and hepatitis C
	Puricase	PEG-urate oxidase	10000	Gout
	Pegasys	peginterferon-2α	40000 (branched)	hepatitis C
Granulocyte colony stimulating factor	Neulasta	pegfilgrastim	20000 (linear)	neutropenia
Growth hormone receptor antagonist	Somavert	pegvisomant	5000 (linear)	Acromegaly
Drug	Macugen	Pegaptanib sodium	40000 (branched)	age-related macular degeneration(AMD)
	Movanti	pegylated naloxol	339	Opoid-induced constipation
Erythropoietin receptor activator	Mircera	Mono-mPEG-epoetin-β	30000 (linear)	Anemia associated with chronic renal failure
Antibody	Cimzia	certolizumab pegol	40000 (branched)	Reducing signs and symptoms of Crohn's disease

Figure 4. (a) The chemical structure and representation of linear PEG chains with different lengths and branched PEG; (b) Table of FDA approved PEGylated drugs.^[23]

PEG is a synthetic polymer of repeating ethylene glycol units. Used as a reagent or additive in a wide range of biological, chemical and industrial settings,^[24] it is commercially available in a range of geometries (linear, branched, star, comb), molecular weights (from 300 Da – 6-7 repeating units – up to 10 MDa - >200,000 repeating units) and can be readily functionalized. PEGylation of nanoparticle surfaces

has been shown to decrease serum protein adsorption, reduce nanoparticle uptake in the liver and prolong circulation lifetimes.^[25] More recently, evidence has been uncovered to suggest PEG can elicit an immunogenic response.^[26] However, the extent and accuracy of the immunogenic response caused by binding of anti-PEG antibodies to PEGylated nanoparticles remains unclear.^[27] PEG remains an FDA approved polymer and is still the most widely used polymeric coating of nanoparticle DDS both in academic and industrial research.

Numerous PEGylated products, such as PEGylated enzymes, proteins, antibodies or oligonucleotides, are FDA-approved (Figure 4). For example, PEGylated liposomal-doxorubicin (Doxil®) has been clinically used for over 20 years in the treatment of select breast and ovarian cancers, multiple myeloma and AIDS-related Kaposi's sarcoma.^[24b]

1.1.3 The PEG dilemma

While PEGylation serves to prolong circulation lifetimes, it also limits the cellular uptake of nanoparticles. This has proved a major obstacle in the targeted delivery of therapeutic cargos, particularly those that must be actively transported across the target cellular membrane.^[28] For instance, in the delivery of oligonucleotides (ODNs) or small interfering RNAs (siRNAs), significantly lower transfection/transduction efficiencies were observed for PEGylated vs. non-PEGylated DDS.^[29] To overcome this 'PEG dilemma', many strategies have been proposed to trigger the shedding of PEG (*i.e.* dePEGylation) from a nanoparticle surface upon reaching the target tumor. In the vast majority of cases, triggered dePEGylation within the target tumor occurs outside of the target cell (extracellular). This leads to one of three scenarios: 1) rupture of the nanoparticle and extracellular drug release (Figure 5a); 2) cellular uptake of the intact nanoparticle-drug complex (Figure 5b) or 3) in the case of liposomal carriers, fusion of the nanoparticle with the target cellular membrane resulting in contents release directly to the cell cytoplasm (*i.e.* avoiding endocytotic uptake) (Figure 5c). In a small number of examples, PEGylated nanoparticles used to be taken up by the cancer cells first whereupon the low pH, reductive and protease-rich environment of the late endosome/lysosome triggers dePEGylation and contents release (Figure 5d).

However, the slow rate of uptake of PEGylated nanoparticles is a major obstacle to these approaches.

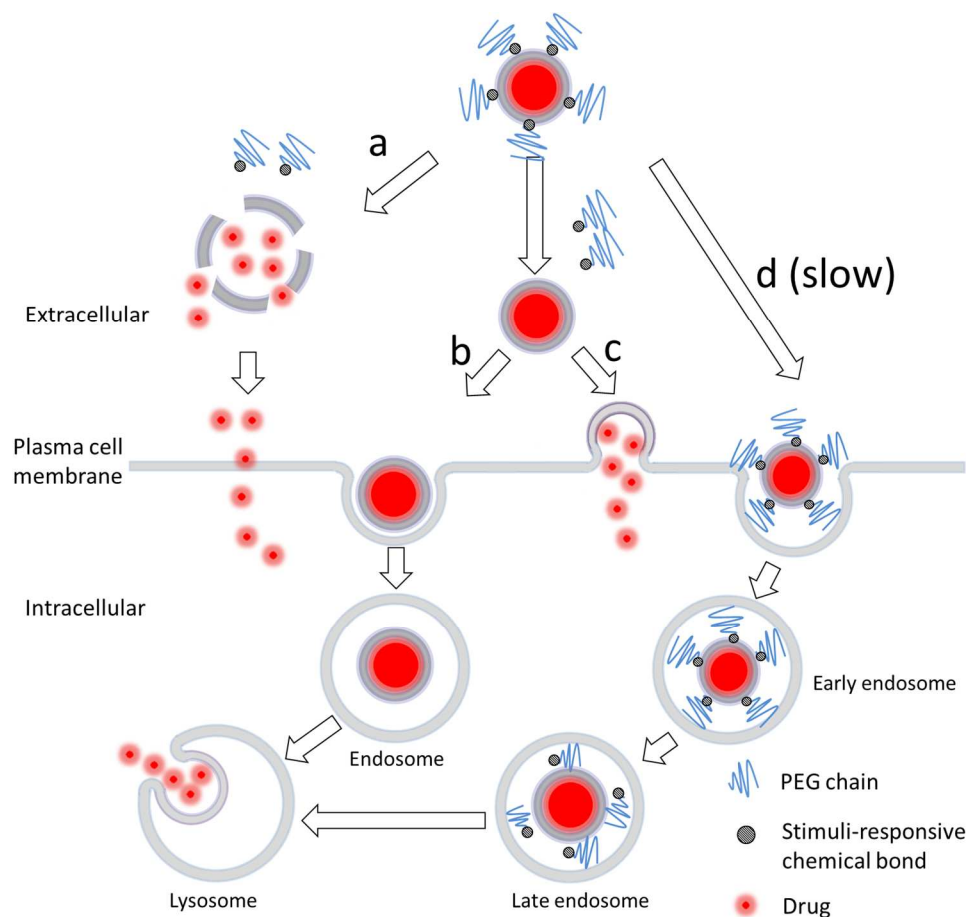


Figure 5. Schematic illustration of the various drug release outcomes following dePEGylation of a nanoparticle: (a) extracellular dePEGylation, nanoparticle rupture and extracellular drug release; (b) extracellular dePEGylation followed by endocytotic uptake and intracellular drug release; (c) extracellular dePEGylation followed by nanoparticle fusion with the plasma cell membrane and drug delivery direct to the cell cytosol; and (d) intracellular dePEGylation following endocytotic uptake of PEGylated nanoparticle and intracellular drug release.

1.2 Physical dePEGylation strategies

Two principal physical approaches to achieve dePEGylation of nanoparticle surfaces have been investigated. The first, most relevant for liposome DDS, relies on the

exchange of PEGylated lipids from a drug carrier (*e.g.* liposome) surface to a target membrane sink (*e.g.* target cancer cell membranes).^[30] Here, the rate at which exchange occurs is heavily dependent on the structure of the lipid anchoring PEG to the liposome membrane (*i.e.* how strongly it is embedded within the liposome membrane).^[31] In a study of three different lipid-PEG conjugates, no lipid-PEG exchange was observed for long chain, saturated lipid anchors (DSPE-PEG, C18:0) whereas exchange occurred in the time frame of hours for shorter saturated lipids (DMPE-PEG; C14:0) or long chain, unsaturated lipids (DOPE-PEG; C18:1).^[32] This time frame enabled efficient accumulation of liposomes in tumor sites *via* the EPR effect (prior to dePEGylation) coupled with increased cellular uptake within the tumor (following dePEGylation). Conversely, a similar study found that only in the case of DSPE-PEG where circulation times was improved to achieve efficient passive accumulation of nanoparticles within the tumor.^[33] These conflicting results highlight the fine balance required to achieve efficient accumulation and subsequent dePEGylation within the tumor microenvironment. The propensity for non-specific PEG exchange with biological membranes *in vivo*, prior to reaching the target tumor, has likely limited the widespread application of this approach.

The second physical approach relies on non-covalent adsorption of PEG onto a nanoparticle surface, for example, carboxylate-functionalized PEG adsorbed to a cationic nanoparticle surface.^[34] In this case, protonation of carboxylate groups within the acidic tumor microenvironment can be expected to lead to dePEGylation. While this approach is conceptually simple, the stability of the absorbed PEG corona in serum and the propensity of premature dePEGylation under physiological conditions (*e.g.* high salt) and/or through competition from other serum components has likewise limited the widespread investigation of this approach.

1.3 Chemical dePEGylation strategies

The most common method to dePEGylate nanoparticle surfaces is through chemical approaches. In these cases, PEG is connected to the nanoparticle *via* a stimuli-responsive covalent chemical bond.^[35] Stimuli can be both endogenous and exogenous. In the case of endogenous stimuli, intrinsic differences between pathological and healthy tissues are exploited, such as the lower pH and reducing

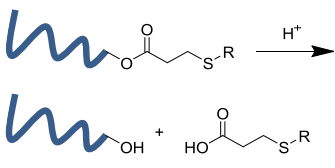
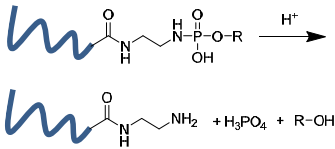
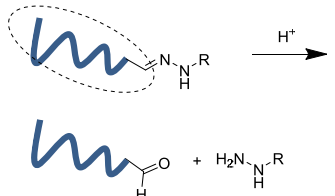
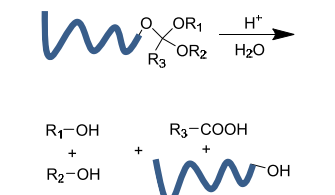
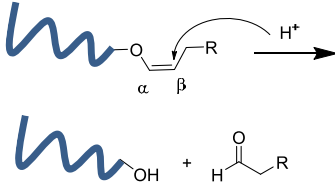
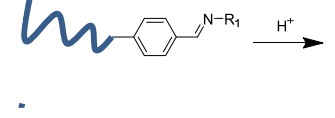
environments within the tumor microenvironment. Exogenous stimuli, including light and heat, have the benefit of being under complete user control in both time and space,^[36] however these approaches rely on the ability to accurately deliver external stimuli to tissues often deep within the body. In next section, stimuli-responsive chemical bonds commonly used in the dePEGylation of nanoparticles are highlighted.

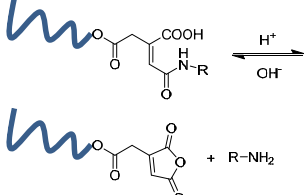
1.4 Stimuli-responsive bonds towards responsive dePEGylation

1.4.1 pH-sensitive dePEGylation

Both the acidic intracellular environment of endosomes (pH 5.0-6.5) and lysosomes (pH 4.5-5.0) and the mildly acidic (pH <7) extracellular environment within tumors have been exploited to trigger the release of PEG from nanoparticles. The most common pH-sensitive bonds used in these DDS are summarized in Table 1.

Table 1. pH sensitive bonds used in PEGylated DDS.

Name	Structure and hydrolysis process	Conjugated polymers	Features
β -thiopropionate		Oligodeoxynucleotide ^[37] or polymer ^[38]	Modify nucleotides; cleaved under endosomal acid conditions
Phosphoramidate		Oligodeoxynucleotide ^[39] or peptide ^[40]	Modify nucleotides; high yield and chemoselectivity
Hydrazone		Lipid ^[41] , drug ^[42] or polymer ^[43]	Controllable sensitivity, predictable pH-sensitivity
Ortho ester		Alkyl ^[44] , lipid ^[45] or polymer ^[46]	Controllable sensitivity, predictable pH-sensitivity
Vinylether		Lipid ^[47]	Controllable sensitivity, predictable pH-sensitivity
Imine bond		Lipid ^[48] , Alkyl ^[49] drug ^[50] or nanoparticles ^[51]	Extracellular dePEGylation, charge shielding

Aconitic anhydride amide		Doxorubicin ^[52]	Mild synthesis
--------------------------	---	-----------------------------	----------------

In several cases, it has been shown possible to fine tune the sensitivity of acid hydrolysis to achieve optimal dePEGylation either within the tumor microenvironment or within endosomes. Walker *et al.* linked polycations (PEI or PLL) to PEG *via* acyl hydrazides or 2-pyridyl hydrazines (compound **1**, **2** and **3**; Figure 6a) and found that while compound **1** and **3** resulted in efficient dePEGylation at endosomal pH (pH=5), hydrolysis of **2** was extremely slow.^[43a] Alternatively, it has been shown that the acid-catalyzed hydrolysis of pH-sensitive ortho esters is heavily affected by its substitution at positions R₁, R₂ and R₃ (Table 1), where methyl or 6-membrered cyclic esters increased the rate of acid catalyzed hydrolysis by at least an order of magnitude.^[45b] At pH 4.0, compound **4** could be completely hydrolyzed while only 30% of **5** was degraded within 30 min (Figure 6b).

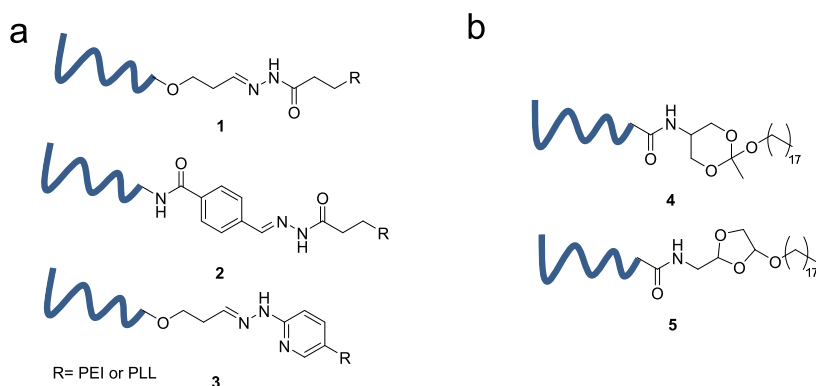


Figure 6. Substitutions of hydrazone (a) and ortho ester bond (b) fine-tune the pH-sensitivity.

1.4.2 Redox-sensitive dePEGylation

Glutathione (GSH), is an abundant reducing agent in most mammalian cells^[53] and has been exploited to trigger redox-sensitive dePEGylation of DDS (Figure 7a). The intracellular concentration of GSH can span the range 2–10 mM, three orders of magnitude greater than the extracellular concentration of GSH (2–20 μ M)^[54] (Figure

7a). Furthermore, the concentration of GSH within the tumor microenvironment is 4 times higher than in normal tissue. Reduced GSH can cleave disulfide (S-S) bonds linking PEG to a nanoparticle surface through a process of disulfide exchange (Figure 7b). PEG-disulfide conjugates can be synthesized through disulfide exchange or through the use of symmetrical/asymmetrical disulfide-containing crosslinkers (Table 2). A variety of symmetrical and asymmetrical disulfide containing crosslinking reagents, such as aldrithiol, cystamine, 2-hydroxyethyl disulfide, 3,3'-dithiodipropionic acid, DTSP and SPDP have been used to generate redox-sensitive PEGylated DDS (Table 2).

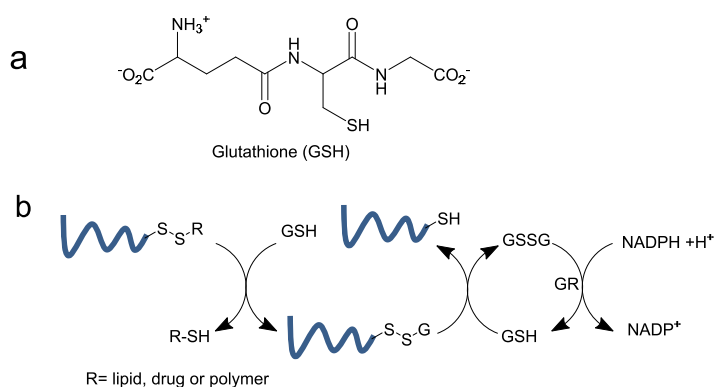
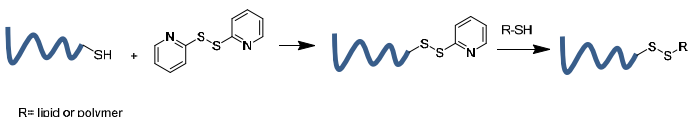
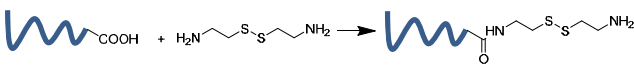
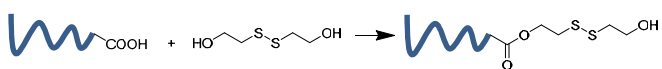
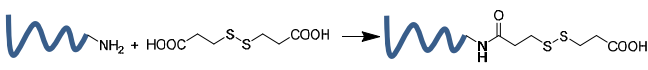
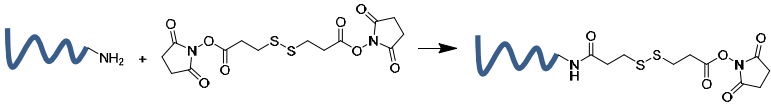
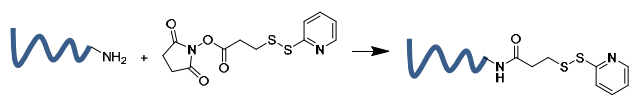


Figure 7. (a) The structure of GSH; (b) GSH mediated reduction of disulfide bonds.

Table 2. Methods and reagents for synthesizing PEGylated compounds containing disulfide bonds.

Crosslinker	Synthesis
Thiol-disulfide exchange	 <p>R= lipid or polymer</p> <p>Aldrithiol^[55]</p>
Symmetrical crosslinker	 <p>Cystamine^[56]</p>
	 <p>2-Hydroxyethyl disulfide^[57]</p>
	 <p>3,3'-dithiodipropionic acid^[58]</p>
	 <p>DTSP^[59]</p>
Asymmetrical crosslinker	 <p>SPDP^[60]</p>

The first example of a redox sensitive PEGylated nanoparticle incorporated mPEG₂₀₀₀-DTP-DSPE within a fusogenic liposome formulation, facilitating rapid and complete content release (Figure 8).^[59] Partial cleavage of grafted PEG from liposomes by thiolytic agents successfully led to destabilization of liposome bilayers and complete contents release within 2 h. However, this system required high concentrations of thiolated agents (10 mM, 1,4-dithiothreitol) limiting its application *in vivo*. To overcome this, a new generation of reductive cleavable PEG-lipid (mPEG-DTB-DSPE) has been shown to undergo complete thiolytic cleavage at greatly reduced thiol concentrations (cysteine, 150 μ M).^[61] Moreover, cleavage of

mPEG-DTB-DSPE liberated unmodified DSPE (*i.e.* leaving no remnant thiol attached) which was essential to the recovery of fusogenicity of the DDS (Figure 8).

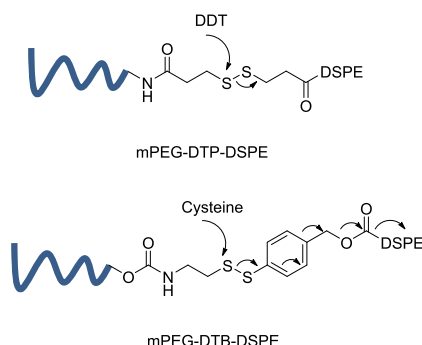


Figure 8. The structure of mPEG-DTP-DSPE and mPEG-DTB-DSPE and their thiolytic cleavage mechanisms.

1.4.3 Enzyme-sensitive dePEGylation

Within the tumor microenvironment, there are high levels of lytic enzymes. These are secreted by tumor cells to degrade the extracellular matrix (ECM) and aid cancer cell migration.^[62] Short peptides containing enzyme-consensus sequences can therefore be used to enzymatically cleave PEG from a nanoparticle surface (Table 3). Two principle proteases have been exploited, matrix metalloproteinases (MMPs) and cathepsin B.

MMPs play an essential role in tumor invasion and metastasis by degrading a variety of extracellular proteins and ECM components.^[63] MMPs, particularly MMP2 and MMP9, are highly expressed within, and secreted by, cancer cells. MMP-sensitive linkers have been employed to achieve tumor-specific and extracellular dePEGylation of various DDS including liposomes,^[64] nanoparticles^[65] and micelles.^[66]

Cathepsin B is an intracellular cysteine protease found abundantly in endosomes and lysosomes. It is highly up-regulated in cancer cells^[67] and cleaves peptides containing one of a variety of short recognition sequences. Cathepsin B-sensitive peptide linkers have been used to achieve endo/lysosomal dePEGylation, however the slow cellular uptake of PEGylated nanoparticles has limited the widespread application of cathepsin B-sensitive linkers.

Table 3. MMP2 and cathepsin B peptide recognition sequences (↓ represents position of enzymatic cleavage)

Enzyme	Peptide Sequences	Cleavage Site
MMP2-sensitive peptides ^[64-66, 68]	GPLG ↓ IAGQ; GGGPQG ↓ IWGQGK; GPL ↓ GIAG; GPL ↓ GV; PLG ↓ LAG	Extracellular
Cat B-sensitive peptides ^[69]	A↓A; A↓L; F↓R; F↓K; AF↓K; GL↓FG; GF↓LG	Intracellular

1.4.4 Light-sensitive bonds

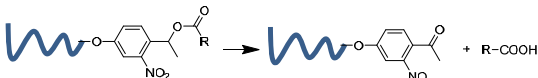
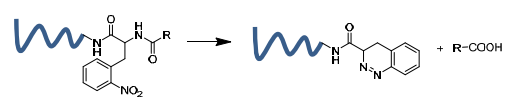
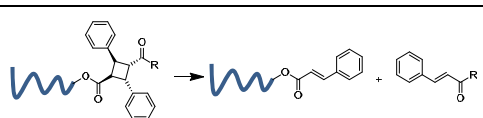
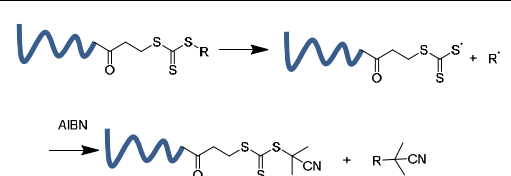
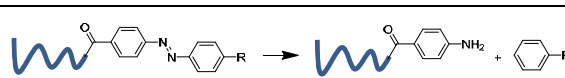
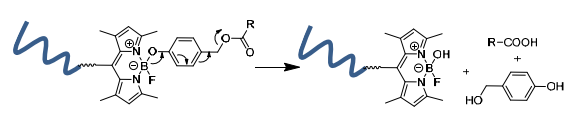
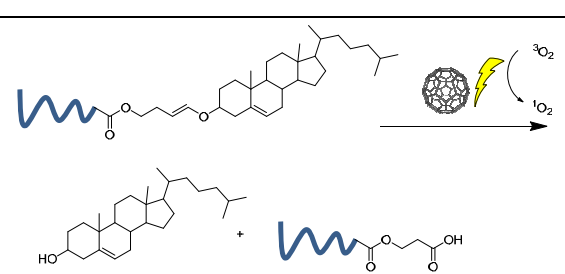
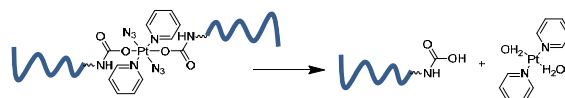
Photolabile chemical bonds have been widely used in both chemistry and biology to precisely control where and when new functionality is revealed.^[70] Unlike endogenous stimuli, such as pH, redox and enzymatic cleavage, the application of light can be precisely controlled in both time, space and intensity (*i.e.* is user defined) and requires no other reactive species (other than, in some cases, water). Light-based therapies have already entered the clinic. For example, photodynamic therapy^[71] combines chemical photosensitizers and light to trigger the local production of cytotoxic singlet oxygen in the body and is used in the clinic to treat a wide range of medical conditions, including acne, atherosclerosis and cancer.^[72]

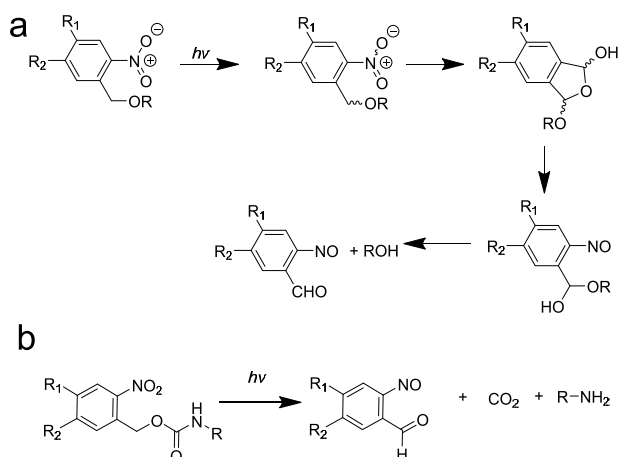
Various photolabile bonds used to dePEGylated nanoparticle surfaces are summarized in Table 4. The vast majority of these are sensitive to high-energy UV light (<400 nm), wavelengths that not only demonstrate poor tissue penetration (100-200 µm) but also yields significant light-induced cytotoxicity.^[73] Therefore several strategies have been developed to alleviate these issues. These include the use of fibre optic light sources to deliver UV light deep within tissue,^[74] the development of photolabile chemical bonds sensitive to longer wavelength light^[75] and increasing the efficiency of photolysis so as to minimize light exposure. One attractive option is to improve the sensitivity of photolabile bonds to two photon light.^[76] Two-photon excitation requires two light sources perpendicular to one another, each delivering photons at twice the wavelength required (*e.g.* 365 nm vs 2 x 730 nm light) for photolysis. Only at the exact point of intersection is enough energy delivered to cleave the photolabile

bond. The use of longer wavelength light not only increases tissue penetration (>1 cm for near-IR light) and reduces the risk of light induced cytotoxicity but, by restricting light activation to the focal point of two photon beams, it provides exquisite spatial control over light activation. We and others have previously shown that *o*-nitrobenzyl groups, the most commonly used photolabile chemical bond, can be efficiently cleaved using 2-photon light.^[77]

The work in this thesis primarily concerns the use of the *o*-nitrobenzyl (*o*-Nb) photolabile functionality. Non-hydrolytic photolysis of *o*-Nb proceeds through a cyclic intermediate followed by the release of the desired alcohol and a nitroso by-product (Scheme 1a).^[78] *O*-Nb groups can also be used to 'photocage' primary amines, through the inclusion of a carbamate linker, producing CO₂ as a photolytic by-product (Scheme 1b). To broaden application in biological areas, modifications, such as substituting R₁ with methoxy groups, have been included to reduce the toxicity of the nitroso photolysis byproduct.

Table 4. Common light-cleavable bonds used in PEGylated DDS.

Photo-responsive group	Active wavelength	Photo-irradiated dePEGylation
Nitrobenzyl ester ^[38, 79]	300-400 nm	
2-nitrophenylalanine ^[80]	365 nm	
Truxillic acid ^[81]	< 260 nm	
Trithiocarbonate ^[82]	232-500 nm	
azobenzene ^[83]	280–450 nm	
Boron dipyrromethene ^[84]	470-490 nm	
Fullerene ^[85]	350–700 nm	
Platinum (IV)–azide complexes ^[86]	360-500 nm	



Scheme 1. The mechanism of cleavage of *o*-Nb substituted with ester (a) and carbamate (b).

1.5 DePEGylation of various drug carriers

1.5.1 Liposomes

Liposomes are formed through the self-assembly of amphiphilic (phospho)lipids in aqueous solution, forming closed spherical particles consisting of a lipid bilayer surrounding an inner aqueous core.^[87] Within these structures, hydrophilic cargos/drugs can be encapsulated within the aqueous interior and hydrophobic cargos/drugs within the hydrophobic membrane. In both cases, cargos are protected from the outside environment. Self-assembly of liposomes is driven by the burial of hydrophobic fatty acid chains ('the hydrophobic effect') and each individual liposome comprises many thousands of individual lipid molecules (approximately 80,000 per 100 nm uni-lamellar liposome). The huge diversity of lipid reagents – both natural and non-natural – means the overall physicochemical properties of the liposome (size, surface charge, rigidity, surface functionalization) can be infinitely fine-tuned for a particular purpose. A selection of common lipids described and/or used throughout this thesis is shown in Table 5.

Table 5. the structure of lipids used in this thesis.

Name	Structure	Charge
(d18:1/12:0) Sphingomyelin		Zwitterionic
18:0 PC (DSPC)		
18:1 (Δ9-Cis) PE (DOPE)		
18:1 (Δ9-Cis) PC (DOPC)		
Cholesterol		Neutral
18:1 TAP (DOTAP)		Cationic
18:1 (Δ9-Cis) PG (DOPG)		Anionic

1.5.1(a) Lipid geometries

Lipid packing within a liposome membrane is heavily influenced by the molecular geometries of individual lipid molecules. Based on the difference between the surface area of the hydrophilic head group and the volume of the hydrophobic fatty acid tail, amphiphilic lipids can be divided into three distinct molecular geometries: cylinder, cone and inverted-cone (Figure 9). The principle lipid components of biological membranes (and those most commonly found in reported liposome membranes) are cylinder shaped. Cylindrical lipids, with equal cross-sectional areas of both hydrophilic

head group and hydrophobic fatty acid tails, pack favorably to form lipid bilayers. Examples include phosphatidyl choline (PC), serine (PS) and glycerol (PG). Lipids such as sphingomyelin (SM), with a larger hydrophilic headgroup and a smaller hydrophobic volume, preferentially form micellar structures.^[88] These smaller self-assembled structures (typically 10-20 nm in diameter) are characterized by a packed hydrophobic core and have no inner aqueous volume. Finally, inverted cone lipids, such as DOPE, do not form stable self-assembled structures in aqueous solution. These lipids preferentially pack into membranes demonstrating negative curvature and form inverted micelles in organic solutions. Although lipid membranes with negative curvature are rare, a key intermediate structure during the fusion of two lipid membranes (*e.g.* during SNARE-mediated fusion) requires lipids which favor negative curvature.^[89]

Liposome membranes can comprise mixtures of different lipids and lipid geometries, so while it is not possible to make stable lipid bilayers using 100% DOPE, this lipid can be efficiently incorporated in stable lipid bilayers formed from cylinder-shaped lipids (*eg.* PC lipids). In all cases, the key driving force determining self-assembly, stability and structure of lipid mixtures in aqueous solution is the efficient burial of the hydrophobic core so as to minimize exposure to water.

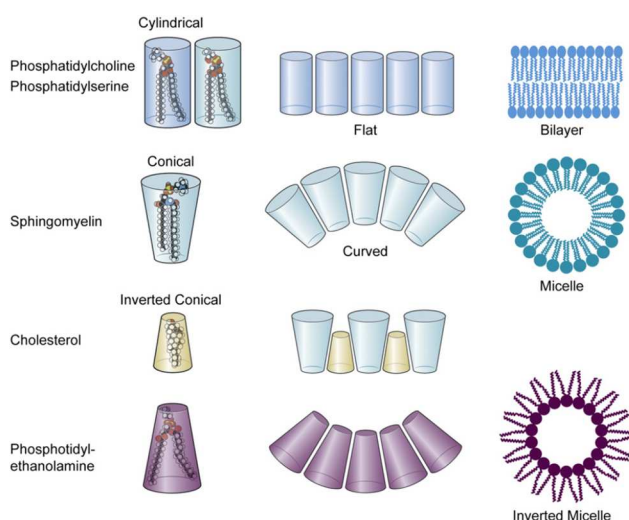


Figure 9. Schematic diagram depicting molecular shape-volumes occupied by various membrane lipid types. Image taken from^[88].

1.5.1(b) Membrane rigidity and thickness

The length and saturation of lipid fatty acid (FA) chains determines both the thickness and rigidity of a liposome membrane. FA chain length within biological membranes typically varies between C12 and C30 – the number of carbon atoms – where a membrane made up of C30 lipids is approximately twice as thick one made up of C12 lipids. A mismatch of different FA chain lengths within a single membrane can lead to phase separation – where FAs of one particular length preferentially assemble together with one another. This can create specific lipid domains within a single continuous lipid membrane.^[90]

FA chains can also be saturated (no double bonds) or unsaturated (1 or more double bond). In general, saturated FAs pack closely together to form rigid lipid membranes. In contrast, unsaturated FAs – with a bend in their FA chains as a result of the double bond – loosely pack to form fluid membranes.^[91] These differences are characterized by variations in melting temperatures (T_m), defined as the temperature at which a lipid membrane transitions between the ‘rigid’ gel state and the ‘fluid’ liquid crystalline state.^[92] Whereas the T_m of DSPC – a saturated C18:0 PC lipid – is 55°C, its unsaturated orthologue, DOPC has a T_m of -17°C. The ‘fluidity’ of liposome membranes is an important consideration in designing liposomal drug carriers as small molecules will more readily leak across fluid membranes than more closely packed ones.

1.5.1(c) Addition of cholesterol

Cholesterol – an endogenous and ubiquitous sterol within the body – rigidifies ‘fluid’ lipid membranes and makes more fluid ‘rigid’ lipid membranes.^[93] As such it is helpful to think of cholesterol as a molecular ‘cork’ – plugging the ‘gaps’ to stabilize fluid lipid membranes and acting as a ‘wedge’ to destabilize rigid membranes. Cholesterol is often used to fine tune drug retention and release profiles of liposome-drug vectors.^[94]

1.5.1(d) Liposome surface functionalization

Surface modification of liposome surfaces, for instance functionalization with active targeting moieties including antibodies and peptides,^[88] can be achieved either

through incorporation of pre-synthesized lipidated reagents during formulation or through post-functionalization of pre-formed liposomes. Various conjugation strategies (e.g. click chemistry) have been used to successfully functionalize pre-formed liposomes.^[95] As mentioned previously, PEGylation of liposome surfaces is known to reduce serum protein adsorption to the liposome surface, prolong circulation lifetimes in the body and maximize passive targeting of solid tumors via the EPR effect.^[96] In the case of PEG₂₀₀₀, approximately 5 mol% lipid-PEG reagents are required to sterically shield the entire liposome surface. Above 9 mol% PEG₂₀₀₀ and the brush-like arrangement of PEG on the liposome surface is thought to destabilize the lipid bilayer.^[24a]

1.5.1.1 DePEGylation of liposome surfaces to reveal new functionalities

Through dePEGylation it is possible to reveal underlying functionality to promote drug delivery to target cells. Shielding functionality *en route* to the target tumor also reduces the risk of off-target interactions with non-target cells. In this vein, several strategies have been investigated and three of them are highlighted in Figure 10.^[60f, 97]

In the first example, a liposome surface was functionalized with two different PEG-lipid conjugates whose PEG chains varied in length (PEG₂₀₀₀ and PEG₁₀₀₀) (Figure 10a).^[68c] To the longer PEG₂₀₀₀ arm a monoclonal antibody, (mAb) 2C5, previously shown to specifically target a range of human cancer cell lines, was conjugated.^[98] To the shorter PEG₁₀₀₀ arm the cell-penetrating TAT peptide was attached.^[99] In the absence of MMP enzymes, the longer PEG₂₀₀₀ effectively shielded the underlying function of the TAT peptide, preventing non-specific cellular interactions, while the 2C5 promoted specific binding to cancer cells. In the presence of MMP enzymes – *i.e.* within the tumor microenvironment – PEG₂₀₀₀ was efficiently cleaved, revealing underlying TAT functionality which enhanced the intracellular uptake of the liposome-drug carrier two-fold as compared to liposomes lacking the TAT peptide.

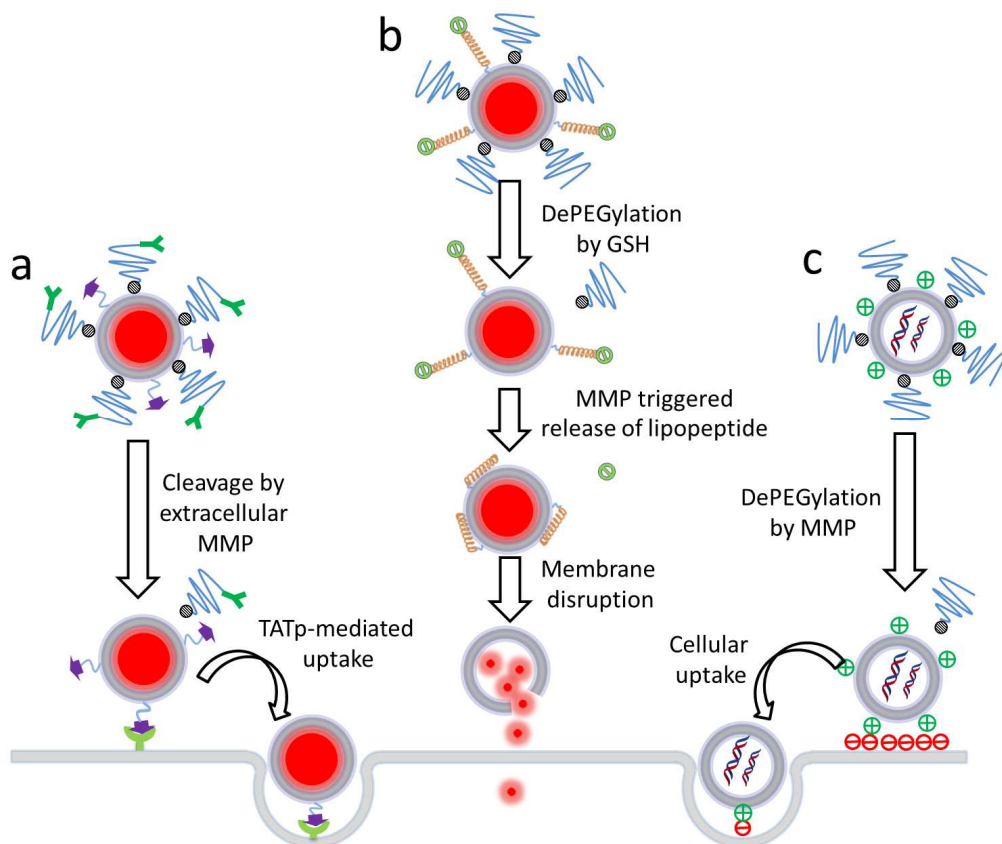


Figure 10. Illustration of PEGylation strategies on different types of liposomes, (A) PEGylated targeted liposomes, (B) PEGylated liposomes with membrane destabilizing peptides, (C) PEGylated cationic liposomes.

A similar dual responsive strategy was employed to promote extracellular drug release within the tumor microenvironment (Figure 10b). In this case, dePEGylation of longer PEG₂₀₀₀ arms was triggered by an increase of extracellular GSH within the tumor microenvironment.^[100] This in turn revealed underlying functionality, which when catalyzed by MMP, released a membrane lytic peptide. In this way, quantitative drug (*i.e.* gemcitabine) release in both 2D and 3D “tumor-like” spheroid cultures as well as suppressed tumor growth in mice following intravenous administration of gemcitabine-encapsulated liposomes was demonstrated. As drug release required exposure to both reductant and protease enzymes, this approach greatly minimized the risk of premature activation and drug release.

DePEGylation has also been successfully used to reveal underlying liposome surface charge (Figure 10c). Cationic liposomes are often employed as a gene delivery system owing to their potential to efficiently condense and protect polyanionic DNA and RNA.^[101] However, cationic nanoparticles are rapidly cleared from circulation due to both non-specific interactions with anionic cell surfaces and extensive adsorption of serum components (opsonisation) and clearance *via* the MPS.^[101] Both extracellular enzymatic^[29] and intracellular^[52] acid catalyzed dePEGylation strategies have been shown to increase the transfection/transduction efficiencies of cationic gene vectors.

1.5.1.2 DePEGylation of liposome surfaces to destabilize liposome membranes

DePEGylation of liposomes has also been used to destabilize the integrity of the liposome membrane itself to trigger drug release. In these cases, dePEGylation results in a change of lipid geometry (*i.e.* loss of large hydrophilic PEG headgroup) generating a lipid composition which no longer packs to form a stable lipid bilayer. By utilizing a cholesteryl hemisuccinate (CHEMS)-PEG conjugate, Dong *et al.* were able to successfully demonstrate dePEGylation – triggered by enzymatic cleavage of the CHEMS-PEG ester linkage – following endocytotic uptake. Subsequent protonation of the newly revealed CHEMS carboxylate groups, within the acidic endosome, resulted in rapid liposome rupture and content release.^[102] This approach did however rely on the cellular uptake of PEGylated liposomes, which as mentioned previously, is extremely slow.^[103]

Another popular strategy has been to take advantage of the ‘fusogenic’ lipid, DOPE, which preferentially adopts a non-bilayer, hexagonal phase (H_{II}) in aqueous solution.^[104] Cone-shaped DOPE can be incorporated at high concentrations within stable lipid bilayers consisting of cylinder and/or cone shaped lipids. If DOPE-rich bilayers are stabilized using a stimuli-responsive lipid-PEG conjugate, dePEGylation results in rapid membrane destabilization and concomitant content release (Figure 11).^[47a]

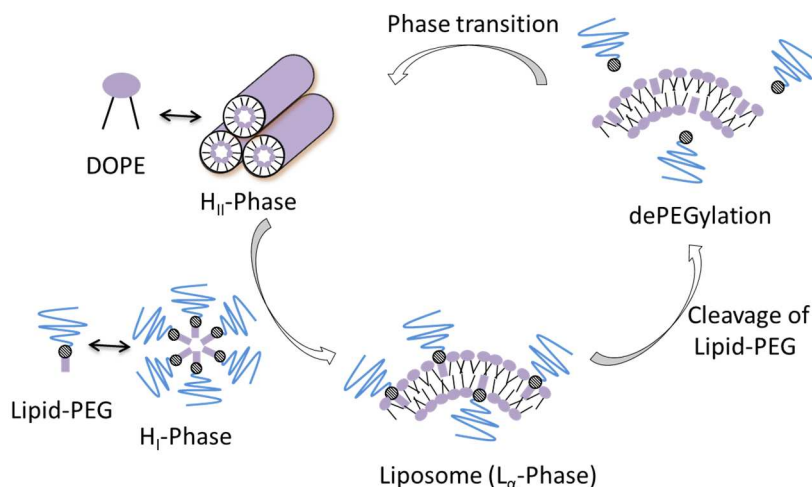


Figure 11. Destabilization of liposomes formed by DOPE and cleavable PEG–lipid upon dePEGylation. Image taken from^[39a].

Zalipsky *et al.* reported the first example of a DOPE-rich liposome membrane stabilized using cone-shaped and redox-sensitive lipid-PEG₂₀₀₀ (mPEG-SS-DSPE) conjugates.^[59] Incorporation of just 3 mol% lipid-PEG conjugate (*i.e.* 97 mol% DOPE) resulted in the formulation of stable liposomes, however in the presence of DTT – a thiolytic agent – loss of PEG led to rapid liposome destabilization and drug release. Inspired by this concept, numerous efforts have been made to design stimuli-responsive PEG-lipids to stabilize DOPE-rich liposomes. These have included dithiobenzyl (DTB) urethane,^[61] diortho ester^[45a] and vinyl ether^[47b] lipid-PEG linkages.

1.5.2 Micelles

Micelles are formed through the self-assembly of cone-shaped amphiphiles in aqueous solution and are characterized by an inner hydrophobic core. Hydrophobic cargos/drugs can be efficiently packed within the micelle core and protected from the outside environment. Micelles have been widely investigated as potential DDS against a variety of human diseases including leukemia^[105], hepatitis^[106], breast cancer^[107] and ovarian cancer.^[108] An important consideration when using micelles is that the concentration of amphiphiles must be above the critical micelle concentration (CMC). Below this concentration, micelles disassemble in solution and as a result the drug/cargo is exposed.

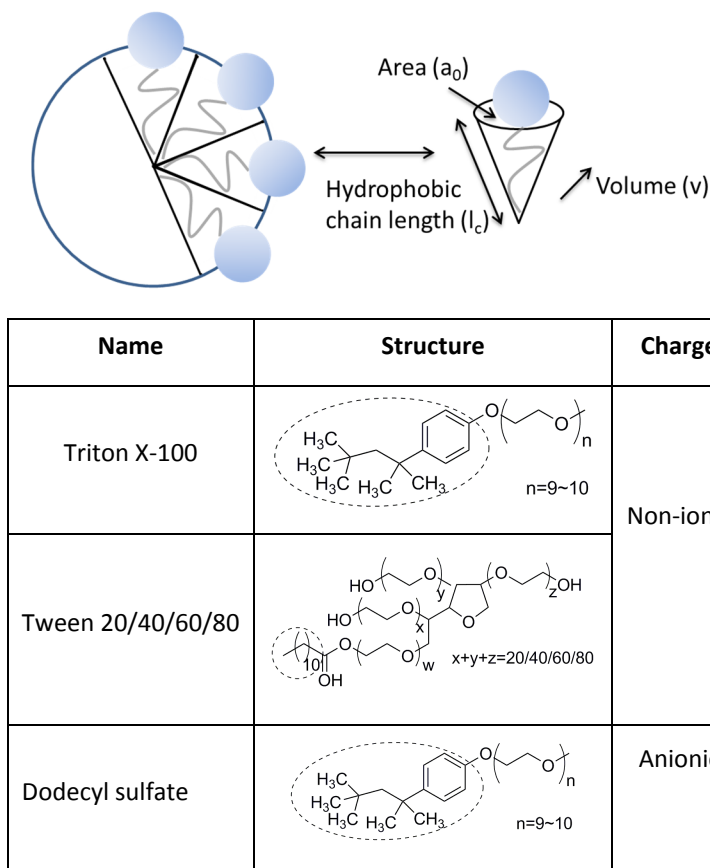


Figure 12. The required geometry of molecules for micelle formation (top) and the structure of some common micelle-forming detergents (bottom); the dash line circled part is hydrophobic component.

To preferentially form micelles over other self-assembled structures, the surface area (a_o) of the hydrophilic head group must be sufficiently large, while the volume (v) of hydrophobic portion must be sufficiently small. Micelles are only formed when the geometric constraint, critical packing parameter ($P = v/a_o l_c$), of the molecules is $< 1/3$. (Figure 12).^[109] Detergents like sodium dodecyl sulfate (SDS) are classic examples of lipid amphiphiles which preferentially form micelles in aqueous solutions.

PEGylated amphiphiles have a natural propensity to form micelles given the large surface area of the hydrophilic PEG headgroup. Upon dePEGylation however, cone-shaped molecular geometries are lost resulting in micelle destabilization. This leads to efficient drug release from the hydrophobic micelle core. Depending on the

hydrophobic component, micelle DDS can be divided into lipid micelles, polymeric micelles, pro-drug micelles and hybrid micelles.

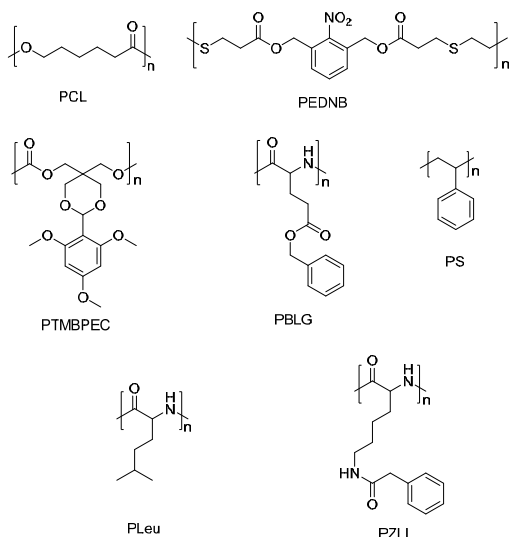
1.5.2.1 Lipid micelles

The most common lipid anchors used to form lipid-PEG amphiphiles have been DSPE^[110], cholesterol^[111] and fatty acids.^[57d] Depending on the hydrophobicity of lipids, the molecular weight of the PEG block ranging from 750 to 5000 Da with the resultant micelle size ranging from tens to hundreds of nanometers have been used. To achieve stimuli responsive drug release, cleavable linkers are often incorporated between the PEG chain and lipid.^[112] After accumulation at the site of a tumor, the dePEGylated micelles are internalized into endosomes/lysosomes, resulting in release of the drugs intracellularly.

1.5.2.2 Polymeric micelles

To obtain polymer-PEG micelles, hydrophobic and biocompatible/biodegradable polymers are required to form a stable hydrophobic micellar core. The most common synthetic polymers used in polymeric micelle designs are shown in Scheme 2.^[57a] Stimuli responsive PEGylated polymeric micelles have been developed to be sensitive to both endogenous (*e.g.* redox^[57a], pH^[38, 79e]) and exogenous (*e.g.* light^[38]) triggers.

Polypeptides, composed of natural and/or non-natural amino acids have also been widely used to form the hydrophobic core of PEGylated, polymeric micelle DDS. In one example, a redox-sensitive co-polymer composed of PEG and poly-L-leucine (PEG-SS-pLeu) was used to control the release of doxorubicin (DOX) under reducing conditions.^[56b] The fully biocompatible system demonstrated no toxicity to cancer cells *in vitro* prior to dePEGylation but rapid and quantitative drug release in the reductive environment of endosomes.



Scheme 2. Overview of polymer blocks conjugated to PEG used polymeric micelles.

1.5.2.3 Polyion complex (PIC) micelles

As a sub-group of polymeric micelles, PIC micelles have been investigated as potential non-viral gene vectors. These copolymer systems comprise a hydrophilic/ionic polymer conjugated to PEG, which upon complexation with oppositely charged cargos (e.g. DNA, RNA or protein) form micellar structures with a charge neutralized hydrophobic core (Figure 13a).^[113] Depending on the associated charge of the complexed cargo, the hydrophilic/ionic polymer can be both polyanionic or polycationic. Common charged polymers used in PIC systems include poly (L-lysine) (PLL),^[43a, 56f] poly (L-aspartate)(pAsp),^[114] polyethylenimine (PEI)^[60g, 68d] and poly(2-(dimethyl-amino)ethylmethacrylate) (PDMAEMA).^[46a]

To extend the function of PIC micelles to the delivery of both hydrophilic and charged cargos as well as small molecule hydrophobic drugs, Torchilin and coworkers incorporated an additional hydrophobic DOPE core to a PEI-PEG polymer construct. In this way, the authors were able to efficiently encapsulate hydrophobic paclitaxel within the DOPE core and simultaneously condense siRNA as a complex with PEI to form a dual therapy (Figure 13b).^[68d]

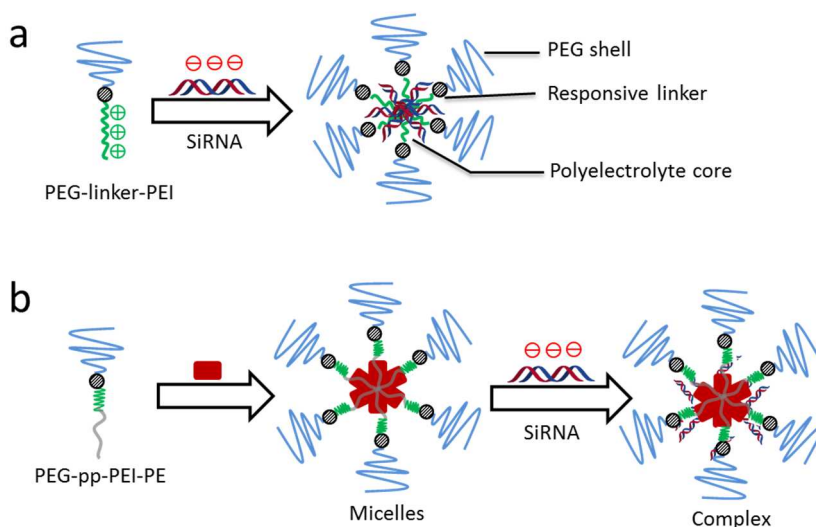


Figure 13. (a) Schematic illustration of PIC micelles formed by PEGylated cationic polymers with anionic biotherapeutics (*e.g.* siRNA). (b) Illustration of PIC micelles as carriers to co-deliver hydrophobic drugs.

1.5.2.4 Prodrug micelles

The principle limitations of polymeric and lipid micelle DDS are poor drug loading efficiencies and premature drug leakage from the micelle core. To address these issues, efforts have been made to develop prodrug micelle DDS in which the therapeutic drugs themselves are used to form the hydrophobic core of the micelle (Figure 14a).^[115] The principle advantages of these systems are higher drug encapsulation efficiencies (w/w) and, as drugs are now covalently linked to the PEG corona, no premature drug leakage. A key disadvantage of these systems is sub-optimal packing of the hydrophobic micelle, resulting in decreased micelles stability.

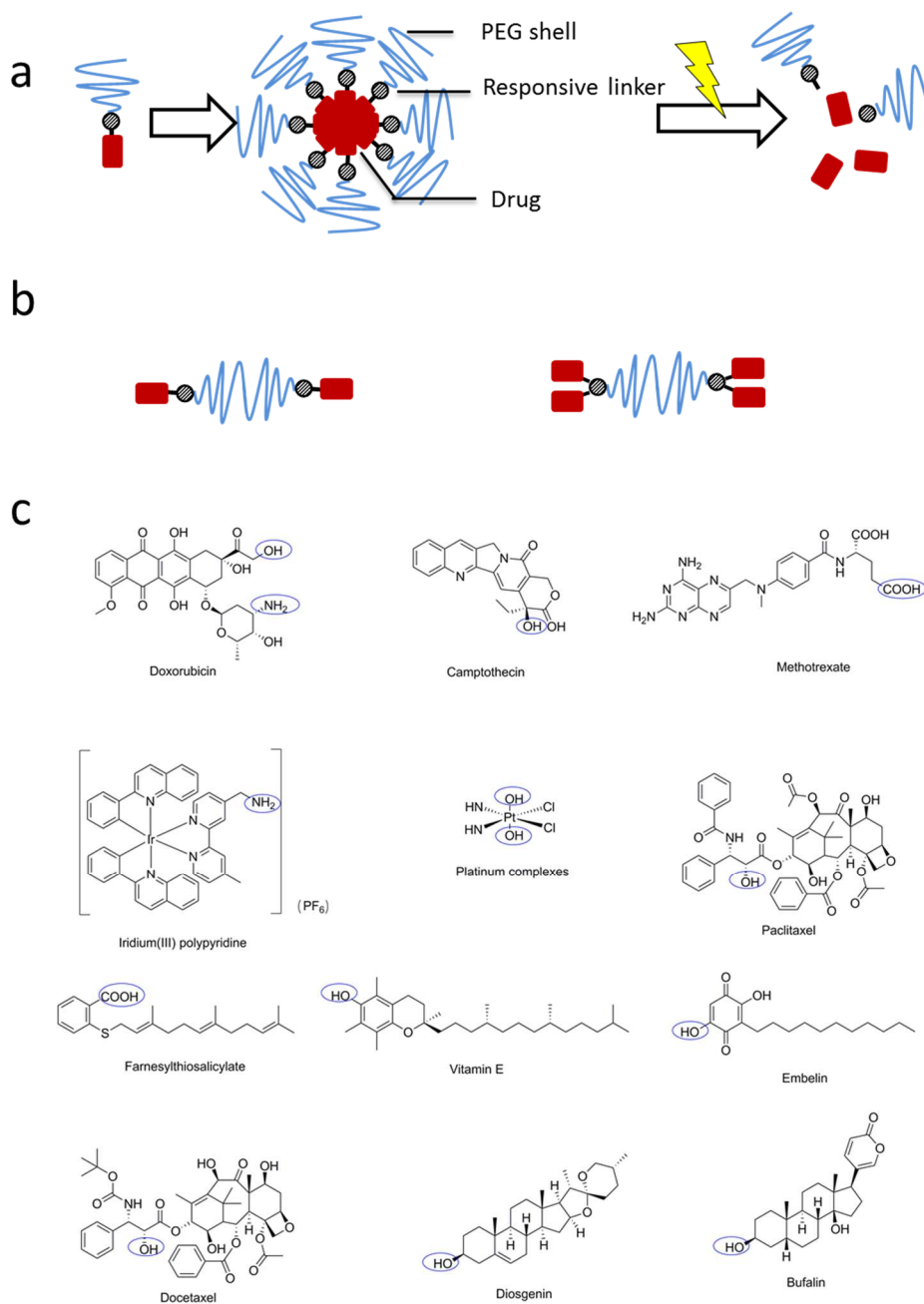


Figure 14. (a) Schematic illustration of micelles formed by PEGylated prodrugs; (b) two tailed prodrugs (c) The structure of anticancer drugs used in stimuli-sensitive PEGylated prodrugs (reactive groups in circles).

A variety of anticancer drugs have been used to construct PEGylated prodrug micelles. These include doxorubicin,^[52a, 116] camptothecin,^[117] methotrexate,^[118] metallic antitumor agents,^[86] bufalin,^[119] vitamin E,^[60h, 120] diosgenin,^[121] paclitaxel,^[122] embelin,^[123] docetaxel^[124] and farnesylthiosalicylic acid (FTS) (Figure 14c).^[125]

To overcome the principle limitation of these systems – namely, low micelle stability due to a high CMC, efforts have been made to stabilize the hydrophobic core using higher drug/PEG ratio (Figure 14b). Wang *et al* investigated the correlation between DOX loading efficiency and PEG chain length (PEG₂₀₀₀, PEG₄₀₀₀ and PEG₆₀₀₀), onto which two DOX molecules were connected to each individual PEG chain through an acid-sensitive linkage.^[126] They achieved up to 37% (w/w) DOX encapsulation (using PEG₂₀₀₀), significantly higher than conventional drug loading method using polymeric micelles, and with greater micelle stability. In another report, Dong *et al* used a branched system to couple up to 8 methotrexate molecules to a single PEG polymer. This resulted in drug-rich pro-drug micelles (26% w/w) with improved *in vivo* stability.^[56m]

1.5.2.6 Hybrid micelles

In many cases, micelles formed from the self-assembly of a single amphiphile building block do not fulfill the optimal requirements of an efficient micellar DDS. For instance, DOX-PEG prodrug micelles typically demonstrate high CMCs (*i.e.* low stability) owing to suboptimal packing of doxorubicin within the hydrophobic core of the micelle. Co-formulation and self-assembly of additional amphiphilic components, to form hybrid micelles, is a common strategy to improve micelle performance of a micellar DDS but also a simple way of adding additional functionality to an existing design.^[127]

An elegant example of a multifunctional, hybrid micelle DDS combined a PEG₂₀₀₀-paclitaxel conjugate, containing an MMP sensitive linkage (PEG₂₀₀₀-MMP-PTX), together with cell penetrating peptide-PEG₁₀₀₀-phosphoethanolamine (TATp-PEG₁₀₀₀-DOPE) and PEG₁₀₀₀-phosphoethanolamine (PEG₁₀₀₀-DOPE) lipid amphiphiles in the ratio of 5:4:1 (mol/mol/mol).^[66] Compared to micelles formed from PEG₂₀₀₀-paclitaxel alone, these micelles were an order of magnitude more stable (3.9 μ M vs 32 μ M). In this system, the longer PEG₂₀₀₀ effectively shielded the

underlying TAT peptide function and extended circulation lifetimes *in vivo* following systemic administration. Once accumulated within the tumor microenvironment, MMP-mediated enzymatic cleavage of the PEG₂₀₀₀ corona revealed the underlying cell penetrating TAT-peptide, driving the efficient internalisation and intracellular drug delivery. Importantly, upon the loss of PEG₂₀₀₀, micelles remained intact, stabilized by the remaining lipid-PEG₁₀₀₀-TAT construct and containing paclitaxel within the hydrophobic core. This served to minimize extracellular release of paclitaxel within the tumor microenvironment. Adding further flexibility to the design of this system, Zhu *et al.* were able to successfully entrap free paclitaxel within the hydrophobic core of a PEG₂₀₀₀-MMP-DOPE/ TATp-PEG₁₀₀₀-DOPE hybrid micelle (Figure 15).^[128] With no additional chemical modification to existing hydrophobic drugs required in this case, this system demonstrates the broad potential of such a hybrid micelle system in delivering diverse therapeutic cargos.

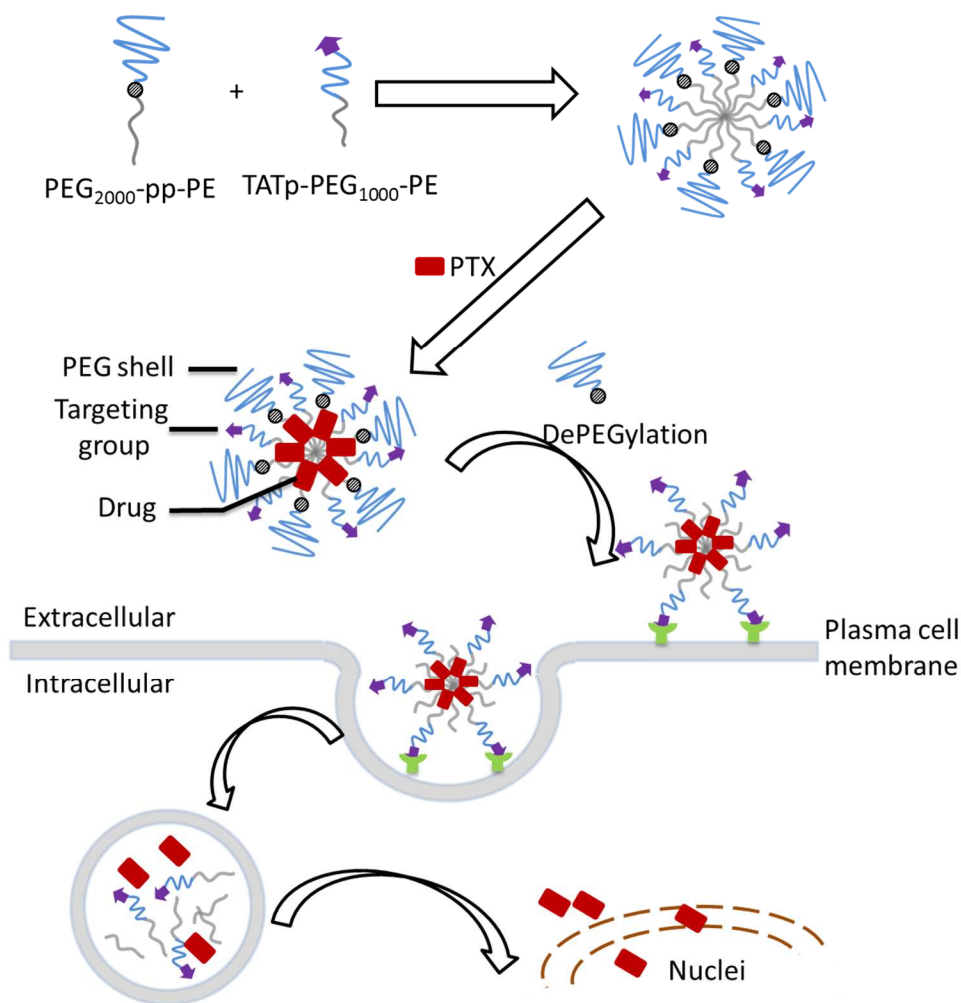


Figure 15. Illustration of hybrid micelles made of PEG₂₀₀₀-Pp-PE and TATp-PEG₁₀₀₀-PE to deliver free drugs.

1.5.3 Polymersomes

Polymersomes are artificial vesicles comprised of a polymer membrane surrounding an inner aqueous core.^[129] Analogous to liposomes, it is possible to load hydrophilic drugs/cargos within the inner aqueous core and hydrophobic drugs within the polymersome membrane interior.^[130] Common polymersome DDS are self-assembled nanostructures composed of linear diblock copolymer amphiphiles (hydrophilic-hydrophobic) or tri-block polymer bola-amphiphiles (hydrophilic-hydrophobic-hydrophilic). Typically, polymersomes are more stable than liposomes in aqueous solution, as reflected in their lower critical aggregation

concentrations (CAC).^[131] Although many polymers (*e.g.* polyesters) are hydrolytically sensitive and degrade over time within the body, the rate of hydrolysis and polymersome destabilization, even under acid-catalyzed conditions (*e.g.* within endosomes), is generally too slow to result in the release of therapeutically relevant drug doses.

DePEGylation of polymersomes has been used as an effective method to rapidly destabilize polymersomes and promote drug release. In these systems, PEG is used as the hydrophilic block of a di- or tri-block polymer and is therefore an integral to polymersome self-assembly. Release of PEG (*i.e.* the hydrophilic block) leads to polymersome destabilization and concomitant drug release occurs. In one of the first examples of polymersome dePEGylation, Hubbell *et al.* were able to demonstrate efficient endosomal drug release from polymersomes composed of redox-sensitive PEG-S-S-poly(propylene sulfide) di-block copolymers.^[132] In this case, polymersome cellular uptake, disruption and quantitative drug release occurred within 10 minutes of incubation with cells *in vitro*. Since then, many reductive PEG copolymers have been designed and applied as building blocks to construct redox-sensitive polymersomes.^[55b, 56f, 57c, 133] Moreover, photo-degradable polymersomes could also be constructed by co-polymers with photo-cleavable moiety, such as PEG-*o*-NB-PCL.^[80] In this kind of polymersomes, under a short UV exposure, content release was accompanied with partially-cleaved PEG and the rearrangement of PCL segments. However, the remaining PEG-PCL still stabilizes the vesicular structure. Only after full cleavage of PEG-PCL, collapse of polymersomes was observed.

1.6 Overview and goals of this thesis

From this review of current technologies, it is clear stimuli-responsive dePEGylation of nanoparticle-based DDS is an effective strategy to potentially enhance therapeutic efficacy. However, no such systems have yet made it to market. For this to happen, a clear cost-to-benefit advantage, over, for example, administering the free drug alone, must be demonstrated. This will only be realized if DDS systems are either simplified (to bring down development and manufacturing costs) and/or efficacy is improved.

The work in this thesis focuses on overcoming various technological inefficiencies associated with current stimuli-responsive nanoparticles. These include: enabling drug delivery directly to the cell cytosol (**chapter 2**), optimizing physicochemical properties and drug retention/release profiles of pro-drug micelles (**chapter 3 and 4**) and exploiting the differing *in vivo* fates of nanoparticles with opposing surface charges (**chapter 5**). In all cases, activation is triggered by light, affording precise spatiotemporal control over where and when dePEGylation/activation occurs.

In **chapter 2**, spatiotemporal control of membrane fusion system is reported through photolabile PEGylation of fusogenic liposomes. In this system, fusion relies on the recognition and binding of complementary peptides displayed on opposing liposome surfaces. Peptide recognition can be efficiently inhibited through liposome surface PEGylation. Light triggered fusion was demonstrated in both liposome-liposome systems and between liposomes and cells. This system paves the way towards controlled drug delivery direct to the cytosol of cells thereby avoiding endocytosis.

In **chapters 3 and 4**, two PEGylated prodrugs, PEG₂₀₀₀-*o*-nitrobenzyl-doxorubicin (**chapter 3**) and PEG₂₀₀₀-*o*-nitrobenzyl-nervonic acid (**chapter 4**) are described. Both conjugates self-assembled into micelles in aqueous solution with the PEG layer as the outer corona. In **chapter 3**, the release behavior of conjugated doxorubicin (DOX) from micelles was investigated and precise spatiotemporal control of drug delivery to cells demonstrated.

In **chapter 4**, a very long chain fatty acid (nervonic acid, NA) was conjugated to PEG via a photo-cleavable linker. Forming close packed micelles, this enabled the efficient incorporation of highly insoluble NA into target cellular membranes. Subsequent photolysis of PEG released free NA, which was subsequently processed by the cells to form very long chain phospholipids. This is expected to result in the thickening of the plasma cell membrane and provides an indirect method to modulate membrane protein activity.

In **chapter 5**, novel cationic lipids were photocaged to form neutral, caged cationic lipids. These could be formulated into liposomes which were shown to be freely circulating following intravenous injection *in vivo*. Following UV irradiation resulting in

photolysis of *o*-Nb, the liposome surface charge rapidly switched from neutral to cationic leading to the non-specific cellular adsorption, uptake and intracellular drug delivery of liposome encapsulated cargos. Switching of surface charge was demonstrated *in situ* and *in vivo* and importantly did not lead to content leakage from the liposome drug carrier.

Finally, in **chapter 6**, the main results and conclusions of this thesis are summarized and the advantages and future perspectives of using photo-cleavable DDS are described.

1.7 References

- [1] R. M. McQuade, V. Stojanovska, R. Abalo, J. C. Bornstein, K. Nurgali, *Front Pharmacol* **2016**, 7.
- [2] S. W. Y. Atiar M Rahman, Michael S Ewer, *Int J Nanomedicine* **2007**, 2, 567–583.
- [3] Y. H. Bae, K. Park, *J Control Release* **2011**, 153, 198-205.
- [4] (a) A. Beck, L. Goetsch, C. Dumontet, N. Corvaia, *Nat Rev Drug Discov* **2017**, 16, 315-337; (b) H. I. Chang, M. K. Yeh, *Int J Nanomedicine* **2012**, 7, 49-60.
- [5] S. C. Alley, N. M. Okeley, P. D. Senter, *Curr Opin Chem Biol* **2010**, 14, 529-537.
- [6] H. L. Perez, P. M. Cardarelli, S. Deshpande, S. Gangwar, G. M. Schroeder, G. D. Vite, R. M. Borzilleri, *Drug Discov Today* **2014**, 19, 869-881.
- [7] R. Haag, *Angew Chem Int Edit* **2004**, 43, 278-282.
- [8] E. Blanco, H. Shen, M. Ferrari, *Nat Biotechnol* **2015**, 33, 941-951.
- [9] H. Maeda, H. Nakamura, J. Fang, *Adv Drug Deliv Rev* **2013**, 65, 71-79.
- [10] L. M. Russell, M. Hultz, P. C. Searson, *J Control Release* **2018**, 269, 171-176.
- [11] H. Maeda, *Journal of Controlled Release* **2012**, 164, 138-144.
- [12] S. Wilhelm, A. J. Tavares, Q. Dai, S. Ohta, J. Audet, H. F. Dvorak, W. C. W. Chan, *Nat Rev Mater* **2016**, 1.
- [13] T. Lammers, F. Kiessling, W. E. Hennink, G. Storm, *J Control Release* **2012**, 161, 175-187.
- [14] M. W. Dewhirst, T. W. Secomb, *Nat Rev Cancer* **2017**, 17, 738-750.
- [15] J. I. Hare, T. Lammers, M. B. Ashford, S. Puri, G. Storm, S. T. Barry, *Adv Drug Deliver Rev* **2017**, 108, 25-38.
- [16] R. J. Y. H. T. Lian, *J Pharm Sci* **2001**, 90, 667-680.
- [17] A. Akbarzadeh, R. Rezaei-Sadabady, S. Davaran, S. W. Joo, N. Zarghami, Y. Hanifehpour, M. Samiei, M. Kouhi, K. Nejati-Koshki, *Nanoscale Res Let* **2013**, 8, 567-578
- [18] M. A. Clond, B. S. Lee, J. J. Yu, M. B. Singer, T. Amano, A. W. Lamb, D. Drazin, B. Kateb, E. J. Ley, J. S. Yu, *Plos One* **2013**, 8, 1026-1030
- [19] M. Longmire, P. L. Choyke, H. Kobayashi, *Nanomedicine (Lond)* **2008**, 3, 703-717.
- [20] Y. N. Zhang, W. Poon, A. J. Tavares, I. D. McGilvray, W. C. W. Chan, *J Control Release* **2016**, 240, 332-348.
- [21] P. Aggarwal, J. B. Hall, C. B. McLeland, M. A. Dobrovolskaia, S. E. McNeil, *Adv Drug Deliv Rev* **2009**, 61, 428-437.

- [22] A. Kolate, D. Baradia, S. Patil, I. Vhora, G. Kore, A. Misra, *J Control Release* **2014**, *192*, 67-81.
- [23] W. Li, P. Zhan, E. De Clercq, H. Lou, X. Liu, *Prog Polym Sci* **2013**, *38*, 421-444.
- [24] (a)G. Pasut, F. M. Veronese, *J Control Release* **2012**, *161*, 461-472; (b)P. L. Turecek, M. J.Bossard, F. Schoetens, I. A. Ivens, *J Pharm Sci* **2016**, *105*, 460-475.
- [25] Y. Maitani, *J Drug Deliv Sci Technol* **2011**, *21*, 27-34.
- [26] R. P. Garay, R. El-Gewely, J. K. Armstrong, G. Garratty, P. Richette, *Expert Opin Drug Del* **2012**, *9*, 1319-1323.
- [27] H. Schellekens, W. E. Hennink, V. Brinks, *Pharm Res-Dordr* **2013**, *30*, 1729-1734.
- [28] H. Hatakeyama, H. Akita, H. Harashima, *Adv Drug Deliv Rev* **2011**, *63*, 152-160.
- [29] H. Y. Xue, P. B. Guo, W. C. Wen, H. L. Wong, *Cur Pharm Des* **2015**, *21*, 3140-3147.
- [30] C. H. John W. Holland, Pieter R. Cullis, and Thomas D. Madden, *Biochemistry-Us* **1996**, *35*, 2618-2624.
- [31] J. R. S. a. M. J. Zuckermann, *Biochemistry-Us* **1993**, *32*, 3153-3161.
- [32] W. M. Li, L. Xue, L. D. Mayer, M. B. Bally, *Bba-Biomembranes* **2001**, *1513*, 193-206.
- [33] M. B. B. Gitanjali Adlakha-Hutcheon, Clifford R. Shew and Thomas D. Madden, *Nat Biotech* **1999**, *17*, 775-779.
- [34] S. Khondee, C. M. Olsen, Y. Zeng, C. R. Middaugh, C. Berkland, *Biomacromolecules* **2011**, *12*, 3880-3894.
- [35] B. Romberg, W. E. Hennink, G. Storm, *Pharm Res* **2008**, *25*, 55-71.
- [36] S. Mura, J. Nicolas, P. Couvreur, *Nat Mater* **2013**, *12*, 991-1003.
- [37] (a) S. S. Motoi Oishi, Yukio Nagasaki and Kazunori Kataoka, *Biomacromolecules* **2003**, *4*, 1426-1432; (b) M. Oishi, F. Nagatsugi, S. Sasaki, Y. Nagasaki, K. Kataoka, *Chembiochem* **2005**, *6*, 718-725; (c) Y. N. Motoi Oishi, Keiji Itaka, Nobuhiro Nishiyama and Kazunori Kataoka, *J. Am. Chem. Soc.* **2005**, *127*, 1624-1625; (d) Z. Y. Lin Zhu, Kun Cheng, Duane D. Miller, and Ram I. Mahato, *Bioconjugate Chem* **2008**, *19*, 290-298.
- [38] Q. Jin, T. Cai, H. Han, H. Wang, Y. Wang, J. Ji, *Macromol Rapid Commun* **2014**, *35*, 1372-1378.
- [39] S. W. K. Ji Hoon Jeong, and Tae Gwan Park, *Bioconjugate Chem.* **2003**, *14*, 473-479.
- [40] N. Nischan, A. Chakrabarti, R. A. Serwa, P. H. Bovee-Geurts, R. Brock, C. P. Hackenberger, *Angew Chem Int Ed Engl* **2013**, *52*, 11920-11924.
- [41] C. L. Chan, R. N. Majzoub, R. S. Shirazi, K. K. Ewert, Y. J. Chen, K. S. Liang, C. R. Safinya, *Biomaterials* **2012**, *33*, 4928-4935.
- [42] F. Li, J. He, M. Zhang, K. C. Tam, P. Ni, *RSC Adv.* **2015**, *5*, 54658-54666.
- [43] (a)G. F. Walker, C. Fella, J. Pelisek, J. Fahrmeir, S. Boeckle, M. Ogris, E. Wagner, *Mol Ther* **2005**, *11*, 418-425; (b)F. Li, J. He, M. Zhang, P. Ni, *Polym. Chem.* **2015**, *6*, 5009-5014.

- [44] (a) J. A. M. Joon Sig Choi, and Francis C. Szoka, Jr., *Bioconjugate Chem* **2003**, *14*, 420–429; (b) J. A. M. Xin Guo, y and Francis C. Szoka, Jr.z, *Biophys J* **2003**, *84*, 1784–1795.
- [45] (a) X. G. a. F. C. S. Jr., *Bioconjugate Chem* **2001**, *12*, 291–300; (b) C. Masson, M. Garinot, N. Mignet, B. Wetzter, P. Mailhe, D. Scherman, M. Bessodes, *J Control Release* **2004**, *99*, 423–434.
- [46] (a) F. D. Song Lin, Yang Wang, Shouping Ji, Zichen Li, *Biomacromolecules* **2008**, *9*, 109–115; (b) R. Ji, J. Cheng, T. Yang, C. C. Song, L. Li, F. S. Du, Z. C. Li, *Biomacromolecules* **2014**, *15*, 3531–3539.
- [47] (a) J. Shin, *J Control Release* **2003**, *91*, 187–200; (b) H. D. I. Jeremy A. Boomer, Zhi-Yi Zhang, Nill Bergstrand, Katarina Edwards, Jong-Mok Kim and David H. Thompson, *Langmuir* **2003**, *19*, 6408–6415; (c) W. G. Zhenghong Xu, Lingli Chen, Yu Gao, Zhiwen Zhang, and Yaping Li, *Biomacromolecules* **2008**, *9*, 3119–3126; (d) J. Shin, P. Shum, J. Grey, S. Fujiwara, G. S. Malhotra, A. Gonzalez-Bonet, S. H. Hyun, E. Moase, T. M. Allen, D. H. Thompson, *Mol Pharm* **2012**, *9*, 3266–3276; (e) H. K. Kim, J. Van den Bossche, S. H. Hyun, D. H. Thompson, *Bioconjug Chem* **2012**, *23*, 2071–2077; (f) M. M. Q. Jeremy A. Boomer, H. Dorota Inerowicz, Robert H. Haynes, V. Srilakshmi Patri, Jong-Mok Kim, and David H. Thompson, *Bioconjugate Chem.* **2009**, *20*, 47–59.
- [48] W.-P. C. Jingxia Gu, Xiaozhong Qu, Jiguang Liu, Sum-Yee Lo and Zhenzhong Yang, *Biomacromolecules* **2008**, *9*, 255–262.
- [49] H. Rongbin, X. Lei, L. Ying, D. Xiangping, C. Xuan, L. Lanfang, Y. Cuiyun, C. Yanming, T. Guotao, *J Pharm Pharmacol* **2016**, *68*, 751–761.
- [50] J. Li, L. Zhang, Y. Lin, H. Xiao, M. Zuo, D. Cheng, X. Shuai, *RSC Adv.* **2016**, *6*, 9160–9163.
- [51] (a) J. Wang, C. Gong, Y. Wang, G. Wu, *Colloids Surf B Biointerfaces* **2014**, *118*, 218–225; (b) J. Wang, C. Gong, Y. Wang, G. Wu, *RSC Adv* **2014**, *4*, 15856.
- [52] (a) D. Sun, J. Ding, C. Xiao, J. Chen, X. Zhuang, X. Chen, *ACS Appl Mater Interfaces* **2014**, *6*, 21202–21214; (b) D. Sun, J. Ding, C. Xiao, J. Chen, X. Zhuang, X. Chen, *Adv Healthc Mater* **2015**, *4*, 844–855.
- [53] T. Sun, A. Morger, B. Castagner, J. C. Leroux, *Chem Commun (Camb)* **2015**, *51*, 5721–5724.
- [54] Q. L. Li, S. H. Xu, H. Zhou, X. Wang, B. A. Dong, H. Gao, J. Tang, Y. W. Yang, *Acs Appl Mater Inter* **2015**, *7*, 28656–28664.
- [55] (a) T. H. Motoi Oishi, Yoshitsugu Akiyama, Seiji Takae, Atsushi Harada, Yuichi Yamasaki, Fumi Nagatsugi, Shigeki Sasaki, Yukio Nagasaki and Kazunori Kataoka, *Biomacromolecules* **2005**, *6*, 2449–2454; (b) L. Jia, D. Cui, J. Bignon, A. Di Cicco, J. Wdziejczak-Bakala, J. Liu, M. H. Li, *Biomacromolecules* **2014**, *15*, 2206–2217; (c) H. Gong, Z. Xie, M. Liu, H. Sun, H. Zhu, H. Guo, *Colloid and Polym Sci* **2015**, *293*, 2121–2128; (d) Y. Wang, N. Han, Q. Zhao, L. Bai, J. Li, T. Jiang, S. Wang, *Eur J Pharm Sci* **2015**, *72*, 12–20; (e) H. Gong, Z. Xie, M. Liu, H. Zhu, H. Sun, *RSC Adv.* **2015**, *5*, 59576–59582.

[56] (a) X. Q. Li, H. Y. Wen, H. Q. Dong, W. M. Xue, G. M. Pauletti, X. J. Cai, W. J. Xia, D. Shi, Y. Y. Li, *Chem Commun (Camb)* **2011**, 47, 8647-8649; (b) T.-B. Ren, W.-J. Xia, H.-Q. Dong, Y.-Y. Li, *Polymer* **2011**, 52, 3580-3586; (c) Q. Guo, P. Luo, Y. Luo, F. Du, W. Lu, S. Liu, J. Huang, J. Yu, *Colloids Surf B Biointerfaces* **2012**, 100, 138-145; (d) H. Wen, C. Dong, H. Dong, A. Shen, W. Xia, X. Cai, Y. Song, X. Li, Y. Li, D. Shi, *Small* **2012**, 8, 760-769; (e) K. Wang, Y. Liu, W.-J. Yi, C. Li, Y.-Y. Li, R.-X. Zhuo, X.-Z. Zhang, *Soft Matter* **2013**, 9, 692-699; (f) T. Ren, W. Wu, M. Jia, H. Dong, Y. Li, Z. Ou, *ACS Appl Mater Interfaces* **2013**, 5, 10721-10730; (g) Y. Ping, Q. Hu, G. Tang, J. Li, *Biomaterials* **2013**, 34, 6482-6494; (h) J. Yu, X. Li, Y. Luo, W. Lu, J. Huang, S. Liu, *Colloids Surf B Biointerfaces* **2013**, 107, 213-219; (i) W. Chen, P. Zhong, F. Meng, R. Cheng, C. Deng, J. Feijen, Z. Zhong, *J Control Release* **2013**, 169, 171-179; (j) J. Ding, J. Chen, D. Li, C. Xiao, J. Zhang, C. He, X. Zhuang, X. Chen, *J. Mater. Chem. B* **2013**, 1, 69-81; (k) T. Thambi, G. Saravanakumar, J.-U. Chu, R. Heo, H. Ko, V. G. Deepagan, J.-H. Kim, J. H. Park, *Macromol Res* **2012**, 21, 100-107; (l) H. Zhu, C. Dong, H. Dong, T. Ren, X. Wen, J. Su, Y. Li, *ACS Appl Mater Interfaces* **2014**, 6, 10393-10407; mH. Dong, C. Dong, W. Xia, Y. Li, T. Ren, *Med. Chem. Commun.* **2014**, 5, 147-152; (n) C. Cui, P. Yu, M. Wu, Y. Zhang, L. Liu, B. Wu, C. X. Wang, R. X. Zhuo, S. W. Huang, *Colloids Surf B Biointerfaces* **2015**, 129, 137-145; (o) W. Hou, F. Xia, C. S. Alves, X. Qian, Y. Yang, D. Cui, *ACS Appl Mater Interfaces* **2016**, 8, 1447-1457.

[57] (a) H. Sun, B. Guo, R. Cheng, F. Meng, H. Liu, Z. Zhong, *Biomaterials* **2009**, 30, 6358-6366; (b) Y. Zhong, W. Yang, H. Sun, R. Cheng, F. Meng, C. Deng, Z. Zhong, *Biomacromolecules* **2013**, 14, 3723-3730; (c) X. Wang, H. Sun, F. Meng, R. Cheng, C. Deng, Z. Zhong, *Biomacromolecules* **2013**, 14, 2873-2882; (d) C. Cui, Y. N. Xue, M. Wu, Y. Zhang, P. Yu, L. Liu, R. X. Zhuo, S. W. Huang, *Biomaterials* **2013**, 34, 3858-3869; (e) L. Jia, Z. Li, D. Zhang, Q. Zhang, J. Shen, H. Guo, X. Tian, G. Liu, D. Zheng, L. Qi, *Polym. Chem.* **2013**, 4, 156-165; (f) Y. Cao, J. Zhao, Y. Zhang, J. Liu, J. Liu, A. Dong, L. Deng, *RSC Adv.* **2015**, 5, 28060-28069.

[58] Y. Wang, Q. J. Luo, L. L. Gao, C. Gao, H. Du, G. Y. Zha, X. D. Li, Z. Q. Shen, W. P. Zhu, *Biomater Sci-Uk* **2014**, 2, 1367-1376.

[59] K. H. Dmitri Kirpotin, Nasreen Mullah, Demetrios Papahadjopoulos, Samuel Zalipsky *FEBS Letters* **1996**, 388, 115- 118.

[60] (a) S. H. Kim, J. H. Jeong, S. H. Lee, S. W. Kim, T. G. Park, *J Control Release* **2008**, 129, 107-116; (b) K. M. McNeeley, E. Karathanasis, A. V. Annapragada, R. V. Bellamkonda, *Biomaterials* **2009**, 30, 3986-3995; (c) W. Y. Rui Kuai, Yao Qin, Huali Chen, Jie Tang, Mingqing Yuan, Zhirong Zhang, and Qin He, *Mol Pharmaceutics* **2010**, 7, 1816-1826; (d) Y. Cui, H. Dong, X. Cai, D. Wang, Y. Li, *ACS Appl Mater Interfaces* **2012**, 4, 3177-3183; (e) L. Mei, L. Fu, K. Shi, Q. Zhang, Y. Liu, J. Tang, H. Gao, Z. Zhang, Q. He, *Int J Pharm* **2014**, 468, 26-38; (f) J. Tang, H. Fu, Q. Kuang, L. Zhang, Q. Zhang, Y. Liu, R. Ran, H. Gao, Z. Zhang, Q. He, *J Drug Target* **2014**, 22, 313-326; (g) J. M. Williford, Y. Ren, K. Huang, D. Pan, H. Q. Mao, *J Mater Chem B Mater Biol*

- Med* **2014**, *2*, 8106-8109; (h) X. Ai, J. Sun, L. Zhong, C. Wu, H. Niu, T. Xu, H. Lian, X. Han, G. Ren, W. Ding, J. Wang, X. Pu, Z. He, *Macromol Biosci* **2014**, *14*, 1415-1428.
- [61] M. Q. Samuel Zalipsky, John A. Walker, Nasreen Mullah, Yolanda P. Quinn, and Shi Kun Huang, *Bioconjugate Chem* **1999**, *10*, 703-707.
- [62] R. K. E. Charles C. Pak, Patrick L. Ahl, Andrew S. Janoj, Paul Meers, *Biochimica et Biophysica Acta* **1999**, *1419* 111-126.
- [63] L. L. H. Benjamin E. Turk, Elizabeth T. Piro, and Lewis C. Cantley, *Nat biotechnol* **2001**, *19*, 661-667.
- [64] P. Yingyuad, M. Mevel, C. Prata, S. Furegati, C. Kontogiorgis, M. Thanou, A. D. Miller, *Bioconjug Chem* **2013**, *24*, 343-362.
- [65] C. Nazli, G. S. Demirer, Y. Yar, H. Y. Acar, S. Kizilel, *Colloids Surf B Biointerfaces* **2014**, *122*, 674-683.
- [66] L. Zhu, T. Wang, F. Perche, A. Taigind, V. P. Torchilin, *Proc Natl Acad Sci U S A* **2013**, *110*, 17047-17052.
- [67] S. J. Lee, Y. I. Jeong, H. K. Park, D. H. Kang, J. S. Oh, S. G. Lee, H. C. Lee, *Int J Nanomedicine* **2015**, *10*, 5489-5503.
- [68] (a) T. Terada, M. Iwai, S. Kawakami, F. Yamashita, M. Hashida, *J Control Release* **2006**, *111*, 333-342; (b) H. Hatakeyama, H. Akita, K. Kogure, M. Oishi, Y. Nagasaki, Y. Kihira, M. Ueno, H. Kobayashi, H. Kikuchi, H. Harashima, *Gene Ther* **2007**, *14*, 68-77; (c) P. K. Lin Zhu, and Vladimir P. Torchilin, *ACS Nano* **2012**, *6*, 3491-3498; (d) L. Zhu, F. Perche, T. Wang, V. P. Torchilin, *Biomaterials* **2014**, *35*, 4213-4222; (e) K. L. Veiman, K. Kunnapuu, T. Lehto, K. Kiisholts, K. Parn, U. Langel, K. Kurrikoff, *J Control Release* **2015**, *209*, 238-247; (f) Y. Tu, L. Zhu, *J Control Release* **2015**, *212*, 94-102; (g) Z. Dai, Q. Yao, L. Zhu, *ACS Appl Mater Interfaces* **2016**, *8*, 12661-12673.
- [69] (a) J. Zhang, *Pharm Res* **2004**, *49*, 185-198; (b) Y. J. Zhong, L. H. Shao, Y. Li, *Int J Oncol* **2013**, *42*, 373-383.
- [70] C. G. Bochet, *J Chem Soc Perk T 1* **2002**, 125-142.
- [71] A. P. Castano, P. Mroz, M. R. Hamblin, *Nat Rev Cancer* **2006**, *6*, 535-545.
- [72] C. M. Allen, W. M. Sharman, J. E. Van Lier, *J Porphyr Phthalocya* **2001**, *5*, 161-169.
- [73] T. J. McMillan, E. Leatherman, A. Ridley, J. Shorrocks, S. E. Tobin, J. R. Whiteside, *J Pharm Pharmacol* **2008**, *60*, 969-976.
- [74] S. H. Yun, S. J. J. Kwok, *Nat Biomed Eng* **2017**, *1*.
- [75] L. Fournier, C. Gauron, L. Xu, I. Aujard, T. Le Saux, N. Gagey-Eilstein, S. Maurin, S. Dubruille, J. B. Baudin, D. Bensimon, M. Volovitch, S. Vriz, L. Jullien, *ACS Chem Biol* **2013**, *8*, 1528-1536.
- [76] X. M. M. Weyel, M. A. H. Fichte, A. Heckel, *ACS Chem Biol* **2017**, *12*, 2183-2190.

- [77] K. Peng, I. Tomatsu, B. van den Broek, C. Cui, A. V. Korobko, J. van Noort, A. H. Meijer, H. P. Spaink, A. Kros, *Soft Matter* **2011**, *7*, 4881.
- [78] (a) Y. V. Il'ichev, M. A. Schworer, J. Wirz, *J Am Chem Soc* **2004**, *126*, 4581-4595; (b) I. Aujard, C. Benbrahim, M. Gouget, O. Ruel, J. B. Baudin, P. Neveu, L. Jullien, *Chem Eur J* **2006**, *12*, 6865-6879.
- [79] (a) F. B. Peters, A. Brock, J. Wang, P. G. Schultz, *Chem Biol* **2009**, *16*, 148-152; (b) J.-M. Schumers, J.-F. Gohy, C.-A. Fustin, *Polym. Chem.* **2010**, *1*, 161-163; (c) J. M. Govan, A. L. McIver, A. Deiters, *Bioconjug Chem* **2011**, *22*, 2136-2142; (d) L. Li, A. Lv, X. X. Deng, F. S. Du, Z. C. Li, *Chem Commun (Camb)* **2013**, *49*, 8549-8551; (e) N. Kalva, N. Parekh, A. V. Ambade, *Polym. Chem.* **2015**, *6*, 6826-6835; (f) K. Ding, L. Shi, L. Zhang, T. Zeng, Y. Yin, Y. Yi, *Polym. Chem.* **2016**, *7*, 899-904.
- [80] S. Z. Joshua S. Katz, Brendon G. Ricart, Darrin J. Pochan, Daniel A. Hammer and Jason A. Burdick, *J. Am. Chem Soc.* **2010**, *132*, 3654–3655
- [81] H. Yang, L. Jia, Z. Wang, A. I. Di-Cicco, D. Lévy, P. Keller, *Macromolecules* **2011**, *44*, 159-165.
- [82] M. Cao, J.-Q. Wang, P.-C. Chen, J.-T. Xu, Z.-Q. Fan, *J Polym Sci Part A: Polym Chem* **2010**, *48*, 3834-3840.
- [83] J. Wang, Y. Ouyang, S. Li, X. Wang, Y. He, *RSC Adv.* **2016**, *6*, 57227-57231.
- [84] N. G. Patil, N. B. Basutkar, A. V. Ambade, *Chem Commun (Camb)* **2015**, *51*, 17708-17711.
- [85] C. Komeda, A. Ikeda, J. Kikuchi, N. Ishida-Kitagawa, H. Tatebe, K. Shiozaki, M. Akiyama, *Org Biomol Chem* **2013**, *11*, 2567-2570.
- [86] D. Zhou, J. Guo, G. B. Kim, J. Li, X. Chen, J. Yang, Y. Huang, *Adv Healthc Mater* **2016**, *5*, 2493-2499.
- [87] D. Tila, S. Ghasemi, S. N. Yazdani-Arazi, S. Ghanbarzadeh, *J Biomater Appl* **2015**, *30*, 3-16.
- [88] F. D. Maria Laura Immordino, Luigi Cattel, *Int J Nanomedicine* **2006**, *1*, 297–315.
- [89] H. R. Marsden, I. Tomatsu, A. Kros, *Chem Soc Rev* **2011**, *40*, 1572-1585.
- [90] A. S. Janoff, *Lab Invest* **1992**, *66*, 655-658.
- [91] S. Leekumjorn, H. J. Cho, Y. F. Wu, N. T. Wright, A. K. Sum, C. Chan, *Bba-Biomembranes* **2009**, *1788*, 1508-1516.
- [92] M. M. Sperotto, O. G. Mouritsen, *Eur Biophys J Biophys* **1988**, *16*, 1-10.
- [93] A. Samad, Y. Sultana, M. Aqil, *Curr Drug Deliv* **2007**, *4*, 297-305.
- [94] M. L. Briuglia, C. Rotella, A. McFarlane, D. A. Lamprou, *Drug Deliv Transl Re* **2015**, *5*, 231-242.
- [95] F. Versluis, J. Voskuhl, B. van Kolck, H. Zope, M. Bremmer, T. Albregtse, A. Kros, *J Am Chem Soc* **2013**, *135*, 8057-8062.
- [96] J. S. Suk, Q. G. Xu, N. Kim, J. Hanes, L. M. Ensign, *Adv Drug Deliver Rev* **2016**, *99*, 28-51.

- [97] J. Tang, L. Zhang, H. Gao, Y. Liu, Q. Zhang, R. Ran, Z. Zhang, Q. He, *Drug Deliv* **2016**, *23*, 1130-1143.
- [98] B. Gupta, T. S. Levchenko, D. A. Mongayt, V. P. Torchilin, *J Drug Target* **2005**, *13*, 337-343.
- [99] H. Brooks, B. Lebleu, E. Vives, *Adv Drug Deliver Rev* **2005**, *57*, 559-577.
- [100] P. S. Kulkarni, M. K. Haldar, R. R. Nahire, P. Katti, A. H. Ambre, W. W. Muhonen, J. B. Shabb, S. K. Padi, R. K. Singh, P. P. Borowicz, D. K. Shrivastava, K. S. Katti, K. Reindl, B. Guo, S. Mallik, *Mol Pharm* **2014**, *11*, 2390-2399.
- [101] G. Byk, C. Dubertret, V. Escriou, M. Frederic, G. Jaslin, R. Rangara, B. Pitard, J. Crouzet, P. Wils, B. Schwartz, D. Scherman, *J Medi Chem* **1998**, *41*, 224-235.
- [102] H. Xu, Y. Deng, D. Chen, W. Hong, Y. Lu, X. Dong, *J Control Release* **2008**, *130*, 238-245.
- [103] T. Wang, J. R. Upponi, V. P. Torchilin, *Int J Pharm* **2012**, *427*, 3-20.
- [104] J. B. a. F. C. S. Harma Ellens, *Biochemistry* **1986**, *25*, 4141-4147.
- [105] Y. Z. Wang, L. Chen, Y. F. Ding, W. L. Yan, *Int J Pharm* **2012**, *422*, 409-417.
- [106] J. Miao, X. G. Zhang, Y. Hong, Y. F. Rao, Q. Li, X. J. Xie, J. E. Wo, M. W. Li, *Carbohydr Polym* **2012**, *87*, 1342-1347.
- [107] S. M. Garg, I. M. Paiva, M. R. Vakili, R. Soudy, K. Agopsowicz, A. H. Soleimani, M. Hitt, K. Kaur, A. Lavasanifar, *Biomaterials* **2017**, *144*, 17-29.
- [108] W. W. Xiao, N. Suby, K. Xiao, T. Y. Lin, N. Al Awwad, K. S. Lam, Y. P. Li, *J Control Release* **2017**, *264*, 169-179.
- [109] J. N. Israelachvili, D. J. Mitchell, B. W. Ninham, *J Chem Soc Farad T 2* **1976**, *72*, 1525-1568.
- [110] K. K. Gill, A. Kaddoumi, S. Nazzal, *J Drug Target* **2015**, *23*, 222-231.
- [111] Z. Y. He, B. Y. Chu, X. W. Wei, J. Li, C. K. Edwards, 3rd, X. R. Song, G. He, Y. M. Xie, Y. Q. Wei, Z. Y. Qian, *Int J Pharm* **2014**, *469*, 168-178.
- [112] C. Zhao, H. Deng, J. Xu, S. Li, L. Zhong, L. Shao, Y. Wu, X. J. Liang, *Nanoscale* **2016**, *8*, 10832-10842.
- [113] Y. Lee, K. Kataoka, *Soft Matter* **2009**, *5*, 3810.
- [114] K. M. Seiji Takae, Makoto Oba, Takehiko Ishii, Nobuhiro Nishiyama, Keiji Itaka, Yuichi Yamasaki, Hiroyuki Koyama and Kazunori Kataok, *J. Am. Chem. Soc.* **2008**, *130*, 6001-6009.
- [115] Q. Tang, B. Cao, G. Cheng, *Chem Comm* **2014**, *50*, 1323-1325.
- [116] (a) Y. Zhao, J. Zhao, C. Hao, M. Han, M. Wang, Y. Guo, X. Wang, *RSC Adv.* **2016**, *6*, 2602-2610; (b) X. Mao, J. Si, Q. Huang, X. Sun, Q. Zhang, Y. Shen, J. Tang, X. Liu, M. Sui, *Adv Healthc Mater* **2016**, *5*, 2517-2527; (c) P. F. Gou, W. W. Liu, W. W. Mao, J. B. Tang, Y. Q. Shen, M. H. Sui, *J Mater Chem B* **2013**, *1*, 284-292.
- [117] (a) Q. Wu, F. Du, Y. Luo, W. Lu, J. Huang, J. Yu, S. Liu, *Colloids Surf B Biointerfaces* **2013**, *105*, 294-302; (b) A. Guiotto, M. Canevari, P. Orsolini, O. Lavanchy, C. Deuschel, N. Kaneda, A.

- Kurita, T. Matsuzaki, T. Yaegashi, S. Sawada, F. M. Veronese, *Bioorg Med Chem Lett* **2004**, *14*, 1803-1805.
- [118] K. Riebeseel, E. Biedermann, R. Loser, N. Breiter, R. Hanselmann, R. Mulhaupt, C. Unger, F. Kratz, *Bioconjug Chem* **2002**, *13*, 773-785.
- [119] T. Liu, X. Yuan, T. Jia, C. Liu, Z. Ni, Z. Qin, Y. Yuan, *Int J Pharm* **2016**, *506*, 382-393.
- [120] J. Lu, Y. Huang, W. Zhao, Y. Chen, J. Li, X. Gao, R. Venkataramanan, S. Li, *Mol Pharm* **2013**, *10*, 2880-2890.
- [121] C. Li, L. Dai, K. Liu, L. Deng, T. Pei, J. Lei, *RSC Adv.* **2015**, *5*, 74828-74834.
- [122] T. Yin, Q. Wu, L. Wang, L. Yin, J. Zhou, M. Huo, *Mol Pharm* **2015**, *12*, 3020-3031.
- [123] (a) J. Lu, Y. Huang, W. Zhao, R. T. Marquez, X. Meng, J. Li, X. Gao, R. Venkataramanan, Z. Wang, S. Li, *Biomaterials* **2013**, *34*, 1591-1600; (b) Y. Huang, J. Lu, X. Gao, J. Li, W. Zhao, M. Sun, D. B. Stolz, R. Venkataramanan, L. C. Rohan, S. Li, *Bioconjug Chem* **2012**, *23*, 1443-1451.
- [124] J. Liu, P. Zahedi, F. Zeng, C. Allen, *J Pharm Sci* **2008**, *97*, 3274-3290.
- [125] (a) X. Zhang, K. Liu, Y. Huang, J. Xu, J. Li, X. Ma, S. Li, *Bioconjug Chem* **2014**, *25*, 1689-1696; (b) X. Zhang, Y. Huang, M. Ghazwani, P. Zhang, J. Li, S. H. Thorne, S. Li, *ACS Macro Letters* **2015**, *4*, 620-623; (c) X. Zhang, J. Lu, Y. Huang, W. Zhao, Y. Chen, J. Li, X. Gao, R. Venkataramanan, M. Sun, D. B. Stolz, L. Zhang, S. Li, *Bioconjug Chem* **2013**, *24*, 464-472; (d) X. Zhang, Y. Huang, W. Zhao, Y. Chen, P. Zhang, J. Li, R. Venkataramanan, S. Li, *Mol Pharm* **2014**, *11*, 2807-2814; (e) Y. Chen, X. Zhang, J. Lu, Y. Huang, J. Li, S. Li, *AAPS J* **2014**, *16*, 600-608.
- [126] H. Wang, J. He, D. Cao, M. Zhang, F. Li, K. C. Tam, P. Ni, *Polym. Chem.* **2015**, *6*, 4809-4818.
- [127] (a) S. Yang, F. Zhu, Q. Wang, F. Liang, X. Qu, Z. Gan, Z. Yang, *J. Mater. Chem. B* **2015**, *3*, 4043-4051; (b) G. Salzano, D. F. Costa, C. Sarisozen, E. Luther, G. Mattheolabakis, P. P. Dhargalkar, V. P. Torchilin, *Small* **2016**, *12*, 4837-4848.
- [128] Z. Dai, Y. Tu, L. Zhu, *J Biomed Nanotechnol* **2016**, *12*, 1199-1210.
- [129] D. E. Discher, F. Ahmed, *Annu Rev Biomed Eng* **2006**, *8*, 323-341.
- [130] M.-H. Li, P. Keller, *Soft Matter* **2009**, *5*, 927.
- [131] L. Messenger, J. Gaitzsch, L. Chierico, G. Battaglia, *Curr Opin Pharmacol* **2014**, *18*, 104-111.
- [132] D. V. Simona Cerritelli, and Jeffrey A. Hubbell, *Biomacromolecules*, **2007**, *8*, 1966-1972.
- [133] T. Thambi, V. G. Deepagan, H. Ko, D. S. Lee, J. H. Park, *J Mater Chem* **2012**, *22*, 22028.

2

Temporal Control of Membrane Fusion through Photolabile PEGylation of Liposome Membranes

Abstract: Membrane fusion results in the transport and mixing of (bio)molecules across otherwise impermeable barriers. In this chapter, we demonstrate, for the first time, temporal control of targeted liposome-liposome membrane fusion and contents mixing using light as an external trigger. Our method relies on the steric shielding and rapid, photo-induced de-shielding of complementary fusogenic peptides tethered to opposing liposomal membranes. In an analogous approach, we are also able to demonstrate precise spatiotemporal control of liposome accumulation at cellular membranes *in vitro*.

Li Kong, Sven H.C. Askes, Sylvestre Bonnet, Alexander Kros and Frederick Campbell, *Angew. Chem. Int. Ed.* **2016**, 128, 1418–1422.

2.1 Introduction

Membrane fusion is a fundamental process of life resulting in the highly regulated transport of (bio)molecules both between and within cells.^[1] To achieve fusion, energetic barriers associated with bringing opposing membranes together and of subsequent membrane destabilization and merging must be overcome.^[2] *In vivo*, large, often multi-component, protein fusion complexes have evolved to carry out this task.^[3]

The development of synthetic systems capable of controlled (non-spontaneous) membrane fusion is a tantalizing prospect, not least for applications in vector (liposomal) based drug and gene delivery *in vitro* and *in vivo*. In this context, fusion of drug-loaded vector with target cellular membranes would result in drug delivery directly to the cell cytoplasm. Crucially, this route to intracellular drug and gene delivery minimizes degradative loss of encapsulated payloads associated with hydro- and proteolytic endocytotic uptake.^[4]

Given the typical size and complexity of native fusion complexes, significant efforts have been made to develop simplified systems capable of membrane fusion.^[5] These can be targeted^[6] or non-targeted^[7] Towards this goal, we have previously reported a supramolecular system capable of inducing rapid and targeted membrane fusion of distinct liposome populations.^[8] Inspired by the native SNARE fusion complex, our targeted fusion system relies on the recognition and binding of complementary coiled-coil forming peptides (E and K) tethered to opposing liposome membranes (Figure 1). In our membrane fusion model, coiled-coil forming peptide pair (E/K) are conjugated to cholesterol via a short polyethylene glycol (PEG) spacer, yielding fusogens, so called CPE/CPK. Upon mixing E- and K-liposomes, membrane fusion and leakage-free, contents mixing occurs spontaneously.

In Nature however, membrane fusion is highly regulated in both time and space, ensuring correct biological function. Likewise, if simplified fusion systems are to be applied to drug and gene delivery systems, the ability to control when and where fusion occurs will be essential in ensuring clinically relevant therapeutic indices. Control of membrane fusion using simplified fusion systems, in either time and/or

space however has yet to be demonstrated. In this communication we first demonstrate precise temporal control of membrane fusion in model (liposome-liposome) systems. This result is achieved through steric shielding and rapid, photo-induced de-shielding of complementary and fusogenic liposome populations (Figure 1).

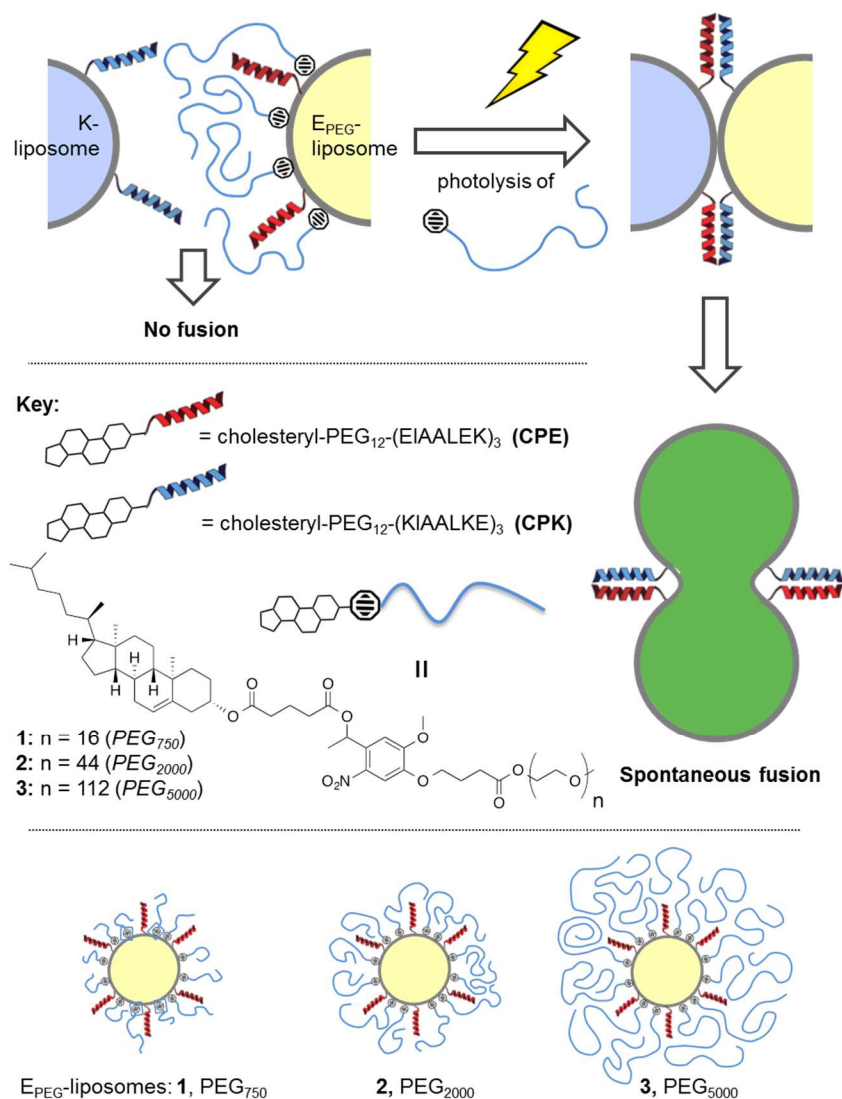


Figure 1. (top) Light induced, temporal control of liposome-liposome fusion through photolabile steric shielding (PEGylation) of fusogenic peptides tethered to opposing liposomal membranes. (bottom) E_{PEG}-liposomes sterically shielded with **1-3**.

Polyethylene glycol (PEG) is chosen as steric ‘shield’ given its widespread use in improving the pharmacokinetics and dynamics of biomolecules, nanoparticles and liposomes.^[9] We have previously shown that 2 mol% PEGylation of both liposomal membranes in our simplified fusion system effectively shuts down membrane fusion through steric shielding of liposome-tethered peptides E and K.^[10]

2.2 Results and discussion

The synthesis and characterization of photolabile cholesterol-*o*-nitrobenzyl-PEG constructs, **1-3**, are outlined in Section 2.4.2 (Figures S1-8). Upon UV light irradiation (365 nm, 3-5 mW/cm²) in H₂O:MeCN:tBuOH (1:1:1), complete photolysis was achieved within 20 min as shown by UV-Vis spectroscopy (see Figure 2a). The appearance of three clear isosbestic points shows clean photoconversion of **2** to its photoproducts. Comparable spectra and rates of photolysis were found for **1** and **3** under identical irradiation conditions (Figure S9). HPLC-ELSD analysis of the photolysis products following irradiation of **2** in both H₂O:MeCN:tBuOH (1:1:1) (Figure S10b and S11) and PBS (Figure 2b) confirmed the conversion of **2** to cholesteryl hemisuccinate as expected. Conversion of **1** and **3** to their expected photoproducts was similarly observed (Figure S10a and S10c).

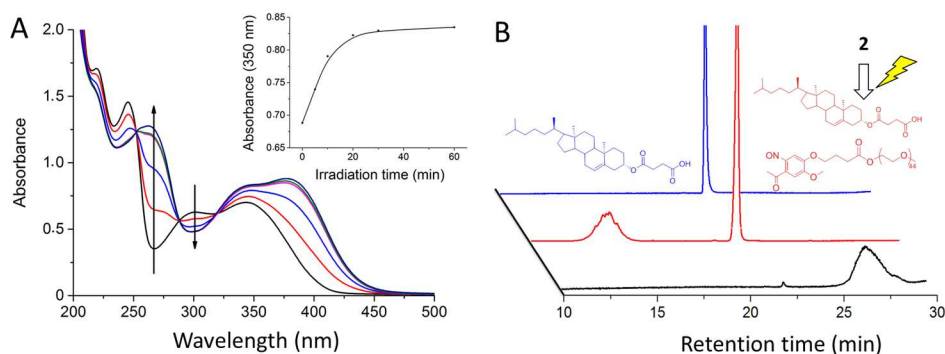


Figure 2. (a) Time evolution of the UV-Vis spectra of a solution of **2** (200 μM; H₂O:MeCN:tBuOH (1:1:1)) during photolysis (365 nm, 3-5 mW/cm²). Inset: Time evolution of the absorbance at 350 nm. (b) HPLC-ELSD analysis of **2** (200 μM in PBS) before (black) and after (red) 30 min UV irradiation (365 nm, 3-5 mW/cm²). Cholesteryl hemisuccinate (200 μM in PBS), an expected photoproduct, is shown in blue.

As a next step, liposomes containing 1 mol% CPE or CPK, referred to as E- and K-liposomes respectively, were formulated via lipid film hydration and sonication. Following previously published protocols,^[11] *in situ* modification of E-liposomes with **1-3** yielded E_{PEG}-liposomes whose outer membrane leaflet contained between 0 and 10 mol% **1-3**. In all cases, liposomes, both before and after *in situ* modification, were ~100 nm in diameter as shown by dynamic light scattering (polydispersity index <0.2) (Figure S12).

For photolabile PEG constructs **2** and **3**, lipid mixing experiments – between K- and E_{PEG}-liposome populations – revealed that the degree of lipid mixing was inversely correlated to the degree of membrane PEGylation (Figure S13). In both cases, 4 mol% PEGylation of E-liposomes alone was sufficient to completely nullify lipid mixing between E- and K-liposomal membranes. For the shorter (PEG750) construct, **1**, the degree of PEGylation bore no influence on the rate or extent of lipid mixing between E_{PEG}- and K-liposomes (Figure 3). This was confirmed by circular dichroism (CD) measurements which, for mixed K- and E_{PEG}-liposomes (4 mol% **1**), shows a significant increase in helical content (Table S1), indicative of the formation of the expected heterodimeric coiled coil complex between peptides E and K (Figure 3). It should be noted that peptides E and K tethered to the liposome membrane are already ~50% folded. This is consistent with previous reports on the conformation of these peptides when tethered to a liposome membrane.^[8a,c,d]

The inability of the shorter PEG construct, **1**, to sterically shield the interaction between peptides E and K reflects a critical length requirement for the steric shield determined by the molecular size of peptides E and K.^[12]

To assess how liposome-liposome fusion was influenced by UV light irradiation, E_{PEG}-liposomes containing 4 mol% **2** and **3** were irradiated for increasing periods of time prior to the addition of K-liposomes. As expected, lipid mixing efficiencies directly correlate with increasing pre-irradiation times (Figure 4). Complete lipid mixing, as compared to E- and K-liposome fusion in the absence of any steric shielding, was achieved following 30 min pre-irradiation of E_{PEG}-liposomes. This result was mirrored in analogous content mixing experiments (Figure S14).

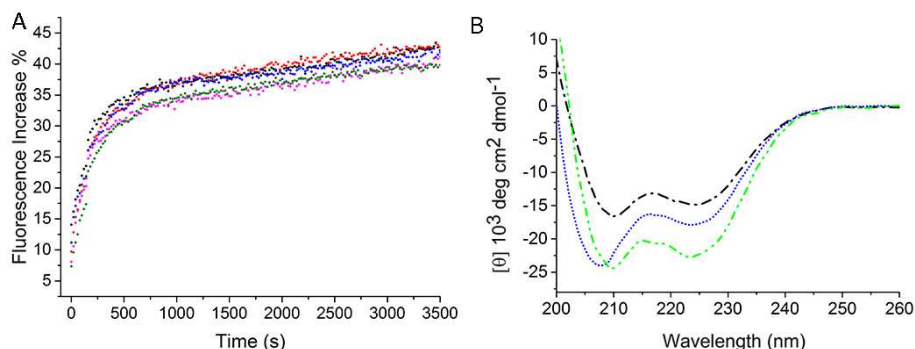


Figure 3. (a) Lipid mixing between E_{PEG^-} and K-liposomes with varying amounts of **1** presented from the E-liposome membrane; 0 mol% (---), 2 mol% (---), 4 mol% (---), 8 mol% (---) and 10 mol% (---). Upon mixing E_{PEG^-} and K-liposomes, membrane merging results in a decrease in Förster resonance energy transfer between donor and acceptor and an increase in donor fluorescence emission. (b) CD spectra of K-liposomes (---) alone, 4 mol% **1** E_{PEG^-} -liposomes alone (---) and mixed solutions of K- and E_{PEG^-} -liposomes (---).

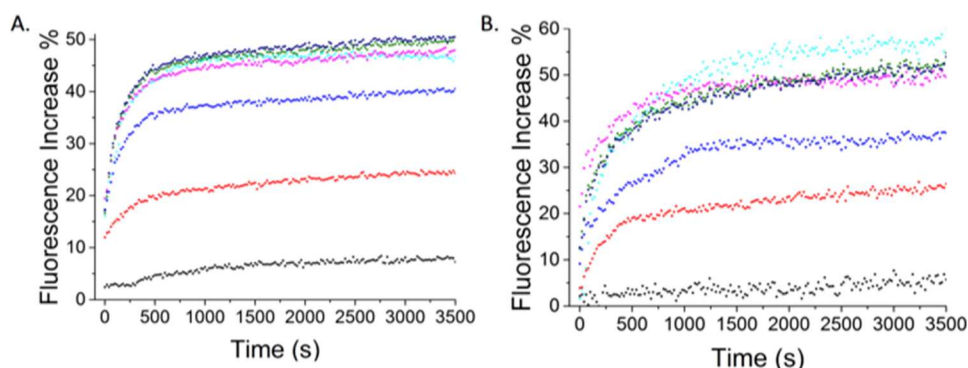


Figure 4. Lipid mixing of E_{PEG^-} (4 mol%) and K-liposomes with increasing irradiation times of the E_{PEG^-} -liposomes prior to mixing with K-liposomes. A: E_{PEG^-} (4 mol% **2**); B: E_{PEG^-} (4 mol% **3**). Time: 0 (---), 5 (---), 10 (---), 20 (---), 30 (---), 60 min (---) irradiation. 0 mol% **2** (---).

To validate that membrane fusion is governed through the interaction of peptides E and K, CD measurements of mixed populations of E_{PEG^-} and K-liposomes were taken both before and after irradiation (Figure 5). In both cases, following irradiation, an increase in helical content together with a shift towards an equal ratio of mean residue molar ellipticities at 208 and 222 nm respectively, confirms the formation of

the expected E/K heterodimeric coiled coil complex (see Table S13 for quantitative CD analysis).

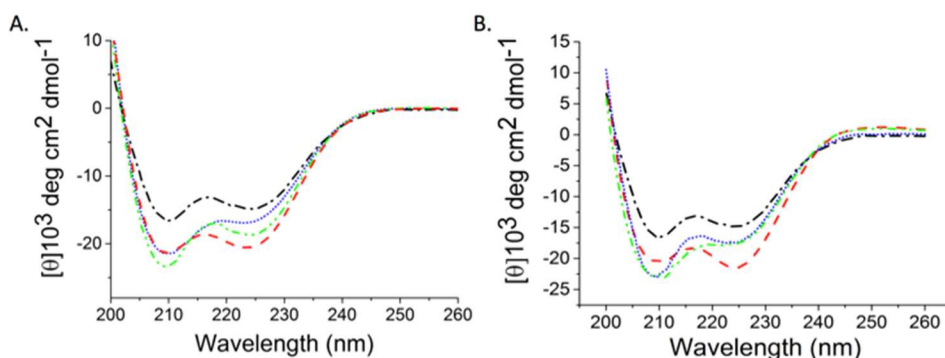


Figure 5. CD spectra: K-liposomes (---), 4 mol% E_{PEG} -liposomes (---), mixed solutions of K- and E_{PEG} -liposomes pre- (---) and post-irradiation (---). **A:** E_{PEG} - (4 mol% **2**); **B:** E_{PEG} - (4 mol% **3**).

To monitor the photolysis and subsequent liposome-liposome fusion *in situ*, populations of E_{PEG} -liposomes (containing 4 mol% **2**) and K-liposomes were pre-mixed and contents mixing monitored simultaneously before and during continuous UV irradiation (Figure 6). In the absence of UV light no content mixing between liposomes was observed, however immediately upon UV irradiation liposome-liposome fusion commences. This demonstrates the direct dependence of liposome-liposome fusion on photolysis of the PEG shield from the E_{PEG} -liposomal membrane enabling precise temporal control of the fusion process. This result was mirrored in the analogous experiment with E_{PEG} -liposomes containing 4 mol% **3** (Figure S16). The influence of continuous UV irradiation upon the rate of fusion between E- and K-liposomes, in the absence of any PEGylation, was found to be insignificant (Figure S15).

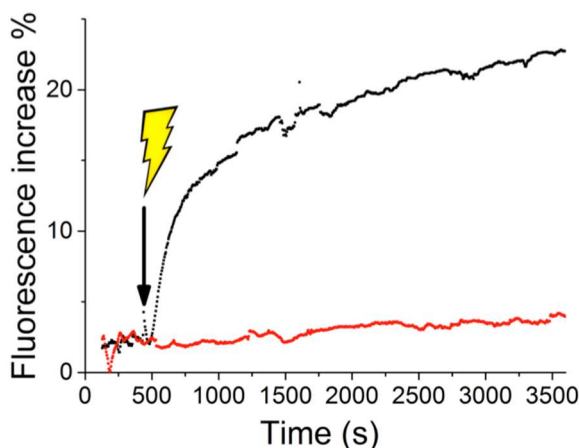


Figure 6. Content mixing following *in situ* photolysis of a 1:1 mixture of E_{PEG}-liposomes (4 mol% **2**) and K-liposomes, upon (---) and in the absence of (---) UV irradiation. Black arrow indicates point at which UV irradiation was turned on. For contents mixing measurements, a self-quenching concentration of a fluorescent dye (sulforhodamine B, 10 mM) is encapsulated within E_{PEG}-liposomes. Upon mixing and fusion with empty K-liposomes, dilution of the dye results in fluorescence dequenching.

Finally, applying this methodology to a biological context, we are able to demonstrate precise spatiotemporal control of liposome accumulation at pre-functionalised cellular membranes (Figure 7). To achieve this, we adapted previously reported protocols,^[13] first incorporating lipopeptide K into the membranes of cells then incubating cells with E_{PEG}-liposomes (4 mol% **2**). 1 mol% fluorescent DOPE-LR was added to the E_{PEG}-liposome membrane composition for visualization. Remarkably, following photolysis of the steric shield from the E_{PEG}-liposomes, the interaction between peptides E and K, displayed from the liposome and cell surface respectively, is both specific and strong enough to enable well-defined, light-templated accumulation of liposomes at the cell surface. We have yet to confirm whether this interaction leads to full fusion of liposome and target plasma membranes. However, even if this results in docking alone, we can expect these liposomes, now localized at the cellular membrane, to be internalised over time, most likely via an endocytotic pathway.^[14] Subsequent liposome degradation and endosomal escape would result in the intracellular release of liposome encapsulated content.

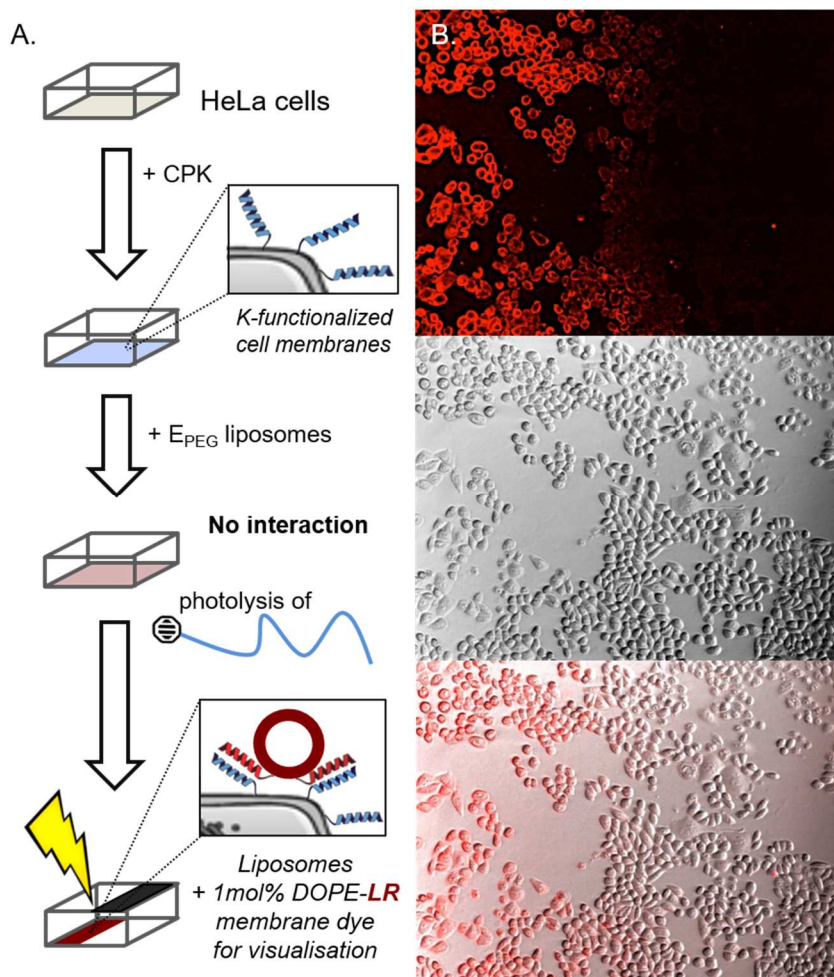


Figure 7. (A) Light directed, spatiotemporal control of liposome accumulation at pre-functionalised HeLa cell membranes *in vitro*. (B) (top) Fluorescence image (10x magnification) of E_{PEG}-liposomes (containing 1mol% DOPE-LR fluorescent probe) docked at pre-functionalised HeLa cell membranes following localised UV irradiation. (middle) Brightfield image (10x magnification). (bottom) Merge. Experimental details: Step 1. CPK solution (5 μ M) incubated with cells for 15 min followed by washing. Step 2. E_{PEG}-liposome solution (250 μ M containing 1 mol% CPE and 1 mol% DOPE-LR fluorescent probe) incubated with cells for 15 min. Step 3. Localised irradiation (10 min, 10 mW/cm²) and further incubation for 15 min. Step 4. Wash and image.

2.3 Conclusions

In this study, we successfully synthesized photolabile cholesterol-o-nitrobenzyl-PEG constructs, **1-3** and incorporated these into E-liposomal membranes. We illustrate the need for a minimum PEG length (≥ 2000 g/mol) to effectively shield the interaction between fusogenic peptides, E and K. And we show rapid photo-induced de-shielding of E_{PEG}-liposomal membranes results in spontaneous, and temporal control of, fusion between distinct liposome populations *in situ*. Applying this approach to a biological context, we are also able to demonstrate light directed spatiotemporal control of liposome accumulation at pre-functionalised cellular membranes *in vitro*. It should be noted, no phototoxicity, arising from the use of UV-A (365 nm) light, was observed in cell experiments. In any event, potential issues of phototoxicity can largely be alleviated through the use of longer wavelength, 2-photon excitation sources, to which o-nitrobenzyl functionalities are photosensitive.^[15] Likewise, whilst UV-A light suffers from poor tissue penetration, the use of 2-photon excitation sources enables light activation up to tissue depths of 1 cm.^[16] In conclusion, the general method described holds significant promise towards non-invasive, user-defined vector based drug and gene delivery both *in vitro* and *in vivo*.

2.4 Experimental

2.4.1 Materials and Instruments

Phospholipids used for liposomes, 1,2-dioleoyl-sn-glycero-3-phosphocholine (**DOPC**), 1,2-dioleoyl-sn-glycero-3-phosphoethanolamine (**DOPE**), 1,2-dioleoyl-sn-glycero-3-phosphoethanolamine-N-(7-nitro-2-1,3-benzoxadiazol-4-yl) (**DOPE-NBD**) and 1,2-dioleoyl-sn-glycero-3-phosphoethanolamine-N-(lissamine rhodamine B sulfonyl) (**DOPE-LR**), were purchased from Avanti Polar Lipids. Cholesterol and all other chemical reagents were purchased at the highest grade available from Sigma Aldrich and used without further purification. All solvents were purchased from Biosolve Ltd. Phosphate buffered saline (PBS): 5 mM KH_2PO_4 , 15 mM K_2HPO_4 , 150 mM NaCl, pH 7.4. Silica gel column chromatography was performed using silica gel grade 40-63 μm (Merck). TLC analysis was performed using aluminium-backed silica gel TLC plates (60F 254, Merck), visualisation by UV absorption at 254 nm and/or staining with KMnO_4 solution. NMR spectra (^1H) were measured on a Bruker AV-400MHz spectrometer. Chemical shifts are recorded in ppm. Tetramethylsilane (TMS) is used as an internal standard. Coupling constants are given in Hz. LCMS analysis was performed on a Jasco HPLC-system coupled to a Perkin Elmer Sciex API 165 mass spectrometer. MALDI-TOF mass spectra were acquired using an Applied Biosystems Voyager System 6069 MALDI-TOF mass spectrometer. α -Cyano-4-hydroxycinnamic acid (CHCA) was used as matrix in all cases. Sample concentrations were ~ 0.3 mg/ml. UV absorption spectra were measured using a Cary 3 Bio UV-vis spectrometer, scanning from 200 nm to 550 nm at 1 nm intervals. Scan rate: 120 nm/min. For the pre-irradiation of E_{PEG} -liposomes, UV light irradiation was performed using a hand-held BLAK-RAY B-100AP high intensity UV lamp (365 nm, 100 W) encased in a cardboard box. Samples were irradiated in quartz cuvettes at a fixed distance of 10 cm from the UV source. HPLC-ELSD analysis was performed using a Shimadzu HPLC setup equipped with two LC-8A series pumps coupled to a Shimadzu ELSD-LT II detection system. Separation (Vydac 214 MS C4 column, 5 μ , 100 \times 4.6 mm, flow rate: 1 mL/min), in all instances, was carried out over a linear gradient of 10-90% **B** over 20 minutes with an initial 5 min hold at 10% **B**. HPLC buffers: **A** – H_2O (0.1% TFA); **B** – Acetonitrile (0.1%

TFA). The drift tube temperature for ELSD was set at 37°C and the nitrogen flow-rate at 3.5 bar.

CPE (cholesterol-PEG₁₂-peptideE) and CPK (cholesterol-PEG₁₂-peptideK) were synthesized and purified as previously reported.^[11] Peptide sequences were (EIAALEK)₃ and (KIAALKE)₃ for E and K respectively.

Liposomes were prepared via lipid film hydration and bath sonication using a Branson 2510 Ultrasonic Cleaner. Sonication was carried out at 55°C.

Size exclusion chromatography (SEC) was carried out using illustra™ NAP™ Sephadex™ G-25 DNA grade pre-made columns (GE Healthcare) and used according to the user instructions.

Particle size distributions were obtained using a Malvern Zetasizer Nano ZS equipped with a peltier controlled thermostatic holder. The laser wavelength was 633 nm and the scattering angle was 173°. To obtain an estimation of the hydrodynamic radius, D_h , the Stokes-Einstein relation was used:

$$D = \frac{K_B T}{3\pi\eta D_h}$$

where, k_B is the Boltzmann constant and η is the viscosity of the solvent. DLS measurements were carried out at room temperature.

Fluorescence measurements for lipid and content mixing using E_{PEG}-liposomes irradiated prior to mixing with K-liposomes were performed on a TECAN Plate Reader Infinite M1000. All experiments were carried out in 96-well plates (PP Microplate, 96 well, solid F-bottom (flat), chimney well). For every experimental well the final experimental volume was 200 μ L. Fluorescent measurements were recorded at 25°C.

CD spectra were measured using a Jasco J-815 spectropolarimeter. The observed ellipticity is given in millidegrees, the conversion to the mean residue molar ellipticity is performed by the following equation:

$$[\theta] = \frac{\theta_{obs}}{lC_M N}$$

where, Θ_{obs} is the observed ellipticity, C_M , the molar total peptide concentration, l , the path length of the cuvette in cm and N , the number of amino acids per peptide. Spectra were obtained at a sample concentration of 3mM total lipids (1 mol% lipopeptide, 4 mol% photolabile cholesterol-PEG construct) in PBS in a 0.1 cm quartz cuvette. All measurements were made at room temperature. Data was collected at 0.2 nm intervals, at a scanning speed of 20 nm/min and a 1 nm bandwidth. Each spectrum was the average of 5 scans.

Helical content was determined using the following formula:

$$\text{rh} = \frac{[\theta]_{222}}{-40 \cdot 10^3 \text{ deg cm}^2 \text{ dmol}^{-1} \left(1 - \frac{4.6}{N}\right)} \times 100$$

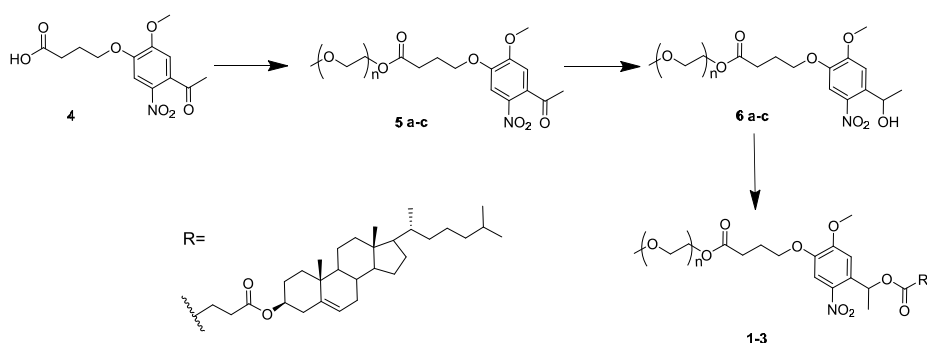
where rh is the helical fraction, Θ_{222} is the ellipticity at 222 nm and N is the number of peptide bonds.

In situ UV irradiation and simultaneous fluorescence measurements were conducted using a custom built setup. All optical parts were connected with FC-UVxxx-2 (xxx = 200, 400, 600) optical fibers from Avantes (Apeldoorn, The Netherlands), with a diameter of 200-600 μm , respectively, and were suitable for the UV-Vis range (200-800 nm). The excitation source was a continuous wave Aries 150 532 nm portable DPSS laser from LaserGlow (Toronto, ON, Canada); the power was controlled using a NDL-25C-4 variable neutral density filter (Thorlabs, Dachau/Munich, Germany) put between the laser and the sample, and was measured using a S310C thermal sensor connected to a PM100USB power meter (Thorlabs). The laser was collimated to a beam of 4 mm diameter to reach an intensity of 80 $\text{mW}\cdot\text{cm}^{-2}$ (10 mW power). The sample was held in a 104F-QS or 104F-OS semi-micro fluorescence cuvette from Hellma GmbH & Co. KG (Müllheim, Germany) in a CUV-UV/VIS-TC temperature-controlled cuvette holder (Avantes), with the long side of the cuvette perpendicular to the excitation source. Emission measurement was performed by means of a 2048L StarLine CCD spectrometer from Avantes under a 90° angle with respect to excitation. A filter holder with a NF533-17 533 nm notch filter (Thorlabs) was placed between cuvette holder and detector to reject the excitation source. For measurements involving additional illumination with UV light, a 365 nm LED (17 mW) in a custom-made mount was fitted on top of the cuvette.

HeLa cells were cultivated in Dulbecco's Modified Eagle's Medium (DMEM), supplemented with 10% fetal calf serum (iron supplied), 2% L-glutamine, 1% penicillin and 1% streptomycin. Cells were cultured in an atmosphere of 5% CO₂ at 37°C. Medium was refreshed every two days and cells passaged at 70% confluence by treatment with trypsin-EDTA (0.05% trypsin). For fluorescence assays, cells (2x10⁵ mL⁻¹) were transferred to 48-well cell culture plates (500 µL, Greiner bio-one, Cellstar®) and cultured for a further 24 h. Immediately prior to testing, the culture medium was carefully removed and the cells washed once with PBS. Fluorescence microscopy was carried out using an Olympus IX81 fluorescence microscope equipped with a filter cube (excitation: 532 – 554 nm, emission: 570 – 613 nm for visualization of DOPE-LR).

2.4.2 Synthesis of 1-3

The right structures are confirmed by both H-NMR and Maldi-TOF (Figure S1-S8).



where **a**, n=16; **b**, n=44; **c**, n=112; **1**, n=16; **2**, n=44; **3**, n=112

Scheme S1. The synthetic scheme to **1**.

4-(4-acetyl-2-methoxy-5-nitrophenoxy)butanoic acid, **4**, was synthesized as previously described.^[17] The synthesis and purification of **1-3** were, aside from the variation in PEG chain length, identical. The representative synthesis of **2** is given below. Characterisation of final compounds **1-3** is reported below.

MethoxyPEG₂₀₀₀ 4-(4-acetyl-2-methoxy-5-nitrophenoxy)butanoate, **5b**

To a stirred solution of **4** (240 mg, 0.81 mmol) in CH₂Cl₂ (5 mL) was added DMAP (98 mg, 0.81 mmol), EDCI (185 mg, 0.97 mmol), DIPEA (209 µL, 1.2 mmol) and

MeO-PEG₂₀₀₀-OH (1.20 g, 0.6 mmol). After overnight stirring, the reaction mixture was diluted with EtOAc (50 mL) and washed with sat. NaHCO₃ (3 x 50 mL) and brine (50 mL). The combined organic fractions were dried (Na₂SO₄) and solvent removed in vacuo to yield an orange powder. Column chromatography (Gradient: CH₂Cl₂ to 20% MeOH in CH₂Cl₂) afforded **5b** as a pale yellow powder (0.83 g, 0.49 mmol, 61%). *R*_f 0.45 (CH₂Cl₂:MeOH, 9:1). ¹H-NMR (CDCl₃, 400 MHz): 7.64 (s, 1H), 6.78 (s, 1H), 4.29 (m, 2H), 4.19(t, J=6 Hz, 2H), 3.99 (s, 3H), 3.45-3.89(m, 176H), 3.41 (s, 3H), 2.62(t, J=8 Hz, 2H), 2.53(s, 3H), 2.23 (m, 2H).

MethoxyPEG₂₀₀₀ 4-(4-(1-hydroxyethyl)-2-methoxy-5-nitrophenoxy)butanoate, 6b

NaBH₄ (18.9 mg, 0.5 mmol) was added to a suspension of **5b** (0.50 g, 0.22 mmol) in MeOH (5 mL). After 3 h, the reaction was acidified to pH 4 by careful addition of aq. citric acid (5% w/v). The solution was diluted with CH₂Cl₂ (100 mL) and washed with water (50 mL) and brine (50 mL). The combined organic fractions were dried (Na₂SO₄) and solvent removed in vacuo to yield **6b** as a viscous orange oil (0.45 g, 0.2 mmol, 90%). This was used without further purification. *R*_f 0.44 (CH₂Cl₂:MeOH, 9:1). ¹H-NMR (CDCl₃, 400 MHz): 7.59 (s, 1H), 7.34 (s, 1H), 5.58 (q, 1H), 4.28 (m, 2H), 4.16(t, J=6 Hz, 2H), 4.00 (s, 3H), 3.45-3.89(m, 176H), 3.41 (s, 3H), 2.61(t, J=8 Hz, 2H), 2.23 (m, 2H), 1.57 (d, J=8 Hz, 3H).

1-(5-methoxy-4-(4-(2-methoxyPEG₂₀₀₀)-4-oxobutoxy)-2-nitrophenyl)ethyl cholesteryl succinate, 2

To a stirred solution of **6b** (400 mg, 0.15 mmol) in CH₂Cl₂ (5 mL) was added DMAP (36.6 mg, 0.30 mmol), EDCI (57.5 mg, 0.30 mmol), DIPEA (78.3 μL, 0.45 mmol) and cholesteryl hemisuccinate (121 mg, 0.25 mmol). After overnight stirring, the reaction mixture was diluted EtOAc (50 mL) and washed with sat. NaHCO₃ (3 x 50 mL) and brine (50 mL). The organic fractions were combined, dried (Na₂SO₄) and solvent removed in vacuo. Column chromatography (Gradient: CH₂Cl₂ to 10% MeOH in CH₂Cl₂) afforded **2** as a colourless waxy solid (195 mg, 0.073 mmol, 50%). *R*_f 0.45 (CH₂Cl₂:MeOH, 9:1). ¹H-NMR (CDCl₃, 400 MHz): 7.60 (s, 1H), 7.06 (s, 1H), 6.49 (q, 1H), 5.37 (t, J=8 Hz, 1H), 4.60 (m, 1H), 4.28 (m, 2H), 4.12 (t, J=6 Hz, 2H), 4.01 (s, 3H), 3.45-3.95 (m, 196H), 3.41 (s, 3H), 0.69-2.66 (m, 56H).

1-(5-methoxy-4-(4-(2-methoxyPEG₇₅₀)-4-oxobutoxy)-2-nitrophenyl)ethyl cholesteryl succinate, 1

¹H-NMR (CDCl₃, 400MHz): 7.59 (s, 1H), 7.06 (s, 1H), 6.49 (q, 1H), 5.36 (t, J=4 Hz, 1H), 4.58 (m, 1H), 4.27 (m, 2H), 4.11 (t, J=6 Hz, 2H), 4.01 (s, 3H), 3.45-3.89 (m, 62H), 3.39 (s, 3H), 0.69-2.66 (m, 56H).

1-(5-methoxy-4-(4-(2-methoxyPEG₅₀₀₀)-4-oxobutoxy)-2-nitrophenyl)ethyl cholesteryl succinate, 3

¹H-NMR (CDCl₃, 400MHz): 7.60 (s, 1H), 7.06 (s, 1H), 6.49 (q, 1H), 5.38 (t, J=4 Hz, 1H), 4.61 (m, 1H), 4.27 (m, 2H), 4.12 (t, J=6 Hz, 2H), 4.01 (s, 3H), 3.45-3.90 (m, 486H), 3.40 (s, 3H), 0.70-2.75 (m, 51H).

2.4.3 Photolysis of 1

A solution of **1-3** (200 μM) in water:acetonitrile:tert-butanol (1:1:1) was irradiated (hand-held BLAK-RAY B-100AP high intensity UV lamp (365 nm, 100 W, 3-5 mW/cm²)), for 5 min, followed immediately by acquisition of the UV-visible absorption spectra. The same sample was then re-irradiated and this cycle repeated for cumulative irradiation time points of 10, 20, 30 and 60 min. The products of the photolysis reaction were analyzed by HPLC-ELSD.

2.4.4 Liposome preparation

Lipid stock solutions in chloroform (or 1:1 chloroform/methanol for CPE and CPK) were mixed and evaporated to a film under a stream of air. This film was re-hydrated with PBS (containing 10 mM sulphorhodamine B for Content Mixing assays), vortexed briefly and bath sonicated for 1-2 min at 55°C, yielding liposomes of approx. 100 nm diameter with polydispersity <0.2. For all lipid and content mixing assays the total lipid concentration in every well was 100 μM.

Lipid compositions

For lipid mixing assays:

Peptide E decorated: DOPC: DOPE: Cholesterol: DOPE-LR: DOPE-NBD: CPE (49:24.5:24.5:0.5:0.5:1 mol%).

Peptide K decorated: DOPC:DOPE:Cholesterol:CPK (49.5:24.75:24.75:1 mol%).

100% lipid mixing control: DOPC: DOPE: Cholesterol: DOPE-LR: DOPE-NBD: CPE (49.75:24.88:24.88:0.25:0.25:1 mol%).

For content mixing assays:

Peptide E decorated: DOPC:DOPE:Cholesterol:CPE (49.5:24.75:24.75:1 mol%) with 10mM sulphorhodamine B encapsulated.

Peptide K decorated: DOPC:DOPE:Cholesterol:CPK (49.5:24.75:24.75:1 mol%).

100% content mixing control: DOPC:DOPE:Cholesterol: (50:25:25 mol%) with 5 mM sulphorhodamine B encapsulated.

Following liposome formulation by sonication, peptide E decorated and the 100% control liposomes used in contents mixing assays were purified by SEC to remove unencapsulated sulphorhodamine B.

***In Situ* Modification of Peptide E decorated liposomes with PEG**

In situ modification of E-liposomes with **1-3** was carried out following procedures previously described. Briefly, hydrated and sonicated solutions of **1-3** (20 μ M) in PBS were added in equal volumes to E-decorated liposomes (200 μ M total [lipid]) in PBS and incubated for 30 min to give a final concentration of E-decorated liposomes (100 μ M total [lipid]) with varying mol% **1-3** displayed from the outer membrane leaflet. As an example, to formulate E-decorated liposomes displaying 5 mol% **1**, 500 μ L E-decorated liposomes (200 μ M total [lipid]), 250 μ L **1** (20 μ M) and 250 μ L PBS were mixed to give 1mL of 5mol% **1** E_{PEG}-liposomes (100 μ M total [lipid]).

2.4.5 Lipid mixing assay

For lipid mixing assays, NBD fluorescence (excitation wavelength: 465 nm; emission wavelength: 530 nm) was measured upon mixing fluorescent E_{PEG}-liposomes and non-fluorescent K-liposomes every 20 s for 3500 s. The 0% value was determined by measuring NBD emission of E_{PEG}-liposomes to which an equal amount of PBS (in place of K-liposomes) was added. The 100% value was determined using liposomes containing half the probe (DOPE-NBD and DOPE-LR) concentrations *i.e.* 0.25 mol%.

The percentage of fluorescence increase ($\%F_{(t)}$) was calculated as: $\%F(t)=(F(t)-F_0)/(F_{\max}-F_0)$ where $F_{(t)}$ is the fluorescence intensity measured at time, t , F_0 is the 0% fluorescence and F_{\max} is the fluorescence intensity measured on liposomes with half the fluorescent probe concentrations.

For measuring the effects of UV irradiation on the rate of lipid mixing, E_{PEG} - liposomes were irradiated for various times prior to the addition of K-liposomes.

2.4.6 Content mixing assay

For content mixing assays, the increase in fluorescence emission of sulforhodamine B (SR-B, 10 mM (self-quenching), excitation wavelength: 520 nm emission wavelength: 58 nm) encapsulated in E_{PEG} -liposomes was measured every 20 s for 3500 s upon mixing peptide E_{PEG} -liposomes and K-liposomes. The 0% value was determined by measuring SR-B emission of E_{PEG} -liposomes to which an equal amount of PBS (in place of K-liposomes) was added. The 100% value was determined using liposomes containing half the probe (SR-B) concentration (5 mM).

The percentage of fluorescence increase ($\%F_{(t)}$) was calculated as: $\%F(t)=(F(t)-F_0)/(F_{\max}-F_0)$ where $F_{(t)}$ is the fluorescence intensity measured at time, t , F_0 is the 0% fluorescence and F_{\max} is the fluorescence intensity measured for liposomes containing 5mM encapsulated SR-B.

For measuring the effects of UV irradiation on the rate of lipid mixing, E_{PEG} - liposomes were irradiated for various times prior to the addition of K-liposomes.

2.4.7 *In situ* UV irradiation and simultaneous fluorescence measurement of content mixing

E_{PEG} - and K-liposomes, prepared as above for contents mixing assays, were mixed in a cuvette (total volume; 600 μL) and fluorescence measurements taken continuously. After approximately 5 min, UV irradiation (365 nm, 15-17 mW/cm^2) above the sample was switched on and left on for the remainder of the experiment whilst simultaneously measuring the increase in SR-B fluorescence emission. The laser intensity was recorded simultaneously and all data was corrected for source intensity fluctuations.

The percentage of fluorescence increase ($\%F_{(t)}$) was calculated as: $\%F_{(t)} = (F_{(t)} - F_0) / (F_{\max} - F_0)$ where $F_{(t)}$ is the fluorescence intensity measured at time, t , F_0 is the 0% fluorescence and F_{\max} is the fluorescence intensity measured for liposomes containing 5mM encapsulated SR-B.

2.4.8 *In vitro* fluorescent assay

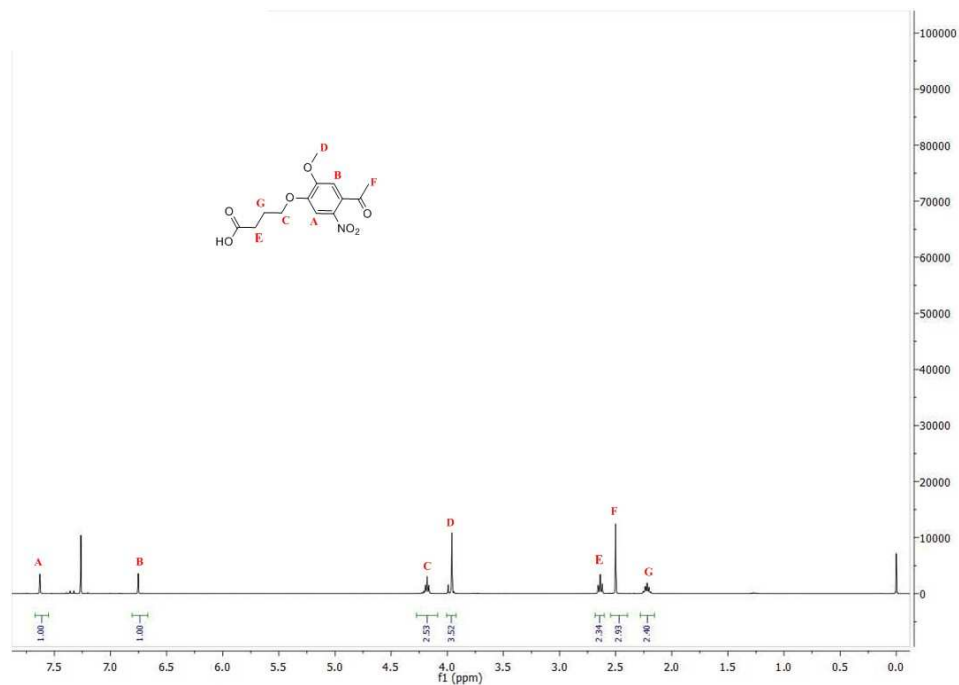
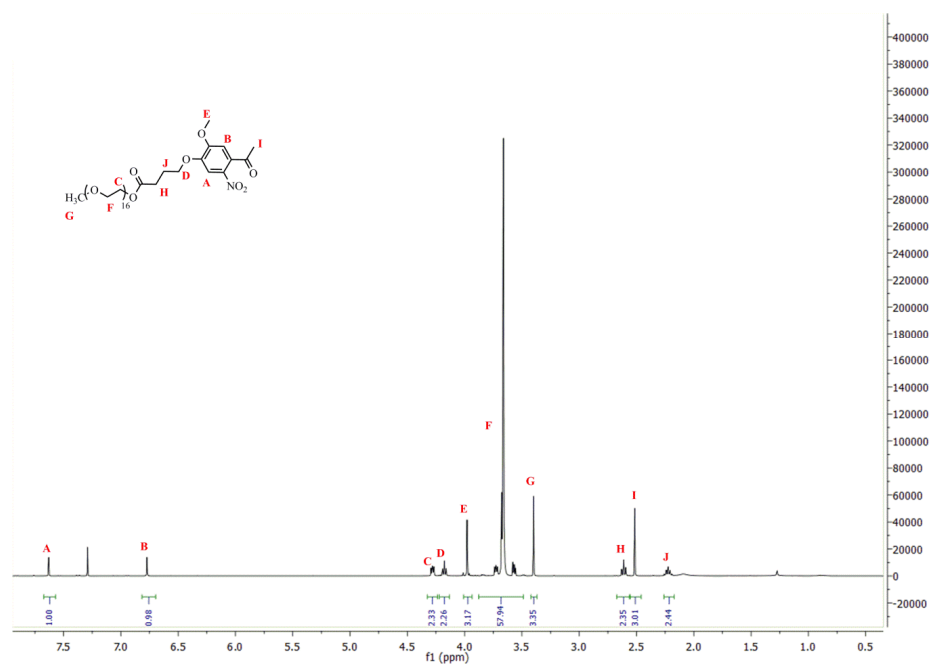
A solution of CPK was prepared by 200-fold dilution of CPK (2 mM) in DMSO with PBS, followed by a further 2x dilution with DMEM (without FCS) to give a 5 μ M CPK solution in PBS:DMEM(-FCS) (1:1). This solution (500 μ L) was added to the cell culture well and incubated for 10-15 minutes at 37 °C (5% CO₂). The CPK solution was carefully removed and the cells washed 3x with PBS:DMEM (-FCS). E_{PEG}-liposomes (500 μ L, 250 μ M, PBS:DMEM(-FCS)) containing 1 mol% CPE, 4 mol% **2**, 1 mol% DOPE-LR probe, were then added to the cells. The cells were then irradiated (365 nm, 10 min, 10 mWcm⁻¹) from directly above the well, of which half was covered with aluminum foil. Following irradiation, the cells were incubated with the E_{PEG}-liposome solution for a further 15 min. The E_{PEG}-liposome solution was then carefully removed and the cells washed 3x with PBS:DMEM (-FCS). The cells were then immediately analysed under the microscope.

2.5 References

- [1] J.E. Rothman, *Angew. Chem. Int. Ed.* **2014**, 53, 12676–12694.
- [2] L.V. Chernomordik, M.M. Kozlov, *Nat. Struct. Mol. Biol.* **2008**, 15, 675–683. (b) S. Martens, H.T. McMahon, *Nat. Rev. Mol. Cell Biol.* **2008**, 9, 543–556.
- [3] R. Jahn, T. Lang, T.C. Südhof, *Cell* **2003**, 112, 519–533.
- [4] D. Luo, W.M. Saltzman, *Nat. Biotechnol.* **2000**, 18, 33–37.
- [5] (a) H. Robson Marsden, I. Tomatsu, A. Kros, *Chem. Soc. Rev.* **2011**, 1572–1585. (b) M. Ma, D. Bong, *Acc. Chem. Res.* **2013**, 46, 2988–2997.
- [6] (a) B. van Lengerich, R.J. Rawle, P.M. Bendix, S.G. Boxer, *Biophys. J.* **2013**, 105, 409–419. (b) G. Pähler, C. Panse, U. Diederichsen, A. Janshoff, *Biophys. J.* **2012**, 2292–2303. (c) K. Meyenberg, A.S. Lygina, G. van den Bogaart, R. Jahn, U. Diederichsen, *Chem. Commun.* **2011**, 47, 9405–9407. (d) A. Kashiwada, M.T.N Takamura, E. Brandenburg, K. B. Matsuda, B. Koksche, *Chem. Eur. J.* **2011**, 17, 6179–6186. (e) A. Kashiwada, M. Tsuboi, K. Matsuda, *Chem. Commun.* **2009**, 695–697. (f) A. Kashiwada, M. Tsuboi, T. Mizuno, T. Nagasaki, K. Matsuda, *Soft Matter* **2009**, 5, 4719–4725. (g) Y-H.M. Chan, B. van Lengerich, S.G. Boxer, *Proc. Natl. Acad. Sci. U.S.A.* **2009**, 106, 979–984. (h) G. Stengel, L. Simonsson, R.A. Campbell, F. Hoök, *J. Phys. Chem. B* **2008**, 112, 8264–8274. (i) M.M. Ma, A. Paredes, D. Bong, *J. Am. Chem. Soc.* **2008**, 130, 14456–14458. (j) G. Stengel, R. Zahnand, F. Hoök, *J. Am. Chem. Soc.* **2007**, 129, 9584–9585. (k) Y. Gong, Y.M. Luo, D. Bong, *J. Am. Chem. Soc.* **2006**, 128, 14430–14431.
- [7] (a) A. Kashiwada, K. Matsuda, T. Mizuno, T. Tanaka, *Chem. Eur. J.* **2008**, 14, 7343–7350. (b) F. Nomura, T. Inaba, S. Ishikawa, M. Nagata, S. Takahashi, H. Hotani, K. Takiguchi, *Proc. Natl. Acad. Sci. U. S. A.* **2004**, 101, 3420–3425. (c) A. Richard, V. Marchi-Artzner, M.N. Lalloz, M.J. Brienne, F. Artzner, T. Gulik-Krzywicki, M.A. Guedeau-Boudeville, J-M Lehn, *Proc. Natl. Acad. Sci. U. S. A.*, **2004**, 101, 15279–15284. (d) B.J. Ravoo, W.D. Weringa, J. Engberts, *Biophys. J.* **1999**, 374–386. (e) R.A. Parente, S. Nir, F.C. Szoka, *J. Biol. Chem.* **1988**, 263, 4724–4730.
- [8] (a) H. Robson Marsden, N.A. Elbers, P.H.H. Bomans, N.A.J.M Sommerdijk, A. Kros, *Angew. Chem. Int. Ed.* **2009**, 48, 2330–2333. (b) F. Versluis, J. Voskuhl, J. Vos, H. Friedrich, B.J. Ravoo, P.H.H Bomans, M.C.A. Stuart, N.A.J.M. Sommerdijk, A. Kros, *Soft Matter* **2014**, 10, 9746–9751. (c) M. Rabe, C. Schwieger, H.R. Zope, F. Versluis, A. Kros, *Langmuir* **2014**, 30, 7724–7735. (d) M.

- Rabe, H.R. Zope, A. Kros, *Langmuir* **2015**, 31, 9953-9964. (e) T. Zheng, J. Voskuhl, F. Versluis, H.R. Zope, I. Tomatsu, H. Robson Marsden, A. Kros, *Chem. Commun.* **2013**, 49, 3649-3651.
- [9] P. Milla, F. Dosio, L. Cattel, *Curr. Drug Metab.* **2012**, 13, 105-119.
- [10] I. Tomatsu, H. Robson Marsden, M. Rabe, F. Versluis, T. Zheng, H.R. Zope, A. Kros, *J. Mater. Chem.* **2011**, 21, 18927-18933.
- [11] F. Versluis, J. Voskuhl, B. van Kolck, H. Zope, M. Bremmer, T. Albrechtse, A. Kros, *J. Am. Chem. Soc.* **2013**, 135, 8057-8062.
- [12] J.F. Stefanik, J.D. Ashley, T. Kiziltepe, B. Bilgicer, *ACS Nano* **2013**, 7, 2935-2947.
- [13] H.R. Zope, F. Versluis, A. Ordas, J. Voskuhl, H.P. Spaink, A. Kros, *Angew. Chem. Int. Ed.* **2013**, 52, 14247-14251.
- [14] L. Kou, J. Sun, Y. Zhai, Z. He, *Asian J. Pharm. Sci.* **2013**, 8, 1-10.
- [15] (a) I. Aujard, C. Benbrahim, M. Gouget, O. Ruel, J-B. Baudin, P. Neveu, L. Jullien, *Chem. Eur. J.* **2006**, 12, 6865-6879. (b) K. Peng, I. Tomatsu, B. van den Broek, C. Cui, A.V. Korobko, J. van Noort, A.H. Meijer, H.P. Spaink, A. Kros, *Soft Matter* **2011**, 7, 4881-4887.
- [16] J. A. Scherschel, M. Rubart, *Microsc Microanal.* **2008**, 14, 492-506.
- [17] B. Yan, J-C. Boyer, D. Habault, N.R. Branda, Y. Zhao, *J. Am. Chem. Soc.* **2012**, 134, 16558-16561.

2.6 Appendix

Figure S1. ¹H-NMR of 4.Figure S2. ¹H-NMR of 5a.

¹H NMR Spectrum (400 MHz, CDCl₃) of 1-(4-methoxy-3-nitrophenyl)-2-methylpropan-1-one

Chemical Structure and Proton Labels:

CC(C)C(=O)c1ccc(OC)c([N+](=O)[O-])c1

- A:** Aromatic proton (ortho to methoxy)
- B:** Aromatic proton (ortho to nitro)
- C, D:** Methyl protons of the isopropyl group
- E:** Methine proton of the isopropyl group
- F:** Methoxy protons
- G:** Aromatic proton (ortho to methoxy)
- H, I:** Aromatic protons (ortho to nitro)
- J:** Aromatic proton (ortho to methoxy)

Peak Data Table:

Label	Chemical Shift (ppm)	Integration
A	~7.3	0.08
B	~6.7	0.08
C, D	~4.0	2.74
E	~3.8	0.99
F	~3.6	9.22
G	~3.4	0.69
H, I	~2.5	1.17
J	~2.3	0.83

75

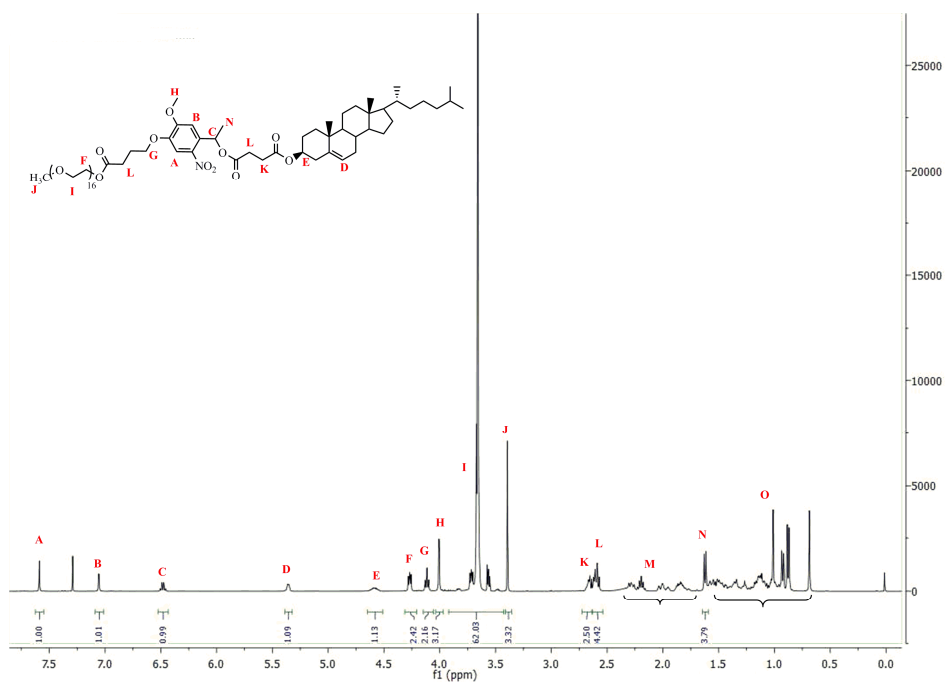


Figure S5. ^1H -NMR of 1.

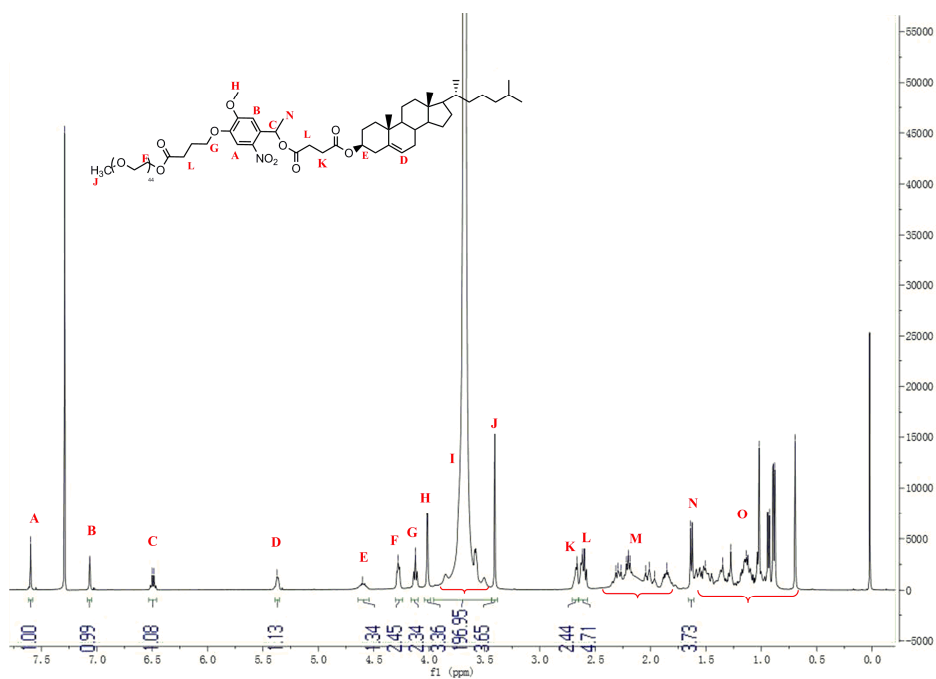


Figure S6. ^1H -NMR of 2.

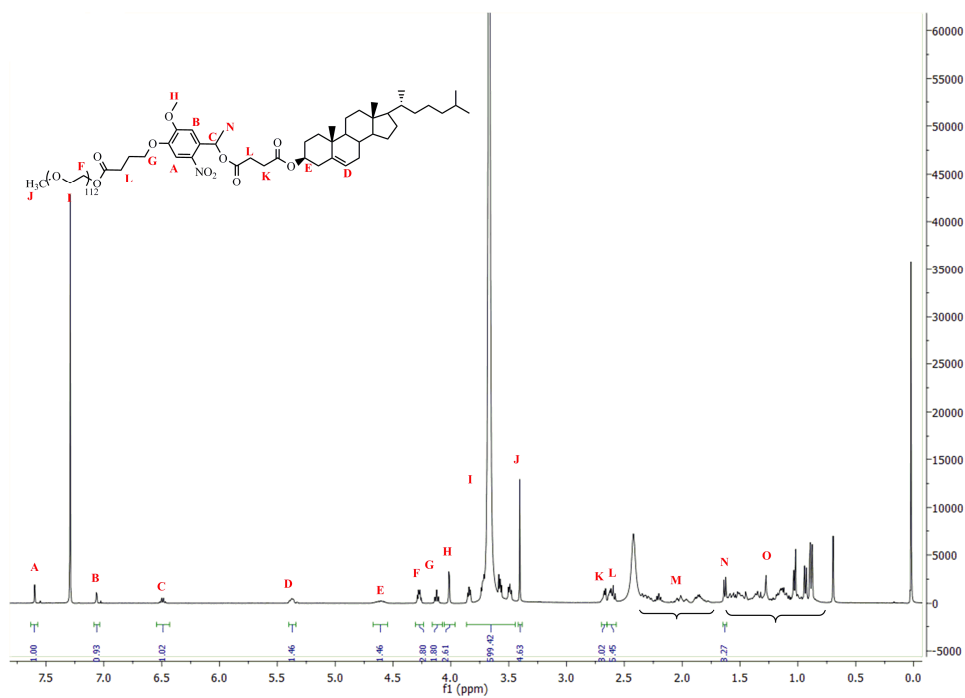
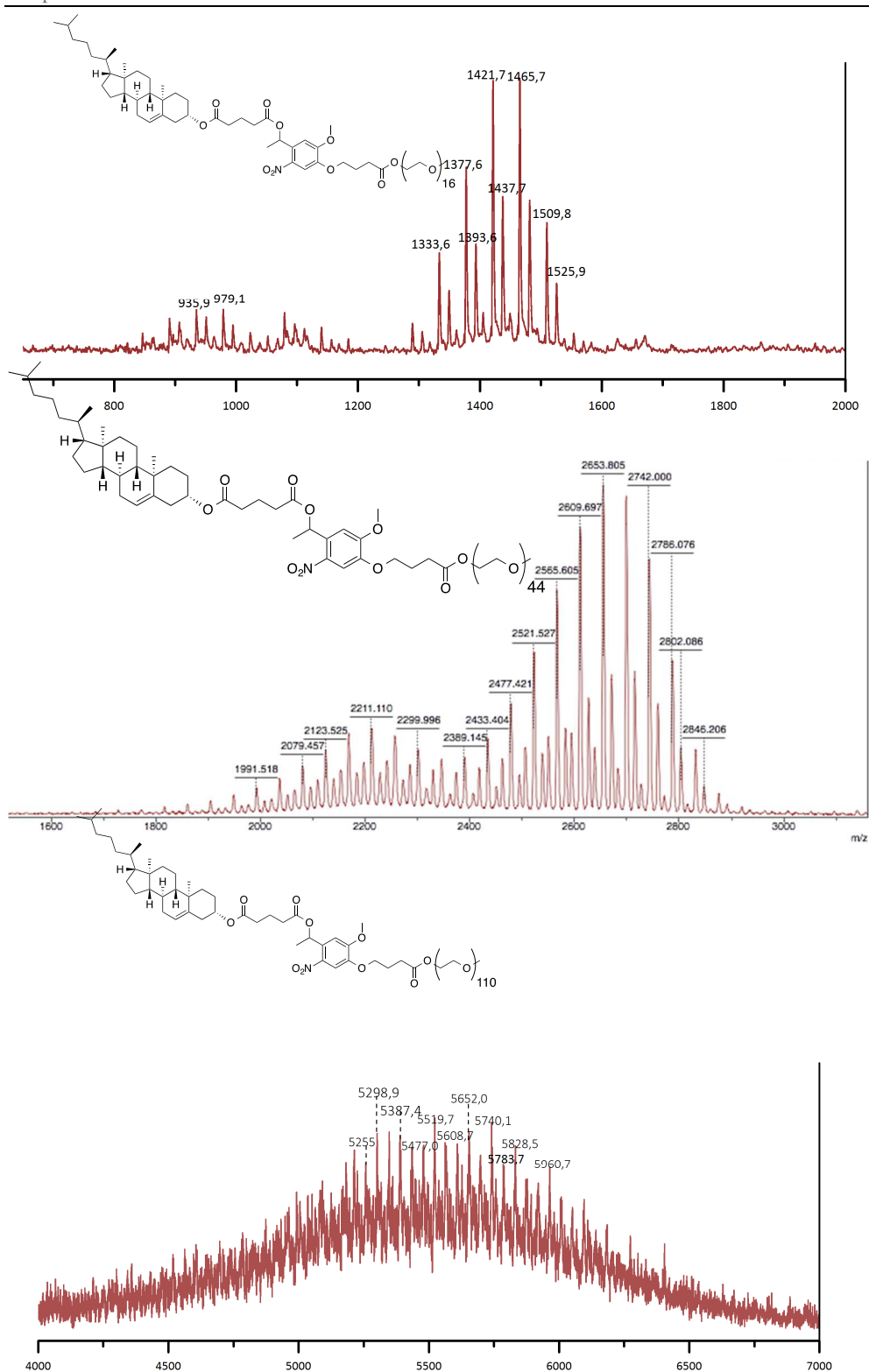


Figure S7. ^1H -NMR of **3**.

**Figure S8.** MALDI-TOF spectra of **1-3**.

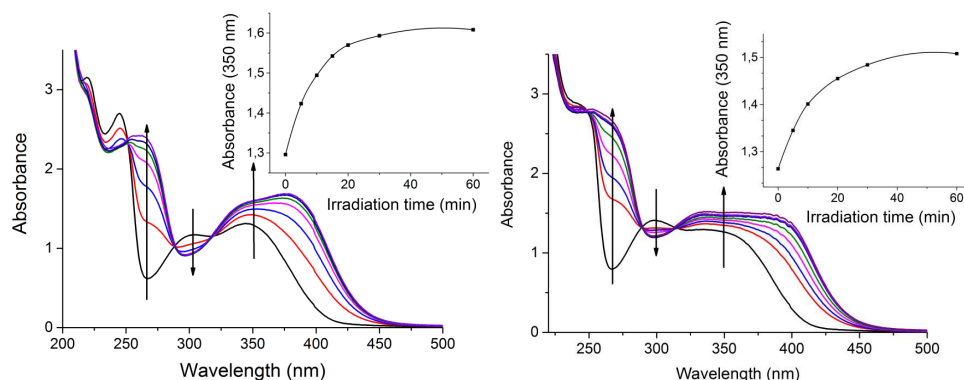


Figure S9. UV-Vis spectra of the photolysis of **1** (left) and **3** (right); all (200 μ M) in water:acetonitrile:tert-butanol (1:1:1). Inset: Reaction profile over time as a function of UV absorption at 350 nm.

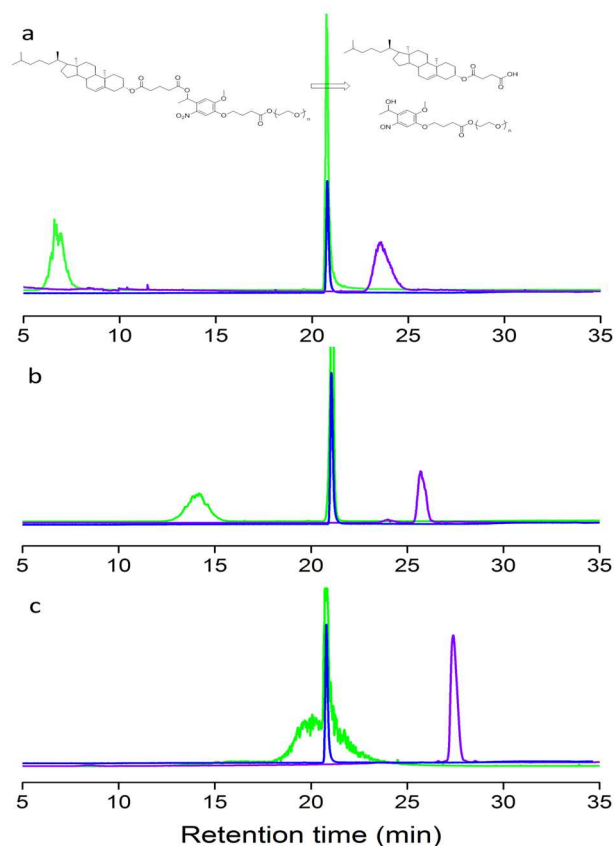


Figure S10. HPLC-ELSD traces of **1**(a), **2**(b) and **3**(c) in PBS before (magenta) and after (green) 60 min UV irradiation. HPLC-ELSD of the expected photolysis products, cholesteryl hemisuccinate (blue).

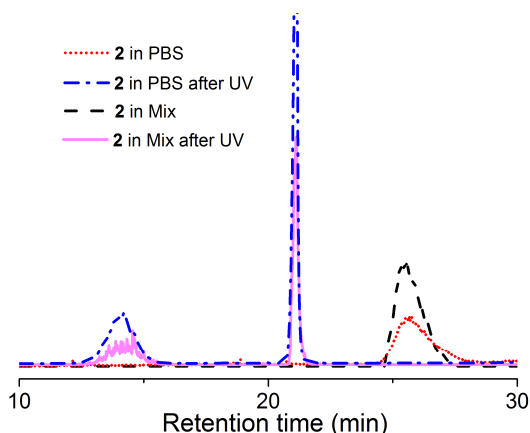


Figure S11. Comparison HPLC-ELSD traces of **2** in PBS and in water:acetonitrile:tert-butanol (1:1:1) before and after 60 min UV irradiation.

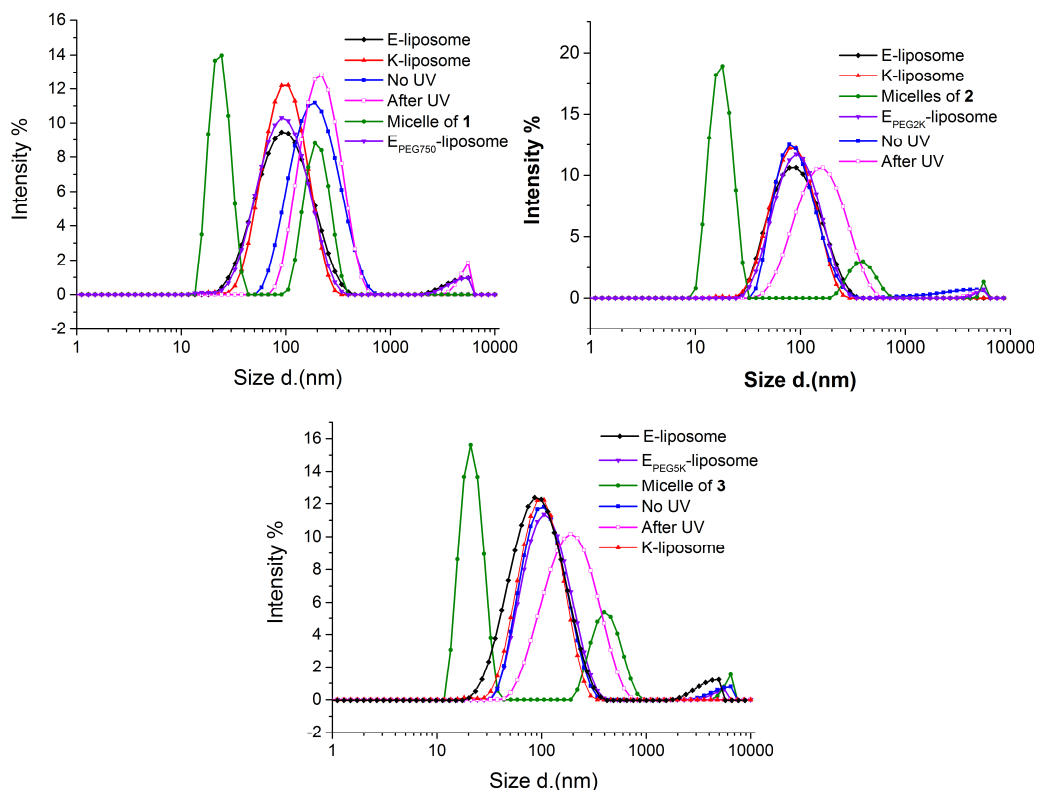


Figure S12. DLS size distributions: **1** (top), **2** (middle), **3** (bottom): **1-3** (20 μ M in PBS), E-liposomes (100 μ M in PBS) alone (black), K-liposomes (100 μ M total [lipid] in PBS) alone, post modified (4mol% **1-3**) E_{PEG}-liposomes (100 μ M total [lipid]) alone, 1:1 mixtures of (4mol% **1-3**) E_{PEG}-liposomes and K-liposomes (100 μ M total [lipid] in PBS) after 60 min, without and following 60 min UV irradiation of E_{PEG}-liposomes prior to mixing with K-liposomes.

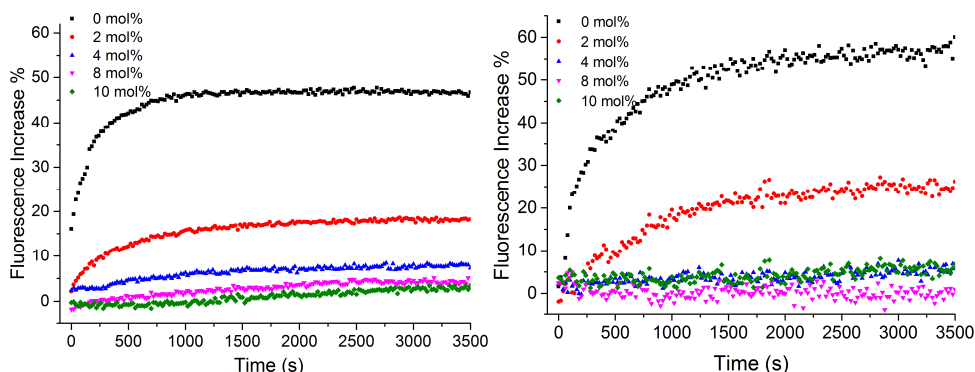


Figure S13. Lipid mixing between E_{PEG}⁻ and K-liposomes with varying amounts of **2** (left) and **3** (right) presented from the E-liposome membrane. 0, 2, 4, 8 and 10 mol%.

Table S1. CD spectra of investigated systems: mean residue molar ellipticities and helical content.

[θ] ($10^3 \text{ deg cm}^2 \text{ dmol}^{-1}$)		[θ] @222 nm	[θ] @208 nm	Helicity	[θ]222/[θ]208
K-liposomes		14,44674	-15,50488	46.2	0.93
1 (4mol%)	E _{PEG} -liposomes	-17,62973	-23,97608	56.4	0.74
	E _{PEG} ⁻ and K-liposomes (pre-irradiation)	-22,37316	-22,9173	71.6	0.97
2 (4mol%)	E _{PEG} -liposomes	-16,881	-20,74584	54.0	0.81
	E _{PEG} ⁻ and K-liposomes (pre-irradiation)	-18,37925	-22,73417	58.8	0.81
	E _{PEG} ⁻ and K-liposomes (post-irradiation)	-20,40157	-20,62402	65.3	0.99
3 (4mol%)	E _{PEG} -liposomes	-17,84379	-22,45793	57.1	0.79
	E _{PEG} ⁻ and K-liposomes (pre-irradiation)	-17,40497	-22,34921	55.7	0.78
	E _{PEG} ⁻ and K-liposomes (post-irradiation)	-20,86163	-20,00899	66.8	1.04

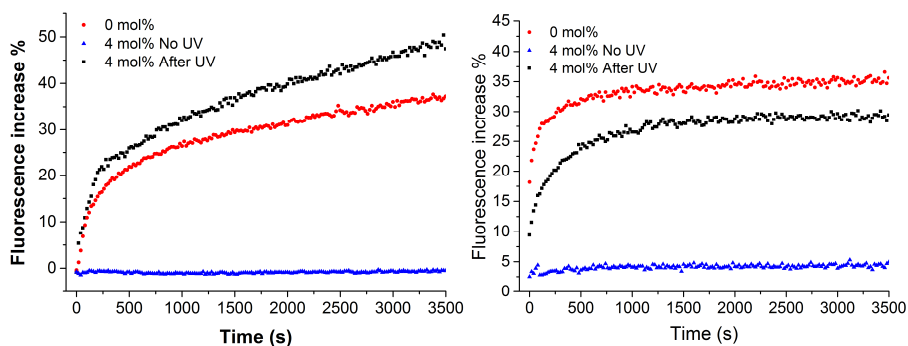


Figure S14. Content mixing of E_{PEG}- and K-liposomes with 0 mol% and 4 mol% **2** (left), **3** (right) presented from the E-liposome membrane, in the absence of UV irradiation and following 60 min prior UV irradiation of E_{PEG}-liposomes.

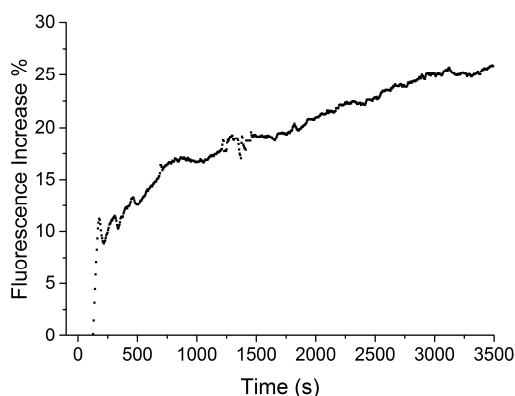


Figure S15. Simultaneous and continuous UV irradiation and monitoring of content mixing between E- and K-liposomes (in the absence of **1-3** presented from the E-liposome membrane).

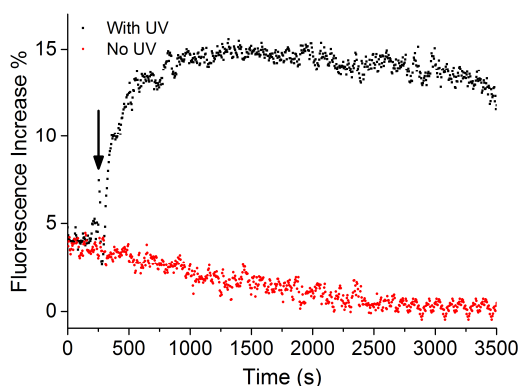


Figure S16. *In situ* photolysis of E_{PEG}-liposomes (4 mol% **3**) and consequent content mixing with K-liposomes, upon (---) and in the absence of (---) UV irradiation.

3

Spatiotemporal Control of Doxorubicin Delivery from “Stealth-Like” Prodrug Micelles

Abstract: In the treatment of cancer, targeting of anticancer drugs to the tumor microenvironment is highly desirable. Not only does this imply accurate tumor targeting but also minimal drug release *en route* to the tumor and maximal drug release once there. Here we describe high-loading, “stealth-like” doxorubicin micelles as a pro-drug delivery system, which upon light activation, leads to burst-like doxorubicin release. Through this approach, we show precise spatiotemporal control of doxorubicin delivery to cells *in vitro*.

3.1 Introduction

Doxorubicin (DOX) is a potent cytotoxic drug used in the clinical treatment of many human cancers. Administered alone, and with no inherent cell selectivity, the clinical efficacy of DOX is however hampered by off-target cardiotoxicity.^[1] This limits the cumulative patient lifetime dose of DOX to just 550 mg/m², irrespective of therapeutic success.^[2] Considerable efforts have been made to improve the therapeutic index of DOX by localizing its extracellular release to the tumor microenvironment alone. Typically, this involves chemical modification or vector entrapment of DOX (*e.g.* within long-circulating liposomes). Within these systems, strategies to enhance tumor targeting and/or local DOX release include the use of active targeting ligands,^[3] steric shielding (*e.g.* PEGylation) of DOX carriers,^[4] exploitation of endogenous (*e.g.* low pH within the tumor environment) and exogenous (*e.g.* heat, magnetism, ultrasound or light) stimuli,^[5] and combinations thereof.^[6]

Of these various approaches, the passive targeting of liposome-entrapped DOX to tumors remains the only strategy approved for clinical use. Liposomal-DOX formulations (*e.g.* Myocet®, Doxil®) are used to treat a variety of malignant human cancers, including select breast and ovarian cancers, multiple myeloma and AIDS-related Kaposi's sarcoma. These liposome formulations, optimally 100 nm in size and administered systemically, are designed to passively accumulate within the tumor via the enhanced permeability and retention (EPR) effect. This phenomenon is characterized by the ill-defined ("leaky") vasculature and poor lymphatic drainage of many tumor pathologies.^[7] Through this approach high local concentrations of DOX are achieved within the tumor following prolonged and passive drug leakage across the liposome membrane. For this strategy to be effective, liposomes with long circulation lifetimes are sought. Care must therefore be taken to balance the conflicting need to both minimize DOX leakage *en route* to the tumor while ensuring therapeutically relevant concentrations are released once there. Drug retention and release profiles can be fine-tuned through judicious choice of drug-to-lipid ratios and liposome lipid composition, and circulation lifetimes can be increased through steric shielding (typically PEGylation) of the liposome surface (to create 'stealth' liposomes)

^[4], however finding the necessary balance between drug retention and release is an intrinsic limitation of these nanoparticle systems.^[8]

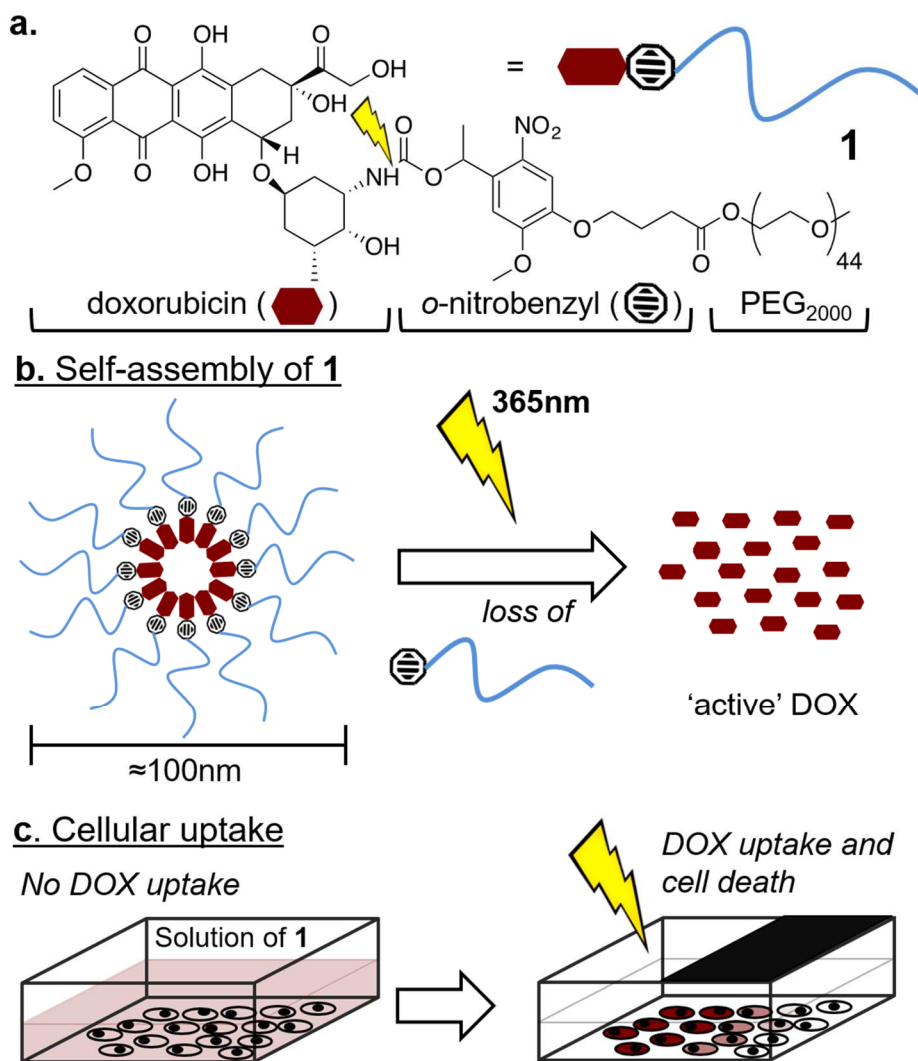


Figure 1. Light activated doxorubicin pro-drug micelles. (a) Doxorubicin-ortho-nitrobenzyl-mPEG2000 construct, **1**; (b) Self-assembly of **1** in aqueous media to 100 nm PEGylated and DOX (doxorubicin)-rich micelles from which quantitative drug release is triggered by light; (c) Light directed DOX release, cell uptake, and cell death.

In this chapter, we describe light activated, DOX-rich (20 wt% drug loading) micelles, which prior to light activation, share analogous physicochemical properties (size, morphology, surface chemistry) to those of long circulating liposomal-DOX

formulations. Crucially however we observe no premature DOX release (and therefore cytotoxicity) in the absence of light. Upon light activation, quantitative drug release is achieved (Figure 1). These properties represent a significant technological improvement over analogous DOX-PEG prodrug systems triggered by tumor-specific, endogenous stimuli (pH,^[9] reduction,^[10] enzymatic^[11]), for which DOX release is typically slow (hours) and incomplete, as well as those reliant on external stimulus, such as light,^[12] for which reported physicochemical properties (size, morphology, surface chemistry) preclude long circulation lifetimes necessary for efficient tumor accumulation via the EPR effect.

3.2 Results and discussion

The synthesis and characterisation of photoactivatable DOX-ortho-nitrobenzyl-PEG construct, **1**, is described in the experimental section. Self-assembly of **1** in aqueous media resulted in particles with mean hydrodynamic diameters of 100 nm and ranging in size from 30 to 300 nm (PDI 0.25, Figure S7). TEM (transmission electron microscopy) measurements revealed “loose” core-shell micelle structures in which the nanoparticle core appears electron-rich (high contrast) and likely contains DOX (Figure 2a). Similar morphologies have been reported for analogous DOX-PEG assemblies.^[9] The critical micelle concentration (CMC) of self-assembled micelles of **1** was determined to be 9.2 μM (approx. 25 $\mu\text{g/mL}$, Figure 2b) and particles were stable over time, over a range of concentrations and diluted in complete cell culture media (Figure S7). Upon low power UV irradiation (365 nm, 3–5 mW/cm^2), complete photolysis of self-assembled **1** to pharmacologically “active” DOX was achieved within 25 min, however significant DOX release was observed following just 5 min low-power UV irradiation (Figure 2c). Drug release was quantitative and importantly, no premature leakage of DOX was observed in the absence of light activation (Figure 2d).

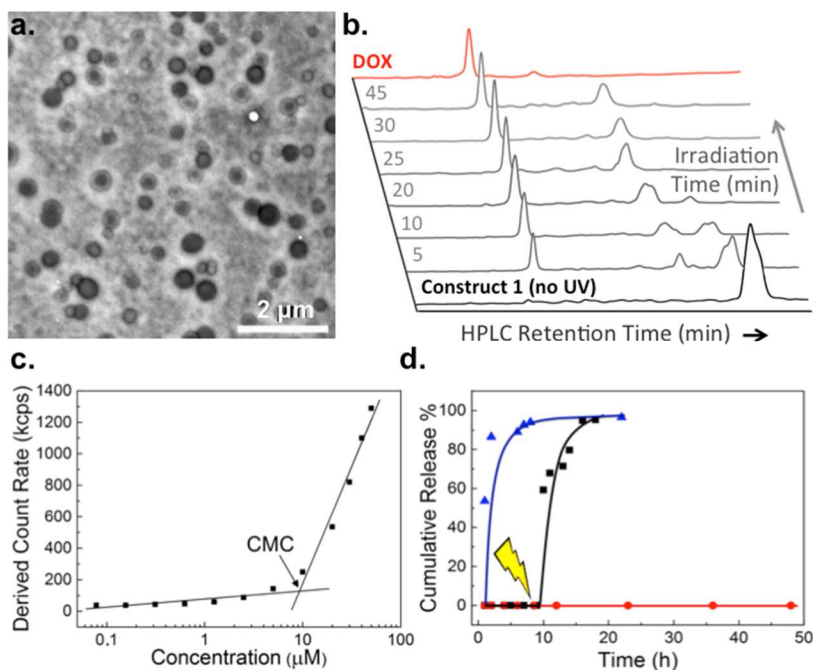


Figure 2. Characterization of doxorubicin pro-drug micelles and light induced drug release. (a) TEM image (uranyl acetate stain) of micelles of **1** (300 μM , approx. 0.7 mg/mL); (b) Time evolution of the HPLC spectra of a solution of **1** (100 μM in PBS) during photolysis (365 nm, 3–5 mW/cm²). Free DOX (100 μM), dissolved in PBS, was used to confirm clean photolysis of **1** to release “active” DOX. HPLC conditions described in Materials and Methods; (c) CMC (critical micelle concentration) determination by light scattering following serial dilution of **1** (100 μM –75 nM) in PBS; (d) *In vitro* DOX release profiles from **1** (300 μM) in PBS. No UV irradiation (red), UV irradiation at 9 h (black) and free DOX control (blue).

Next, the cytotoxicity of **1** was assessed against cancer (HeLa) cells *in vitro*. While the measured IC₅₀ value of free DOX was 3 μM , **1** showed no cytotoxic effect up to the highest concentration tested (100 μM) in the absence of light (Figure 3a). Upon light activation (365 nm, 15–17 mW/cm²) however, DOX induced cytotoxicity correlated, as expected, with both increased concentrations of **1** as well as increasing irradiation time (Figure 3b).

Importantly, UV-A light induced cytotoxicity (due to UV-A induced oxidative stress),^[13] only resulted in significant cell death following > 30 min continuous irradiation (Figure 3b, pink line, and Figure S8). This is significantly longer than the irradiation time

required to release effective concentrations of DOX (released from 20 μM solutions of **1**) achieving > 50% cell death. It is also important to note, below its CMC (9.2 μM), the cytotoxicity of **1** was also insignificant. While this is likely due to the membrane impermeability of individual DOX-PEG constructs, these systems will no longer exist as nanoparticle assemblies and will likely demonstrate very different *in vivo* pharmacokinetic profiles (*i.e.* low vascular retention, rapid renal filtration) compared to 100 nm micelles of **1**.^[14]

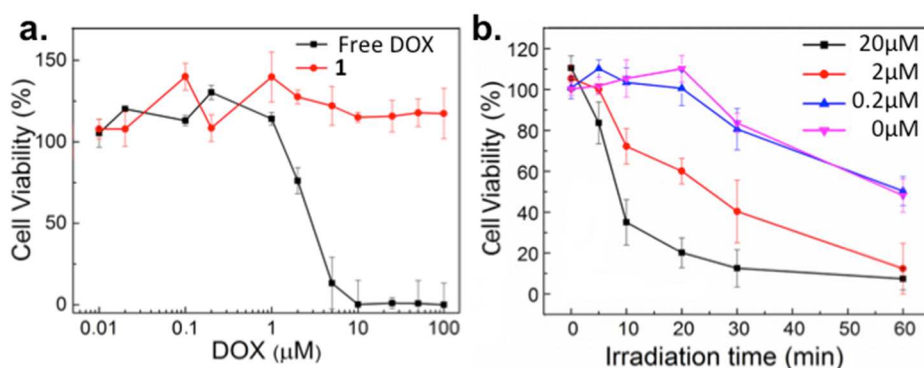


Figure 3. Viability of HeLa cells *in vitro* treated with doxorubicin pro-drug micelles. (a) Cell viability following incubation with varying concentrations (10 nM–100 μM) of free DOX (**black**) and **1** (**red**) in the absence of light; (b) Viability of HeLa cells *in vitro* treated with varying concentrations of **1** and irradiated (365 nm, 15–17 mW/cm^2) for up to 1h. Pink line corresponds to photoinduced cytotoxicity.

Increasing DOX cellular uptake with increasing time of light activation of **1** was confirmed by FACS analysis (Figure S9) and to demonstrate the precision afforded by the described DOX delivery prodrug system, micelles of **1** were first incubated with cells then UV light applied over just half the well plate (Figure 4a). The result was clear spatial delineation of DOX cellular uptake *in vitro* (Figure 4b), highlighting not only efficient photolysis of **1** but also rapid cellular uptake of DOX once released.

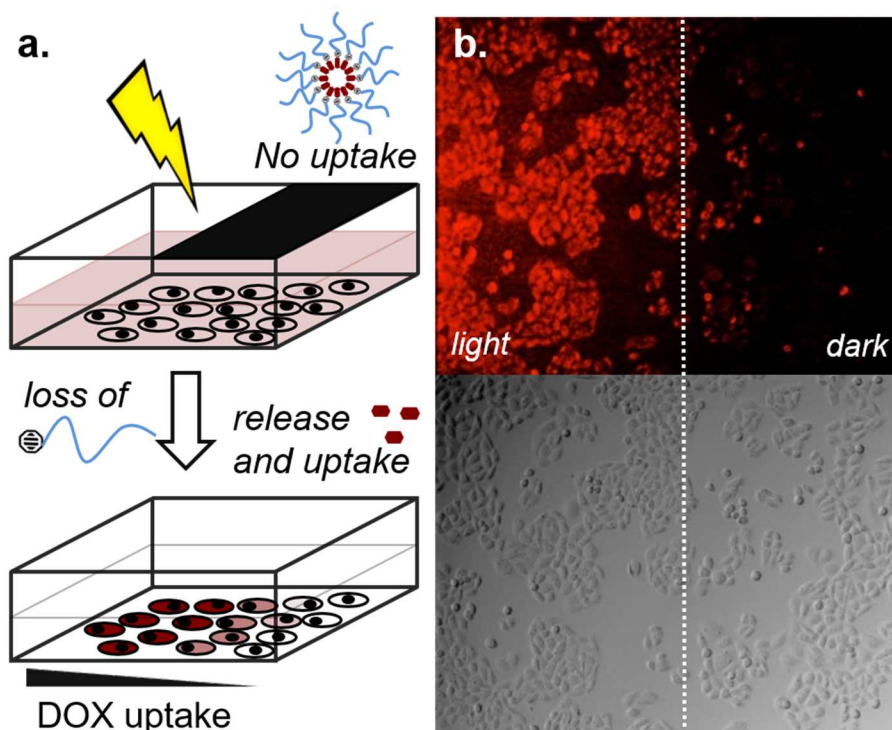


Figure 4. Light templated doxorubicin delivery *in vitro*. Patterned light (365 nm, 15–17 mW/cm²) activation of **1** (300 μ M) and cellular uptake of DOX (**red**).

3.3 Conclusions

Here we demonstrate rapid and quantitative release of DOX from self-assembled micelles of **1** triggered by light. Prior to light activation, DOX-PEG conjugate based micelles are not cytotoxic, do not release DOX prematurely and share near identical physicochemical character to that of marketed and long-circulating liposome-DOX formulations (*e.g.* Doxil®). Towards tumor targeting of DOX *in vivo*, it is envisaged that micelles of **1**, administered systemically, will first passively accumulate within the tumor microenvironment via the EPR effect whereupon drug release could be triggered by light, on demand. Given the limited tissue penetration of single photon UV light, options to apply UV light to tumors residing deep within the body include the use of fiber-optic endoscopic techniques^[15] or 2-photon light activation.^[16] Alternatively, strategies rendering this system sensitive to longer wavelength, single photon, near-infrared (NIR) light can be considered.^[17] Future studies will focus on the

application of these micelles *in vivo* and their potential use as an anti-cancer drug delivery system. In particular, care must be taken to maintain the concentration of **1** above the CMC following dilution in blood (approximately 5 L for an adult human).^[18] For the system described, this equates to an injected dose of > 130 mg/5L of **1**—approximately 30 mg DOX. This figure is below the FDA recommended dosage for DOX·HCl (40–60 mg/m² administered every 21–28 days) currently used in the treatment of a wide range of human cancers.

3.4 Experimental

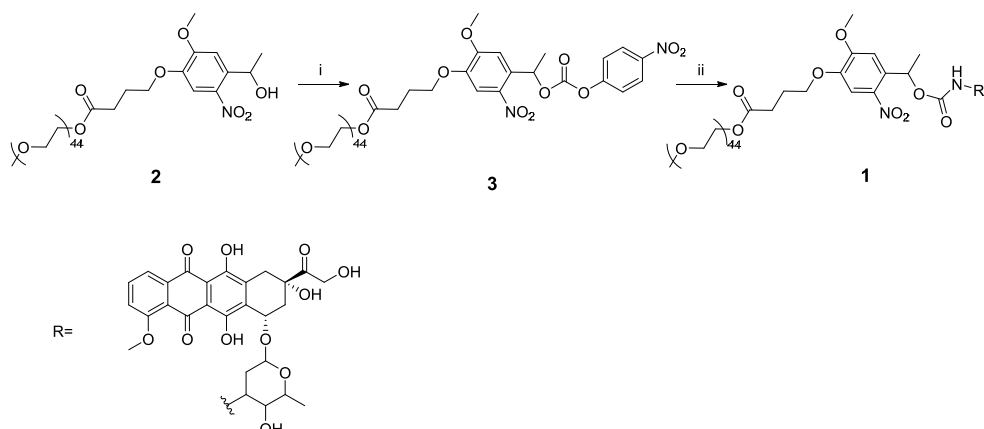
3.4.1 Materials and Instruments

Doxorubicin hydrochloride (DOX·HCl) was purchased from Cayman Chemical Company (Ann Arbor, MI, USA) and used without further purification. All other chemical reagents were purchased from Sigma-Aldrich (Zwijndrecht, Netherlands) and used without further purification. All solvents were purchased from Biosolve Ltd (Valkenswaard, Netherlands). Phosphate buffered saline (PBS): 5 mM KH_2PO_4 , 15 mM K_2HPO_4 , 150 mM NaCl, pH 7.4. Silica gel column chromatography was performed using silica gel grade 40–63 μm (Merck & co., Amsterdam, Netherlands). TLC analysis was performed using aluminum-backed silica gel TLC plates (60F254, Merck, Amsterdam, Netherlands), visualization by UV absorption at 254 nm and/or staining with KMnO_4 solution. NMR (nuclear magnetic resonance) spectra were measured on a AV-400MHz spectrometer (Bruker Nederland BV, Leiderdorp, MA, USA). Chemical shifts are recorded in ppm. Tetramethylsilane (TMS) is used as an internal standard. Coupling constants are given in Hz. LCMS analysis was performed on a Nanoacquity UPLC system-Synapt G2Si mass spectrometer (Waters Corporation, Milford, MA, USA) operating MassLynx software. Separation (Acquity UPLC M-Class 300 μm \times 50 mm column, packed with BEH C4 material of 1.7 μm diameter and 300Å pore size particles, flow rate: 2 $\mu\text{L}/\text{min}$; Waters Corporation, Milford, MA, USA) was carried out over a linear gradient of 10–90% **B** over 20 min. Buffers: **A**— H_2O (0.1% Formic Acid); **B**—Acetonitrile (0.1% Formic Acid). Electro-spray ionization (ESI) via Nano-spray source with ESI emitters (New Objective Inc., Woburn, MA, USA) fused silica tubing 360 μm OD \times 25 μm ID tapered to 5 ± 0.5 μm (5 nL/cm void volume). MS (mass spectrometry) settings (positive resolution mode): source temperature of 80 °C, capillary voltage 4.5 kV, nano flow gas of 0.25 Bar, purge gas 250 L/h, trap gas flow 2.0 mL/min, cone gas 100 L/h, sampling cone 25 V, source offset 25, trap CE 32 V, scan time 3.0 sec, mass range 400–2400 m/z . Lock mass acquiring was done with a mixture of Leu-Enkephalin (556.2771) and [Glu1]-fibrinopeptide B (785.84265), lockspray voltage 3.5 kV, [Glu1]-fibrinopeptide B fragmentation was used as calibrant. MaxEnt 1 was used for mass deconvolution of the envelopes (Cambridge, UK). HPLC (high-performance liquid chromatography) analysis was performed using a Shimadzu

HPLC setup equipped with two LC-8A series pumps (Shimadzu Europa GmbH, 's-Hertogenbosch, Netherlands). Separation: Prep (Kinetex EVO, C18 column, 5u, 150 × 21.2 mm, flow rate: 15 mL/min; Phenomenex B.V., Utrecht, Netherlands), analytical (Vision HT, C18 column, 5 u, 150 × 4.6 mm, flow rate: 1 mL/min; Phenomenex B.V., Utrecht, Netherlands), in all instances, was carried out over a linear gradient of 10–95% **B** over 25 min with an initial 5 min hold at 10% **B**. HPLC buffers: **A**—H₂O (0.1% TFA); **B**—Acetonitrile (0.1% TFA). UV detection at 254 nm.

For experiments not involving cells, UV light irradiation was performed using a hand-held BLAK-RAY B-100AP high intensity UV lamp (365 nm, 100 W; Fisher Scientific, Hampton, NH, USA) encased in a cardboard box. Samples were irradiated in quartz cuvettes at a fixed distance of 10 cm from the UV source. For all cell experiments, UV light irradiation was performed using a high-power LED (365 nm, 15–17 mW/cm², Roithner Laser Technik GmbH, Vienna, Austria) mounted at a fixed distance of 1 cm above the cells.

3.4.2 Synthesis of 1



Scheme S1. Synthetic scheme to **1**. (i) 4-nitrophenylchloroformate, Et₃N, CH₂Cl₂. (ii) Et₃N, DMF.

MethoxyPEG₂₀₀₀ 4-(4-(1-hydroxyethyl)-2-methoxy-5-nitrophenoxy)butanoate (2) was synthesized as the method in chapter 2.

MethoxyPEG₂₀₀₀ 4-(2-methoxy-5-nitro-4-(1-(((4-nitrophenoxy)carbonyl)oxy)ethyl)phenoxy)butanoate, 3

To a stirred solution of **2** (500 mg, 0.22 mmol) and 4-nitrophenyl chloroformate (265

mg, 1.31 mmol, 6 eq.) in CH_2Cl_2 (20 mL) was added Et_3N (305 μL , 2.19 mmol, 10 eq.). The reaction mixture was stirred at room temperature in the dark overnight. Following solvent removal *in vacuo*, purification by column chromatography (*Gradient*: CH_2Cl_2 to 15% MeOH in CH_2Cl_2) afforded **3** (278 mg, 0.11 mmol, 52%) as a yellow powder. **R_f**: 0.30 (CH_2Cl_2 :MeOH; 12:1). ¹**H-NMR** (CDCl_3 , 400 MHz): 8.26 (d, $J = 8$ Hz, ArH-*o*-NO₂, 2H); 7.61 (s, ArH-*o*-NO₂, 1H); 7.35 (d, $J = 8$ Hz, ArH-*m*-NO₂, 2H); 7.11 (s, ArH-*m*-NO₂, 1H); 6.52 (q, $J = 8$ Hz, CH(CH₃)OCO, 1H); 4.26 (m, COOCH₂CH₂O, 2H); 4.14 (t, $J = 8$ Hz, OOCCH₂CH₂CH₂O, 2H); 4.00 (s, CH₃O, 3H); 3.45-3.95 (m, OCH₂CH₂, 196H); 3.32 (s, CH₃OCH₂CH₂O, 3H); 2.59 (m, CH₂CH₂CH₂O, 2H); 2.19 (m, COOCH₂CH₂O, 2H); 1.78 (d, $J = 8$ Hz, CH(CH₃)OCO, 3H).

MethoxyPEG₂₀₀₀4-(4-(1-(((3-hydroxy-2-methyl-6-(((1S,3S)-3,5,12-trihydroxy-3-(2-hydroxyacetyl)-10-methoxy-6,11-dioxo-1,2,3,4,6,11hexahydrotetracen-1-yl)oxy)tetrahydro-2H-pyran-4yl)carbamoyl)oxy)ethyl)-2-methoxy-5-nitrophenoxy)butanoate, 1

To a stirred solution of **3** (86 mg, 0.034 mmol) and doxorubicin.HCl (20 mg, 0.037 μmol) in DMF (500 μL) was added Et_3N (47.2 μL , 0.34 mmol, 10 eq.). The reaction mixture was stirred at RT in the dark overnight. CH_2Cl_2 (20 mL) was then added to the reaction mixture and the solution washed with brine (15 mL). The organic fraction was dried (Na_2SO_4) and solvent removed *in vacuo*. Column chromatography (*Gradient*: CH_2Cl_2 to 2% MeOH in CH_2Cl_2 to 10% MeOH in CH_2Cl_2) yielded **1** (58.1 mg, 61%) as a red powder. **R_f**: 0.20 (CH_2Cl_2 :MeOH; 12:1). ¹**H-NMR** (CDCl_3 , 400 MHz): Partial peak assignment annotated in S3. ¹H-NMR of DOX with partial peak assignment included in S2. **MS** – despite numerous attempts to characterize this compound (MALDI, ESI), MS data was inconclusive – most likely due to compound instability and/or poor ionization of this compound during mass spec analysis. Following UV irradiation however, the MS of the photolysis products could be clearly detected (Figure S5 and S6). These products – nitroso-PEG and DOX – can only arise from the photolysis of **1**.

3.4.3 Preparation and Characterization of Light-Activated DOX-PEG Prodrug Micelles

Micelles of **1** were prepared via thin film hydration followed by sonication. Bath sonication (Branson 2510 Ultrasonic Cleaner, Branson Ultrasonics, Danbury, CT, USA) was carried out at 50 °C for 5 min. Particle size distributions were determined using a

Malvern Zetasizer Nano ZS (Malvern Instruments Ltd, Malvern, UK) equipped with a peltier controlled thermostatic holder, a fixed wavelength at 633 nm and scattering angle of 173°. DLS measurements were carried out at room temperature. For TEM observation, a drop of **1** (300 µM) was placed onto a nitrocellulose membrane covered TEM copper grid and dabbed dry through the underside of the grid with a tissue. This was then washed three times with ddH₂O. A drop of uranyl acetate (2% w/v) in H₂O was then added and the sample left to dry in the dark. Transmission electron microscopy (TEM JEOL 1010; *JEOL Ltd.*, Tokyo, Japan; Nieuw-Vennep, Netherlands) was run at an accelerating voltage of 60 kV.

3.4.4 *In vitro* Drug Release

To monitor the release profile of DOX following light irradiation, 1 mL of **1** (300 µM, > CMC) in PBS were placed in dialysis tubing (MWCO: 3.5 KDa) and dialyzed against 10 mL of dialysis buffers (PBS + 0.5% (w/w) Tween 80). At various time intervals, 3.0 mL of dialysis buffer was removed and replaced with fresh buffer. The amount of free DOX was quantified by UV–Vis absorbance measurements at 480 nm. To monitor light activated release of DOX, a sample of **1** was removed from the dialysis tubing at 9 h and irradiated for 30 min. This solution was returned to the dialysis tubing and the experiment continued. As a positive control, free DOX (300 µM) in PBS was subjected to the identical experimental conditions.

3.4.5 WST Cell Proliferation Assay

HeLa cells were seeded in 96-well plates at a density of 10000 cells per well and incubated overnight. Cells were washed once with PBS, then micelles of **1** (100 µL, varying concentrations in 1:1 PBS:DMEM+FCS), free DOX solutions (100 µL varying concentrations in 1:1 PBS:DMEM+FCS) or DMEM+FCS alone (100 µL) were added and the cells incubated for 12 h. Cells were then washed three times (DMEM+FCS), fresh DMEM+FCS added and incubated for a further 24 h. Cell media was removed and 200 µL Cell Proliferation Reagent; WST-1 (Sigma Aldrich, Zwijndrecht, Netherlands) added to each well. Cells were incubated (37 °C) for a further 3 h, according to the supplier guidelines. To determine cell viability, absorbance at 450 nm was measured. All experiments were carried out in quadruplicate.

3.4.6 FACS Analysis

HeLa cells were incubated with **1** (300 μ M in PBS, > CMC) for 30 min then irradiated (365 nm, 15–17 mW/cm²) for 15 min. Following irradiation, the solution was carefully removed, cells washed with PBS, trypsinized and immediately analyzed by flow cytometry. Counting and characterization was performed by measuring 10,000 events in triplicate and concatenation of this data. For manual gating, the outermost ring of the dot plot was selected. Quadrants were manually selected to illustrate fluorescence plots. No compensation was required.

3.4.7 Light Templated DOX Delivery to Cells

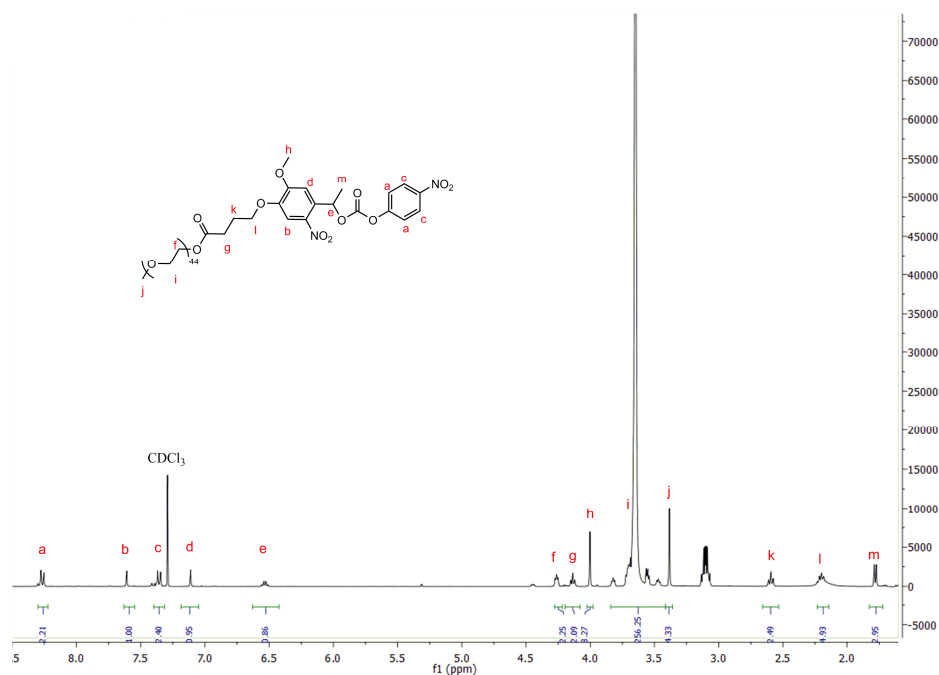
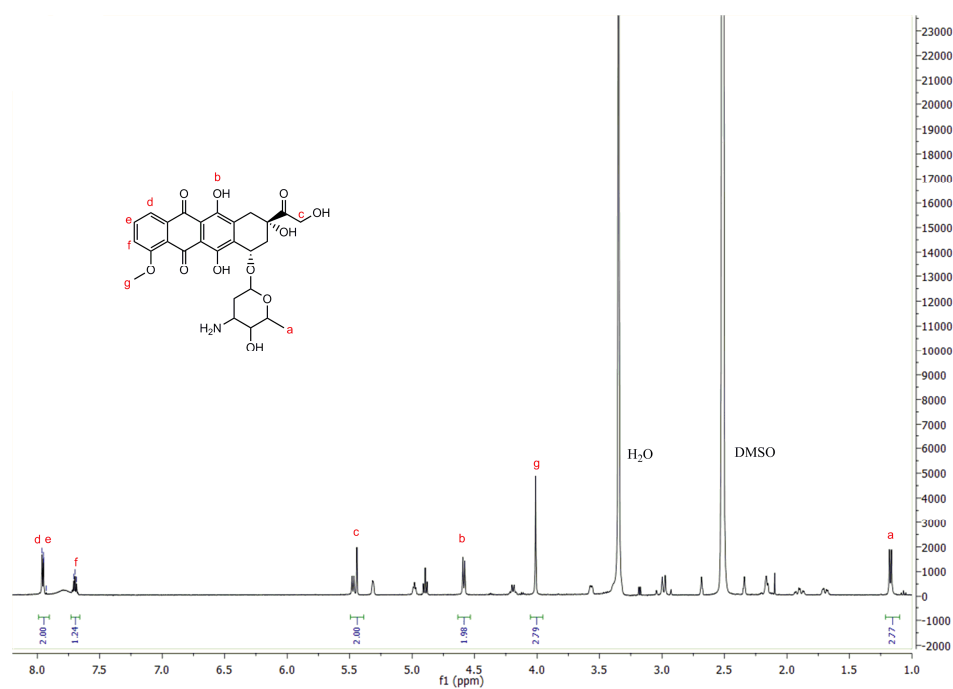
HeLa cells were seeded in 24-well plates (6 \times 10⁴ cells per well) and incubated overnight. Cells were washed once with PBS, then micelles of **1** (300 μ M in PBS, > CMC) added and incubated for 30 min. Next, half of the well was covered with aluminum foil followed by UV irradiation (365 nm, 15–17 mW/cm²) from above for 15 min. Following irradiation, the solution was carefully removed, cells washed (3 \times DMEM+FCS) and immediately analyzed under the fluorescence microscope.

3.5 References

- [1] Chatterjee, K.; Zhang, J.; Honbo, N.; Karliner, J.S. *Cardiology* **2010**, 115, 155–162.
- [2] Swain, S.M.; Whaley, F.S.; Ewer, M.S. *Cancer* **2003**, 97, 2869–2879.
- [3] Byrne, J.D.; Betancourt, T.; Brannon-Peppas, L. *Adv. Drug Deliv. Rev.* 2008, 60, 1615–1626.
- [4] Immordino, M.L.; Dosio, F.; Cattel, L., *Int. J. Nanomed.* **2006**, 1, 297–315.
- [5] Du, J.; Lane, L.A.; Nie, S., *J. Control. Release* **2015**, 219, 205–214.
- [6] Torchilin, V.P., *Nat. Rev. Drug Discov.* **2014**, 13, 813–827.
- [7] Maeda, H.; Nakamura, H.; Fang, J., *Adv. Drug Deliv. Rev.* 2013, 65, 71–79.
- [8] Allen, T.M.; Cullis, P.R., *Adv. Drug Deliv. Rev.* **2013**, 65, 36–48.
- [9] (a) Gou, P.; Liu, W.; Mao, W.; Tang, J.; Shen, Y.; Sui, M., *J. Mater. Chem. B Mater. Biol. Med.* **2013**, 1, 284–292; (b) Wei, T.; Chen, C.; Liu, J.; Liu, C.; Posocco, P.; Liu, X.; Cheng, Q.; Huo, S.; Liang, Z.; Fermeglia, M.; Pricl, S.; Liang, X.-J.; Rocchi, P.; Peng, L., *Proc. Natl. Acad. Sci. U. S. A.* **2015**, 112, 2978–2983; (c) Wang, H.; He, J.; Cao, D.; Zhang, M.; Li, F.; Tam, K.C.; Ni, P., *Polym. Chem.* **2015**, 6, 4809–4818; (d) Xu, Z.; Zhang, K.; Hou, C.; Wang, D.; Liu, X.; Guan, X.; Zhang, X.; Zhang, H., *J. Mater. Chem. B Mater. Biol. Med.* **2014**, 2, 3433–3437.
- [10] Tu, Y.; Zhu, L., *J. Control. Release* **2015**, 212, 94–102.
- [11] Sun, D.; Ding, J.; Xiao, C.; Chen, J.; Zhuang, X.; Chen, X., *ACS Appl. Mater. Interfaces* **2014**, 6, 21202–21214.
- [12] (a) Ibsen, S.; Zahavy, E.; Wrasidlo, W.; Hayashi, T.; Norton, J.; Su, Y.; Adams, S.; Esener, S., *Photochem. Photobiol.* **2013**, 89, 698–708; (b) Dcona, M.M.; Mitra, D.; Goehe, R.W.; Gewirtz, D.A.; Lebman, D.A.; Hartman, M.C.T., *Chem. Commun.* **2012**, 48, 4755–4757; (c) Johnson, J.A.; Lu, Y.Y.; Burts, A.O.; Lim, Y.H.; Finn, M.G.; Koberstein, J.T.; Turro, N.J.; Tirrell, D.A.; Grubbs, R.H., *J. Am. Chem. Soc.* **2011**, 133, 559–566; (d) Choi, S.K.; Thomas, T.; Li, M.H.; Kotlyar, A.; Desai, A.; Baker, J., *Chem. Commun.* **2010**, 46, 2632–2634; (e) Ibsen, S.; Zahavy, E.; Wrasidlo, W.; Berns, M.; Chan, M.; Esener, S., *Pharm. Res.* **2010**, 27, 1848–1860.
- [13] McMillan, T.J.; Leatherman, E.; Ridley, A.; Shorrocks, J.; Tobi, S.E.; Whiteside, J.R., *J. Pharm. Pharmacol.* **2008**, 60, 969–976.

- [14] E.; Shen, H.; Ferrari, M., *Nat. Biotechnol.* **2015**, 33, 941–951.
- [15] Huang, Z., *Technol. Cancer Res. Treat.* **2005**, 4, 283–293.
- [16] Peng, K.; Tomatsu, I.; Korobko, A.V.; Kros, A., *Soft Matter* **2010**, 6, 85–87.
- [17] Shanmugam, V.; Selvakumar, S.; Yeh, C.-S., *Chem. Soc. Rev.* **2014**, 43, 6254–6287.
- [18] Trivedi, R.; Kompella, U.B., *Nanomedicine* **2010**, 5, 485–505.

3.6 Appendix

Figure S1. ^1H -NMR of **3**.Figure S2. ^1H -NMR of Doxorubicin.

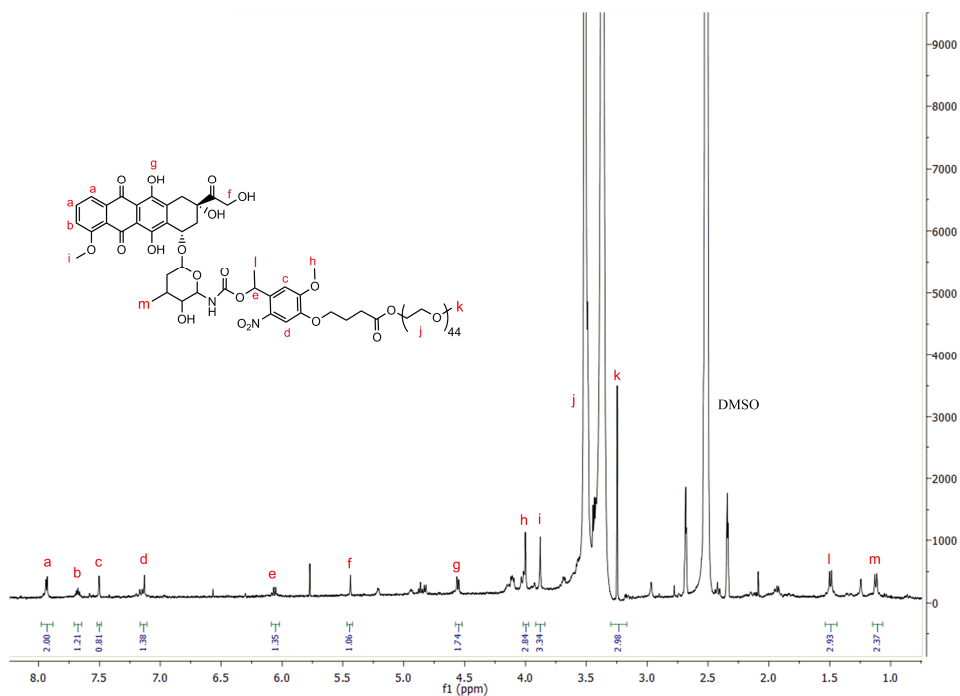


Figure S3. ^1H -NMR of **1**.

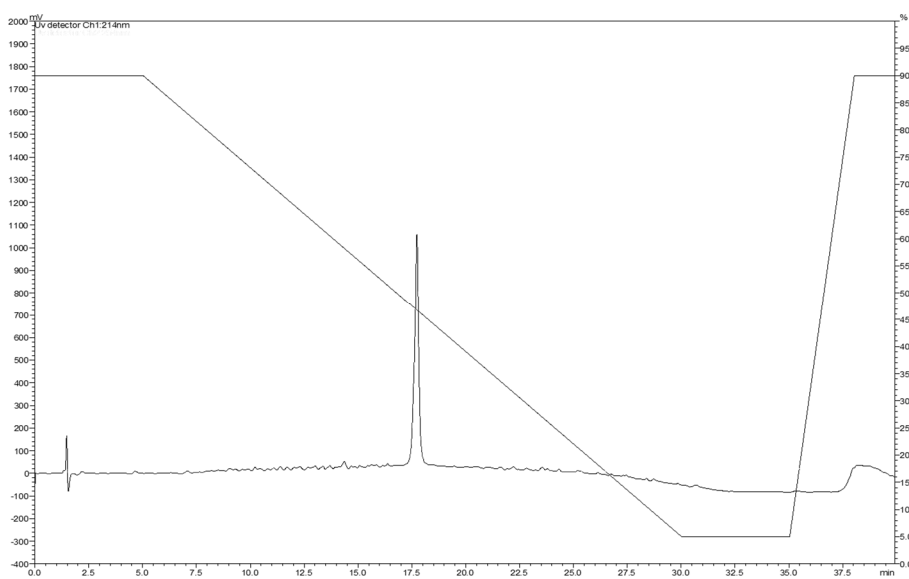


Figure S4. HPLC trace of **1**. Retention time – 17.8 min. UV detection – 214 nm.

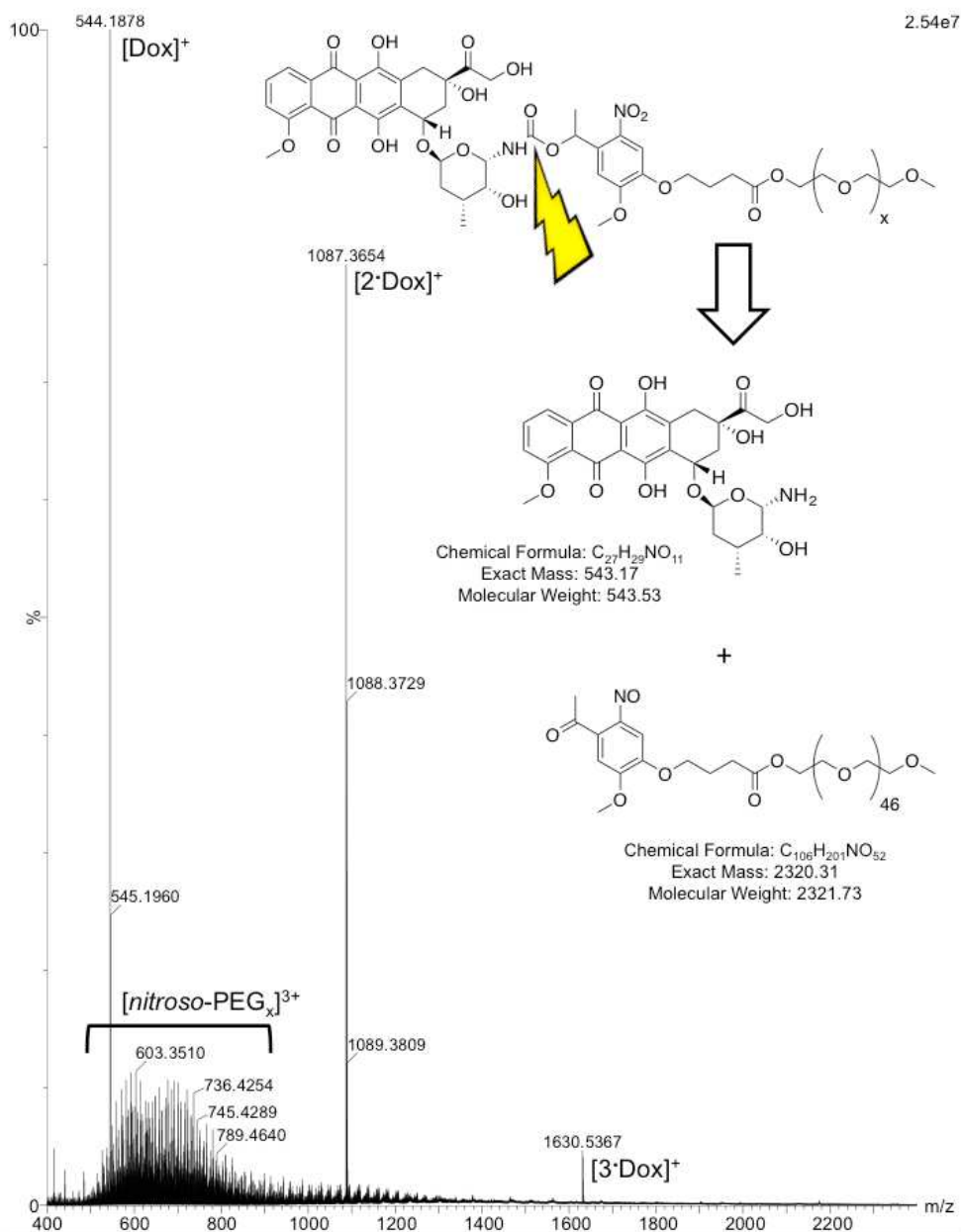


Figure S5. ESI-MS spectra (raw data) following photolysis of **1** and showing the expected photoproducts – DOX and nitroso-benzyl-PEG2000 – as the only significant species present. The presence of DOX clusters – $[2 \cdot DOX]^+$ and $[3 \cdot DOX]^+$ - in the raw spectra arise from ‘soft’ electrospray ionization techniques.

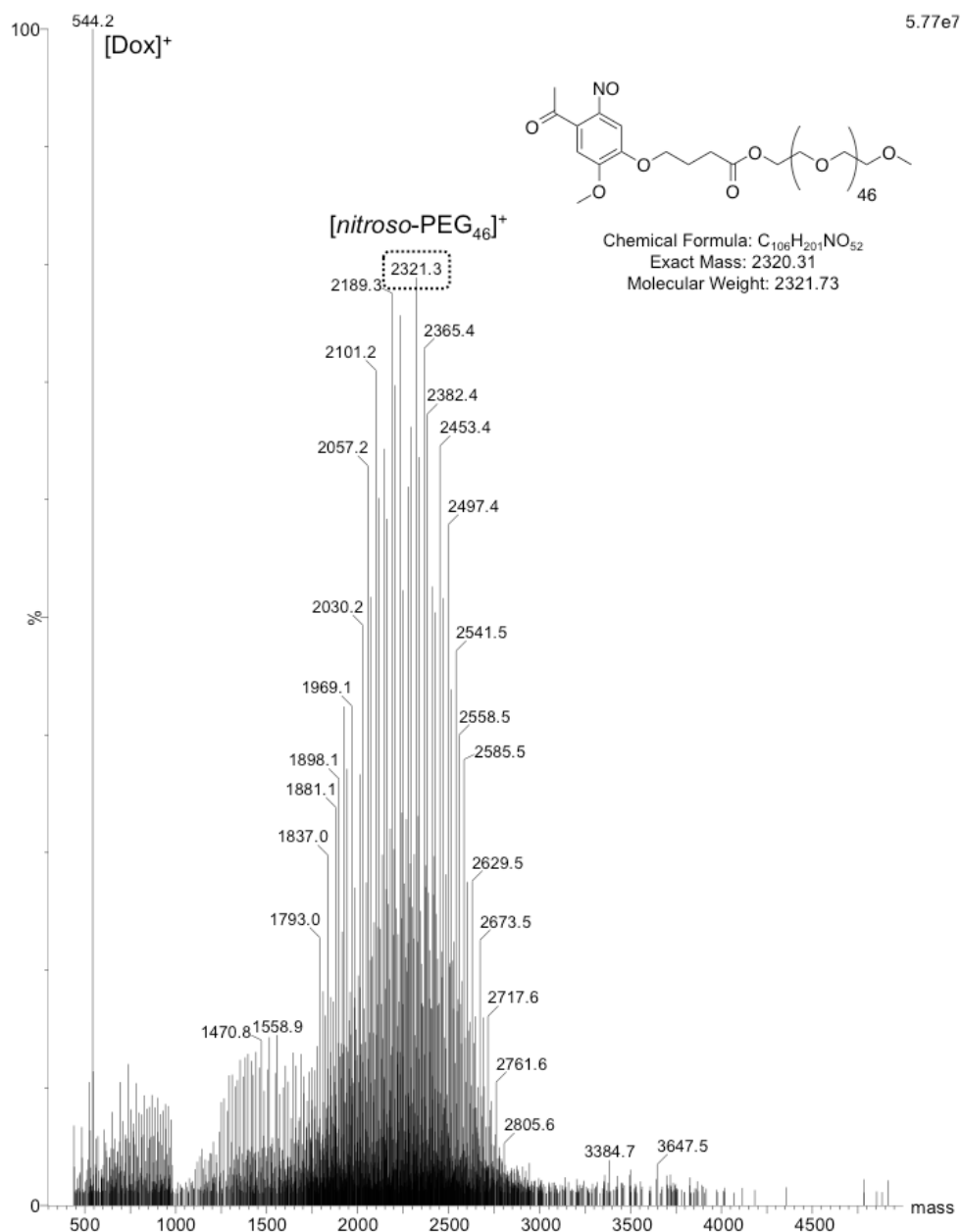


Figure S6. Deconvoluted (*software: MaxEnt1*) mass spectra of nitroso-PEG envelope signals.

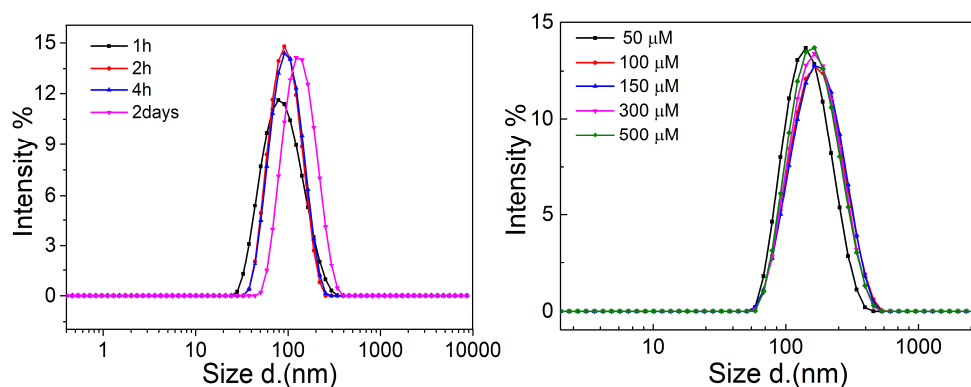


Figure S7. (left) Time course DLS size distributions of **1** (300 μM in PBS) diluted (1:1) in DMEM+FCS. (right) DLS size distributions of **1** (varying concentrations) in PBS.

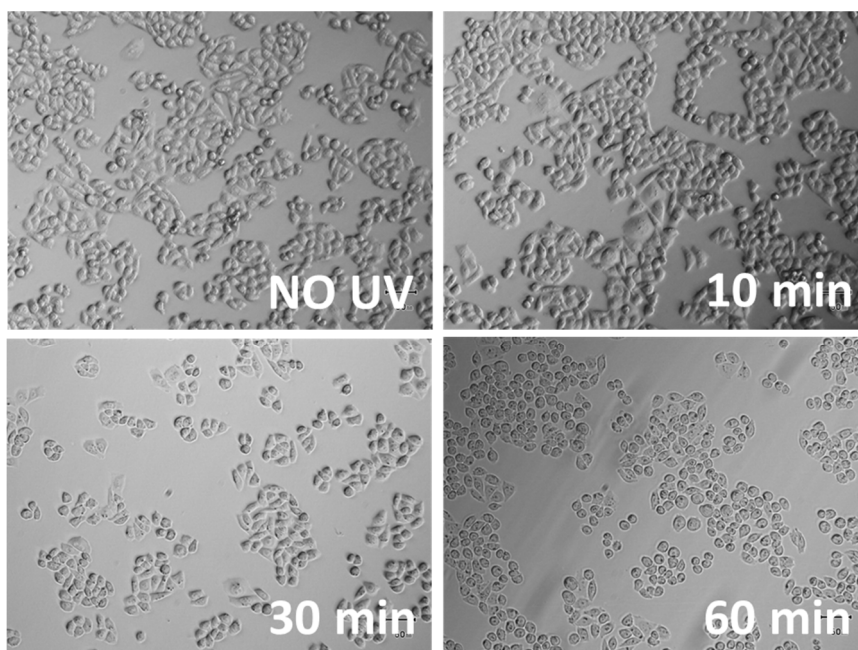


Figure S8. Cells (bright field) irradiated for varying times (UV-A, 365 nm, 15-17 mWcm^{-2}) and imaged immediately. As UV-A irradiation times increase cells become smaller (shrinkage) and more rounded, hallmarks of the onset of UV-A induced apoptosis.

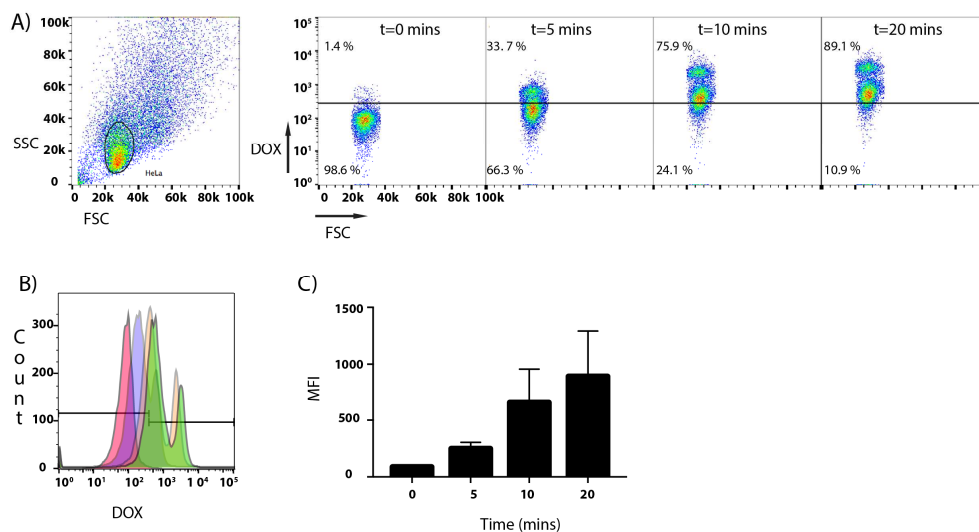


Figure S9. FACS analysis showing increased uptake of DOX (released from a solution of **1** (300 μ M in PBS)) by HeLa cells with increasing irradiation times. A) Dot plots of HeLa cells after $t=0$, 5, 10 and 20 min of irradiation; cell population was gated based on FSC-A vs SSC-A (cell doublets were gated out using FSC-A vs FSC-H). B) Histograms of HeLa cells after $t=0$ min (pink) $t=5$ min (blue), $t=10$ min (orange) and $t=20$ min (green) irradiation. C) Mean Fluorescence Intensity (MFI) of HeLa cells after different irradiation times. Error bars \pm SD.

4

Light Induced Modulation of the Very Long Chain Fatty Acid Composition of Cell Membranes

Abstract: Membrane protein function is highly dependent on the properties of the surrounding lipid bilayer. Herein, we report a chemical and solvent-free method to enrich cellular membranes with very long chain fatty acids (vlcFAs). In this way, we are able to modulate cell membrane lipid composition, thickness and potentially membrane protein activity. Supplementing cell membranes with vlcFAs is notoriously difficult due to their extreme insolubility in aqueous solution. To solve this, we create light sensitive micelles, composed of PEG-nervonic acid (FA24:1) conjugates, which spontaneously disassemble in the presence of lipid bilayers. Once embedded, light is used to cleave off PEG, leaving free nervonic acid within the target membrane. When applied to living cells, released nervonic acid was processed by the cell to generate various species of phospholipids with elevated amounts of incorporated vlcFAs.

Li Kong¹, Edgar Dawkins², Frederick Campbell¹, Edith Winkler², Rico J.E. Derks⁴, Martin Giera⁴, Frits Kamp², Harald Steiner^{2,3} and Alexander Kros¹

¹Leiden Institute of Chemistry, Leiden University, The Netherlands

²BMC, Metabolic Biochemistry, Ludwig-Maximilians University, Munich, Germany

³German Center for Neurodegenerative Diseases (DZNE), Munich, Germany

⁴Center for Proteomics and Metabolomics, Leiden University Medical Center (LUMC), The Netherlands

4.1 Introduction

Phospholipid bilayers, as the main constituent of cellular membranes, act as scaffolds maintaining structural integrity and correct cellular function. Membrane bilayers are involved in numerous cellular processes, regulating bidirectional molecular traffic and supporting numerous membrane associated proteins and receptors (*e.g.* G-protein coupled receptors). The activity and function of membrane proteins is heavily dependent on the local properties of the lipid bilayer in which they are embedded. The transmembrane domains (TMD) of many membrane proteins are highly evolved to prefer a specific lipid environment. In turn, slight changes of bilayer thickness, fluidity, curvature, and/or lipid headgroup chemistry may lead to destabilization of protein structure and affect function and activity.^[1,2]

Very long-chain fatty acids (vlcFAs), with a chain-length of ≥ 22 carbon atoms, play a vital role to many cellular functions including spermatogenesis, skin barrier formation and myelin maintenance.^[3] Free, unesterified vlcFA can rapidly diffuse across lipid bilayers and redistribute among various cellular compartments.^[4,5] When incorporated within endogenous phospholipids (*e.g.* sphingo- and glycerophospholipids), vlcFAs are key modulators of cell membrane fluidity and thickness, facilitating the formation of lipid rafts/domains within cellular membranes.^[6] Furthermore, vlcFAs are important precursors of inflammation-resolving lipid mediators and several disorders in the synthesis of vlcFAs (*e.g.* elongation of stearic acid to saturated or mono-unsaturated vlcFAs), as well as defects in vlcFA metabolism, can lead to severe diseases such as Stargardt disease and adrenoleukodystrophy.^[3]

A change in the thickness of a lipid bilayer can create a mismatch in size with the hydrophobic TMD of an embedded protein.^[7] To minimize unfavorable interactions (*e.g.* exposure of hydrophobic amino acids to water), a change in membrane thickness forces a membrane protein to alter its conformation to the most energetically favourable orientation, for instance, by tilting and bending the TMDs in the new membrane landscape. This in turn can alter the ability of the protein to carry out its function and in extreme cases may lead to a complete loss of function.^[8] The activity

of ion channels, enzymes and substrate transporters have all been shown sensitive to changes in lipid membrane thickness.^[9–12]

Membrane thickness depends on cholesterol content and particularly esterified vlcFA content of endogenous phospholipids. Delivery of vlcFAs to cells is therefore an attractive option to artificially modulate the thickness of cell membranes, and thereby the activity of membrane proteins, as acyl-chain remodeling pathways readily incorporate exogenous fatty acids into cellular phospholipids.^[13,14] However, the delivery of vlcFAs to cells is complicated by their extreme insolubility in water. This is particularly problematic in the case of vlcFAs with a low degree of unsaturation, *e.g.* nervonic acid (NA, FA24:1). These species immediately form insoluble aggregates upon dilution in aqueous media. Our motivation for this study was to find ways of solubilizing vlcFAs in aqueous media to enable efficient incorporation into target cellular membranes. Once embedded in the plasma membrane, we hypothesized that delivered vlcFAs would be taken up into cellular compartments, enter membrane remodeling pathways^[14] and eventually be incorporated into cellular phospholipids. If successful, this would create a larger hydrophobic domain within the bilayer of cellular membranes and potentially alter the activity of embedded membrane proteins.^[1,8]

Herein, we describe a photo-inducible approach to enrich cell membranes with vlcFAs, leading to enrichment of cellular phospholipids with delivered vlcFAs. To achieve this, we conjugated NA to poly-ethylene-glycol (PEG) *via* a photocleavable (*o*-nitrobenzyl) linker (**1**). These amphipathic constructs self-assemble to form close-packed micelles in aqueous solution as illustrated in Figure 1a and 1b.

These micelles spontaneously disassemble in the presence of model and cell membranes, embedding **1** within the target membrane sink (Figure 1c). Once within the membrane, photolysis of PEG leaves unesterified NA within the membrane. By applying this technique to HEK293 cells we demonstrate increased incorporation of esterified vlcFA in cellular phospholipids using lipidomics analysis.

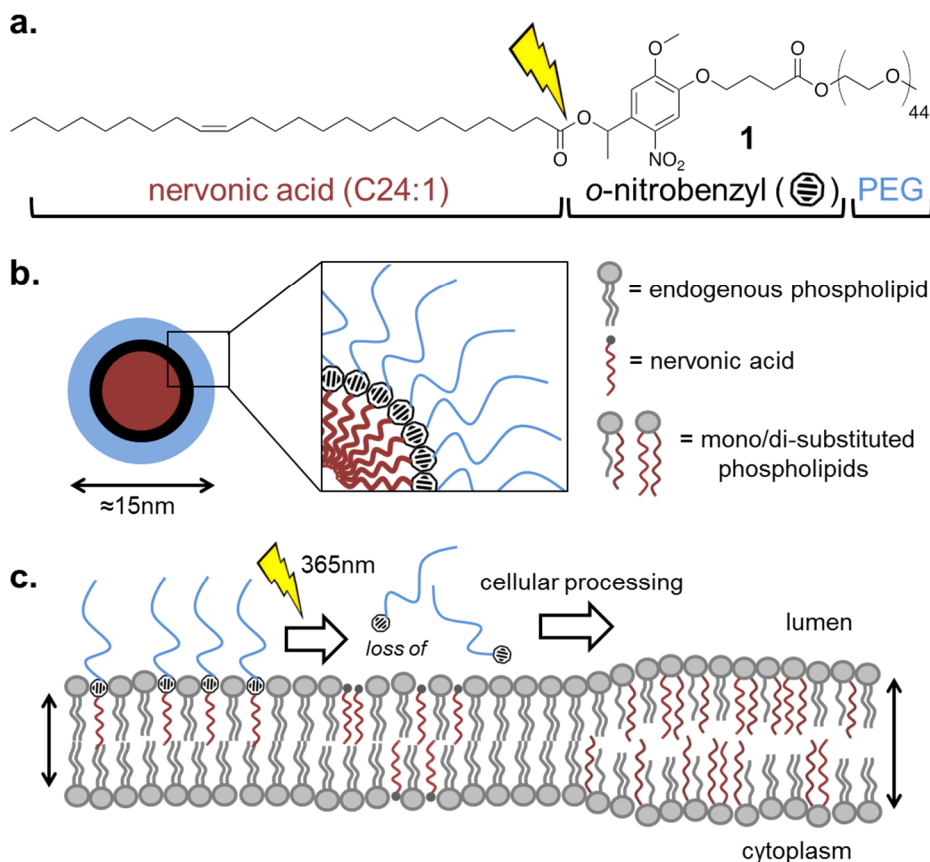


Figure 1. Schematic showing the delivery of nervonic acid to cells using light activatable micelles. (a) chemical structure of photo-cleavable nervonic acid-PEG (**1**); (b) the micellar structure of PEGylated nervonic acid; (c) incorporation, light activation and biotransformation of nervonic acid to vlCPLs and ultimately a thicker cell membrane.

4.2 Results and discussion

The synthesis and characterization of photolabile, nervonic acid-*o*-nitrobenzyl-PEG₂₀₀₀, **1** (Figure 1a), is described in the Supporting Information (Scheme S1, Figures S1, S2). Upon UV light irradiation in PBS, complete photolysis was achieved within 30 min (Figure 2a, b). The appearance of a clear isosbestic point at 320 nm in the UV-Vis absorption spectra indicates clean photoconversion of **1** to its photoproducts. HPLC-ELSD analysis of the photolysis products confirmed the expected release of NA (Figure 2c). Self-assembly of **1** in aqueous media resulted in close-packed micelles. The size of these micelles was approximately 20 nm in size as determined by electron

microscopy (Figure 2d) and dynamic light scattering (DLS, Figure S4). The critical micelle concentration (CMC) of **1** was 2.9 μM (Figure S3) and particles were stable up to at least 1 mM (Figure S4).

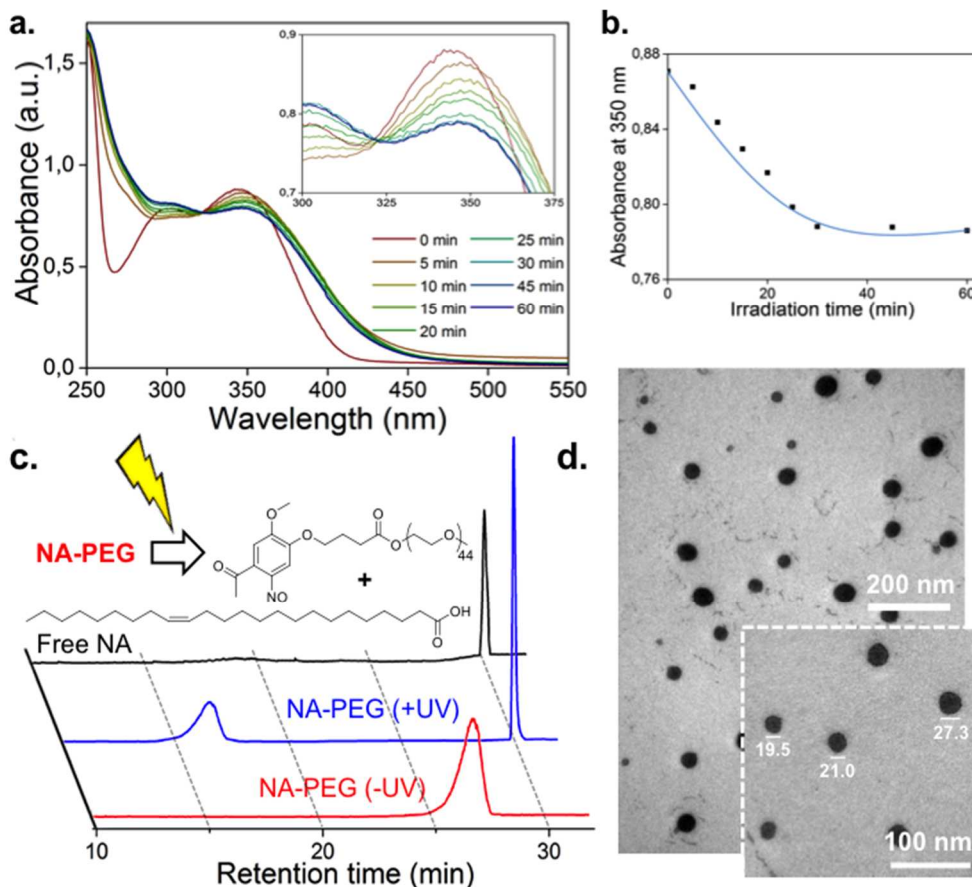


Figure 2. (a) Time evolution of the UV-Vis spectra of a solution of **1** during photolysis (365 nm, 3-5 mW/cm²); (b) Time evolution of the UV absorbance at 350 nm during photolysis. (c) HPLC-ELSD analysis of **1** before (red) and after (blue) UV irradiation. HPLC-ELSD analysis of free NA (black) was used to confirm photolysis of **1** to free NA. (d) TEM image (uranyl acetate stain) of micelles of **1** (500 μM , approx. 1.31 mg/mL).

Next, the incorporation of **1** into model phospholipid (POPC) membranes was assessed (Figure 3). An aliquot of concentrated micelles of **1** (1 mM, in PBS) were mixed with preformed POPC liposomes (large unilamellar vesicles) at a 1:10 molar ratio (50 μM **1**, and 500 μM POPC lipid, respectively). Successful incorporation of **1** into the POPC liposome membrane was, in part, confirmed by a small increase in the

hydrodynamic radius (r_h) of the liposomes (as measured by DLS) prior to light activation. This we attribute to the additional PEG corona now presented from the outer leaflet of the liposome membrane. As expected, upon light irradiation and cleavage of the PEG corona, the r_h returned to the original size of the parent POPC liposome, and a significant decrease in the surface charge was observed. The latter is attributed to the liberated carboxylate functionality of free NA upon UV irradiation. These observations confirm successful incorporation of NA into model lipid bilayers by our procedure. In contrast, addition of NA (via ethanol injection (*i.e.* addition of an aliquot of a concentrated stock solution of NA in ethanol)) to POPC liposomes resulted in no significant change to the liposome surface charge (Figure 3), highlighting the difficulties in incorporating highly insoluble vlcFAs into lipid membranes by conventional methods.

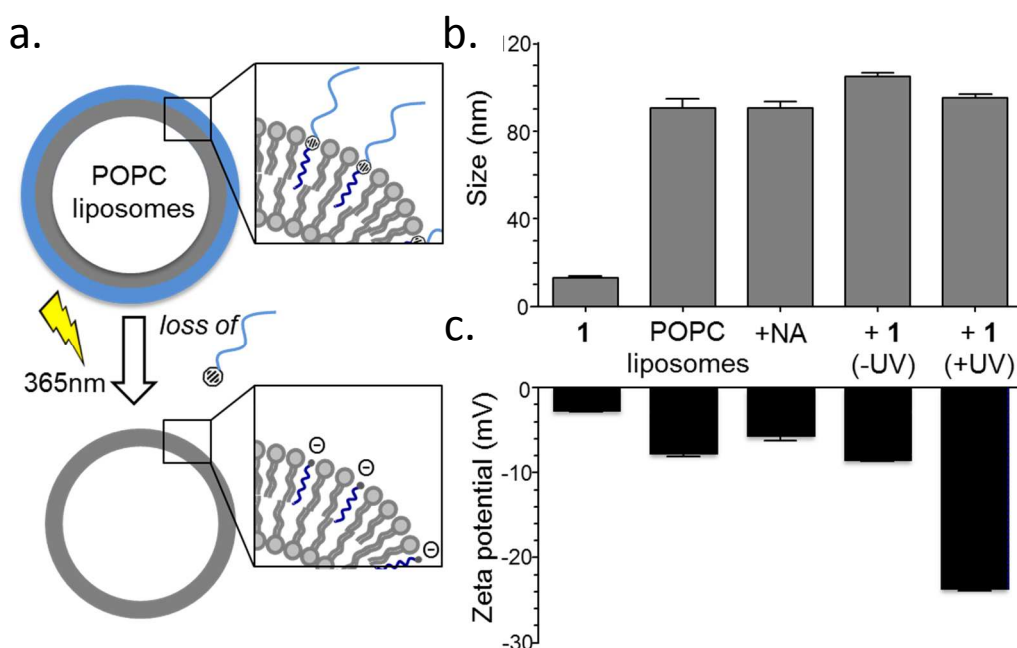


Figure 3. Incorporation and activation of **1** in model lipid membranes. (a): Cartoon of the procedure. (b) Measured hydrodynamic radii (r_h) and (c) zeta potentials of micelles of **1** and POPC liposomes. From l to r: micelles of **1**, unmodified POPC liposomes, POPC liposomes after ethanol injection of **1**, and, alternatively: POPC liposomes incubated with **1** (10:1 molar ratio), followed with subsequent UV light irradiation and photolytic loss of PEG.

To verify analogous incorporation of **1** into biological membranes, we prepared micelles of **1** containing 1 mol% fluorescently-labeled nervonic acid (**NA-Fluo**, see Supporting Information for synthesis and characterization). When mixed micelles of **1** and **NA-Fluo** were incubated with HeLa cells, a homogenous distribution of fluorescence across all cells was immediately observed (Figure S5 and S6). This indicated **NA-Fluo** had spontaneously incorporated into cellular membranes during the process of dissolution of mixed micelles and subsequent transfer of **1** to cell membranes.

Having established the delivery of NA to cellular membranes by our procedure, we next investigated whether HEK293 cells could process free NA, following photolysis of **1**, to generate elevated levels of specific phospholipids with incorporated vlcFAs. First, in a control experiment, we tested the potential for UV induced cytotoxicity to cells (Figure S8). Interestingly, while untreated cells (in PBS) showed significant UV induced cell death (approx. 80% cell viability following 15 min irradiation; determined by WST cell viability assay), cells modified with **1** showed no significant UV induced cytotoxicity following at least 20 min irradiation. This result is consistent with previous observations showing supplemental monounsaturated fatty acids could protect cells from oxidant injury.^[15] Alternatively, quenching of UV light by nitrobenzyl-PEG might have protected the cells. Subsequently, following cell membrane incorporation of **1** (100 μ M) and subsequent light activation (10 min), cells were incubated for 72 h to allow for the processing of free NA and incorporation into membrane lipids. After incubation, cells were pelleted and cellular lipids extracted and analyzed by thin layer chromatography (Figure S7). Phosphatidylcholine lipids (PC) are the most common class of endogenous phospholipids in cells^[16] and incorporation of vlcFAs into PC lipids, thereby increasing the hydrophobic content, leads to reduced retention on the silica TLC plate. Indeed, for cells incubated with **1** and subsequently irradiated, an upshift in the PC lipid content was observed on the TLC plate (Figure S7). Subsequently, from the same samples the relative amounts of 61 cellular PC, 31 phosphatidyl-ethanolamine (PE), 12 sphingomyelin (SM) and 15 free fatty acid (FA) species were analyzed and compared by LC-MS lipidomics (see SI for methods).

Figure 4a demonstrates the changes, focusing on species with incorporated vlcFA. Remarkably, five PC species (PC (22:1/22:1), PC (24:1/24:1), PC(24:1/16:0), PC(24:1/16:1) and PC (24:1/18:1)) as well as one PE species (PE(24:1/18:1)) were increased significantly at the expense of common PC species (PC(16:0/18:1), PC(18:0/18:1), PC(18:1/18:1)) and PE(18:1/18:1). This redistribution demonstrates that indeed, due to the procedure, liberated NA had been taken up by the cell and incorporated into cellular phospholipids. Thus, part of the NA had been esterified into phospholipids by acyl-transferases and/or in *de novo* synthesis pathways of phospholipids. Moreover, a fraction of NA was shortened to erucic acid (FA22:1) which was subsequently incorporated to yield among others PC (22:1/22:1). Also the profile of SM species had altered. Although these phospholipids represent only a minor (<5%) fraction of membrane lipids, those containing vlcFA accumulate into rafts, thereby increasing locally the membrane thickness.^[17] Remarkably, in the treated cells, specific SM species containing vlcFA (*i.e.* SM (d14:2/20:0), SM (d14:1/26:0), SM (d14:1/28:0) and SM (d14:1/28:2)) were down-regulated, whereas prevailing SM (d18:1/16:0) and SM (d18:1/24:1) remained the same. Possibly, this redistribution of SM species compensates for increased levels of vlcFA-PC lipids accumulating into membrane rafts, taking over the local membrane thickening function of vlcFA-SM. Interestingly, the distribution of free fatty acids remained shifted dramatically towards vlcFA in the cells to which NA had been delivered, compared to the control (-UV) (Figure 4c). Remarkably, even after 72 h incubation of the cells, still 38 % of the circulating FA were presented by NA (compared to 5% in the control), whereas common FA such as palmitic acid (FA 16:0) and stearic acid were decreased. Interestingly, erucic acid was increased corroborating our above-mentioned observation that a fraction of NA was β -oxidized to erucic acid (FA 22:1). It appears that the initial high levels of released NA were not toxic for the cells and during the incubation only a fraction of the delivered NA had been esterified and/or β -oxidized while the cells down-regulated common long-chain fatty acids. This is in line with known high affinity of fatty acids to bind to cellular membranes, which easily accommodate 2 mole % fatty acids under physiological conditions.^[18] In summary, these results demonstrate that the distribution of several of lipid species in cells can be altered significantly by our procedure of delivery of large amounts of NA.

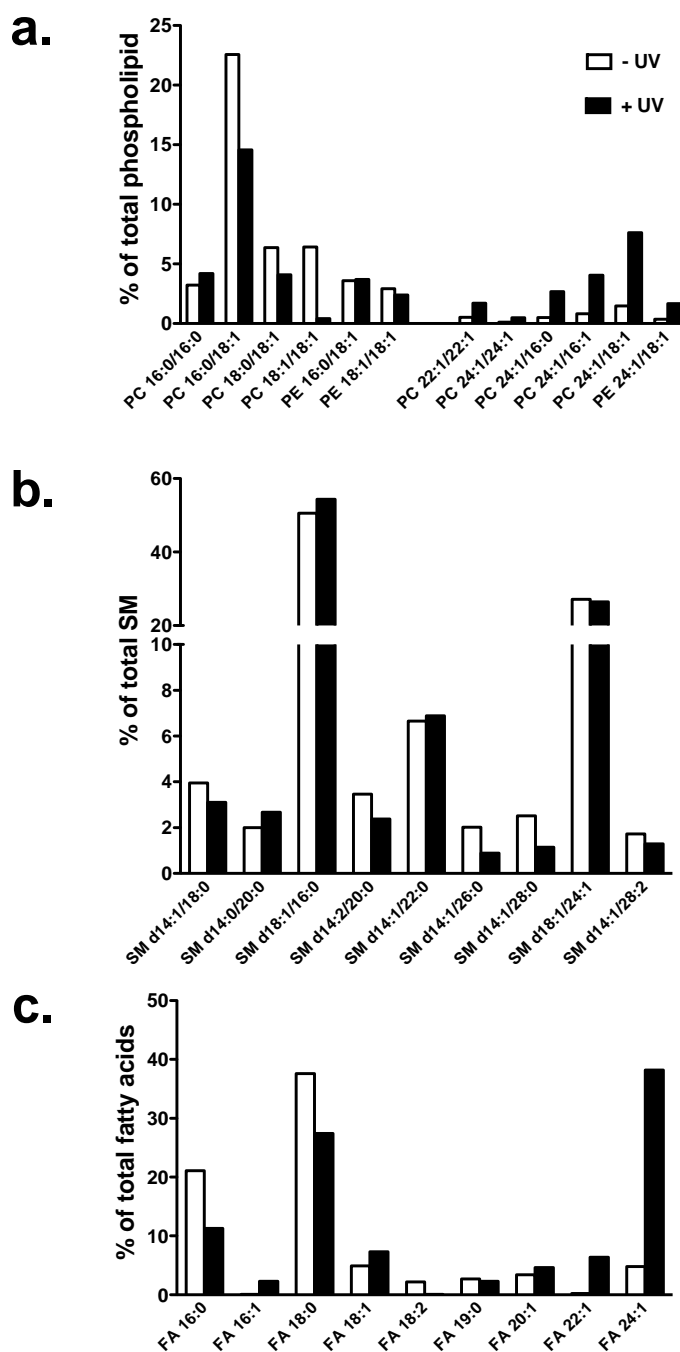


Figure 4. Membrane remodeling in HEK293 cells due to delivery of NA by **1**. Changes in the distribution of (a) glycerophospholipid (PC and PE), (b) sphingomyelin (SM) and (c) free fatty acid (FA) species, after UV release of PEG and subsequent 72 h incubation of the cells at 37 °C.

4.3 Conclusions

In this chapter, we demonstrate efficient delivery of vlcFAs to cell membranes, through the use of light sensitive micelles, composed of PEG-nervonic acid (FA24:1) conjugates. In the absence of light, PEG-NA micelles spontaneously disassembled in the presence of a cell membrane to leave individual PEG-NA molecules embedded within the membrane. Upon light irradiation, PEG is cleaved, leaving free vlcFAs within the cell membrane. Subsequent cellular processing of vlcFAs led to elevated levels of cellular phospholipids. Our approach overcomes the conventional difficulties associated with supplementing cell membranes with highly insoluble vlcFAs and is expected to be transferable to the delivery of any vlcFA or other very hydrophobic lipid species to cell membranes. This procedure has the potential to open new venues in research ranging from studies of membrane protein activities to cellular mechanisms of disease-related altered levels of vlcFA.

4.4 Experimental

4.4.1 Materials and Instruments

Phospholipids used for liposomes, 1-palmitoyl-2-oleoyl-sn-glycero-3-phosphocholine (POPC), were purchased from Avanti Polar Lipids. All chemical reagents, including nervonic acid, were purchased from Sigma Aldrich and used without further purification. All solvents were purchased from Biosolve Ltd. Phosphate buffered saline (PBS): 5 mM KH_2PO_4 , 15 mM K_2HPO_4 , 150 mM NaCl, pH 7.4. Silica gel column chromatography was performed using silica gel grade 40-63 μm (Merck). TLC analysis was performed using aluminum-backed silica gel TLC plates (60F 254, Merck), visualization by UV absorption at 254 nm. NMR spectra were measured on a Bruker AV-400MHz spectrometer. Chemical shifts are recorded in ppm. Tetramethylsilane (TMS) is used as an internal standard. Coupling constants are given in Hz. LCMS analysis was performed Jasco HPLC-system coupled to a Perkin Elmer Sciex API 165 mass spectrometer. MALDI-TOF mass spectra were acquired using an Applied Biosystems Voyager System 6069 MALDI-TOF mass spectrometer. α -Cyano-4-hydroxycinnamic acid (CHCA) was used as matrix in all cases. Sample concentrations were ~ 0.3 mg/ml. HPLC-ELSD analysis was performed using a Shimadzu HPLC setup equipped with two LC-8A series pumps coupled to a Shimadzu ELSD-LT II detection system. Separation (Vydac 214 MS C4 column, 5 μ , 100 \times 4.6 mm, flow rate: 1 mL/min), in all instances, was carried out over a linear gradient of 10-90% **B** over 20 minutes with an initial 5 min hold at 10% **B**. HPLC buffers: **A** – H_2O (0.1% TFA); **B** – Acetonitrile (0.1% TFA). The drift tube temperature for ELSD was set at 37°C and the nitrogen flow-rate at 3.5 bar. UV absorption spectra were measured using a Cary 3 Bio UV-Vis spectrometer, scanning from 200 nm to 500 nm at 1 nm intervals. Scan rate: 150 nm/min.

Particle size distributions and zeta potential measurements were obtained using a Malvern Zetasizer Nano ZS equipped with a peltier controlled thermostatic holder. The laser wavelength was 633 nm and the scattering angle was 173°. To obtain an estimation of the hydrodynamic radius, D_h , the Stokes-Einstein relation was used:

$$D = \frac{K_B T}{3\pi\eta D_h}$$

where, k_B is the Boltzmann constant and η is the viscosity of the solvent. DLS measurements were carried out at room temperature. Zeta potentials were measured at room temperature, at 500 μ M total lipid concentration and 10 mM NaCl concentration. All reported DLS measurements and zeta potentials are the average of three measurements.

For experiments not involving cells, UV light irradiation was performed using a hand-held BLAK-RAY B-100AP high intensity UV lamp (365 nm, 5 mW/cm²) encased in a cardboard box. Samples were irradiated in quartz cuvettes at a fixed distance of 10 cm from the UV source. For all cell experiments, UV light irradiation was performed using a high-power LED (365 nm, 15-17 mW/cm², Roithner Laser Technik, GmbH) mounted at a fixed distance of 1 cm above the cells.

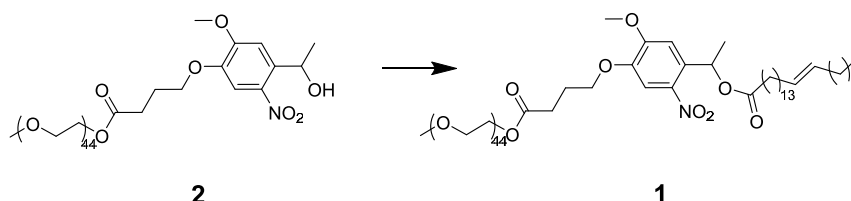
Micelles of **1** were prepared *via* thin hydration (PBS) and bath sonication (Branson 2510 Ultrasonic Cleaner, 50 °C, 5 min). POPC liposomes (10 mM) were prepared by *via* thin hydration and extrusion at room temperature (Mini-extruder, Avanti Polar Lipids, Alabaster, US). Hydrated lipids were passed 11 times through 2 x Confrim 400 nm polycarbonate (PC) membranes (Nucleopore Track-Etch membranes, Whatman), followed by 11 times through 2 x 100 nm PC pores. POPC liposomes were used immediately after formulation.

The structure of the micelles of **1** were characterized using (TEM) operated at 70 kV TEM transmission electron microscopy (TEM, JEOL 1010, USA). The sample was dropped on copper grids with carbon film and washed 3 times with water. All the samples were stained with 0.5% uranyl acetate in water for 2 min. Next, the samples were dried under a N₂ atmosphere in the dark.

Cells (HeLa and HEK293) were cultivated in Dulbecco's Modified Eagle's Medium (DMEM), supplemented with 10% fetal calf serum (FCS, iron supplied), 2% L-glutamine, 1% penicillin and 1% streptomycin. Cells were cultured in an atmosphere of 5% CO₂ at 37°C. Medium was refreshed every two days and cells passaged at 70% confluence by treatment with trypsin-EDTA (0.05% trypsin). For fluorescence imaging

(Figure S5), HeLa cells were seeded (1×10^5 cells/cm²) in 48-well plates (500 μ L, Greiner bio-one, Cellstar®) and cultured (in DMEM+FCS) for a further 24 h. Prior to testing, culture medium was carefully removed and the cells washed once with PBS. Fluorescence microscopy was carried out using an Olympus IX81 fluorescence microscope equipped with a filter cube (Excitation wavelength, 470/40 nm; Emission wavelength, 525/50 nm) or visualization of fluorescein-labeled nervonic acid. For lipid analysis, HEK293 cells were seeded 1×10^6 cells/cm² in 12 well plates and cultured (in DMEM+FCS) overnight. Prior to testing, culture medium was carefully removed and the cells washed once with PBS.

4.4.2 Synthesis of **1**



Scheme S1. Synthetic scheme to **1**.

Methoxy-PEG₂₀₀₀-4-(4-(1-hydroxyethyl)-2-methoxy-5-nitrophenoxy)butanoate (**2**) was synthesized as reported in Chapter 2.

Methoxy-PEG₂₀₀₀-4-(2-methoxy-5-nitro-4-(1-(tetracos-15 enoyloxy) ethyl) phenoxy) butanoate (1**)**

To a stirred solution of **2** (370 mg, 0.16 mmol) in CH₂Cl₂ (5 mL) was added DMAP (12.2 mg, 0.1 mmol), EDCI (57.5 mg, 0.30 mmol), DIPEA (78.3 mL, 0.45 mmol) and nervonic acid (92 mg, 0.25 mmol). After overnight stirring under N₂, the reaction mixture was diluted by EtOAc (50 mL) and washed with sat. NaHCO₃ (3 x 50 mL) and brine (50 mL). The organic fractions were combined, dried (Na₂SO₄) and solvent removed under vacuum. Column chromatography (*Gradient*: CH₂Cl₂ to 10% MeOH in CH₂Cl₂) afforded **1** as a light yellow waxy solid (208 mg, 0.08 mmol, 50%). *R_f*: 0.38 (CH₂Cl₂:MeOH; 10:1). ¹H-NMR (CDCl₃, 400 MHz): 7.60 (s, 1H), 7.02 (s, 1H), 6.49 (q, *J* = 8 Hz, 1H), 5.37 (t, *J* = 4 Hz, 1H), 4.28 (m, 2H), 4.13 (t, *J* = 4 Hz, 2H), 4.02 (s, 3H), 3.45-3.95 (m, 174H), 3.41 (s, 3H), 2.60 (t, *J* = 4 Hz, 2H), 2.35 (m, 2H), 2.23 (m, 2H), 2.03 (m, 4H), 1.63 (d, *J* = 8 Hz, 1H), 1.28 (m, 32H), 0.9 (t, *J* = 6 Hz, 3H).

4.4.3 Synthesis of fluorescein-labeled nervonic acid, NA-Fluo

To a stirred solution of nervonic acid (20 mg, 0.05 mmol) in CH_2Cl_2 (2 mL) was added HCTU (80 mg, 0.2 mmol), DIPEA (70 μL , 0.4 mmol) and fluoresceinamine (70 mg, 0.2 mmol). After stirring for 5h, the reaction solution was evaporated under vacuum. The residue was dissolved in DCM (10 mL) and washed with sat. NaHCO_3 (3 x 20 mL) and brine (20 mL). Column chromatography (*Gradient*: CH_2Cl_2 to 10% MeOH in CH_2Cl_2), afforded fluorescein-labeled nervonic acid as a yellow solid (15 mg, 0.02 mmol, 45%). Purity (>90%) was confirmed by HPLC-ELSD (Figure S5). R_f : 0.27 (CH_2Cl_2 :MeOH; 10:1).

MS-ESI: (m/z) *found*: 696.2 $[\text{M}+\text{H}]^+$, *expected*: 695.42.

4.4.4 Photolysis of **1**

A solution of **1** (100 μM) in PBS was irradiated (365 nm, 3-5 mW/cm^2) for 5 min, followed immediately by acquisition of the UV-visible absorption spectra. The same sample was then re-irradiated and this cycle repeated for cumulative irradiation time points of 10, 20, 30 and 60 min. The products of the photolysis reaction were confirmed by HPLC-ELSD analysis.

4.4.5 Interaction between micelles of **1** and POPC liposomes

To four solutions of preformed POPC liposomes (10 μL , 10 mM in PBS) were independently added a) 90 μL PBS – to give a 1mM of unmodified POPC liposomes, 2 x b) 10 μL of micelles of **1** (1 mM) followed by 80 μL of PBS – to give get POPC liposomes modified with **1** (1:10 mol ratio; POPC: **1**), c) 10 μL of nervonic acid solution (1 mM in EtOH). The solutions were pipette mixed and left for 15 min at room temperature. UV irradiation (365 nm, 3-5 mW/cm^2) of 1 x b) sample was performed for 20 min. DLS and zeta potential measurements were taken immediately.

4.4.6 Delivery micelles of **1** and NA-FA to cells

For fluorescence imaging and cell viability assays, HeLa cells were seeded (1×10^5 cells/ cm^2) in 48-well plates (500 μL , Greiner bio-one, Cellstar®) and cultured for a further 24 h. Prior to testing, culture medium was carefully removed and the cells washed once with PBS. Micelles of **1** containing 1% of **NA-Fluo** were prepared by film hydration with PBS and sonication as for non-fluorescent micelles of **1**. Fluorescently

labeled micelles (500 μ M total, 5 μ M **NA-Fluo**, 500 μ L) were added to HeLa cells and incubated for 20 min. The micelle solution was subsequently removed and cells washed with PBS (3x) and re-suspended in DMEM+FCS. Cells were imaged immediately under the fluorescent microscope using an Olympus IX81 fluorescence microscope equipped with a filter cube (Ex. 470/40; Em. 525/50).

4.4.7 Lipid analysis of cell lysates with TLC

For analysis of cellular lipids, HEK293 cells were seeded (8.57×10^5 cells/cm²) in 12 well plates and cultured for a further 24 h prior to the addition of **1** at a final concentration of 100 μ M. Cells were irradiated (10 min, 365 nm, 15-17 mW/cm²) and incubated for a further 72 h. Cells were then scraped and washed twice in ice-cold PBS by centrifugation at 2500 g for 10 min at 4°C. 25-50% of the cell pellet was re-suspended in CHCl₃:MeOH (1:2). To extract cellular lipids, pellets were briefly (bath) sonicated before centrifugation at 17000 g for 10 min at 4°C. The supernatant containing cellular lipids was resolved by TLC using a mobile phase of CHCl₃:MeOH:H₂O (65:25:4). In this solvent system, the phospholipids phosphatidylcholine, phosphatidylinositol and phosphatidylserine co-migrate as one spot (PL). Synthetic 24:1 PC, 22:1 PC and POPC were used as standards. TLC analysis was performed using Silica HPTLC plates (Millipore Cat no: 1.05644.001), developed by spraying with 10% CuSO₄ (w/v) in 8% phosphoric acid (v/v) and charring at 95°C overnight on a hot plate.

4.4.8 Cell viability assay

HeLa cells were seeded in 96-well plates at a density of 10^4 cells per well and incubated overnight. Cells were washed once with PBS, then micelles of **1** (100 μ L, varying concentrations in 1:1 PBS:DMEM+FCS), free DOX solutions (100 μ L varying concentrations in 1:1 PBS:DMEM+FCS) or DMEM+FCS alone (100 μ L) were added and the cells incubated for 12 h. Cells were then washed three times (DMEM+FCS), re-suspended in DMEM+FCS and incubated for a further 24 h. Cell media was removed and 200 μ L Cell Proliferation Reagent; WST-1 (Sigma) added to each well. Cells were incubated (37°C) for a further 3 h, according to the supplier guidelines. To determine cell viability, absorbance at 450 nm was measured. All experiments were carried out in quadruplicate.

4.4.9 Lipidomics

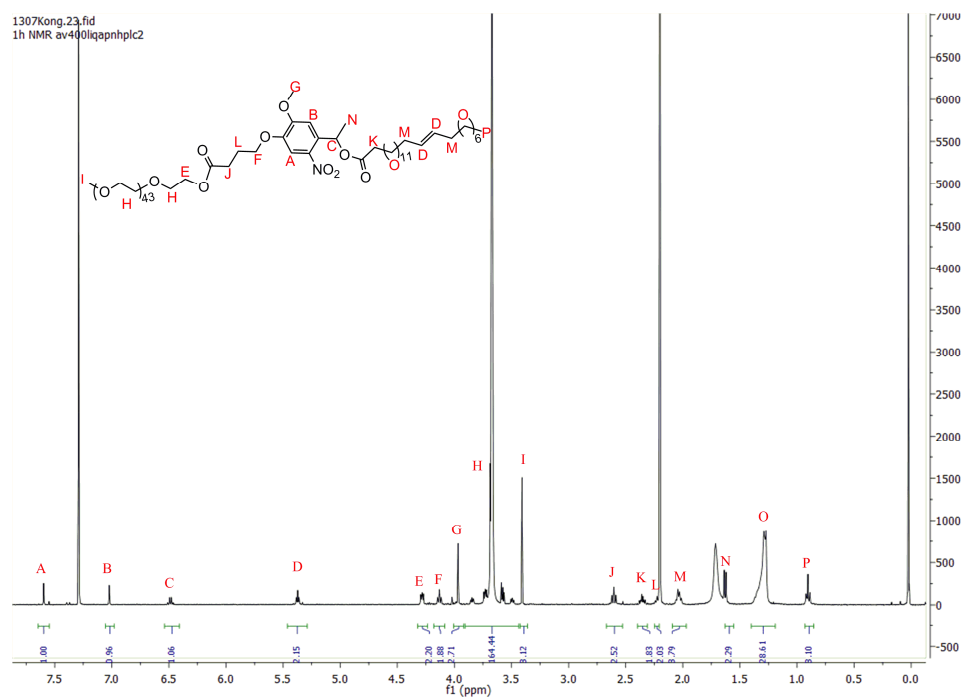
Lipidomic analysis of HEK293 lipid extracts was performed using a LC-MS/MS based lipid profiling method. A Shimadzu Nexera LC-30 (Shimadzu, 's Hertogenbosch, The Netherlands) was used to deliver a gradient of water/acetonitrile 80:20 v/v (eluent A) and water/acetonitrile/2-propanol 1:90:9 v/v (eluent B). Both eluents contained 5 mM ammonium formate and 0.05% formic acid. The applied gradient, with a column flow of 300 μ L/min, was as follows: 0 min 40% B, 10 min 100% B, 12 min 100% B. A Phenomenex Kinetex C18, 2.7 μ m particles, 50 x 2.1 mm (Phenomenex, Utrecht, The Netherlands) was used as column. The injection volume was 10 μ L. The MS was a Sciex TripleTOF 6600 (AB Sciex Netherlands B.V., Nieuwerkerk aan den IJssel, The Netherlands) operated in positive (ESI+) and negative (ESI-) ESI mode, with the following conditions: Ion Source Gas 1, 2 and Curtain gas 30 psi, temperature 350°C, acquisition range m/z 100-1200, IonSpray Voltage 5500 V (ESI+) and -4500 V (ESI-), declustering potential 80 V (ESI+) and -80 V (ESI-). An information dependent acquisition (IDA) method was used to identify lipids, with the following conditions for MS analysis: collision energy ± 10 , acquisition time 250 ms and for MS/MS analysis: collision energy ± 45 , collision energy spread 25, ion release delay 30, ion release width 14, acquisition time 40 ms. The IDA switching criteria were set as: for ions greater than m/z 300, which exceed 200 cps, exclude former target for 2 s, exclude isotopes within 1.5 Da, max. candidate ions 20.

Before data analysis, raw MS data files were converted with the Reifycs Abf Converter (v1.1) to the Abf file. MS-DIAL (v2.74), with the FiehnO (VS27) database, was used to align the data and identify the different lipids. PC and PE lipids were manually curated to confirm their identity. Due to overlap of triglyceride (TG) species, MS-DIAL could not sufficiently identify lipid species, in turn a modified identification approach was applied. Initially, MS-DIAL was used to get the total number of carbons and double bonds of a TG. This information together with the MS/MS spectrum was used to search the glycerolipid MS/MS predicted database on LipidMaps. TG's with all their neutral loss of lipid species fragments matched were assigned as correctly identified.

4.5 References

- [1] O. S. Andersen, R. E. Koeppe, *Annu. Rev. Biophys. Biomol. Struct.* **2007**, *36*, 107–130.
- [2] H. J. Sharpe, T. J. Stevens, S. Munro, *Cell* **2010**, *142*, 158–169.
- [3] A. Kihara, *J. Biochem.* **2012**, *152*, 387–395.
- [4] F. Zhang, F. Kamp, J. A. Hamilton, *Biochemistry* **1996**, *35*, 16055–16060.
- [5] F. Kamp, J. A. Hamilton, *Prostaglandins Leukot. Essent. Fat. Acids* **2006**, *75*, 149–159.
- [6] J. Bernardino de la Serna, G. J. Schütz, C. Eggeling, M. Cebecauer, *Front. Cell Dev. Biol.* **2016**, *4*, DOI 10.3389/fcell.2016.00106.
- [7] J. A. Killian, *Biochim. Biophys. Acta - Rev. Biomembr.* **1998**, *1376*, 401–415.
- [8] A. G. Lee, *Biochim. Biophys. Acta - Biomembr.* **2004**, *1666*, 62–87.
- [9] A. . Lee, *Biochim. Biophys. Acta - Biomembr.* **2003**, *1612*, 1–40.
- [10] A. G. Lee, *Trends Biochem. Sci.* **2011**, *36*, 493–500.
- [11] F. X. Contreras, A. M. Ernst, F. Wieland, B. Brügger, *Cold Spring Harb. Perspect. Biol.* **2011**, *3*, 1–18.
- [12] E. Winkler, F. Kamp, J. Scheuring, A. Ebke, A. Fukumori, H. Steiner, *J. Biol. Chem.* **2012**, *287*, 21326–21334.
- [13] A. A. Spector, R. E. Kiser, G. M. Denning, S. W. Koh, L. E. DeBault, *J Lipid Res* **1979**, *20*, 536–547.
- [14] A. Yamashita, Y. Hayashi, Y. Nemoto-Sasaki, M. Ito, S. Oka, T. Tanikawa, K. Waku, T. Sugiura, *Prog. Lipid Res.* **2014**, *53*, 18–81.
- [15] C. Hart, J. Tolson, E. Block, *Am J Physiol* **1991**, *260*, L481–488.
- [16] G. van Meer, D. R. Voelker, G. W. Feigenson, *Nat. Rev. Mol. Cell Biol.* **2008**, *9*, 112–124.
- [17] M. Oda, T. Matsuno, R. Shiihara, S. Ochi, R. Yamauchi, Y. Saito, H. Imagawa, M. Nagahama, M. Nishizawa, J. Sakurai, *J. Lipid Res* **2008**, *49*, 1039–1047.
- [18] J. A. Hamilton, F. Kamp, *Diabetes* **1999**, *48*, 2255–2269.

4.6 Appendix

**Figure S1.** ¹H-NMR of **1**.

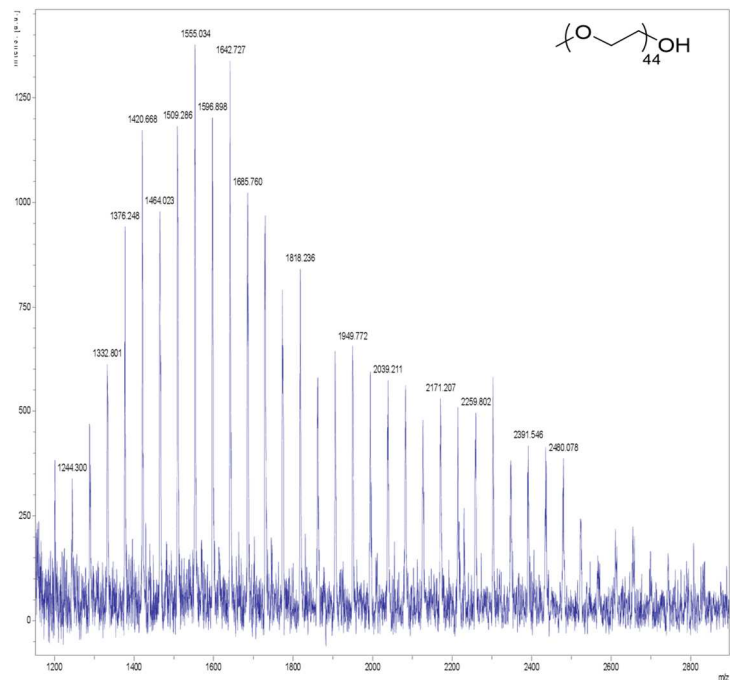


Figure S2. Maldi-TOF spectrum of mPEG₂₀₀₀ and **1**. (The mass difference between mPEG₂₀₀₀ and **1** is 630 g/mol which is the exact mass value of the extra part of nitrobenzyl-nervonic acid).

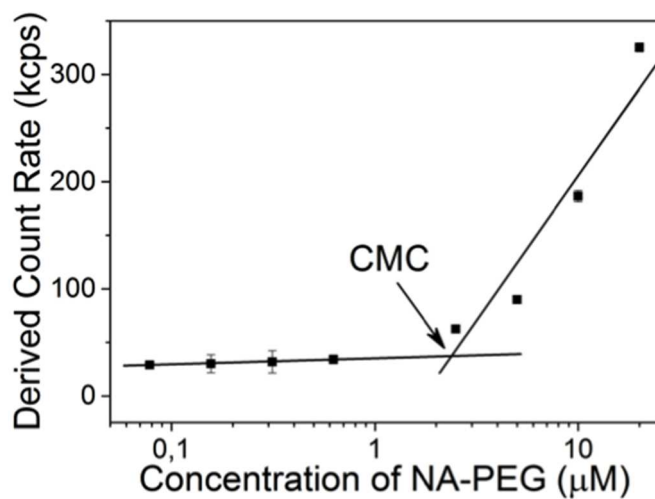


Figure S3. CMC determined by measuring light scattering intensity (raw count rate) as a function of concentration of **1** in PBS.

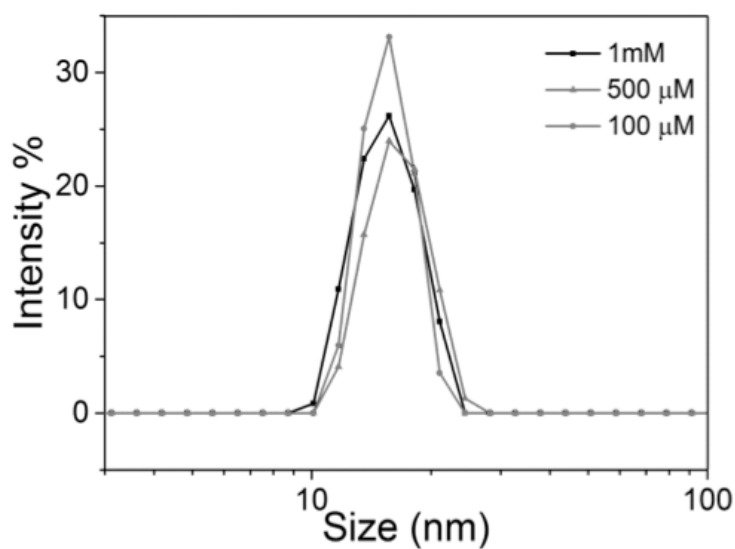


Figure S4. DLS size measurement of micelles of **1** at varying concentrations in PBS.

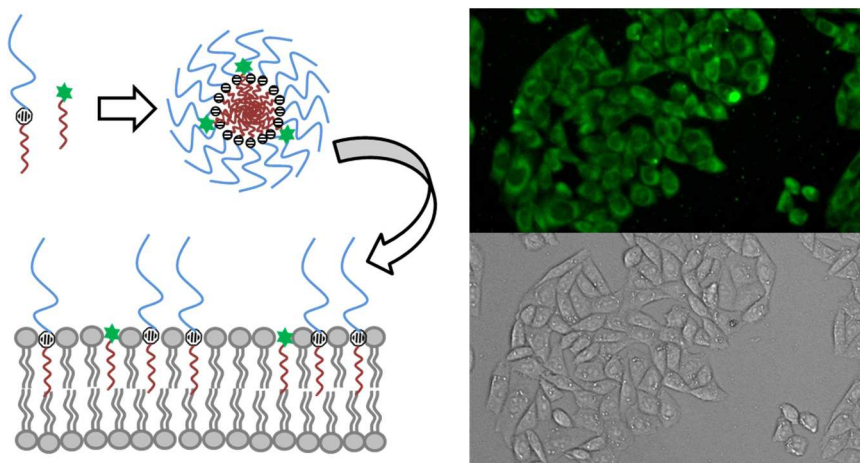


Figure S5. Brightfield and fluorescence image of HeLa cells following incubation of **1** micelles (containing 1 mol% **NA-Fluo**).

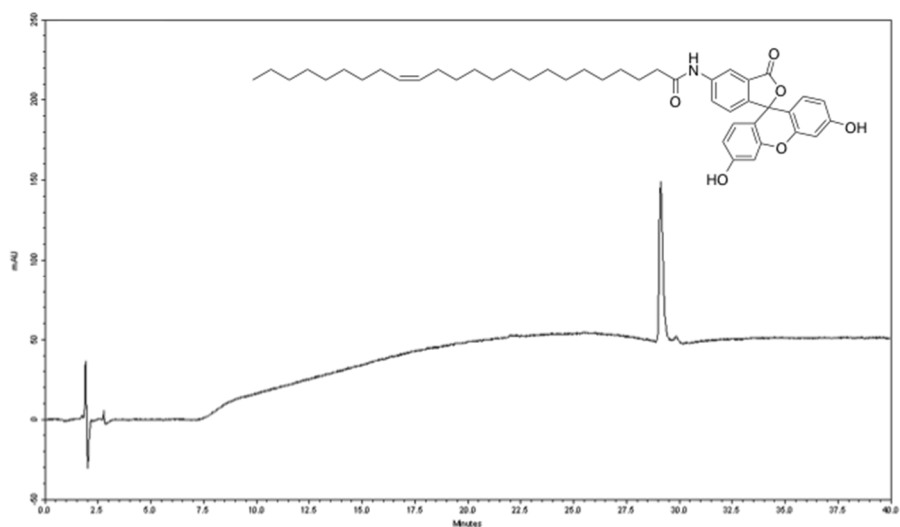


Figure S6. Analytical HPLC trace of purified **NA-Fluo**. *HPLC conditions:* Linear gradient of 10-90% **B** over 20 minutes with an initial 5 min hold at 10% **B**. HPLC buffers: **A**: H₂O (0.1% TFA); **B**: Acetonitrile (0.1% TFA). Detection at 254 nm.

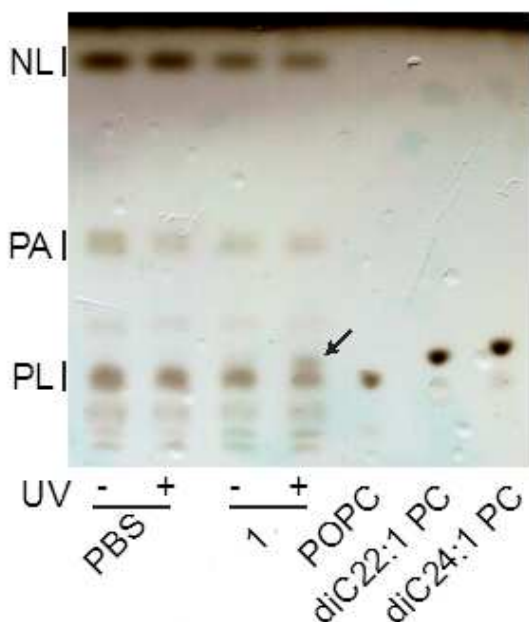


Figure S7. Thin layer chromatography of lipids extracted from HEK293 cells following treatment with **1**. In controls, PBS was added. PL: phospholipids (predominantly PC); PA: phosphatidic acid; NL: neutral lipids (predominantly cholesterol). The arrow indicates formation of slightly more hydrophobic phospholipids, *i.e.* species with incorporated vclFA.

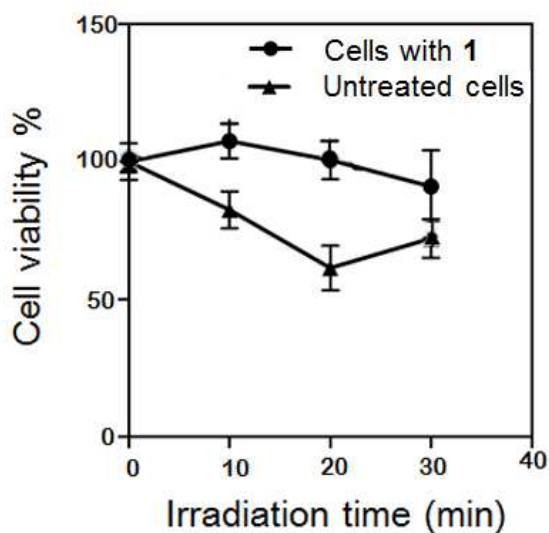


Figure S8. Cell viability following UV irradiation.

5

Charge-Switchable Liposomes for Drug Delivery *in Vitro* and *in Vivo*

Abstract: Surface charge significantly affects how nanoparticles distribute *in vivo* as well as how they are taken up by cells. Herein, we report liposomal drug carriers whose surface charge can be rapidly switched *in situ* and *in vivo* using light. Prior to light activation, liposomes are neutrally charged and freely circulate within the bloodstream of an embryonic zebrafish following systemic (*i.v.*) administration. Upon light activation however, the liposome surface charge is rapidly switched from neutral to positively charged leading to rapid cellular adsorption and uptake. Switching of surface charge does not disrupt the integrity of the carrier membrane and small molecule cargos remain entrapped within liposomes and are taken up by cells.

Li Kong¹, Gabriela Arias Alpizar¹, Alexander Rabe², Michel Meijer¹, Sylvestre Bonnet¹, Stefan Vogel², Alexander Kros¹ and Fred Campbell¹

¹Leiden Institute of Chemistry, Leiden University, The Netherlands

²Department of Physics, Chemistry and Pharmacy, University of Southern Denmark, Odense, Denmark

5.1 Introduction

Nanoparticle-based approaches to target drugs to cancer cells have predominantly focused on long-circulating formulations designed to passively target tumors *via* the EPR effect. Doxil® and Myocet® are two liposomal-doxorubicin formulations clinically approved to treat a variety of human cancers in this way.^[1] Doxil® is a PEGylated liposomal formulation (ePC:Cholesterol:DSPE-mPEG₂₀₀₀;55:40:5) whereas Myocet® (POPC:Cholesterol:55:45) is non-PEGylated.^[2] Both formulations are 100-200nm in size and demonstrate extended circulation lifetimes (hours – days). The principle reason for this is reduced absorption of serum proteins (opsonisation) and avoidance of the MPS (*i.e.* recognition, uptake and clearance by plasma exposed macrophages, primarily in the liver and spleen). While Doxil® and Myocet® can efficiently accumulate within target tumors, their ability to evade cellular interactions *en route* to the tumor means they do not efficiently interact with target cancer cells. Drug delivery in these cases is achieved through passive diffusion of doxorubicin across the liposome membrane over time within the tumor.^[3] It is often therefore challenging to reach therapeutically relevant drug concentrations within tumors. In addition, given the fact that drug release occurs extracellular, these technologies are limited to the delivery of drugs which themselves can cross target cancer cell membranes. These technologies cannot easily be extended to the delivery of larger and/or more hydrophilic, membrane impermeable therapies (*e.g.* proteins and oligonucleotides).

In contrast, nanoparticles with a cationic surface charge are rapidly internalized by cells.^[4] This is caused by non-specific adsorption to anionic cell membranes (and/or the polyanionic glycocalyx) followed by endocytosis.^[5] In addition, it is thought that cationic nanoparticles can destabilize endosomal membranes facilitating endosomal escape and drug release to the cytosol of the cell.^[6] For these reasons, cationic nanoparticles have been extensively used as vehicles to deliver oligonucleotides (DNA and RNA) to cells *in vitro* (*e.g.* transfection agents such as Lipofectamine®).^[7] Here, they have the added advantage of efficiently condensing/complexing polyanionic genetic material. However the non-specific adsorption of cationic nanoparticles to cells, together with extensive adsorption of anionic serum proteins (opsonisation),^[8] has hampered the translation of these technologies *in vivo*. Efforts to sterically shield

nanoparticle cationic surface charge using PEG have been investigated,^[9] however unpublished work for our group has demonstrated this is an ineffectual method to prevent non-specific cellular interactions and therefore the rapid removal of nanoparticles from circulation (Figure S2). There are currently no cationic nanoparticle-based drug delivery systems approved for clinical use.

Previous work from our group utilized the embryonic zebrafish as a convenient animal model to assess the biodistribution of nanoparticles *in vivo*, at high (cellular) resolution and across a whole living organism.^[10] Here, it was found that the surface charge of liposomes significantly affects biodistribution. Notably, neutral liposomes based on the lipid composition of Myocet® were found to freely-circulate, whereas cationic liposomes, based on the lipid composition of EndoTAG-1^[11] – a positively charged liposomal-paclitaxel formulation currently in phase 3 clinical trials – were found to ‘stick’ across the entire endothelium of the fish (Figure S3). For a brief description of the embryonic zebrafish and its current applications in biomedical research, please see the supporting information.

Taking advantage of the contrasting biodistribution of differently charged liposomes *in vivo*, we here report an efficient strategy to convert freely circulating neutral liposomes to ‘sticky’ cationic liposomes *in situ* and *in vivo* using long-wave UV light as a trigger. We achieve this through the incorporation of neutrally charged, photocaged cholesterol analogues within liposome membranes. Upon light activation, photolysis of the photocage reveals a primary amine at the headgroup of cholesterol, which, protonated at physiological pH, results in a cationic liposome surface charge (Figure 1). In contrast to existing light activated liposomal drug delivery systems (DDS), a key feature of this system is not only surface charge switching but that this transformation does not lead to disruption of the liposome membrane and extracellular drug release. This technology provides the basis for the light targeted delivery of membrane impermeable cargos to target cells *in vivo*. A handful of similar strategies have been reported for micelle, polymersome and mesoporous silica based nanoparticle systems.^[12] All, however, rely on endogenous stimuli (both pH and enzymatic cleavage), with charge reversal occurring over the time frame of hours to days. These systems are therefore limited to applications where a) nanoparticles can

efficiently accumulate at the site of disease (*e.g.* tumor microenvironment) and b) there is an exploitable, pathological distinction between diseased and healthy tissue (*e.g.* low pH of tumor microenvironment).

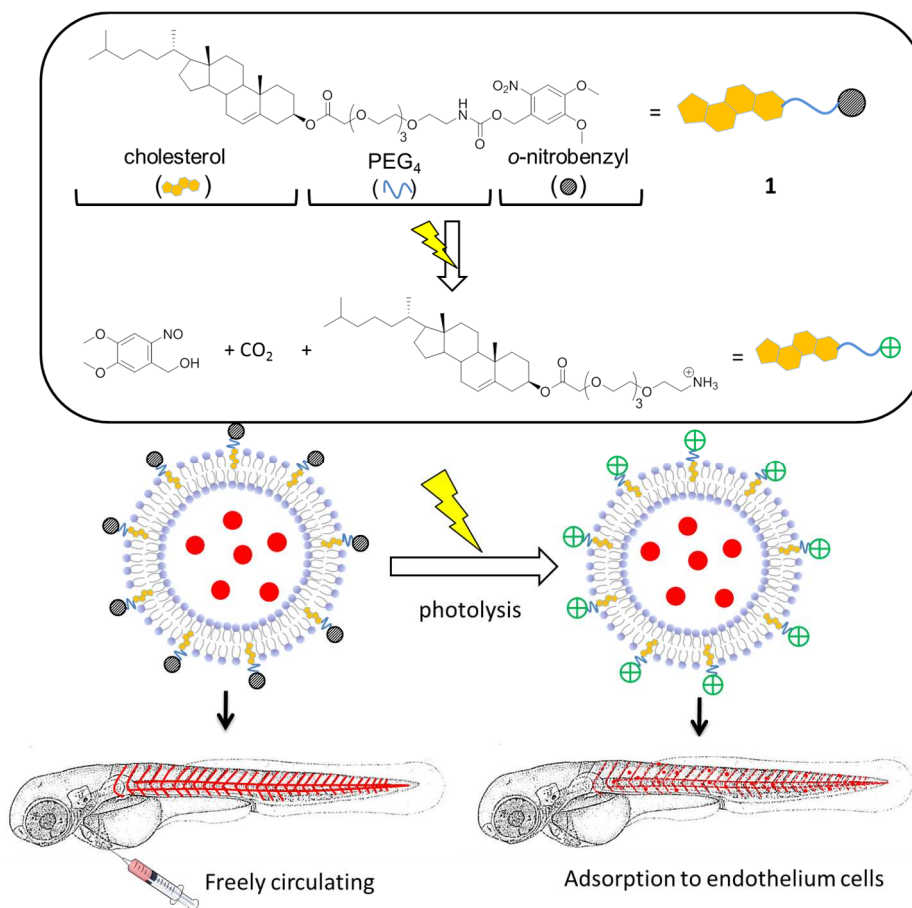
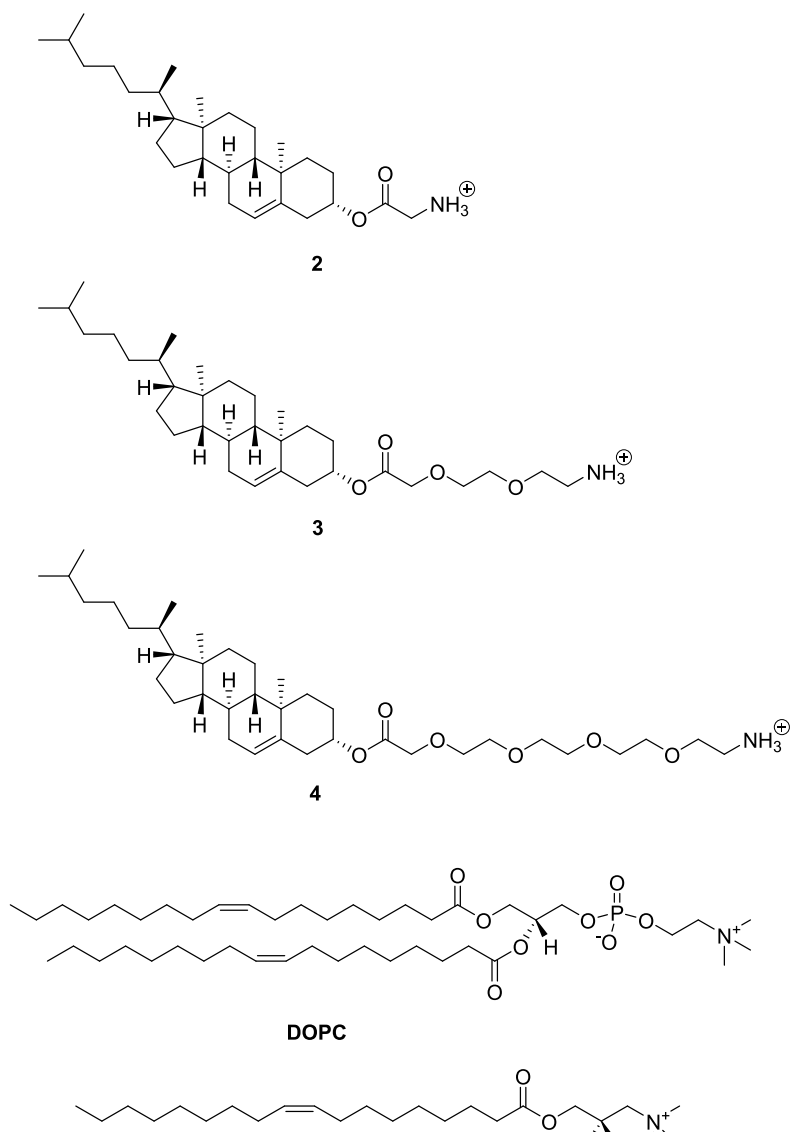


Figure 1. Schematic illustration of charge switchable liposome and its distribution *in vivo* before and after UV irradiation. The caged liposomes are freely circulating in the zebrafish prior to UV irradiation, while the cationic liposomes, triggered by UV light, stick to all endothelial cells and are endocytosed.

5.2 Results and discussion

To ensure sufficient cationic surface charge following photolysis of the *o*-nitrobenzyl photocage, a series of cationic lipids, based on cholesterol, were synthesized and tested. These lipids were co-formulated at 1:1 molar ratios with DOPC – to broadly match the lipid composition of Myocet®. As cholesterol is known to sit deeper within

phospholipid membranes – the hydroxyl headgroup being roughly in line with the phosphate group of adjacent phospholipids^[13] – a series of spacers, between cholesterol and primary amine, were designed to establish the optimal exposure of the terminal primary amine. Spacers chosen were glycine (**2**), PEG-2 (*i.e.* 2 ethylene glycol units; **3**) and PEG-4 (*i.e.* 4 ethylene glycol units; **4**), see Scheme 1.



Scheme 1. Structures of three cationic lipids with different spacers, DOPC and DOTAP.

From zeta potential measurements, it became clear that increasing the spacer length between cholesterol and terminal primary amine leads to a greater surface cationic charge (Figure 2a). In the case of DOPC:4 liposomes, a similar cationic surface charge was measured as compared to cationic liposomes formulated using the commercially available cationic lipid, DOTAP.^[14] As expected decreasing the mol% of these cationic lipids within the liposome formulation resulted in reduced overall cationic surface charge (Figure 2a).

Next, the biodistribution of liposomes containing each of these three cholesterol amine lipids mixed with DOPC (1:1 molar ratio) was assessed following intravenous (*i.v.*) injection in embryonic zebrafish. In all three cases, liposomes showed the expected non-specific adsorption across the entire endothelium of the embryonic fish (Figure 2b). From these experiments, it was decided that the cholesterol amine spacer with the longest (PEG₄) spacer would be taken forward, photocaged and assessed as a light activated drug delivery platform.

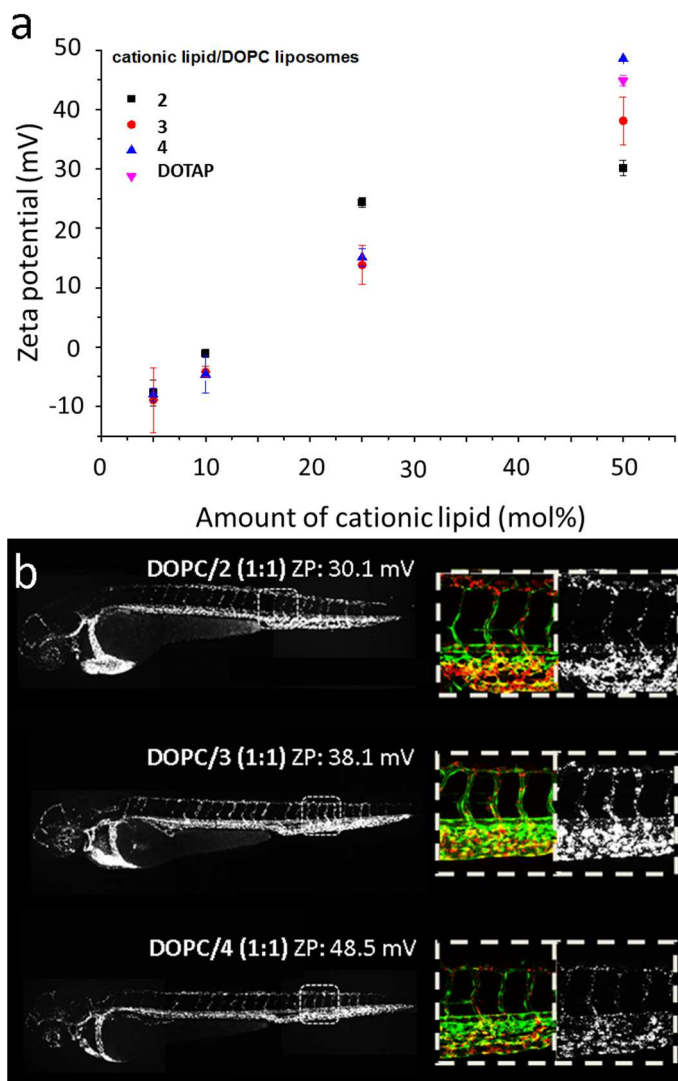


Figure 2. (a) Zeta potential of liposomes composed of mixtures of DOPC and cationic lipid: **2**, **3** or **4**. (b) Biodistribution of cationic liposomes containing 50 mol% of **2**, **3** or **4** injected (i.v.) in *kdrl:GFP* zebrafish embryos (2 days post fertilization, dpf). Embryos stably expressing GFP in all endothelial cells. Images acquired 1 hour post-injection (hpi). *Whole embryo images* (10x magnification): liposomes (white); *Boxed images* (40x magnification): left – blood vessels (green), liposomes (red); right: liposomes (white).

The synthesis and characterisation of photocaged, cholesterol amine (**1**) is described in the Supporting Information. A *o*-nitrobenzyl protection group was selected as a photocage for the amine given its ease of synthesis.^[15] Furthermore, it is well

characterized, neutral charged and has rapid photolysis kinetics, and can therefore be used in numerous biological scenarios. Upon UV light irradiation (365 nm, 15-17 mW/cm²) of **1** in H₂O:MeCN:^tBuOH (1:1:1), complete photolysis of the *o*-Nb functionality was achieved within 2 min (see Figure 3a and 3b). The appearance of three clear isosbestic points (295 nm and 365 nm) shows clean photoconversion of **1** to its photoproducts. To confirm that photolysis resulted in the generation of **4** with concomitant switching of liposome surface charge, zeta potential measurements of DOPC:**1** (1:1 mol ratio) liposomes were taken during photolysis (Figure 3c). This revealed a rapid switching of surface charge, from slightly anionic (-10 mV) to strongly cationic (+25 mV), within 2 min irradiation time. As expected, irradiation of control liposomes (100% DOPC) had no effect on surface charge. We are not currently able to explain the differences in zeta potential between DOPC:**4** liposomes formed following complete photolysis of **1** at the liposome surface (+25 mV) and those formulated directly as DOPC:**4** (+45 mV) liposomes. Importantly, light triggered charge switching of the liposome surface did not lead to apparent destabilization of the liposome membrane^[16] with liposome size and population polydispersity remaining constant before and after UV irradiation (Figure 3d). Caged, neutral liposomes (DOPC:**1**; 1:1) were stable for at least 2 days at 37 °C in biologically relevant solutions (buffer + serum) while kept in the dark, as the size of liposomes and corresponding polydispersity (PDI) barely changed over the time (Figure S9).

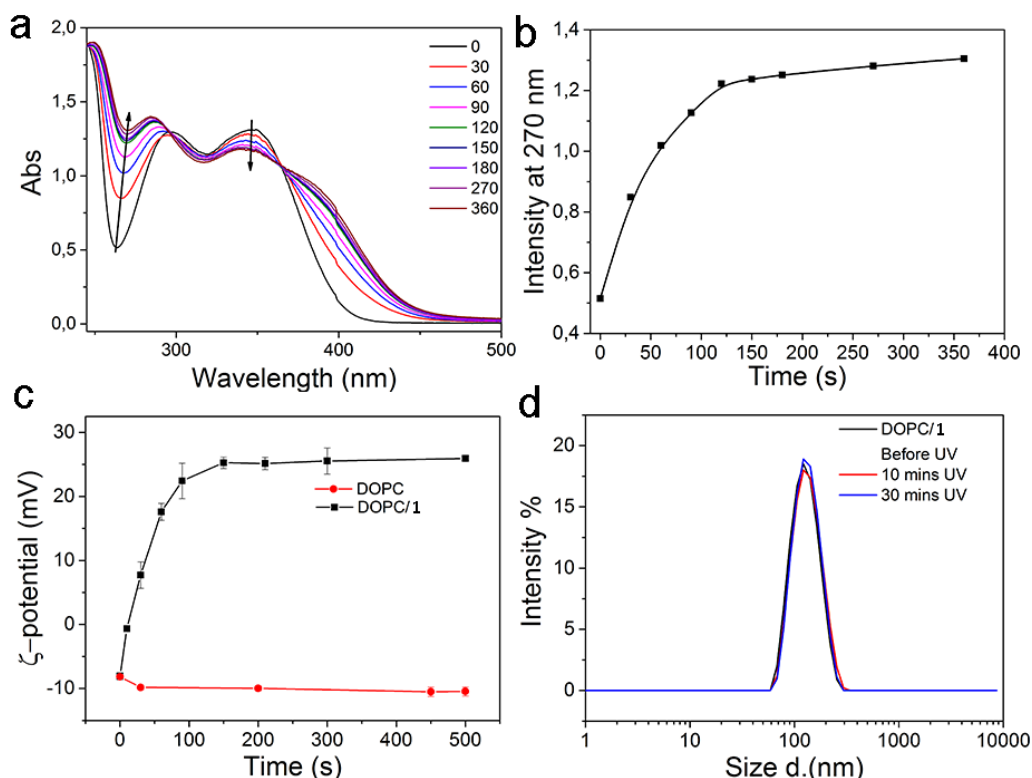


Figure 3. (a) Time evolution of the UV-VIS spectrum of **1** (100 μ M; H₂O:MeCN:^tBuOH (1:1:1)) during UV irradiation (365 nm, 15-17 mW/cm²), time points in seconds; (b) Time evolution of the UV absorbance at 270 nm; (c) The zeta potential of caged liposomes (DOPC/**1** 1:1) and DOPC liposomes with prolonged UV irradiation time; (d) The size distributions of caged liposomes (DOPC/**1** 1:1) before and after UV.

To investigate the biodistribution of DOPC:**1** liposomes (containing 1 mol% fluorescent probe) before and after light activation, liposomes were injected (*i.v.*) into embryonic zebrafish (approximately 2 dpf) and whole embryo images taken using a confocal fluorescent microscope (Figure 4). Prior to light activation, liposomes were freely circulating – as evidenced by the homogenous distribution of liposome associated fluorescence across the whole embryo – and largely restricted to the vasculature of the fish. No significant liposome interactions with either endothelial and/or plasma-exposed macrophages were observed. Following UV irradiation (365 nm, 15-17 mW/cm², 20 min) of the fish, liposomes – within the same embryo – are now clearly seen adsorbed to endothelial cells and across the entire vasculature of the fish. Photocaged liposomes in controls where animals were not exposed to light,

and imaged at the same time points, remained freely circulating (data not shown). From this, we concluded that a) liposomes prior to light activation are freely circulating, b) efficient photolysis of lipid **1** can be achieved *in situ* and *in vivo* and c) charge switching of liposome surface charge lead to the rapid adsorption of liposomes to endothelial cells of the fish vasculature.

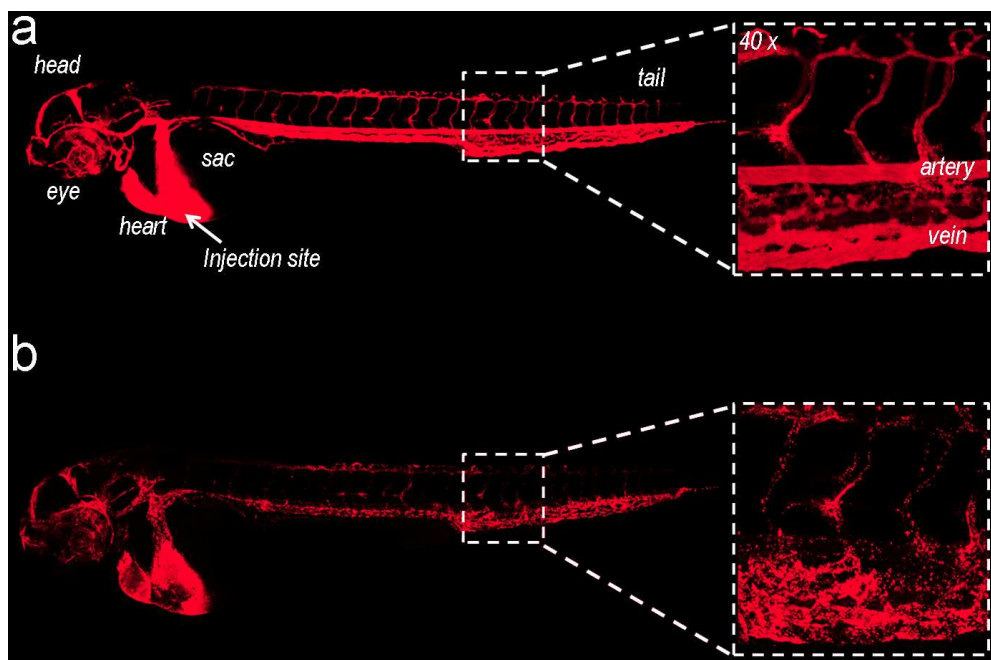


Figure 4. Biodistribution of caged liposomes (DOPC/**1** 1:1, containing 0.1% mol membrane dye; 1mM total lipids) in zebrafish embryos (2 dpf) before (a) and after (b) UV irradiation (365 nm, 15-17 mW/cm², 20 min). Images acquired 2 hpi, liposome-associated fluorescence in red. Injection (i.v.) volume: 1-2 nL.

For optimal application as a potential drug delivery system, we next investigated whether encapsulated contents remained entrapped within liposomes before, during and after UV irradiation. For this, we encapsulated a self-quenching concentration (10 mM) of the fluorescent dye sulforhodamine B (SR-B),^[17] and monitored the release (and associated fluorescence de-quenching) before and after UV irradiation (Figure 5a). From this data, it is clear that the dye remains encapsulated upon charge switching of the liposome membrane. Likewise, UV irradiation of control DOPC liposomes with encapsulated SR-B, which are insensitive to light activation, showed

also no dye release as expected. This confirmed that UV light does not itself physically compromise the integrity of liposome membranes. Transmission electron microscopy (TEM) imaging of SR-B encapsulated within DOPC:1 liposomes confirmed the presence of electron-rich (*i.e.* high contrast) SR-B within the core of the liposome before and after UV irradiation (Figure 5b and 5c). Importantly, these images also show the preservation of liposome morphology following charge switching of the liposome membrane.

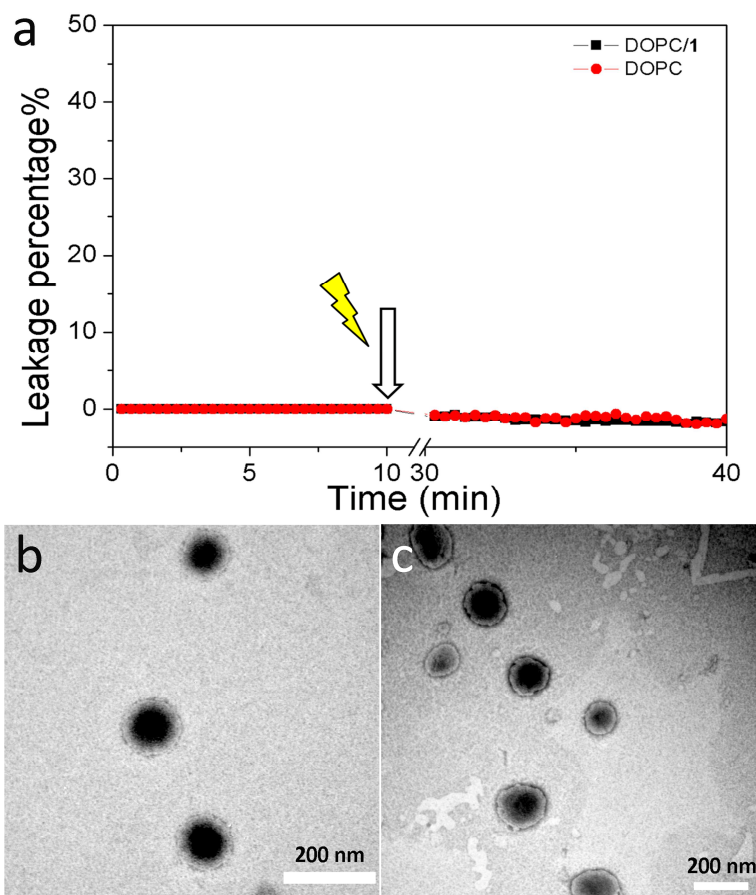


Figure 5. (a) Content leakage test on caged liposomes (DOPC/1 1:1) and DOPC liposomes containing sulforhodamine B (10 mM) with UV irradiation (365 nm, 15-17 mW/cm²). Arrow indicates the point at which samples were UV irradiated for 20 min. The observed minor drop in fluorescence can be attributed to UV irradiation induced photo bleaching. TEM images of caged liposomes containing SR-B (10 mM) prior to (b) and after (c) UV irradiation (365 nm, 15-17 mW/cm², 20 min).

Having established the successful light activated switching of liposome surface charge and drug encapsulation, we next investigated the potential for light triggered drug delivery to cells *in vitro*. Again using encapsulated self-quenching concentrations of SR-B, DOPC:1 liposomes were incubated with HeLa cells and imaged before and after 10 min UV irradiation (Figure 6). Prior to light activation, no delivery of SR-B to cells was observed, however following UV activation, increasing concentration of SR-B in the cells could be seen over time. The release of SR-B into the cell cytosol (and consequent de-quenching of fluorescence) requires active uptake of liposomes and subsequent endosomal escape. This accounts for the time delay between, presumably near instantaneous, liposome-cell membrane interactions following light activation and the visualization of released dye within the cell. These experiments confirm that liposomes are efficiently taken up by cells following light activation and surface charge switching, and that this leads to the successful intracellular delivery of membrane impermeable cargos to the cytosol of cells.

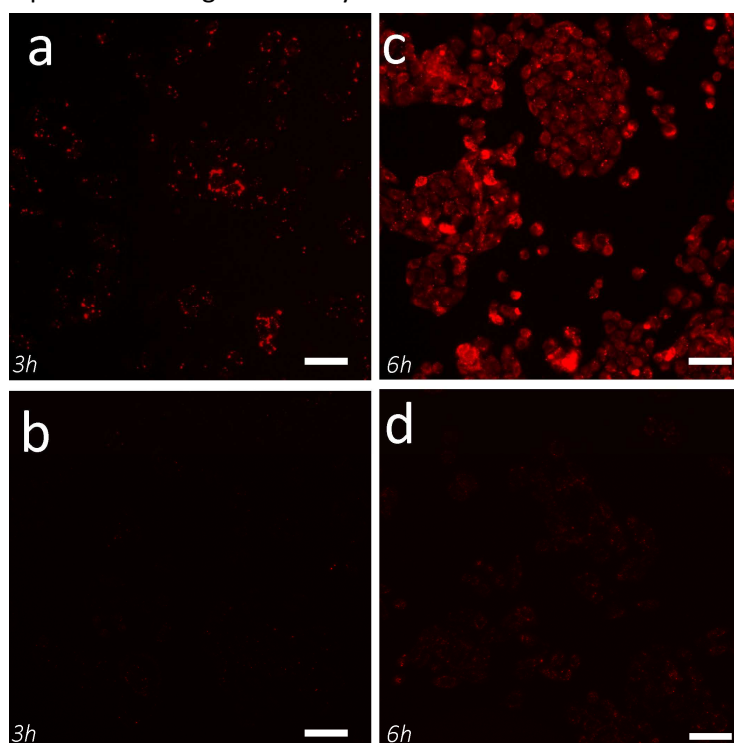


Figure 6. Fluorescent images of the cellular uptake of caged liposomes containing SR-B (10 mM), at 3 and 6 h post incubation, following (a,c) and without (b,d) UV irradiation. The scale bar represents 200 μm .

Finally, we assessed light triggered drug delivery via charge switching of liposome membranes *in vivo*. For this, we encapsulated propidium iodide (PI, 15 mM), a cell impermeable nuclear stain, within fluorescent (DOPE-Atto633, 0.5 mol%) photocaged liposomes composed of DOPC:1 (1:1 molar ratio). These liposomes were injected into a 2 dpf zebrafish embryo and imaged before and after irradiation *in situ* (365 nm, 15-17 mW/cm², 20 min). Without UV irradiation, caged liposomes freely circulated within the blood vessels of the embryonic fish (Figure 7a, blue). Following irradiation however, immobile liposomes can now be clearly seen absorbed across the entire vascular endothelium of the fish, appearing as distinct fluorescent punctae (Figure 7b, blue). Crucially, delivery of encapsulated PI, primarily to endothelial cells, is significantly enhanced following light activation and photoswitching of liposome surface charge (Figure 7, red). Endothelial cells are long and thin and PI associated fluorescence therefore appears to delineate the blood vessel lining. The larger and brighter fluorescent cells containing PI are plasma-exposed macrophages. Low level uptake of caged liposomes by these cells is observed in the absence of light activation (Figure 7a, white arrows). This data confirms that liposomes not only adsorb to cells following light activation but are taken up and are able to release the encapsulated cargos over time. This paves the way for light directed delivery of membrane impermeable therapeutic cargos *in vivo*.

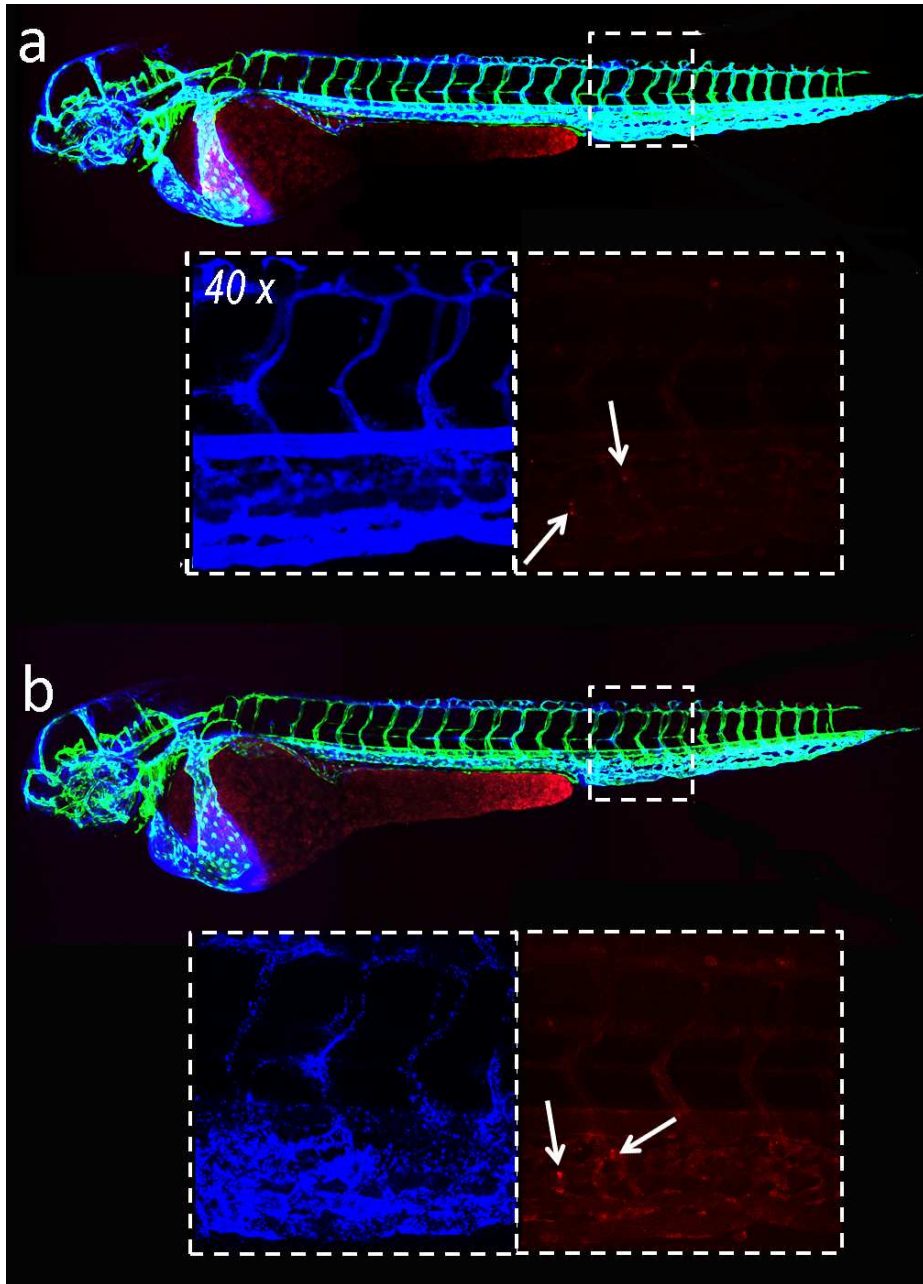


Figure 7. The distribution and cellular uptake of caged liposomes (DOPC/1 1:1 + 0.1% mol DOPE-ATTO633; 4 mM total lipids) containing 15 mM encapsulated PI in *kdrl:GFP* zebrafish embryos (2dpf) - before (a) and after (b) UV irradiation (365 nm, 15-17 mW/cm², 10 min). Injection volume: 1-2 nL. Images acquired 2 hpi. Blood vessels (green), liposomes (blue), PI (red).

5.3 Conclusions

In this work, we demonstrated successful switching of liposome surface charge *in situ* and *in vivo* using light as a trigger for activation. Prior to light activation, photocaged liposomes showed no interaction with cells *in vitro* and *in vivo* (following *i.v.* injection in embryonic zebrafish) and were freely circulating. Upon the light activation, the liposome surface charge switched rapidly to become cationic and as a result the liposomes adhered to, and were taken up by endothelial cells across the entire vasculature of the embryonic fish. Importantly, the encapsulated content was retained within the liposome before and after light activation. In this way, we were able to successfully demonstrate light targeted drug delivery of membrane impermeable cargos to cells *in vivo*. Compared to existing technologies, this approach offers complete (user defined) spatiotemporal control over drug delivery *in vivo* as well as the potential to deliver non-drug like and membrane impermeable therapies (*e.g.* proteins and oligonucleotides). It is important to note that light is used currently used in clinical application (*e.g.* during photodynamic therapy) and the maximal tolerable light dose (MTD) in humans is 1500–3700 J.^[18] In our experiments, embryonic zebrafish are subjected to a light dose of 4.85 J/cm² (145.5 mJ for the whole fish), several orders of magnitude below the MTD limit. In any event, the potential phototoxicity could be alleviated by using 2-photon excitation sources to obtain better tissue penetration with less harm to normal tissues.^[19]

5.4 Experimental

5.4.1 Materials and Instruments

1,2-dioleoyl-sn-glycero-3-phosphocholine (**DOPC**), 1,2-dioleoyl-3-trimethylammonium-propane (chloride salt) (**DOTAP**) and 1,2-dioleoyl-sn-glycero-3-phosphoethanolamine-N-(lissamine rhodamine B sulfonyl) (ammonium salt) (**DOPE-LR**) were purchased from Avanti Polar Lipids. 1,2-dioleoyl-sn-glycero-3-phosphoethanolamine-ATTO633 dye (**DOPE-ATTO633**) was purchased from ATTO-TEC GmbH. Cholesterol and all other chemical reagents were purchased at the highest grade available from Sigma Aldrich and used without further purification. All solvents were purchased from Biosolve Ltd. HEPES buffer: 10 mM HEPES, NaOH, pH 7.4. Phosphate buffered saline (PBS): 5 mM KH_2PO_4 , 15 mM K_2HPO_4 , 150 mM NaCl, pH 7.4. Sulforhodamine B solution (10 mM, pH=7.4) and propidium iodide (15 mM, pH=7.4) were prepared in PBS buffer. Silica gel column chromatography was performed using silica gel grade 40-63 μm (Merck). TLC analysis was performed using aluminium-backed silica gel TLC plates (60F 254, Merck), visualisation by UV absorption at 254 nm and/or staining with KMnO_4 solution. NMR spectra (^1H) were measured on a Bruker AV-400MHz spectrometer. Chemical shifts are recorded in ppm. Tetramethylsilane (TMS) is used as an internal standard. Coupling constants are given in Hz. Size exclusion chromatography was carried out using illustraTM NAPTM SephadexTM G-25 DNA grade pre-made columns (GE Healthcare) and used according to the user instructions.

Particle size distributions were obtained using a Malvern Zetasizer Nano ZS equipped with a peltier controlled thermostatic holder. The laser wavelength was 633 nm and the scattering angle was 173° . To obtain an estimation of the hydrodynamic radius, D_h , the Stokes-Einstein relation was used:

$$D = \frac{\kappa_B T}{3\pi\eta D_h}$$

where, k_B is the Boltzmann constant and η is the viscosity of the solvent. DLS measurements were carried out at room temperature.

UV irradiation was performed using a high-power LED (365 nm, 15-17 mW/cm², Roithner Laser Technik GmbH, Vienna, Austria) mounted at a fixed distance of 1 cm above the samples.

Fluorescence measurements for content leakage of liposomes were performed on a TECAN Plate Reader Infinite M1000. All experiments were carried out in 96-well plates (PP Microplate, 96 well, solid F-bottom (flat), chimney well). For every well the final volume was 200 µL. Fluorescent measurements were recorded at 25 °C.

The structure of the liposomes containing sulforhodamine B (SR-B) was characterized using transmission electron microscopy (TEM) operated at 70 kV (JEOL 1010, USA). a droplet of the sample was placed on a copper grid coated with a carbon film for 3 minutes and washed 3 times with water. Next the sample was stained with 0.5% uranyl acetate.

Zeta potentials were measured on a Zetasizer Nano ZS (Malvern) equipped with a dip-cell electrode. All samples (in 10 mM HEPES) were measured three times and at room temperature.

Size exclusion chromatography (SEC) was carried out using illustraTM NAPTM SephadexTM G-25 DNA grade pre-made columns (GE Healthcare) and used according to the user instructions.

HeLa cells were cultivated in Dulbecco's Modified Eagle's Medium (DMEM), supplemented with 10% fetal calf serum (iron supplied), 2% L-glutamine, 1% penicillin and 1% streptomycin. Cells were cultured in an atmosphere of 5% CO₂ at 37°C. Medium was refreshed every two days and cells passaged at 70% confluence by treatment with trypsin-EDTA (0.05% trypsin).

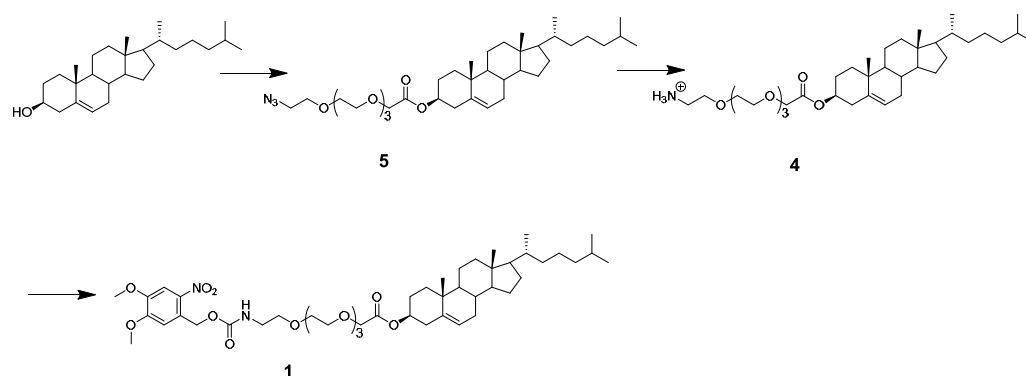
Fluorescence microscopy imaging of cells was done using an Olympus IX81 fluorescence microscope equipped with a filter cube (wavelength settings for SR-B Ex/Em: 565/586 nm).

Fluorescent images of zebrafish were acquired on Leica TCS SP8 confocal laser scanning microscope. Leica application suite advanced fluorescence software (LAS AF, Leica Microsystems B.V., Rijswijk, The Netherlands) and ImageJ (developed by the

National Institutes of Health) were used for image analysis and liposome colocalization studies. Wavelength settings for GFP Ex/Em: 485/530 nm (Ex laser: 488 nm), for propidium iodide Ex/Em: 535/617 nm (Ex laser: 543 nm), for NBD Ex/Em: 455/530 nm (Ex laser: 488 nm) and for ATTO 633 Ex/Em: 635/653 nm (Ex laser: 635 nm).

5.4.2 Synthesis of **1**

Photo-active lipid **1** was synthesized according to the following scheme.



Scheme 1. Synthesis scheme of photo-active lipid **1**.

Synthesis of **5**

Cholesterol (194 mg, 502 μmol , 1.00 eq.), 14-azido-3,6,9,12-tetraoxatetradecanoic acid (139 mg, 502 μmol , 1.00 eq.) and a catalytic amount of DMAP (6 mg, 50 μmol , 0.10 eq.) were dissolved in dry DCM (5 mL). A solution of EDC•HCl (192 mg, 1.00 mmol, 2.00 eq.) and DIPEA (0.13 mL, 753 μmol , 1.50 eq.) in dry DCM (5 mL) was added to the reaction mixture at 0 °C. The solution was stirred for 20 h at room temperature. DCM (40 mL) was added and the solution was washed with 1 M aqueous hydrochloric acid (2 x 50 mL) and a saturated aqueous sodium chloride solution (50 mL). The organic phase was dried over magnesium sulfate and the solvent was removed under reduced pressure. The crude product was purified by flash-column chromatography (petroleum ether (40 – 60 °C)/ethyl acetate 1:0 to 4:1 to 3:1 to 2:1) to obtain **5** (127 mg, 197 μmol , 39%) as a white solid. R_f = 0.37 (Pet. Ether: EtOAc; 1:1). $^1\text{H-NMR}$ (400 MHz, CDCl_3): δ (ppm) = 5.37 (s, 1H, $\text{C}=\text{CH}$), 4.80 – 4.60 (m, 1H, OCH_{chol}), 4.12 (s, 2H, CH_2COO), 3.78 – 3.60 (m, 14H, $\text{OCH}_2\text{CH}_2\text{O}$),

3.39 (d, $J = 2.2$ Hz, 2H, CH_2N_3), 2.33 (d, $J = 7.4$ Hz, 2H, $\text{CH}_2\text{C}=\text{CH}$), 2.07 – 0.80 (m, 38H, H_{chol}), 0.67 (s, 3H, CH_3CCH). **HR-MS** (ESI^+): calc. ($\text{C}_{37}\text{H}_{63}\text{N}_3\text{O}_6\text{Na}$): $m/z = 668.46091$, found: $m/z = 668.46063$.

Synthesis of 4

5 (105 mg, 163 μmol , 1.00 eq.) was dissolved in dry THF (8 mL) and a solution of 1 M trimethylphosphine in toluene (0.49 mL, 489 μmol , 3.00 eq.) was added dropwise at 0 °C. The solution was warmed to room temperature and stirred for 3.5 h. A 1 M aqueous sodium hydroxide solution (25 mL) was added and the mixture was stirred for 1 h at room temperature. The solution was extracted with DCM (3 x 30 mL), the organic phase was washed with a saturated aqueous sodium chloride solution (30 mL) and dried over magnesium sulfate. The solvent was removed under reduced pressure. The crude product was purified by flash-column chromatography (DCM/MeOH 1:0 to 99:1 to 97:3 to 95:5 to 9:1, the eluent contained 1% of a 33% aqueous ammonia solution) to obtain **4** (37.4 mg, 60.2 μmol , 37%) as a white solid. $R_f = 0.21$ (CH_2Cl_2 :MeOH:aq. NH_3 (33%); 9:1:0.1). **$^1\text{H-NMR}$** (400 MHz, CDCl_3): δ (ppm) = 5.36 (d, $J = 3.9$ Hz, 1H, $\text{C}=\text{CH}$), 4.75 – 4.60 (m, 1H, OCH_{chol}), 4.10 (s, 2H, CH_2COO), 3.77 – 3.56 (m, 14H, $\text{OCH}_2\text{CH}_2\text{O}$), 3.50 (t, $J = 5.2$ Hz, 1H, $\text{CH}_2\text{CH}_2\text{NH}_2$), 2.85 (t, $J = 5.2$ Hz, 1H, $\text{CH}_2\text{CH}_2\text{NH}_2$), 2.31 (d, $J = 7.8$ Hz, 2H, $\text{CH}_2\text{C}=\text{CH}$), 2.07 – 0.83 (m, 38H, H_{chol}), 0.65 (s, 3H, CH_3CCH). **HR-MS** (ESI^+): calc. ($\text{C}_{37}\text{H}_{66}\text{NO}_6$): $m/z = 620.48847$, found: $m/z = 620.48854$.

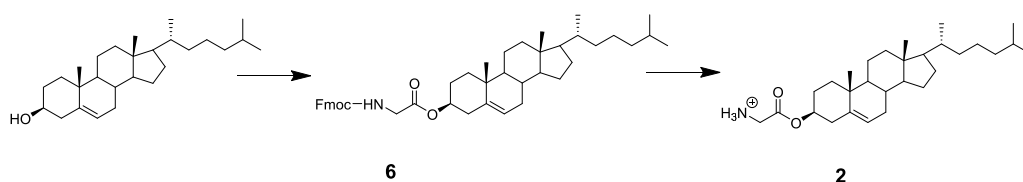
Synthesis of 1

The chloride salt of **4** (39.5 mg, 60.2 μmol , 1.00 eq.) and DIPEA (16 μL , 90.3 μmol , 1.50 eq.) were dissolved in DCM (3 mL). A solution of 4,5-Dimethoxy-2-nitrobenzyl chloroformate (33.2 mg, 120 μmol , 2.00 eq.) in DCM (3 mL) was added at 0 °C and the solution was stirred for 18 h at room temperature. DCM (10 mL) was added and the solution was washed with a 1 M aqueous hydrochloric acid solution (10 mL) and a saturated aqueous sodium chloride solution (10 mL). The organic phase was dried over magnesium sulfate and the solvent was removed under reduced pressure. The crude product was purified by flash-column chromatography (petroleum ether (40 – 60 °C)/ethyl acetate 1:0 to 3:1 to 1:1 to 1:3 to 0:1) to obtain **1** (10.6 mg, 12.3 μmol , 21%) as a colorless solid. $R_f = 0.18$ (Pet. Ether: EtOAc; 1:1). **$^1\text{H-NMR}$**

(300 MHz, CDCl_3): δ (ppm) = 7.72 (s, 1H, H_{Ar}), 7.07 (s, 1H, H_{Ar}), 5.70 – 5.58 (m, 1H, NH), 5.52 (s, 2H, CH_2, NOVC), 5.43 – 5.26 (m, 1H, $\text{C}=\text{CH}$), 4.79 – 4.59 (m, 1H, OCH_{chol}), 4.11 (s, 2H, CH_2COO), 3.99 (s, 3H, OMe), 3.95 (s, 3H, OMe), 3.77 – 3.65 (m, 4H, $\text{OCH}_2\text{CH}_2\text{O}$), 3.60 (t, $J = 4.9$ Hz, 2H, NHCH_2CH_2), 3.44 (dt, $J = 5.2, 4.8$ Hz, 2H, NHCH_2), 2.32 (d, $J = 7.3$ Hz, 2H, $\text{CH}_2\text{C}=\text{CH}$), 2.09 – 0.83 (m, 38H, H_{chol}), 0.67 (s, 3H, CH_3CCH). **HR-MS** (ESI^+): calc. ($\text{C}_{47}\text{H}_{74}\text{N}_2\text{O}_{12}\text{Na}$): $m/z = 881.51340$, found: $m/z = 881.51353$.

5.4.3 Synthesis of 2

Cationic lipid **2** was synthesized according to the following scheme.



Scheme S2. Synthesis scheme of cationic lipid **2**.

Synthesis of 6

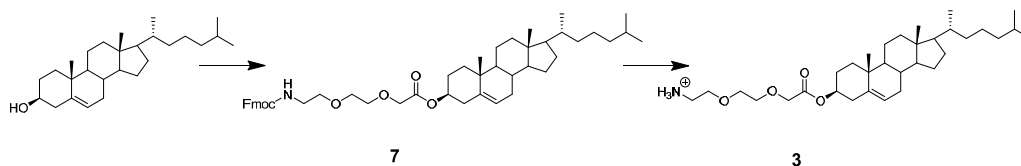
Cholesterol (500 mg, 1.29 mmol, 1.00 eq.), Fmoc-Gly-OH (577 mg, 1.94 mmol, 1.50 eq.) and EDC·HCl (744 mg, 3.88 mmol, 3.00 eq.) were dissolved in dry DCM (25 mL). A catalytic amount of DMAP (16 mg, 129 μmol , 0.10 eq.) was added and the reaction mixture was stirred 24 h at room temperature. DCM (25 mL) was added and the solution was washed with a 1 M aqueous hydrochloric acid solution (2 x 50 mL), distilled water (50 mL) and a saturated aqueous sodium chloride solution (50 mL). The organic phase was dried over sodium sulfate and the solvent was removed under reduced pressure. The crude was purified by flash-column chromatography to obtain **6** (604 mg, 0.91 mmol, 70%) as a colorless solid. $R_f = 0.34$ (Pet. Ether(40 – 60 °C): EtOAc; 4:1). **$^1\text{H-NMR}$** (400 MHz, CDCl_3): δ (ppm) = 7.77 (d, $J = 7.5$ Hz, 2H, H_{Ar}), 7.61 (d, $J = 7.5$ Hz, 2H, H_{Ar}), 7.40 (t, $J = 7.5$ Hz, 2H, H_{Ar}), 7.32 (td, $J = 7.5, 1.0$ Hz, 2H, H_{Ar}), 5.38 (d, $J = 4.0$ Hz, 1H, $\text{C}=\text{CH}$), 5.29 (t, $J = 5.4$ Hz, 1H, NH), 4.77 – 4.63 (m, 1H, OCH_{chol}), 4.40 (d, $J = 7.1$ Hz, 2H, CH_2, Fmoc), 4.24 (t, $J = 7.1$ Hz, 1H, CH_{Fmoc}), 3.98 (d, $J = 5.4$ Hz, 2H, CH_2NH), 2.34 (d, $J = 7.8$ Hz, 2H, $\text{CH}_2\text{C}=\text{CH}$), 2.09 – 1.04 (m, 26H, H_{chol}), 1.02 (s, 3H, $\text{CH}_3\text{CC}=\text{CH}$), 0.91 (d, $J = 6.5$ Hz, 3H, CH_3CHCH), 0.87 (d, $J = 1.8$ Hz, 3H, CH_3CHCH_3), 0.86 (d, $J = 1.8$ Hz, 3H, CH_3CHCH_3), 0.68 (s, 3H, CH_3CCH).

Synthesis of 2

6 (201 mg, 302 μmol) was dissolved in DCM/DEA (1:1, 4 mL) and stirred for 3 h at room temperature. The solvent was removed under reduced pressure and DEA residues were co-evaporated with methanol (3 x 10 mL). The crude was dissolved in DCM and purified by flash-column chromatography (DCM/MeOH 1:0 to 99:1 to 95:5) to obtain **2** (87.4 mg, 197 μmol , 65%) as a pale yellow solid. R_f = 0.34 (CH_2Cl_2 :MeOH; 9:1). $^1\text{H-NMR}$ (400 MHz, CDCl_3): δ (ppm) = 5.38 (d, J = 3.7 Hz, 1H, C=CH), 4.73 – 4.60 (m, 2H, NH_2), 3.41 (s, 2H, CH_2NH_2), 2.32 (d, J = 7.9 Hz, 2H, $\text{CH}_2\text{C}=\text{CH}$), 2.06 – 1.04 (m, 26H, H_{chol}), 1.01 (s, 3H, $\text{CH}_3\text{CC}=\text{CH}$), 0.91 (d, J = 6.3 Hz, 3H, CH_3CHCH), 0.87 (s, 3H, CH_3CHCH_3), 0.85 (s, 3H, CH_3CHCH_3), 0.67 (s, 3H, CH_3CCH).

5.4.4 Synthesis of 3

Cationic lipid **3** was synthesized according to the following scheme.



Scheme S3. Synthesis scheme of cationic lipid **3**.

Synthesis of 7

Cholesterol (100 mg, 259 μmol , 1.00 eq.), 2-(2-(Fmoc-amino)ethoxy)ethoxy]acetic acid (100 mg, 259 μmol , 1.00 eq.) and *cat.* amounts of DMAP (6.00 mg, 49.1 μmol , 0.20 eq.) were dissolved in dry DCM (2 mL). A solution of EDC-HCl (99.2 mg, 517 μmol , 2.00 eq.) and DIPEA (0.07 mL, 389 μmol , 1.50 eq.) in dry DCM (4 mL) was added dropwise to the reaction mixture at 0 °C. The solution was allowed to warm up to room temperature and stirred for 18 h. The reaction mixture was diluted with DCM (20 mL), washed with 1 M aq. hydrochloric acid (2 x 30 mL), water (30 mL) and brine (30 mL). The organic phase was dried over magnesium sulfate and the solvent was removed under reduced pressure. The crude was purified by flash-column chromatography (petroleum ether (40 – 60 °C)/ethyl acetate 1:0 to 4:1 to 2:1 to 1:1) to obtain **7** (125 mg, 166 μmol , 64%) as colorless solid. R_f = 0.21 (CH_2Cl_2 : MeOH; 17:3). $^1\text{H-NMR}$ (400 MHz, CDCl_3): δ (ppm) = 7.76 (d, J = 7.5 Hz, 2H, H_{Ar}), 7.62 (d, J = 7.4 Hz,

2H, H_{Ar}), 7.39 (t, $J = 7.5$ Hz, 2H, H_{Ar}), 7.31 (td, $J = 7.4, 0.9$ Hz, 2H, H_{Ar}), 5.52 (t, $J = 5.2$ Hz, 1H, NH), 5.32 (d, $J = 4.2$ Hz, 1H, C=CH), 4.77 – 4.66 (m, 1H, OCH_{chol}), 4.37 (d, $J = 7.2$ Hz, 2H, CH_{2, Fmoc}), 4.22 (t, $J = 7.2$ Hz, 1H, CH_{Fmoc}), 4.11 (s, 2H, CH₂COO), 3.78 – 3.64 (m, 4H, OCH₂CH₂O), 3.60 (t, $J = 5.1$ Hz, 2H, NHCH₂CH₂), 3.43 (q, $J = 5.1$ Hz, 2H, NHCH₂), 2.32 (d, $J = 7.9$ Hz, 2H, CH₂C=CH), 2.10 – 1.00 (m, 26H, H_{chol}), 0.98 (s, 3H, CH₃CC=CH), 0.91 (d, $J = 6.5$ Hz, 3H, CH₃CHCH), 0.88 (d, $J = 1.9$ Hz, 3H, CH₃CHCH₃), 0.86 (d, $J = 1.8$ Hz, 3H, CH₃CHCH₃), 0.66 (s, 3H, CH₃CCH).

Synthesis of **3**

7 (104 mg, 138 μ mol) was dissolved in DCM/DEA (1:1, 4 mL) and stirred for 3 h at room temperature. The solvent was removed under reduced pressure and DEA residues were co-evaporated with methanol (3 x 30 mL). The crude was dissolved in DCM and purified by flash-column chromatography (DCM/MeOH 1:0 to 9:1 to 17:3) to obtain **3** (28.4 mg, 53.4 μ mol, 39%) as a pale yellow solid. $R_f = 0.21$ (CH₂Cl₂:MeOH; 17:3). ¹H-NMR (400 MHz, CDCl₃): δ (ppm) = 6.86 (s_{br}, 2H, NH₂), 5.37 (s, 1H, C=CH), 4.77 – 4.53 (m, 1H, OCH_{chol}), 4.12 (s, 2H, CH₂COO), 3.85 (s, 2H, NH₂CH₂CH₂), 3.72 (s, 4H, OCH₂CH₂O), 3.26 (s, 2H, NH₂CH₂), 2.31 (d, $J = 7.6$ Hz, 2H, CH₂C=CH), 2.10 – 1.03 (m, 26H, H_{chol}), 1.00 (s, 3H, CH₃CC=CH), 0.90 (d, $J = 6.0$ Hz, 3H, CH₃CHCH), 0.86 (s, 3H, CH₃CHCH₃), 0.84 (s, 3H, CH₃CHCH₃), 0.66 (s, 3H, CH₃CCH).

5.4.5 Photolysis of **1**

The photolysis process of compound **1** was monitored by UV-VIS spectroscopy. A solution of **1** (100 μ M) in acetonitrile:tert-Butanol:water (1:1:1) was irradiated under a LED UV lamp (365 nm, 17 mW) at a fixed distance of 1 cm for 30 seconds and a UV spectrum scan was taken. UV absorption spectra were measured using a Cary 3 Bio UV-vis spectrometer, scanning from 200 nm to 550 nm at 1 nm intervals, scan rate: 120 nm/min. Next, the sample was irradiated for different time periods (60, 90, 120, 150, 180, 270 and 360 seconds) and spectra were measured.

5.4.6 Liposome preparation

Liposomes were prepared *via* extrusion using a mini-extruder (Mini-extruder, Avanti Polar Lipids, Alabaster, US). Lipid stock solutions in chloroform were prepared firstly with a total lipid concentration of 10 mM. For each sample, the relevant lipid film

including membrane dye (DOPE-ATTO633) was formed by evaporating organic solvents under N₂, and hydrated for 20 min using HEPES buffer. The hydrated lipid film was vortexed for at least 1 min to obtain a suspension ([lipid]=10 mM with 0.5 mol% of DOPE-ATTO633). The solution was extruded 11 times through a 400 nm pore membrane to form multilayer vesicles (MLVs) at room temperature. Next the MLVs suspension was sequentially extruded 11 times through a 100 nm pore membrane to generate liposomes. The size distribution and PDI of prepared liposomes was determined by dynamic light scatter (DLS) spectroscopy.

For liposomes containing sulforhodamine B (SR-B) or propidium iodide (PI), the same method was applied, except the hydration buffer was HEPES containing sulforhodamine B (10 mM)/propidium iodide (15 mM). A sephadex G25 size exclusion column was used to remove unencapsulated dye.

5.4.7 Content leakage assay

For content leakage assays, the fluorescence emission of SR-B (10 mM, excitation: 520 nm, emission: 580 nm) encapsulated liposomes ([lipid]=10 mM) was measured prior to UV irradiation for 10 min. The sample was measured again after 20 min of UV irradiation.

5.4.8 *In vitro* cellular uptake

For the cellular uptake experiments, cells (2×10^5 mL⁻¹) were transferred to 48-well cell culture plates (500 µL, Greiner bio-one, Cellstar®) and cultured for 24 h. Cage or activated liposomes (500 µL, [lipid]=10 mM) solution were added to the cells and incubated for 3 or 6 h. Before imaging, the excess of liposomes was removed and the cells were washed three times with DMEM medium.

5.4.9 Zebrafish injection

Zebrafish (strain AB/TL, line Tg(kdrl:egfp)s843)^[20] were handled according to the guidelines from the Zebrafish Model Organism Database, the directives of the local animal welfare committee of Leiden University and the common Directive 2010/63/EU of the European Parliament and the Council. Fertilization was performed by natural spawning at the beginning of the light period and eggs were raised at 28.5

°C in egg water (60 µg/ml Instant Ocean see salts). Liposome solutions were injected into zebrafish embryos (2 dpf) according to a modified microangiography protocol. The embryos were anesthetized in 0.01% tricaine and embedded in agarose gel (0.4%) containing tricaine. 1 nL volumes were calibrated and injected into the sinus venosus/duct of Cuvier. A small pyramidal space, in which the liposome solutions ([lipid]=4 mM) were injected, was created by penetrating the skin with the glassy injection needle and gently pulling it back. The experimental zebrafish was irradiated directly under a UV source (365 nm, 15-17 mW/cm², 10 min) at a distance of 3 cm and imaged again. Embryos were excluded from the experiments in case there was no backward translocation of venous erythrocytes or when the yolk ball was damaged, which would reduce the amount of liposomes in circulation.

5.4.10 Light actinometry

The optical power density of the LED light source used was determined using an integrating sphere setup. For this, the 365-nm LED (H2A1-365, Roithner Lasertechnik, Vienna, Austria), driven by a custom-built LED driver ($I = 350$ mA), was positioned precisely 5 cm above the 6.0 mm aperture of an integrating sphere (AvaSphere-30-IRRAD, Avantes, Apeldoorn, The Netherlands). This sphere was connected by an optical fibre (FC-UV600-2, Avantes) to a UV-Vis spectrometer (AvaSpec-ULS2048L StarLine CCD spectrometer, Avantes). The setup was calibrated using a NIST-traceable calibration light source (Avalight-HAL-CAL-ISP30, Avantes). The LED was switched on, and allowed to warm up for 1 min, before a spectrum was recorded. The obtained spectrum was integrated to obtain the total incident optical power density (in mW/cm²). Light dosages (in J) per zebrafish were obtained by multiplying the optical power density by the average surface area of a zebrafish (0.03 cm²), and the irradiation time (600 s).

5.5 References

- [1] (a) Y. Barenholz, *Journal of Controlled Release* **2012**, *160*, 117-134; (b) C. E. Swenson, W. R. Perkins, P. Roberts, A. S. Janoff, *Breast* **2001**, *10*, 1-7.
- [2] M. Marty, *Breast* **2001**, *10*, 28-33.
- [3] A. Gabizon, R. Isacson, E. Libson, B. Kaufman, B. Uziely, R. Catane, C. G. Bendor, E. Rabello, Y. Cass, T. Peretz, A. Sulkes, R. Chisin, Y. Barenholz, *Acta Oncol* **1994**, *33*, 779-786.
- [4] (a) J. H. Kang, W. Y. Jang, Y. T. Ko, *Pharm Res* **2017**, *34*, 704-717; (b) B. B. Christina R. Miller, Shannon D. McLean, Kathy A. McGovern, and David F. O'Brien, *Biochemistry* **1998**, *37*, 12875-12883.
- [5] M. Schmitt-Sody, S. Strieth, S. Krasnici, B. Sauer, B. Schulze, M. Teifel, U. Michaelis, K. Naujoks, M. Dellian, *Clin Cancer Res* **2003**, *9*, 2335-2341.
- [6] E. Blanco, H. Shen, M. Ferrari, *Nat Biotechnol* **2015**, *33*, 941-951.
- [7] F. Cardarelli, L. Digiacomo, C. Marchini, A. Amici, F. Salomone, G. Fiume, A. Rossetta, E. Gratton, D. Pozzi, G. Caracciolo, *Sci Rep-Uk* **2016**, *6*, 25879-25887.
- [8] D. E. Owens, N. A. Peppas, *Int J Pharm* **2006**, *307*, 93-102.
- [9] (a) P. Yingyuad, M. Mevel, C. Prata, S. Furegati, C. Kontogiorgis, M. Thanou, A. D. Miller, *Bioconjug Chem* **2013**, *24*, 343-362; (b) C. L. Chan, R. N. Majzoub, R. S. Shirazi, K. K. Ewert, Y. J. Chen, K. S. Liang, C. R. Safinya, *Biomaterials* **2012**, *33*, 4928-4935; (c) T. Gjetting, R. I. Jolck, T. L. Andresen, *Adv Healthc Mater* **2014**, *3*, 1107-1118.
- [10] F. Campbell, F. L. Bos, S. Sieber, G. A. Alpizar, B. Koch, J. Huwyler, A. Kros, J. Bussmann, *ACS Nano*, **2018**, accepted. DOI: 10.1021/acsnano.7b06995
- [11] P. Metz, O. Gottschalk, M. Schmitt-Sody, S. Luedemann, M. Eichhorn, B. Schulze, H. Bohnenkamp, E. Guenzi, U. Michaelis, M. Funk, *Ann Rheum Dis* **2007**, *66*, 288-288.
- [12] (a) D. J. Lee, Y. T. Oh, E. S. Lee, *Int J Pharm* **2014**, *471*, 127-134; (b) S. Tang, Q. Meng, H. Sun, J. Su, Q. Yin, Z. Zhang, H. Yu, L. Chen, W. Gu, Y. Li, *Biomaterials* **2017**, *114*, 44-53; (c) J. S. Hersey, C. M. LaManna, H. Lusic, M. W. Grinstaff, *Chem Phys Lipids* **2016**, *196*, 52-60; (d) Q.

Han, W. Wang, X. Jia, Y. Qian, Q. Li, Z. Wang, W. Zhang, S. Yang, Y. Jia, Z. Hu, *ACS Appl Mater Interfaces* **2016**, *8*, 18658-18663.

[13] S. AmitKessel. NirBen-Tal, *Biophysical Journal* **2001**, *81*, 643–658.

[14] B. K. Kim, G. B. Hwang, Y. B. Seu, J. S. Choi, K. S. Jin, K. O. Doh, *Bba-Biomembranes* **2015**, *1848*, 1996-2001.

[15] S. H. C. A. Li Kong, Sylvestre Bonnet, Alexander Kros and Frederick Campbell, *Angew. Chem. Int. Ed.* **2016**, *55*, 1396 –1400.

[16] S. J. Leung, M. Romanowski, *Theranostics* **2012**, *2*, 1020-1036.

[17] W. Bae, T. Y. Yoon, *Biophys J* **2013**, *104*, 88a-88a.

[18] S. K. P. Satish Krishnamurthy, Peggy Witmer and Tony Brown, *Lasers in Surgery and Medicine* **2000**, *27*, 224–234.

[19] K. Peng, I. Tomatsu, B. van den Broek, C. Cui, A. V. Korobko, J. van Noort, A. H. Meijer, H. P. Spaink, A. Kros, *Soft Matter* **2011**, *7*, 4881.

[20] L. D. Covassin, A. F. Siekmann, M. C. Kacergis, E. Laver, J. C. Moore, J. A. Villefranc, B. M. Weinstein, N. D. Lawson, *Dev Biol* **2009**, *329*, 212-226.

5.6 Supporting information

5.6.1 Zebrafish embryo, a Developmental Model Organism

Zebrafish are vertebrates which have been widely used in the scientific study of embryo development and gene function.^[1] Zebrafish embryos develop rapidly outside of the mother with all major organs, such as heart, brain and intestine, functionally developed by 36 hours post fertilization (hpf). By 36 hpf, zebrafish embryos have a closed circulatory system whose vasculature develops in anatomical form (Figure S1).

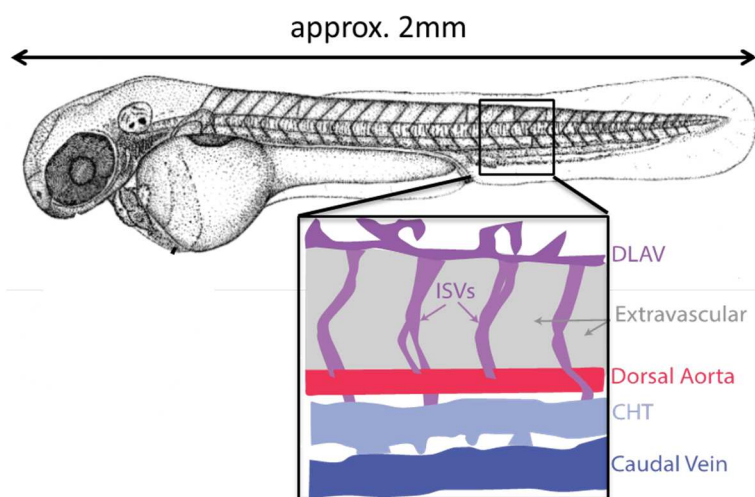


Figure S1 The caudal vascular system of zebrafish in the larval stage. The dorsal longitudinal anastomotic vessel (DLAV), the intersegmental vessels (ISVs), the extravascular tissue, the dorsal aorta, the caudal hematopoietic tissue (CHT) and the caudal vein are indicated.

There are various advantages of using zebrafish as a model organism system in scientific research. 1) The genome of zebrafish has fully sequenced and 70% homologous to humans. In the case of genes encoding disease-causing human proteins, this number increases to 82%. There have been numerous models of human diseases established in zebrafish.^[2] 2) Zebrafish are highly fecund, produce large clutches (100-200 embryos) and embryonic development is rapid and external of the mother. Testing can be carried out on large sample sets of animals and the cost of raising and maintaining zebrafish is much lower than that of mammals. 3) Zebrafish embryos are small and transparent allowing the *in vivo* observation of internal development and function, over the entire organism, using simple microscopy setups. The utility of zebrafish has been significantly enhanced by the generation of tissue-specific fluorescent transgenic zebrafish.

As a vertebrate model, zebrafish have wide biological applications, such as gene mapping, genome mutagenesis, transgenesis, chimeric embryo analysis, protein overexpression or

knockdown and chemical screens.^[3] Zebrafish mutant phenotypes, identified in forward genetic screens, have provided valuable insight into corresponding human disease pathophysiology.^[4] Likewise high-throughput chemical screens have proved invaluable as pre-clinical toxicological tests prior to initial screening in rodent models.^[5]

5.6.2 Additional figures

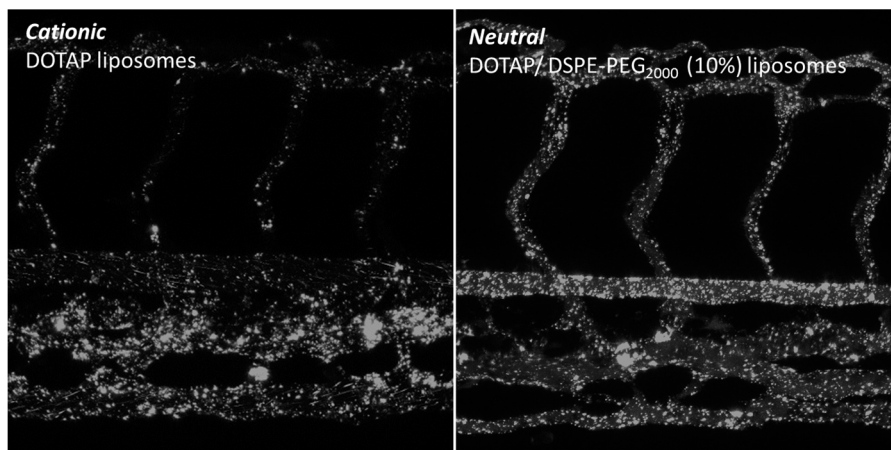


Figure S2. The distribution of cationic liposomes (DOTAP) and PEGylated cationic liposomes (DOTAP/DSPE-PEG₂₀₀₀; 9:1) within a zebrafish embryo. Fluorescently labeled liposomes ([lipid]= 1 mM, containing 1 mol% Rhod-PE) were injected into the duct of Cuvier of the embryonic fish at 54 hpf. Confocal microscopy was performed in a defined region caudal to the yolk extension at 1hpi. Image taken from unpublished data.

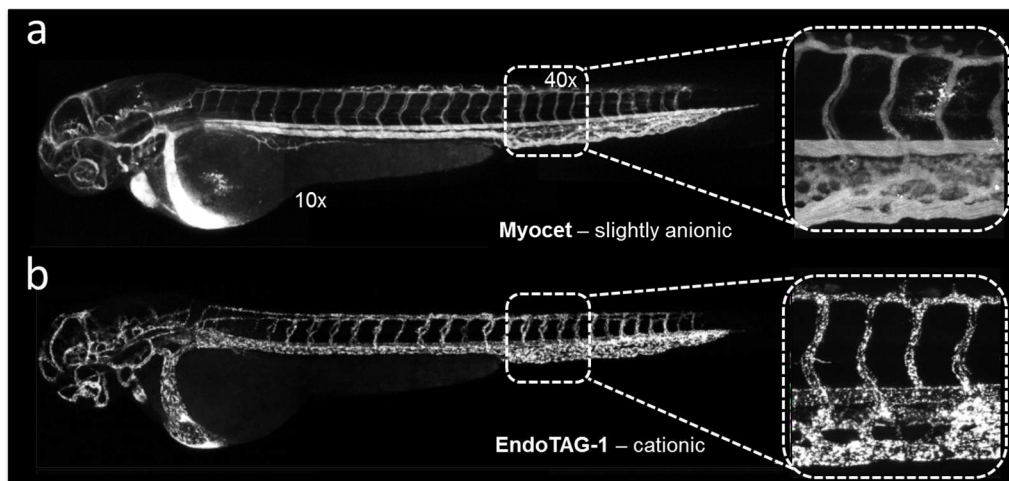


Figure S3. The distribution of neutral liposomes (Myocet) and cationic liposomes (EndoTAG-1) in zebrafish embryo.

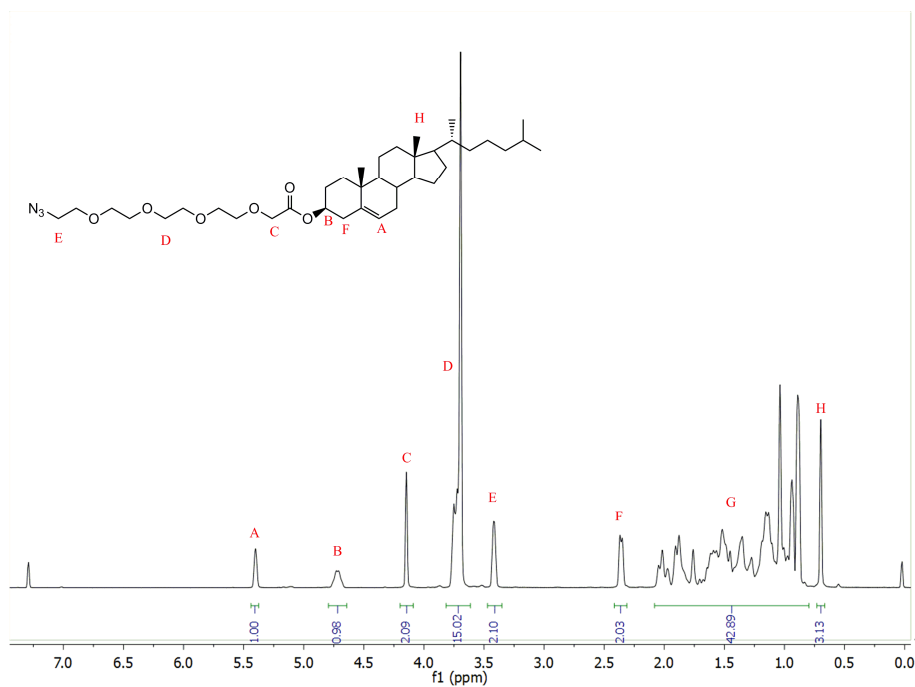


Figure S4. The ^1H -NMR structure of **5**.

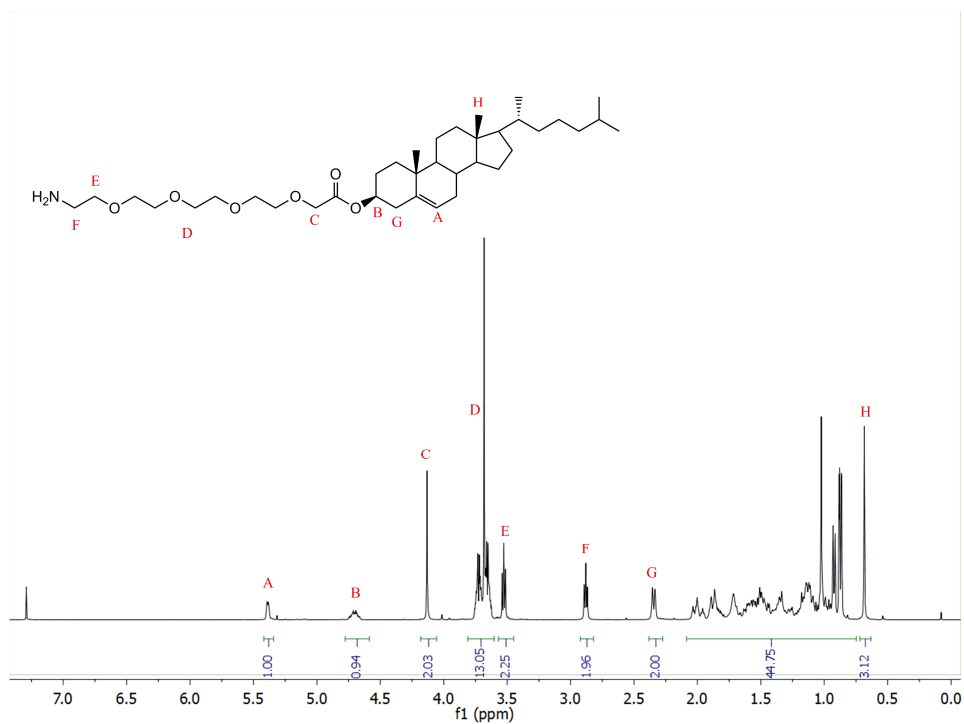


Figure S5. The ¹H-NMR structure of **4**.

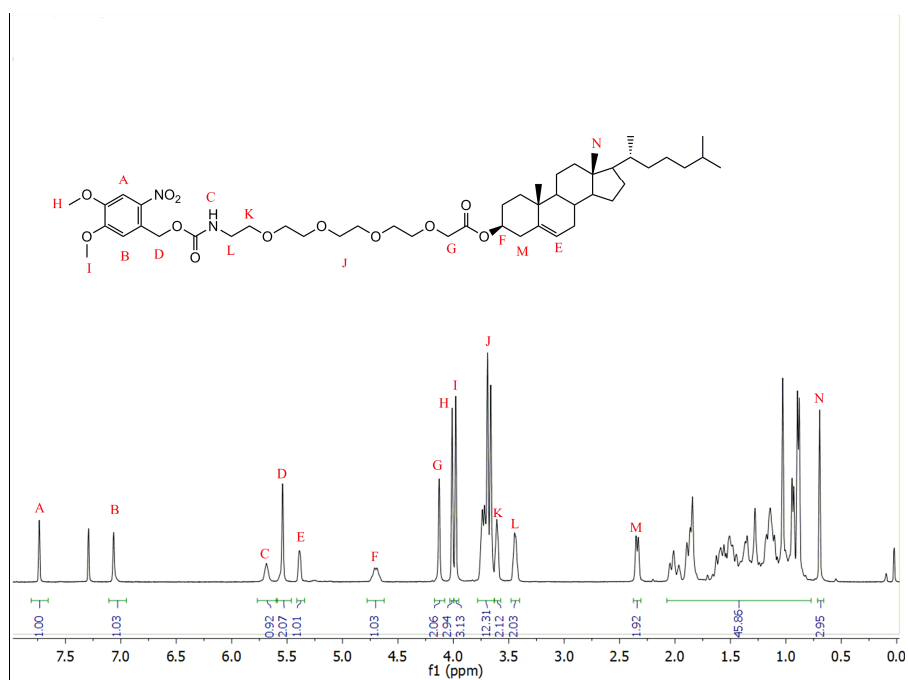


Figure S6. The ¹H-NMR structure of **1**.

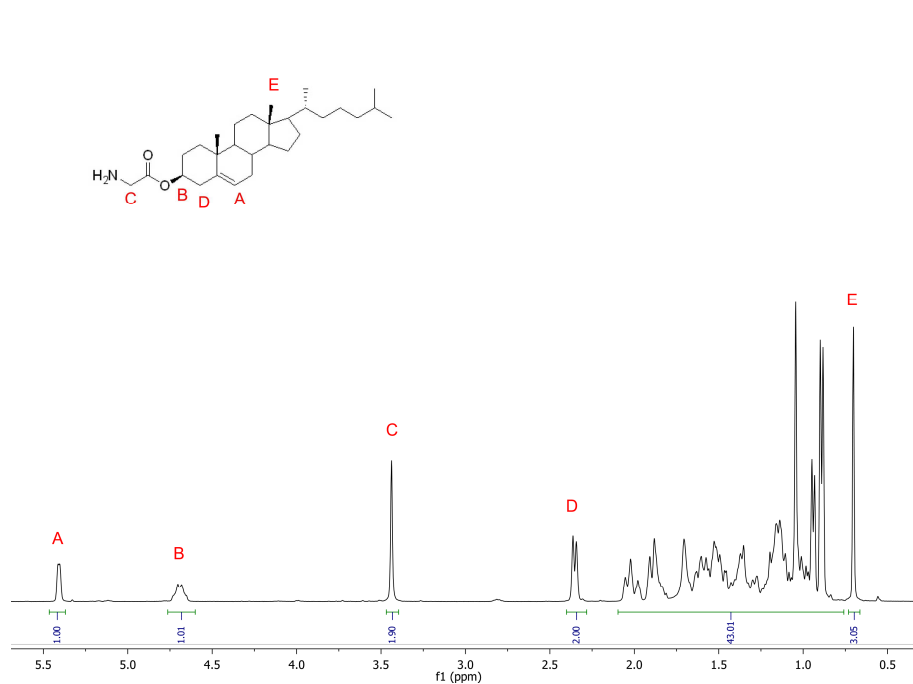


Figure S7. The ^1H -NMR structure of **2**.

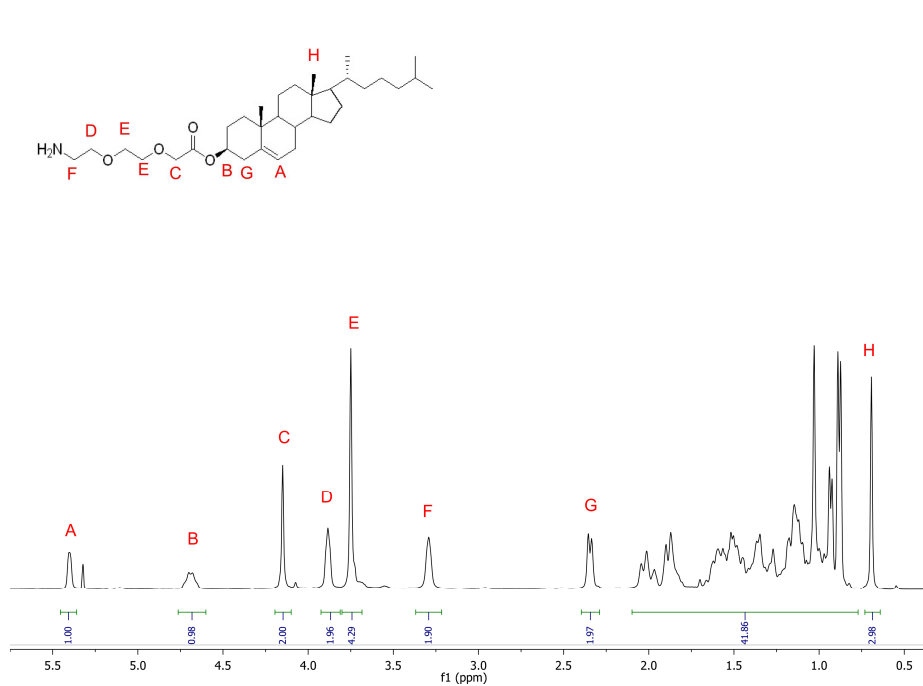


Figure S8. The ^1H -NMR structure of **3**.

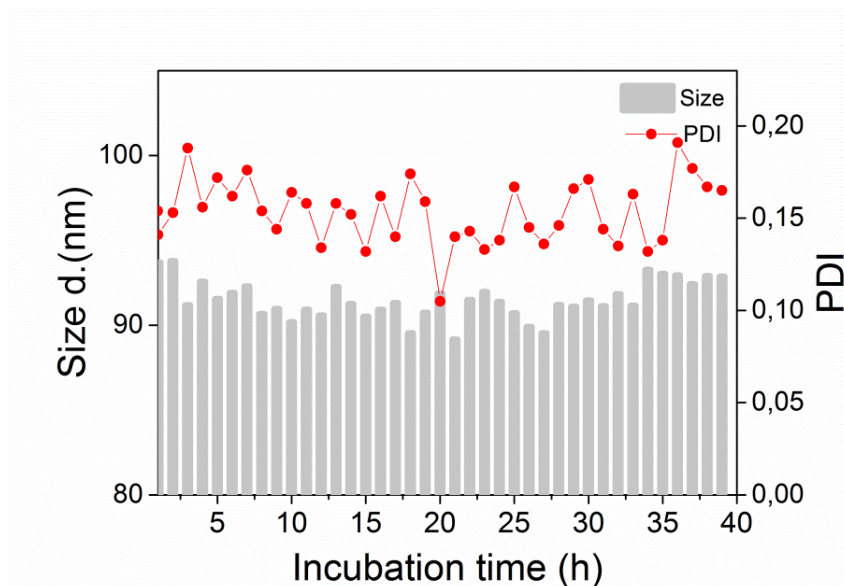


Figure S9. The size change and PDI of caged liposomes (DOPC/1 1:1) incubated with DMEM (+10% FCS) as a function of time.

References:

- [1] H. R. Zope, F. Versluis, A. Ordas, J. Voskuhl, H. P. Spaink, A. Kros., *Angew. Chem. Int. Ed.* **2013**, 52, 14247–14251.
- [2] A. F. Schier., *Nature*, **2013**, 496, 443–444.
- [3] G.N. Wheeler, A. W. Brandli, *Dev Dyn*, **2009**, 238,1287-1308.
- [4] G.J. Lieschke, P.D. Currie, *Nat Rev Genet*, **2007**, 8, 353-367.
- [5] (a) S. J. Poureetezadi, E. Donahue, R. A. Wingert, *J Vis Exp*, **2014**, 93, 5, 2063; (b) S. A. Brittijn, S. J. Duivesteijn, M. Belmamoune, L. F. M. Bertens, W. Bitter, J. D. De Bruijn, D. L. Champagne, E. Cuppen, G. Flik, C. M. R.A.J.Janssen, I.M.L.De Jong, E.R. De Kloet, A. Kros, A.H.Meijer, J. R. Metz, A. M. van der Sar, M. J.Schaaf,S. Schulte-Merker , H.P. Spaink, P. P Tak, F. J. Verbeek, M. J. Vervoordeldonk,F.J. Vonk, F. Witte, H. Yuan, M. K. RichardsonInt, *J Dev Biol.* **2009**, 53, 835-850.

6

Summary and perspective

O-Nitrobenzyl groups have been widely used as molecular photocages in both organic chemistry^[1] and biology^[2]. Photocaging a molecule temporarily blocks its function. Function is regained upon light irradiation. The ability to precisely control where and when light is delivered means it is possible to precisely control where and when a photocaged molecule becomes 'active'. Applied to drug delivery systems, light can be used to direct exactly where drugs are released within the body.

O-Nitrobenzyl groups have been used to cage various therapeutic agents^[3], including small drug molecules, peptides, proteins and nucleic acids but have also been incorporated within more complex, multicomponent drug delivery systems, including hydrogels, micelles, liposomes and inorganic nanoparticles.^[4] In this thesis, *o*-nitrobenzyl groups are used either as photolabile linkers, connecting polyethylene glycol (PEG) to various nanoparticle drug delivery systems (**Chapters 2-4**), or as photocage of specific chemical functionality (**Chapter 5**). In all cases, the use of *o*-nitrobenzyl enables precise control over where and when systems are 'activated'.

In **chapter 2**, I described a strategy to precisely control membrane fusion of two distinct liposome populations. This was achieved by the introduction of a photolabile PEG corona on the surface of fusogenic liposomes. This efficiently blocked the interaction between two complementary lipopeptides displayed from opposing membranes. This work revealed a minimum critical length requirement of PEG necessary to effectively shield this peptide-peptide interaction and a direct correlation between the time of light irradiation and fusion efficiency. Using high power LED light sources, triggered membrane fusion was spontaneous and, by extending our strategy to biological scenarios, precise spatiotemporal control of liposome docking to cell membranes was demonstrated *in vitro*. In this case, cells pre-functionalised with fusogenic lipopeptides were incubated with PEGylated liposomes containing complementary lipopeptides. After light triggered dePEGylation of the liposome surface, the spontaneous interaction between complementary lipopeptides resulted in the well-defined and light templated accumulation of liposomes at the cell surface. This work represents the first demonstration of user-controlled membrane fusion. In Nature, membrane fusion is precisely controlled in time and space to ensure correct cellular function. The ability to control membrane fusion in this way paves the way for

more efficient drug delivery systems, in which liposome-encapsulated drugs are delivered, not only with spatiotemporal precision, but potentially directly to the cell cytosol, avoiding degradative endocytotic uptake.

In **chapters 3 and 4**, the *o*-nitrobenzyl group was used within two prodrug systems: PEG₂₀₀₀-*o*-nitrobenzyl-doxorubicin (**chapter 3**) and PEG₂₀₀₀-*o*-nitrobenzyl-nervonic acid (**chapter 4**). In **chapter 3**, the prodrug, PEG₂₀₀₀-*o*-nitrobenzyl-doxorubicin, formed high loading (20 wt%) doxorubicin micelles, which upon light activation resulted in rapid and quantitative DOX release. Prior to light activation, these prodrug micelles closely resembled, in size and surface chemistry, clinically approved liposomal-doxorubicin formulations (*e.g.* Doxil®). These therapeutic liposomes passively target solid tumors *via* the EPR effect. However, unlike these formulations, no premature drug release was observed – a factor that can lead to adverse side effects for a patient (*e.g.* cardiomyopathy).

Upon low power UV irradiation, complete photolysis to pharmacologically ‘active’ DOX was achieved within 25 minutes and, in the absence of light, no cytotoxicity was observed up to a prodrug concentration of 100 μ M. Importantly, the light dose required to fully release DOX neither caused significant photoinduced cytotoxicity. Upon light activation the cytotoxicity of released DOX correlated with both irradiation time and prodrug concentration. To showcase the precision afforded by this system, we showed exquisite spatiotemporal control of DOX delivery to cells in culture. This system has the potential not only to passively target solid tumors *via* the EPR effect, but by preventing premature drug leakage *en route* to the tumor while ensuring on demand and quantitative release once there, it could result in significantly reduced side effects compared to current targeted cancer nanomedicines.

The lipid composition and thickness of cell membranes has been shown to significantly influence the activity of membrane embedded proteins. To generate thicker cell membranes, it is necessary to supplement cells with very long chain fatty acids (vlcFAs) as biosynthetic precursors of very long chain phospholipids (vlcPLs). The delivery of vlcFAs to cells has however been severely hampered by the extreme insolubility of these reagent in aqueous solutions. In **chapter 4**, we overcome this issue by synthesizing light sensitive, vlcFA-PEG (PEG₂₀₀₀-*o*-nitrobenzyl-nervonic acid;

FA24:1) amphiphiles which self-assemble into close-packed micelles in aqueous solutions. These micelles spontaneously disassembled in the presence of lipid bilayers (both liposome membranes and cell membranes) to efficiently embed vlcFA-PEG amphiphiles within the target bilayer. Subsequent light irradiation released conjugated PEG, leaving free nervonic acid remnant within the membrane. When this experiment was performed on cultured cells, free nervonic acid was subsequently processed to form cellular phospholipids with increased vlcFA content. This approach offers, for the first time, an efficient method to modulate the composition and potentially the thickness of cell membranes. In future studies we will assess the effect of vlcPL enriched cell membranes on the activity of γ -secretase. This membrane bound protease is central to the pathogenic onset of Alzheimer's disease. As reported, the relative amounts of aggregation prone and pathogenic A β peptide variants are significantly reduced when γ -secretase is embedded in model membranes composed of very long chain phospholipids (vlcPLs, *e.g.* diC24:1, nervonyl).^[5] Given the opportunity to precisely modulate cell membrane composition and thickness, our approach offers an attractive approach to allosterically modulate γ -secretase activity and potentially reduce the risk of Alzheimer's disease.

Unlike the dePEGylation strategies described in other chapters, in **chapter 5**, *o*-nitrobenzyl groups were used to photocage the cationic, primary amine headgroups of novel lipid reagents to form neutral, photocaged lipids. Liposomes formulated with these caged lipids circulated freely following intravenous injection into zebrafish embryos. Subsequent photolysis of *o*-Nb photocages, *in situ* and *in vivo*, revealed the underlying amine functionality at the liposome surface causing spontaneous switching of liposome surface charge from neutral to cationic. This, in turn, led to non-specific adsorption of liposomes across the entire vascular endothelium of the embryonic zebrafish, uptake by endothelial cells and delivery of liposome-encapsulated contents to these cells. By exploiting the contrasting *in vivo* fate of nanoparticles with opposing surface charges, we were able to demonstrate the potential for targeted drug delivery without the need for physiological differences between the diseased and healthy state (*e.g.* over expressed receptors, EPR effect *etc.*). In addition, this is the first example of a light sensitive drug delivery system in which the integrity of the drug carrier (*i.e.* the

liposome) is neither compromised nor destroyed upon light activation. Both scenarios leading to extracellular drug release. This is an important step if the targeted delivery of membrane impermeable cargos (*e.g.* DNA, peptides and proteins) to cells *in vivo* is to be realized.

The experimental studies described in this thesis exemplify the use of light as a tool to precisely control where and when drug delivery takes place. However, it is poignant to also recognize the disadvantages of using light as a therapeutic trigger as well as the steps being taken to overcome these limitations. For *o*-nitrobenzyl groups, optimal photolysis occurs on exposure to high energy UV light (365 nm, UV-A). This wavelength has limited tissue penetration (100-200 μm) and can also cause significant photoinduced cytotoxicity. In taking these technologies forward into the clinic, it will be necessary to address these issues. One solution has been the use of fibre optic endoscopic techniques to deliver short wavelength blue light deep into tissue. These techniques are already routinely used within the clinic for the application of various photodynamic therapies.^[6] A second option is to use two-photon excitation, where two photons of light – each twice the wavelength required for photolysis (*i.e.* 2 x 730 nm for *o*-nitrobenzyl) – are simultaneously used to irradiate the target tissue. Only at the exact point of intersection of both photons is enough energy delivered for photolysis.^[7] The advantages of two-photon excitation come from the use of longer wavelength near-infrared light, offering both increased tissue penetration (>1 cm) and negligible photoinduced cytotoxicity, as well as the exquisite spatiotemporal control afforded by this technique (light activation can be constrained to a volume of just 1 femtoliter). The main disadvantage is a significant loss in efficiency of photolysis efficiency compared to single photon excitation. While we and others have successfully demonstrated photolysis of *o*-Nb groups using 2-photon excitation sources, the development of new photocages with improved 2-photon absorption profiles will vastly improve the potential applications of this technology in the clinic.^[8]

Each chapter in this thesis describes a new technology aimed at addressing limitations of current drug delivery technologies and advancing the current state of the art in nanomedicine. This includes: spatiotemporal control of nanoparticle uptake and drug delivery (**chapter 2**), ensuring optimal physicochemical characteristics and drug

retention/release profiles both before and after activation (**chapter 3**), new methods to deliver insoluble drugs (**chapter 4**) and photo-activated targeting of DDSs in vivo (**chapter 5**) are all addressed in this thesis. Even though, on the current research stage, these studies are a proof-of-concept, as research methodology moves ever more into living organisms, and as technologies enabling light activation in patients continuously improve, these studies become more and more relevant to the ultimate goal of clinical application. The future is bright for light targeted nanomedicines!

References:

- [1] N. Kretschy, A. K. Holik, V. Somoza, K. P. Stengele, M. M. Somoza, *Angew Chem Int Edit* **2015**, *54*, 8555-8559.
- [2] P. Klan, T. Solomek, C. G. Bochet, A. Blanc, R. Givens, M. Rubina, V. Popik, A. Kostikov, J. Wirz, *Chem Rev* **2013**, *113*, 119-191.
- [3] (a) S. K. Choi, M. Verma, J. Silpe, R. E. Moody, K. Tang, J. J. Hanson, J. R. Baker, *Bioorgan Med Chem* **2012**, *20*, 1281-1290; (b) C. Marini, J. Offer, R. Longhi, P. E. Dawson, *Bioorgan Med Chem* **2004**, *12*, 2749-2757.
- [4] M. S. Kim, J. Gruneich, H. Y. Jing, S. L. Diamond, *J Mater Chem* **2010**, *20*, 3396-3403.
- [5] Winkler, E.; Kamp, F.; Scheuring, J.; Ebke, A.; Fukumori, A.; Steiner, H. *J. Biol. Chem.* **2012**, *287*, 21326–21334.
- [6] M. E. J. Ortner, K. Caca, F. Berr, J. Liebetrueth, U. Mansmann, D. Huster, W. Voderholzer, G. Schachschal, J. Mossner, H. Lochs, *Gastroenterology* **2003**, *125*, 1355-1363.
- [7] F. Helmchen, W. Denk, *Nat Methods*, **2005**, *2*, 932-940.
- [8] (a) T. Furuta, S. S. H. Wang, J. L. Dantzker, T. M. Dore, W. J. Bybee, E. M. Callaway, W. Denk, R. Y. Tsien, *P Natl Acad Sci USA*, **1999**, *96*, 1193-1200; (b) K. Peng, I. Tomatsu, B. van den Broek, C. Cui, A. V. Korobko, J. van Noort, A. H. Meijer, H. P. Spaink, A. Kros, *Soft Matter*, **2011**, *7*, 4881–4887.

Samenvatting en Perspectiven

O-Nitrobenzyl groepen worden veel gebruikt als moleculaire beschermgroepen die met licht verwijderd kunnen worden. Deze zogenaamde photocages worden reeds vaak toegepast in zowel de organische chemie^[1] als in de biologie^[2]. Photocaging blokkeert de functionaliteit van een molecuul en deze kan weer verwijderd worden door middel van licht met een specifieke golflengte. De mogelijkheid om precies te controleren waar en wanneer het beschermde molecuul belicht wordt maakt het mogelijk om precies te controleren waar en wanneer een photocaged molecuul geactiveerd wordt. Toepassing van photocages bij geneesmiddel bezorgsystemen (nanomedicijnen) leidt er toe dat men de afgifte van medicijnen kan controleren door middel van licht.

O-Nitrobenzylgroepen worden gebruikt voor het beschermen/inactiveren van verscheidene therapeutica^[3], zoals bijvoorbeeld, eiwitten en nucleïne zuren, maar ze worden ook toegepast op complexe meercomponentsystemen zoals nanomedicijnen, hydrogelen, micellen, liposomen en anorganische nanodeeltjes.^[4] In dit proefschrift zijn *o*-nitrobenzyl groepen gebruikt als fotolabiele verbindingsgroep tussen het wateroplosbare polymeer polyethyleenglycol (PEG) en verschillende type nano medicijnen (**Hoofdstukken 2-4**), of als lichtactiveerbare beschermgroep voor specifieke chemische functionaliteiten (**Hoofdstuk 5**). In deze voorbeelden leidde het gebruik van de *o*-nitrobenzyl groep tot volledige controle over waar en wanneer een nanomedicijn geactiveerd wordt.

In **Hoofdstuk 2**, beschrijf ik de strategie om membraanfusie tussen twee complementaire liposoompopulaties te controleren. Dit werd bereikt door de introductie van een fotolabiele PEG-corona op het oppervlak van deze fusogene liposomen. De PEG-corona blokkeert effectief de interactie tussen twee complementaire liposoom populaties. De minimaal noodzakelijke lengte van PEG die nodig is om effectief peptide-peptide interacties te verhinderen werd bepaald en er bleek een directe correlatie te zijn tussen de tijd van belichting en de mate van membraanfusie. Gebruikmakend van een LED lichtbron kon membraanfusie direct

geïnitieerd worden. Door deze methode toe te passen bij levende cellen kon de interactie met liposomen gecontroleerd worden met controle over waar en wanneer deze interactie plaatsvond. Door middel van licht werden de PEG-corona verwijderd van het oppervlak van liposomen wat leidde tot de spontane interactie met de cellen (voorzien van complementaire lipopeptides) resulterend in de accumulatie van liposomen op het cel oppervlak. Dit project is het eerste voorbeeld van gecontroleerde membraanfusie door middel van licht. Membraanfusie is in de Natuur een sterk gereguleerd proces, in tijd en plaats, om cellulaire functies goed te laten verlopen. De beschreven mogelijkheid om membraanfusie te controleren met licht maakt het in de toekomst mogelijk om meer efficiënte nanomedicijnen te ontwikkelen, gebaseerd op in liposoom geëncapsuleerde geneesmiddelen die met controle over tijd en plaats hun medicijnen kunnen afgeven. Door gebruik te maken van membraanfusie worden de medicijnen direct afgegeven in het cytosol van cellen waarmee opname door middel van endocytose vermeden wordt wat kan leiden tot een meer efficiënte medicijnafgifte.

In de **hoofdstukken 3 en 4** werd de *o*-nitrobenzyl groep gebruikt in 2 prodrugsystemen: PEG₂₀₀₀-*o*-nitrobenzyl-doxorubicine (**hoofdstuk 3**) en PEG₂₀₀₀-*o*-nitrobenzyl-nervonzuur (**hoofdstuk 4**). In **hoofdstuk 3**, vormt de prodrug PEG₂₀₀₀-*o*-nitrobenzyl-doxorubicine micellen welke door lichtactivatie uiteenvallen en daardoor snel en kwantitatief doxorubicine (DOX) afgeven. Deze prodrug-micellen lijken qua grootte en oppervlakte chemie veel op de voor klinisch gebruik goedgekeurde liposoom-doxorubicine formuleringen zoals bijvoorbeeld Doxil®. Dit nanomedicijn wordt passief opgenomen in vaste tumoren via het zogenaamde “enhanced permeation and retention” (EPR) effect. Een nadeel van Doxil zijn de cardiotoxische neveneffecten die ontstaan door voortijdig verlies van doxorubicine buiten de tumor. De hier beschreven prodrug heeft dit probleem niet en is daardoor interessant voor verdere studies als medicijn voor de behandeling van vaste tumoren.

Onder invloed van lage intensiteit UV-straling werd complete fotolyse van de prodrug tot het farmacologisch actieve DOX bewerkstelligd binnen 25 minuten. In de afwezigheid van licht werd geen cytotoxiciteit waargenomen voor prodrug concentraties tot 100 µM. De lichtdosering die nodig is voor de volledige conversie

van de prodrug naar DOX volledig leidde niet tot significante foto-geïnduceerde cytotoxiciteit. De door licht geactiveerde cytotoxiciteit van de vrijgekomen DOX was gecorreleerd met zowel stralingstijd als prodrug concentratie. Spatiotemporele controle over de DOX-afgifte aan cellen in kweek kon verkregen worden door middel van deze methode. Dit systeem heeft de potentie om zich niet alleen passief te richten op de vaste tumoren via het EPR effect, maar ook door het voorkomen van lekkage van geneesmiddelen onderweg naar de tumoren. Terwijl de kwantitatieve afgifte gewaarborgd blijft, kunnen de bijwerkingen significant vermindert worden in vergelijking met huidige generatie goedgekeurde kanker-nanomedicijnen.

Het is bekend dat de lipide-samenstelling en de dikte van de celmembranen significante invloed kan hebben op de activiteit van specifieke membraaneiwitten. De celmembraandikte verandert indien cellen vetzuren met extra lange keten (vlcFA) als biosynthetische voorlopers van extra lange fosfolipiden (vlcPL) op kunnen nemen. De opname van de vlcFA's wordt echter bemoeilijkt door de extreme onoplosbaarheid van deze vetzuren in water. In **hoofdstuk 4** werd dit probleem opgelost door het synthetiseren van lichtgevoelige vlcFA-PEG (PEG₂₀₀₀-*o*-nitrobenzyl-nervonzuur; FA24:1) amfifiele conjugaten die in water spontaan micellen vormen. Deze micellen worden spontaan opgenomen in lipide bilagen (zowel liposoom membranen als cel membranen) waardoor vlcFA-PEG in de bilaag komt. Door middel van licht werd de binding tussen het vetzuur en PEG verbroken waardoor het vrije nervonzuur achterbleef in het (cel)membraan. Afgifte van nervonzuur in gekweekte cellen leidde tot de verwerking van dit vetzuur tot cellulaire fosfolipiden met een verhoogd vlcFA gehalte. Deze methode is dus een efficiënte manier om de compositie en dus de dikte van celmembranen te modificeren. In toekomstige studies willen we de effecten van vlcPL verrijkte celmembranen op de activiteit van γ -secretase bepalen. Dit membraan gebonden protease speelt een belangrijke rol in het ontstaan van de ziekte van Alzheimer. In vitro studies hebben aangetoond dat de concentratie van door γ -secretase gevormde pathogene A β -peptides sterk vermindert indien γ -secretase ingebed is in "dikke" membranen bestaande uit extra lange fosfolipiden (vlcPL, bijv. diC24:1, nevon).^[5] De hier beschreven mogelijkheid om de celmembraan compositie aan te kunnen passen maakt onze aanpak potentieel attractieve om de allosterisch

γ -secretase activiteit te moduleren en daarmee het risico op de ziekte van Alzheimer te reduceren.

In tegenstelling tot de dePEGylering strategieën beschreven in de hoofdstukken 2-4 werd in **hoofdstuk 5** de *o*-nitrobenzyl groep om de lading van liposomen te veranderen van neutraal naar kationisch onder invloed van licht. Liposomen geformuleerd met beschermde (“caged”) lipiden circuleerden vrij in de bloedvaten van zebravis embryo’s. Fotolyse van *o*-Nb photocages *in situ* en *in vivo* resulteerde in een verandering van de oppervlaktelading van de liposomen van neutraal naar kationisch. Dit op zijn beurt leidde tot niet-specifieke adsorptie van de liposomen in alle bloedvaten van de zebravis. De liposomen werden vervolgens opgenomen door de endotheel cellen waardoor de inhoud van de liposomen in deze cellen vrijkwam. Door het in-situ aanpassen van de oppervlaktelading van liposomen werd dus controle gekregen over het in vivo gedrag van deze nanomedicijnen. Daarnaast is dit het eerste voorbeeld van een lichtgevoelig nanomedicijn waarvan de integriteit van de geneesmiddelen drager (het liposoom) niet aangetast of zelfs vernietigd werd door lichtactivatie. Dit is een belangrijke stap om gerichte afgifte van membraan ondoordringbare ladingen (bijv. DNA, peptiden en eiwitten) in cellen *in vivo* te realiseren.

De hoofdstukken beschreven in dit proefschrift laten zien dat licht gebruikt kan worden om precieze controle te verkrijgen over waar en wanneer geneesmiddelenafgifte plaatsvindt. Het is belangrijk om ook de nadelen van het gebruik van licht als activator van therapeutica te zien om daarmee deze beperkingen in de toekomst op te kunnen heffen. Voor de in dit proefschrift gebruikte *o*-nitrobenzyl groep vindt optimale fotolyse plaats met energierijk UV licht (365 nm, UV-A). Deze golflengte heeft een beperkte weefsel penetratiediepte (100-200 μm) en kan gepaard gaan met significante cytotoxiciteit als neveneffect. Voor het verder ontwikkelen van deze technologie om toepassingen in de kliniek mogelijk te maken moeten deze kwesties aangepakt worden. Een mogelijke oplossing is het gebruik van glasvezel-gebaseerde endoscopische technieken om het licht dieper in het weefsel te krijgen. Deze techniek wordt al routinematig gebruikt bij foto-dynamische therapieën.^[6] Een tweede optie is gebruik te maken van twee-foton excitatie, waarbij

2 licht fotonen combineren om de *o*-nitrobenzylgroep te activeren.^[7] De voordelen van twee-foton excitatie zijn het gebruik van nabij-infrarood licht waardoor de penetratiediepte van dit licht in het weefsel groter is (>1 cm). Tevens is de cytotoxiciteit van het licht verwaarloosbaar. Echter het grootste nadeel van twee-foton excitatie is het significante verlies in fotolyse efficiëntie ten opzichte van één-foton excitatie. Daarom is de ontwikkeling van nieuwe photocages met verbeterde 2-foton absorptie profielen van groot belang voor deze technologie.^[8]

Elk hoofdstuk in dit proefschrift beschrijft een nieuwe technologie gericht op het overkomen van de limitatie van de huidige nanomedicijnen. De beschreven onderzoeken zijn op dit moment fundamenteel van aard. Echter doordat dit onderzoek steeds meer verschuift richting studies in levende organismen en doordat de technologie die lichtactivatie mogelijk maakt in patiënten steeds verder verbetert zullen de beschreven onderzoeken steeds relevanter worden om uiteindelijk toegepast te worden in klinische toepassingen. Licht-geactiveerde nanomedicijnen gaan een schitterende toekomst tegemoet!

Referenties:

- [1] N. Kretschy, A. K. Holik, V. Somoza, K. P. Stengele, M. M. Somoza, *Angew Chem Int Edit* **2015**, *54*, 8555-8559.
- [2] P. Klan, T. Solomek, C. G. Bochet, A. Blanc, R. Givens, M. Rubina, V. Popik, A. Kostikov, J. Wirz, *Chem Rev* **2013**, *113*, 119-191.
- [3] (a) S. K. Choi, M. Verma, J. Silpe, R. E. Moody, K. Tang, J. J. Hanson, J. R. Baker, *Bioorgan Med Chem* **2012**, *20*, 1281-1290; (b) C. Marini, J. Offer, R. Longhi, P. E. Dawson, *Bioorgan Med Chem* **2004**, *12*, 2749-2757.
- [4] M. S. Kim, J. Gruneich, H. Y. Jing, S. L. Diamond, *J Mater Chem* **2010**, *20*, 3396-3403.
- [5] Winkler, E.; Kamp, F.; Scheuring, J.; Ebke, A.; Fukumori, A.; Steiner, H. *J. Biol. Chem.* **2012**, *287*, 21326–21334.

[6] M. E. J. Ortner, K. Caca, F. Berr, J. Liebetrueth, U. Mansmann, D. Huster, W. Voderholzer, G. Schachschal, J. Mossner, H. Lochs, *Gastroenterology* **2003**, *125*, 1355-1363.

[7] F. Helmchen, W. Denk, *Nat Methods*, **2005**, *2*, 932-940.

[8] (a) T. Furuta, S. S. H. Wang, J. L. Dantzker, T. M. Dore, W. J. Bybee, E. M. Callaway, W. Denk, R. Y. Tsien, *P Natl Acad Sci USA*, **1999**, *96*, 1193-1200; (b) K. Peng, I. Tomatsu, B. van den Broek, C. Cui, A. V. Korobko, J. van Noort, A. H. Meijer, H. P. Spaink, A. Kros, *Soft Matter*, **2011**, *7*, 4881–4887.

Abbreviations

A	Alanine
CD	Circular dichroism
CPE	Cholesterol-PEG ₁₂ -(EIAAIEL) ₃
CPK	Cholesterol-PEG ₁₂ -(KIAALKE) ₃
DCM	Dichloromethane
DDT	Dithiothreitol
DEA	Diethanolamine
DIPEA	N,N-Diisopropylethylamine
DMAP	4-Dimethylaminopyridine
DOPC	1,2-dioleoyl-sn-glycero-3-phosphocholine
DOPE	1,2-dioleoyl-sn-glycero-3-phosphoethanolamine
DOPE-LR	1,2- dioleoyl-sn-glycero-3-phosphoethanolamine- N-(lissamine rhodamine B sulfonyl)
DOPE-NBD	1,2-dioleoyl-sn-glycero-3- phosphoethanolamine- N-(7-nitro-2-1,3-benzoxadiazol-4-yl)
DOPE-Atto633	1,2-dioleoyl-sn-glycero-3-phosphoethanolamine- ATTO633
DOPG	1,2-dioleoyl-sn-glycero-3-phospho-(1'-rac-glycerol) (sodium salt)
DOTAP	1,2-dioleoyl-3-trimethylammonium -propane (chloride salt)
DSPC	1,2-distearoyl-sn-glycero-3-phosphocholine
DSPE	1,2-Distearoyl-sn-glycero-3-phosphoethanolamine
E	Glutamate
EDCI	1-Ethyl-3-(3-dimethylaminopropyl)carbodiimide
EDC·HCl	N-(3-Dimethylaminopropyl)-N'-ethylcarbodiimide hydrochloride
ELSD	Evaporative light scattering detector
Et₃N	Triethylamine
F	Phenylalanine
FACS	Fluorescence-activated cell sorting
FCS	Fetal Calf Serum
G	Glycine
HCTU	2- (6-chloro-1 H -benzotriazole-1-yl) -1,1,3,3-tetramethylaminium

	hexafluorophosphate
HEPES	4-(2-hydroxyethyl)-1-piperazineethanesulfonic acid
HPLC	High-performance liquid chromatography
I	Isoleucine
IC₅₀	Half maximal inhibitory concentration
K	Lysine
L	Leucine
LED	Light-emitting diode
MeCN	Acetonitrile
NaBH₄	Sodium borohydride
NMR	Nuclear Magnetic Resonance spectroscopy
OND	Oligodeoxynucleotide
P	Proline
PDI	Polydispersity Index
PBS	Phosphate buffered saline
PEG	Polyethylene glycol
PEI	Polyethylenimine
PLL	Poly-L-lysine
POPC	1-palmitoyl-2-oleoyl-sn-glycero-3-phosphocholine
Q	Glutamine
R	Arginine
SEC	Size exclusion chromatography
SR-B	Sulforhodamine B
tBuOH	Tert-Butanol
TEM	Transmission electron microscope
TFA	Trifluoroacetic acid
UV	Ultraviolet
V	Valine
vlcFAs	Very long chain fatty acids
W	Tryptophan

Curriculum Vitae

Li Kong was born on 16th October 1986 in Qufu City, Shandong Province, China. She attended the Qufu No.1 Middle school, where she obtained her high school diploma in 2005. In the same year she started her study program of Chemistry in Shandong University and obtained her BSc degree in 2009 under supervision of Prof. Jingcheng Hao. After that, she was recommended to continue her master study in Organic Chemistry, Shandong University, under supervising of Pro. Aiyu Hao. Her research focused on cyclodextrin-based organogel and received her MSc degree in 2012. At the same time, she was awarded a research scholarship from Chinese Scholarship Council. With this grant, she joined as a PhD candidate the Supramolecular & Biomaterials Chemistry group in the Leiden Institute of Chemistry, Leiden University, under supervision of Prof. dr. Alexander Kros and Dr. Frederick Campbell. Her research, photo-activated drug delivery systems, is described in this thesis. From October 2017, Li continued her research as a post-doctoral-researcher in the same group. Her current research concerns the study of dendritic cell targeting liposomes in skin using microneedles.

List of Publications

L. Kong, A. Rabe, G. A. Alpizar, M. Meijer, S. Bonnet, S. Vogel, A. Kros, F. Campbell, "Charge-Switchable Liposomes for Drug Delivery in Vitro and in Vivo", Manuscript in preparation.

L. Kong, E. Dawkins, F. Campbell, E. Winkler, R. J.E. Derks, M. Giera, F. Kamp, H. Steiner, A. Kros, "Light Induced Modulation of the Very Long Chain Fatty Acid Composition of Cell Membranes", Manuscript in preparation.

F. Zhang, ‡ **Li Kong**, ‡ D. Liu, W. Li, E. Mäkilä, A. Correia, R. Lindgren, J. Salonen, J. J. Hirvonen, H. Zhang, A. Kros, H. A. Santos, "Transformable Delivery System by Photo-Triggered Zwitterization with Dual-Antifouling Surface for Cell Recognition", *Advanced therapeutics*, 2018, accepted.

L. Kong, D. Poulcharidis, G. F. Schneider, F. Campbell, A. Kros, "Spatiotemporal Control of Doxorubicin Delivery from "Stealth-Like" Prodrug Micelles", *Int. J. Mol. Sci.*, **2017**, 18, 2033.

L. Kong, S. H. C. Askes, S. Bonnet, A. Kros, F. Campbell, "Temporal Control of Membrane Fusion through Photolabile PEGylation of Liposome Membranes", *Angew.Chem.Int. Ed.* **2016**, 55, 1396–1400.

L. Kong, F. Zhang, P. Xing, X. Chu, A. Hao, "A binary solvent gel as drug delivery carrier". *Colloids and Surfaces A: Physicochem. Eng. Aspects*, **2017**, 522, 577–584.

L. Kong, P. Xing, X. Chu, A. Hao, "A dual-solvents gel based on native cyclodextrin as drug carrier", *Journal of Controlled Release*, **2017**, 259, e77.

L. Kong, T. Sun, F. Zhang, F. Xin, A. Hao. "Supramolecular Smart Organogel Based on Cholesterol". *Progress in Chemistry*, **2012**, 24, 135-145.

L. Kong, T. Sun, F. Xin, W. Zhao, H. Zhang, Z. Li, Y. Li, Y. Hou, S. Li, A. Hao, "Lithium Chloride-induced Organogel Transformed from Precipitate based on Cyclodextrin Complexes". *Colloid and Surface A : Physicochemical and Engineering Aspects*, **2011**, 392, 156–162.